Intelligent Approaches for Energy-Efficient Resource Allocation in the Cognitive Radio Network

Deepa Das

Department of Electrical Engineering
National Institute of Technology Rourkela

Intelligent Approaches for Energy-Efficient Resource Allocation in the Cognitive Radio Network

Dissertation submitted to the

National Institute of Technology Rourkela

in partial fullfillment of the requirements

of the degree of

Doctor of Philosophy

in

Electrical Engineering

by

Deepa Das
(Roll No: 512EE1016)

under the supervision of
Prof. Susmita Das

Department of Electrical Engineering,
National Institute of Technology, Rourkela,
Rourkela-769 008, Odisha, India
2012-2016

Electrical Engineering
National Institute of Technology Rourkela

July 3, 2017

Certificate of Examination

Roll Number: <u>512EE1016</u>
Name: Deepa Das
Title of Dissertation:
Intelligent Approaches for Energy-Efficient Resource Allocation in the Cognitive Radio Network

We the below signed, after checking the dissertation mentioned above and the official record book (s) of the student, hereby state our approval of the dissertation submitted in partial fulfillment of the requirements of the degree of Doctor of Philosophy in Electrical Engineering at National Institute of Technology Rourkela. We are satisfied with the volume, quality, correctness, and originality of the work.

_____

Prof. Susmita Das
Principal Supervisor

_____   _____

Prof. Dipti Patra   *Prof. Sarat Kumar Patra*
Member (DSC)   Member (DSC)

_____   _____

Prof. Ratnakar Dash   *Prof. Debarati Sen*
Member (DSC)   Examiner

_____   _____

Prof. Anup Kumar Panda   *Prof. Jitendriya Kumar Satapathy*
Chairman (DSC)   HOD, EE Dept.

Electrical Engineering
National Institute of Technology Rourkela

Prof./Dr. Susmita Das
Associate Professor

July 3, 2017

Supervisor's Certificate

This is to certify that the work presented in this dissertation entitled "*Intelligent Approaches for Energy-Efficient Resource Allocation in the Cognitive Radio Network*" by "*Deepa Das*", Roll Number 512EE1016, is a record of original research carried out by her under my supervision and guidance in partial fulfillment of the requirements of the degree of *Doctor of Philosophy* in *Electrical Engineering*. Neither this dissertation nor any part of it has been submitted for any degree or diploma to any institute or university in India or abroad.

Susmita Das
Associate Professor

Dedicated

to

to my Parents

for their
endless love, support and sacrifices

Deepa Das

Declaration of Originality

I, Deepa Das, Roll Number 512EE1016 hereby declare that this dissertation entitled *"Intelligent Approaches for Energy-Efficient Resource Allocation in the Cognitive Radio Network"* represents my original work carried out as a doctoral student of NIT Rourkela and, to the best of my knowledge, it contains no material previously published or written by another person, nor any material presented for the award of any other degree or diploma of NIT Rourkela or any other institution. Any contribution made to this research by others, with whom I have worked at NIT Rourkela or elsewhere, is explicitly acknowledged in the dissertation. Works of other authors cited in this dissertation have been duly acknowledged under the section "Bibliography". I have also submitted my original research records to the scrutiny committee for evaluation of my dissertation.

I am fully aware that in case of any non-compliance detected in future, the Senate of NIT Rourkela may withdraw the degree awarded to me on the basis of the present dissertation.

July 3, 2017
NIT Rourkela

Deepa Das

Acknowledgment

Abstract

The cognitive radio (CR) is evolved as the promising technology to alleviate the spectrum scarcity issues by allowing the secondary users (SUs) to use the licensed band in an opportunistic manner. Various challenges need to be addressed before the successful deployment of CR technology. This thesis work presents intelligent resource allocation techniques for improving energy efficiency (EE) of low battery powered CR nodes where resources refer to certain important parameters that directly or indirectly affect EE. As far as the primary user (PU) is concerned, the SUs are allowed to transmit on the licensed band until their transmission power would not cause any interference to the primary network. Also, the SUs must use the licensed band efficiently during the PU's absence. Therefore, the two key factors such as protection to the primary network and throughput above the threshold are important from the PU's and SUs' perspective, respectively. In deployment of CR, malicious users may be more active to prevent the CR users from accessing the spectrum or cause unnecessary interference to the both primary and secondary transmission. Considering these aspects, this thesis focuses on developing novel approaches for energy-efficient resource allocation under the constraints of interference to the PR, minimum achievable data rate and maximum transmission power by optimizing the resource parameters such as sensing time and the secondary transmission power with suitably selecting SUs.

Two different domains considered in this thesis are the soft decision fusion (SDF)-based cooperative spectrum sensing CR network (CRN) models without and with the primary user emulation attack (PUEA). An efficient iterative algorithm called iterative Dinkelbach method (IDM) is proposed to maximize EE with suitable SUs in the absence of the attacker. In the proposed approaches, different constraints are evaluated considering the negative impact of the PUE attacker on the secondary transmission while maximizing EE with the PUE attacker. The optimization problem associated with the non-convex constraints is solved by our proposed iterative resource allocation algorithms (novel iterative resource allocation (NIRA) and novel adaptive resource allocation (NARA)) with suitable selection of SUs for jointly optimizing the sensing time and power allocation. In the CR enhanced vehicular ad hoc network (CR-VANET), the time varying channel responses with the vehicular movement are considered without and with the attacker. In the absence of the PUE attacker, an interference-aware power allocation scheme based on normalized least mean square (NLMS) algorithm is proposed to maximize EE considering the dynamic constraints. In the presence of the attacker, the optimization problem associated with the non-convex and time-varying constraints is solved by an efficient approach based on

genetic algorithm (GA). Further, an investigation is attempted to apply the CR technology in industrial, scientific and medical (ISM) band through spectrum occupancy prediction, sub-band selection and optimal power allocation to the CR users using the real time indoor measurement data. Efficacies of the proposed approaches are verified through extensive simulation studies in the MATLAB environment and by comparing with the existing literature. Further, the impacts of different network parameters on the system performance are analyzed in detail. The proposed approaches will be highly helpful in designing energy-efficient CRN model with low complexity for future CR deployment.

List of Acronyms

Acronym	Description
AES	Advanced Encryption Standard
AP	Access Point
AF	Amplify-and-Forward
ANN	Artificial Neural Network
AWGN	Additive White Gaussian Noise
BAN	Body Area Network
BPSK	Binary Phase Shift Keying
BSs	Base Stations
CCDA	Common Control Data Attack
CORAL	Cognitive Radio Learning
CR	Cognitive Radio
CR-VANET	Cognitive Radio Vehicular Ad Hoc Network
CRNs	Cognitive Radio Networks
CRUs	Cognitive Radio Users
CSS	Cooperative Spectrum Sensing
DC	Difference of Convex
DF	Decode-and-Forward
DHCA	Distributive Heuristic Channel Assignment
DoS	Denial-of-Service
DSRC	Dedicated Short-Range Communications
ED	Energy Detector
EE	Energy Efficiency
EGC	Equal Gain Combining
EPA	Exact Power Allocation
EPG	Energy per Goodbit
FC	Fusion Center
FCC	Federal Communications Commission
FLANN	Functional Link Artificial Neural Network
FW	Frank-and-Wold
GA	Genetic Algorithm
GLRT	Generalized Likelihood Ratio Test
GPS	Global Positioning System
HDF	Hard Decision Fusion
HMM	Hidden Markov Model
I2V	Infrastructure-to-vehicle

List of Acronyms (*continued*)

Acronym	Description
IDM	Iterative Dinkelbach Method
IEEE	Institute of Electrical and Electronics Engineers
IFCI	Interference Free Communication Index
i.i.d	Independent Identically Distributed
ISM	Industrial, Scientific, and Medical
ITU	International Telecommunication Union
IWO	Invasive Weed Optimization
KKT	Karush-Kuhn-Tucker
LAN	Local Area Network
LRT	Likelihood Ratio Test
MAN	Metropolitan Area Network
MDC	Modified Deflection Coefficient
MEESS	Modified Energy-Efficient Sensor Selection
MF	Matched Filter
MLE	Maximum Likelihood Estimates
MLP	Multi Layer Perceptron
MLR	Maximum Likelihood Ratio
MOCSO	Multi-objective Cat Swarm Optimization
MO hybrid IWOPSO	Multi-objective Hybrid Invasive Weed Optimization and Particle Swarm Optimization
MOPSO	Multi-objective Particle Swarm Optimization
MPDA	Maximum Probability of Detection Algorithm
MRC	Maximal Ratio Combining
MSE	Mean Square Error
MSs	Mobile Stations
MU	Malicious User
N-P	Neyman-Pearson
NARA	Novel Adaptive Resource Allocation
NIRA	Novel Iterative Resource Allocation
NLMS	Normalized Least Mean Square
NSGA-II	Nondominated Sorting Genetic Algorithm-II
NSIWO	Nondominated Sorting Invasive Weed Optimization
NTIA	National Telecommunications and Information Administration
OFA	Objective Function Attack
OFDM	Orthogonal Frequency Devision Multiplexing
PA-GABC	Population Adaptive Gbest-guided Artificial Bee Colony

List of Acronyms (*continued*)

Acronym	Description
PDF	Probability Distribution Function
PR	Primary Receiver
PSD	Power Spectral Density
PSO	Particle Swarm Optimization
PU	Primary User
PUEA	Primary User Emulation Attack
QoS	Quality of Service
RBF	Radial Basis Function
RBW	Resolution Bandwidth
SA	Spectrum Analyzer
SCN	Selfish Channel Negotiation
SDF	Soft Decision Fusion
SDR	Software Defined Radio
SINR	Signal-to-Interference-plus-Noise Ratio
SLS	Square-Law Selection
SNR	Signal-to-Noise Ratio
SP-CAF	Symmetry Property of Cyclic Autocorrelation Function
SR	Secondary Receiver
SS	Spectrum Sensing
SSDF	Spectrum Sensing Data Falsification
SU	Secondary User
TCP	Transmission Control Protocol
TDoA	Time Difference of Arrival
TECCL	Transmission Encapsulation based on the Connected Component Labeling
TV	Television
UHF	Ultra High Frequency
V2I	Vehicle-to-Infrastructure
V2V	Vehicle-to-vehicle
VANETs	Vehicular Ad Hoc Networks
VBW	Video Bandwidth
VHF	Very High Frequency
VSUs	Vehicular Secondary Users
WBAN	Wireless Body Area Network
WFAC	Water Filling Factors Aid Search
WiFi	Wireless Fidelity

List of Acronyms (*continued*)

Acronym	Description
WiMAX	Worldwide Interoperability for Microwave Access
WLAN	Wireless Local Area Network
WRAN	Wireless Regional Area Network
WSPRT	Wald's Sequential Probability Ratio Test

List of Symbols & Notations

Symbol & Notation	Description
a_1	Average rate of arrival of vehicles into the sensing range
a_2	Average rate of arrival of vehicles into the protective range
a_m	Acceleration of the mth vehicle
A_0	Absence of the attacker
A_1	Presence of the attacker
b_k	Compromising factor
C_{out}	User defined constant
C_{th}	User defined constant
d_m	Distance between the PU and the mth SU
d_0	Reference distance (1m)
d_S	Safety distance between the vehicles
D_R	Protective range of the PU
D_S	Sensing range of the PU
Eff_k	Balancing efficiency
f_n	Discrete frequency point
f_r	Frequency resolution
f_s	Sampling frequency
F_{span}	Frequency span
h_{arm}	Sub-channel co-efficient between the attacker and the mth SR
h_{asm}	Sub-channel co-efficient between the attacker and the mth SU
$H_n{}^1$	Busy state of the nth sub-band
$H_n{}^2$	Idle state of the nth sub-band
$H_n{}^3$	Underutilized state of the nth sub-band
h_{prm}	Sub-channel co-efficient between the PU and the mth SR
h_{ps}	Sub-channel co-efficient between the PU and the SU
h_{sdm}	Sub-channel co-efficient between the mth SU and the PR
h_{srm}	Sub-channel co-efficient between the mth SU and the corresponding SR
H_0	Idle state of the licensed band
$\hat{H}_0$	Decision made by the SU about the PU's absence
H_1	Busy state of the licensed band
$\hat{H}_1$	Decision made by the SU about the PU's presence
$\mathbb{I}$	Total number of discrete time instants
I_{th}	Interference threshold
I_{total}	Total interference introduced to PR

Symbol & Notation	Description
$\mathbb{J}$	Total number of frequency points
$L_f(\mathfrak{p})$	Floor penetration loss factor (dB) where $\mathfrak{p}$ is the number of floors between the two terminals
M_1	Number of vehicles expected only in the sensing region
M_2	Number of vehicles expected only in the protective region
M_L	Lower bound of SUs
M_U	Upper bound of SUs
N	Number of samples
$\mathcal{N}$	Number of sub-bands
N_F	CR noise floor
N_p	Noise power
N_{points}	Number of trace points in the Agilent N9342C handheld SA
O_{th}	Outage threshold
P_d	Local probability of detection
P_f	Local probability of false alarm
P_{H0}	Probability of PU's absence
P_{H1}	Probability of PU's presence
P_L	Path loss
P_{md}	Local miss detection probability
P_{outm}	Outage at mth SU
P_S	Sensing power
P_{tmax}	Maximum transmission power from the SUs
P_T	Total power consumption
$\mathscr{P}_V$	PDF of V
Q_d	Global probability of detection
$\bar{Q}_d$	Target global detection probability
Q_f	Global false alarm probability
Q_{md}	Global miss detection probability
R_{th}	Minimum achievable throughput
$s(n)$	PU's transmitted signal at nth instant
$s_a(n)$	Transmitted signal from the PUE attacker at nth instant
S_R	Sensing rounds
S_{Rmin}	Minimum sensing rounds
S_T	Shortest distance between the PU and the edge of the road segment
T_{span}	Time span
u	Busy rate

Symbol & Notation	Description
v	Idle rate
V_{Im}	Initial velocity of the mth vehicle
V_{max}	Maximum velocity of the vehicle
V_{min}	Minimum velocity of the vehicle
w	Weight vector
$x(n)$	Received signal at the SU
Y_G	Global test statistic at the FC
Y_m	Output of the ED of mth SU
α	Path-loss exponent
β	Probability of attacker's presence in the CRN
$\eta(n)$	AWGN at nth instant
Γ	Duration of the frame
γ_{am}	Received SNR at the mth SU in the presence of the attacker
γ_m	Received SNR at the mth SU
λ	Local decision threshold
λ_g	Global threshold
$\bar{\mu}$	Step size
$\bar{\Omega}$	Distance power loss coefficient
$\sigma_a{}^2$	Variance of $s_a(n)$
$\sigma_s{}^2$	Variance of $s(n)$
$\sigma_\eta{}^2$	Noise variance
τ_d	Data transmission duration
τ_r	Reporting duration
τ_s	Sensing time
Υ	Dinkelbach parameter
φ	Learning rate

Contents

List of Figures

List of Tables

List of Algorithms

Chapter 1

Introduction

1.1   Introduction

NOW-A-DAYS, communication through the wireless media is becoming one of the inevitable necessities of people around the globe. The ever-growing interests in the wireless devices and their applications induce the demand of high data rate which may result in traffic congestion problem. According to the traditional fixed frequency allocation policy, the spectrum band is assigned to the licensed holders who have the authentication to use that band for a specific time basis over a large geographical region [1, 2]. Though the spectrum is specifically allotted to the licensed users, some portions of the spectrum still remain underutilized or unutilized [3]. According to Federal Communications Commission (FCC), the entire utilization of the spectrum varies between 15% to 85% over time and frequency. This unused portions of the licensed spectrum are defined as whitespace or spectrum holes. The spectrum hole concept is illustrated in Figure 1.1.
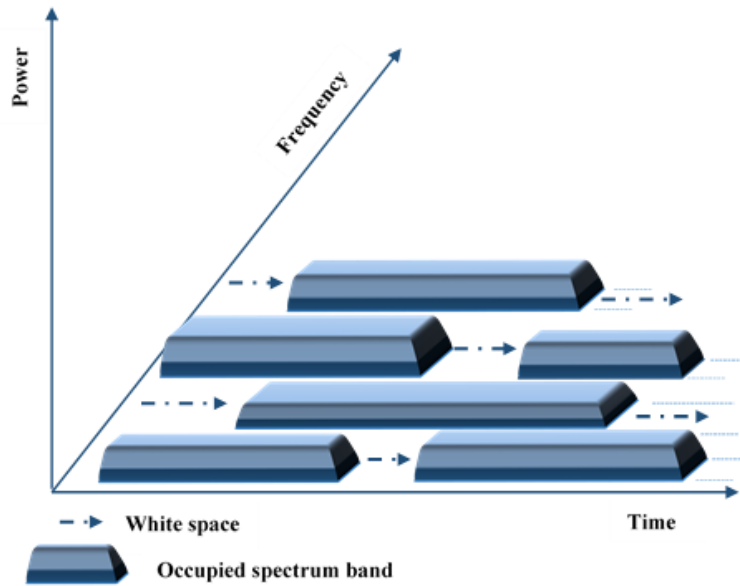
Figure 1.1: Spectrum hole concept.

The radio frequency band is divided into the licensed and unlicensed band. The improper and inefficient usage of spectrum band leads to the development of dynamic spectrum access(DSA) technique which exploits the licensed band in an opportunistic manner. Depending on the licensed band's occupancy statistics, the whitespace is categorized into three types [4, 5].

- White hole/Spectrum hole:The licensed band is vacant.

- Grey hole: The licensed band is partially occupied i.e. the licensed user transmits with a very low power.

- Black hole: The licensed band is fully occupied i.e. the licensed user transmits with high power.

Recently, cognitive radio (CR) is introduced as a promising solution to alleviate the spectrum scarcity problem by effectively exploiting the underutilized spectrum band [6]. In CR, the licensed users and the unlicensed users are referred as the primary users (PUs) and the secondary users (SUs), respectively. In May 2004, FCC declared the use of unlicensed operation in VHF and UHF TV bands [7]. Then, IEEE 802 local area network/metropolitan area network (LAN/MAN) working group created 802.22 committee on wireless regional area networks (WRANs) based on CR which allows unlicensed users in very high frequency (VHF) and ultra high frequency (UHF) (54-862 MHz) bands ensuring sufficient protection to the incumbent user [8].

1.1.1 Cognitive radio

The term "Cognitive Radio" was first introduced by Joseph Mitola in his doctoral thesis in 2002. The CR was presented as an advanced version of software defined radio (SDR) [9, 10]. The CR concept was defined by the several regulatory bodies presenting the same contexts. The well-known definition adopted by FCC is [11]

> *"Cognitive radio: A radio or system that senses its operational electromagnetic environment and can dynamically and autonomously adjust its radio operating parameters to modify system operation, such as maximize throughput, mitigate interference, facilitate interoperability, access secondary markets."*

Hence, the CR is a reconfigurable radio, it can adaptively change its operational parameters according to the dynamic surrounding environment to enable the SUs to select the white space in the frequency band and use that band until they do not cause any harmful interference to the legitimate user.The primary objectives of the CR are

- To facilitate efficient utilization of the limited spectrum, thereby achieving the demands for more data rate and quality of service (QoS).

- To protect the PUs from any harmful interference caused by the SUs.

- To provide highly secure communication to all the users present in the cognitive radio networks (CRNs).

So, the main operational features of the CR are cognitive capability and reconfigurability [2, 5, 12].Cognitive capability refers to the ability of the CR to

identify the unutilized spectrum band from the temporal and spatial varying radio environment at the specific time and required location. In order to cope of with the real-time environment, the CR must be aware of the changes occurring in the surrounding. Hence, it has to perform spectrum sensing (SS), spectrum analysis, spectrum decision and spectrum mobility as shown in Figure 1.2. Reconfigurability refers to the capability of the CR to reconfigure the operating parameters according to the dynamic radio environment. So, the CR can be programmed to transmit and receive on any frequency bands, and to use different access technologies supported by its hardware design. The reconfigurable parameters include operating frequency, modulation scheme, transmit power limited by the maximum power constraint and communication network access.
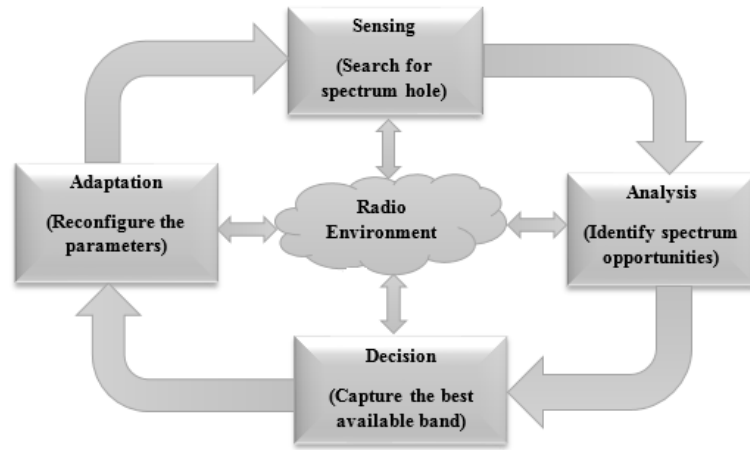
Figure 1.2: General working principles of CR.

The CRN's architecture is designed so as to meet the challenges from all the users' perspective. From the PU's perspective, SUs are allowed to access the licensed band until they do not create any interference to the PU. From the SUs' perspective, they must avail the service facilities efficiently to maximize their data transmission rate. Further, the deployment of CRNs should not affect other networks. The basic components of the CRN are mobile stations/ CR nodes (MSs/CR nodes), CR base stations (CR-BSs) and the backbone/core networks. Basically, there are three types of architectures; infrastructure architecture, ad hoc architecture and mesh architecture [13]. The infrastructure refers to the central controller entity CR-BS at which the local information from CR nodes is collected. The CRs present under the same CR-BS are allowed to communicate with each other via CR-BS. Thus, each CR node can access the CR-BS only in a one-hop manner. In accordance with the final decision by the BS, the CR nodes adopt their operating parameters. The ad hoc network refers to the non-existence of the CR-BSs. The links between the CR nodes act as ad hoc networks either by using the existing communication protocols (e.g.

WiFi, Bluetooth) or by dynamically selecting the spectrum holes. The mesh architecture is also called hybrid wireless mesh networks, and is formed by implementing the concepts of both infrastructure and ad hoc Networks. The CR nodes can connect to the BS either directly or by using other nodes as relay. Hence, the communication process to the BS may be done in a one-hop or multi-hop manner.

1.1.2 Working principles of CR

The working principles of CR are to perform SS, to analyze, to learn from the surroundings and to adapt its internal parameters according to the statistical variations of the real-time environments. So, the main working mechanisms of the CR are SS, spectrum management, spectrum sharing and spectrum mobility.

Spectrum sensing

SS is the primary task amongst all the processes. It enables the CR nodes to correctly identify the spectrum holes and to detect the PU's activity on the licensed band. The PU has no rights to change its characteristics in order to share the authenticated band with the SUs. Hence, the CR nodes need to perform SS continuously to obtain the information about the occupancy statistics. Figure 1.3 shows the classification of SS techniques on different bases [14–19]. Primarily, SS is classified based on the number of SUs that participate in the detection and decision-making process.

- In non-cooperative SS technique, the single SU makes its own decision regarding the availability of the licensed band and reconfigures its parameters according to its own observation.

- In cooperative SS (CSS), multiple SUs participate in the detection process in centralized or decentralized or relay-assisted manner. Each SU can use any of the local sensing methods, and the global decision is obtained by combining all the local decisions.

Specifically, SS is performed at two instants, periodically and demand basis which are defined as follows.

- Proactive (periodical) SS: The SUs perform SS periodically in the licensed band.

- Reactive (demand) SS: SS is performed on the demand basis when the SUs intend to transmit their data on the licensed band.
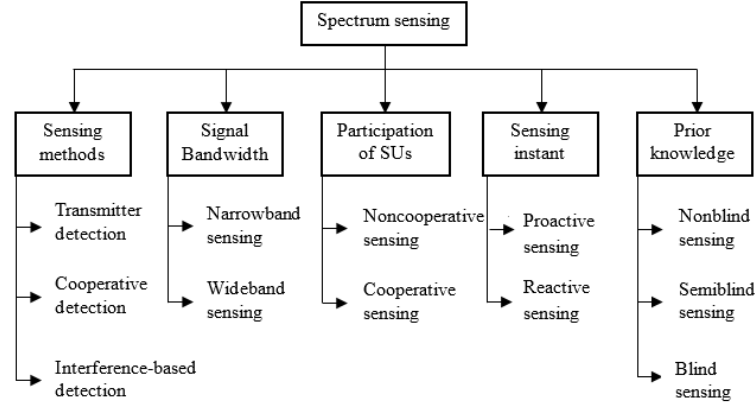
Figure 1.3: Classification of spectrum sensing techniques.

Based on the bandwidth of the spectrum to be detected, the SS technique chooses either the narrowband or wideband sensing. Narrowband SS techniques include matched filtering [20], energy detection [21], feature detection [22], waveform based detection [23], eigenvalue based SS [24], covariance based SS [25], etc. Similarly, the wideband SS techniques include filter-bank based detection [26], wavelet based [27], multi-tapper spectrum estimation [28], compressed SS [29], blind source separation based [30], etc. Also, depending on the requirements of the priori information for detecting the PU, the SS techniques are classified into

- Non-blind SS: It requires some specific parameters about the PU's signal and noise variance for the detection purpose (e.g. matched filtering, waveform based and feature detection method).

- Semi-blind SS: It requires only the noise variance for spectrum detection (e.g. energy detection, filter-bank based detection, wavelet and multi-tapper spectrum estimation method).

- Blind SS: It requires no information regarding the PU system or noise variance for detection purpose (e.g. eigenvalue based, covariance based, compressed SS and blind source separation based method).

The primary focus of the SS is the PU's transmitter detection which is based on the local observations of the SUs. So, the methods of SS are broadly classified into transmitter detection (non-cooperative detection), cooperative detection and interference-based detection [2]. The non-cooperative SS schemes may not provide accurate detection of the PU in an adversarial environmental condition. In the practical wireless environment, due to the presence of multipath fading and shadowing, the PU's signal is heavily attenuated and signal-to-noise ratio (SNR) value decreases. When the received SNR at the SU falls below a certain threshold, the SU can not detect the PU

signal and starts transmitting the data. It will cause severe interference to the primary receiver (PR), if that receiver is present in the SU's transmission range. This is called hidden node problem. Further, single SU can not provide reliable detection probability, and may induce false alarm probability and miss detection probability. These serious outcomings of non-cooperative SS techniques can be overcome by sharing the individual decision with other SUs to obtain the promised sensing performance. This prompts the idea of CSS [31]. The CSS includes the local sensing by the SUs, reporting of their decisions and the information fusion. Specifically, there are two types of channels; sensing channel and the reporting channel. The physical channel between the PU and the SU is called the sensing channel, and the channel between the SU and the fusion center (FC) is called reporting channel. Further, FCC introduced interference temperature for interference measurement. So, that the interference at the receiver side is controlled by the interference temperature limit i.e when the transmission power of the SU exceeds the above limit, it will cause interference to the receiver. Thus, the SUs are allowed to access the spectrum band as long as the transmission power is below the interference temperature limit [32].

Spectrum management

After SS, considering the dynamic behavior of the spectrum, the SUs are capable of selecting the best spectrum band out of the available unused licensed and unlicensed band in order to achieve its promising QoS. The spectrum management function is classified into spectrum analysis and spectrum decision which are related to the upper layers.

- Spectrum analysis: Before selecting the appropriate spectrum band for the specific application, the spectrum bands are analyzed considering the time-varying characteristics, the frequency of operation and the PU activity. Hence, the spectrum analysis is performed on the basis of certain factors such as system capacity, path loss, holding time, delay, interference level, etc.

- Spectrum decision: After the spectrum analysis, the SUs select the suitable band for data transmission achieving the QoS requirements.

Spectrum sharing

The spectrum sharing depends on the coordination between the SUs. The first classification of spectrum sharing is based on the architecture which states that the spectrum sharing is controlled by either the central unit called centralized spectrum sharing or by the individual SU in the distributive manner which is called distributed spectrum sharing. Spectrum sharing technique is also classified on the basis of spectrum allocation i.e cooperative and non-cooperative spectrum sharing. It is obvious that cooperative scheme always outperforms the non-cooperative scheme in

improving the system performance and throughput. Further, spectrum sharing is also classified in terms of spectrum access techniques such as overlay spectrum sharing in which the SUs use the unused portion of the licensed band and vacant that band on the arrival of the PU so as to avoid the unnecessary interference to the PU. In underlay spectrum sharing, the SUs coexist with the PU on the licensed band provided that its transmission power is below the interference temperature limit. Sometimes, in a certain portion of the spectrum the transmission power from the SUs appears as noise to the licensed user.

Spectrum mobility

In order to operate on the best available frequency band, the SUs have the ability to change the frequency of operation which is known as spectrum mobility. Spectrum mobility occurs to support the dynamic characteristic of the licensed band. It leads to the concept of spectrum handoff when the SUs change the operating frequency and accordingly, the protocols in the upper layers modify their operational parameters.

1.1.3 Research challenges in the CRN

Being one of the emerging areas, the CR attracts lots of researchers in different application domains, obtaining with new interesting results. Still, there are some technical challenges, that need to be addressed before successful deployment of CR technology in near future [17, 33]. There are numerous challenges arising due to the operational characteristics to support the real-time environment and the working mechanism of CR in the application domain. Here, some of the important research challenges are described below.

- Decision making:To utilize the spectrum more efficiently, it is always required for the SUs to select the best band. The decision-making process entirely relies on the identification of available vacant bands, strategies to select a suitable band and on the designing of the decision-making algorithm. Though there are lots of optimization algorithms available in the literature, still, it needs further analysis and development of the new algorithm which can give accurate results even in the adversarial real time scenario with less complexity.

- SUs selection:The SUs involved in the sensing process play a vital role in improving the detection performance and spectral efficiency. Usually, the SUs having higher received SNR provide better detection probability. It is a challenging issue to select an optimum number of SUs and eligible SUs for different scenarios such as correlated shadowing, energy consumption, security, and mobility.

- Sensing time and delay: The delay in CSS refers to the sensing delay, reporting delay and data transmission delay. The sensing time delay is the time taken by the SUs for identifying the PU. In the CRN, the CR users must be perfectly synchronized, and their sensing results should be available at the FC instantly. More specifically, the reporting delay is very less as compared to the sensing and transmission delay. Further, longer sensing duration provides better detection probability but leaving a short duration for data transmission. Certainly, this reduces the system throughput. Hence, the sensing time must be chosen so as to maintain a trade-off between the detection performance and system throughput. Transmission delay occurs when the SUs accurately detect the PU or false alarm occurs. False alarm probability deprives the SUs from accessing the band, hence leads to delay in data transmission.

- Power allocation: Transmission power allocation to the SUs is one of the precious resources which maximizes the system throughput preventing the primary network from interference. Usually, the CR devices are low powered battery devices. During the data transmission, there may be chances of sudden increase of the transmission power that crosses the interference limit of the PU. So, proper power allocation algorithms should be developed which increase system throughput providing sufficient protection to the legitimate users from any harmful interference.

- Security issues:The special characteristics of the CRN provide unique opportunities to the attackers. The attackers introduce a new suite of threats targeting to damage the entire normal activities of the communication networks [34]. Besides this, the CR management experiences different kinds of anomalous behavior from the other Access points (APs) [35] such as misbehaving AP, selfish AP, cheat AP and Malicious AP. The physical layer is the lowest layer of the protocol stack and provides an interface to the communication medium. In the CR technology, the SUs are considered to be aware of any changes in the surroundings, adapt the physical layer parameters and access the spectrum dynamically, which makes the operation more challenging. Primary user emulation attack (PUEA) is one of the serious attacks in the physical layer where the malicious user (MU) mimics the PU's signal characteristics and sends the similar type signal, thereby causing the SUs to erroneously identify the attacker as the PU [36].Thus, it reduces the efficient utilization of the spectral resources.

1.1.4   Application domains of CR

The characteristics of CR increase the interest of researchers to use its functionality and capability in multidisciplinary applications such as vehicular network, smart grid, healthcare, military, satellite communication, etc.

Vehicular ad hoc networks (VANETs) have been introduced as an emerging technology to improve the road safety by enabling certain applications such as collision warning, traffic information and monitoring [37, 38]. IEEE 802.11p standard allows vehicular communication to use only 75 MHz of spectrum in 5.9 GHz band (5.850 - 5.925 GHz), which is dedicated for short-range communications (DSRC). But the spectrum gets congested during the busy traffic hour. The vehicular network deployment in the TV white space using the CR technology can solve this problem. The CR-enabled vehicles can improve the spectral efficiency by utilizing the available bandwidth for VANET. The smart grid requires integration of high-speed, reliable and secure data information into it. However, due to the adversarial environmental condition, the sharing of information among the multiple networks gets affected due to interference and collision in the information, noise, etc [39]. Hence, CR application in the smart grid allows the smart devices to identify the unutilized spectrum and utilize them under interference constraint. Wireless body area network (WBAN) which enables continuous monitoring of the patient through integration of wireless sensors worn by the patient. But simultaneously it allows new challenges in the operating wireless channel environment. Hence, CR is introduced in WBAN to improve the QoS by reducing interference between the medical devices [40]. In the military application, when an adversary sends a jamming signal to block the communication link, the CR sensor node has the ability to detect and switch over to a different frequency band [41]. Even in the satellite communication, to utilize the terrestrial and satellite spectrum efficiently, CR can be employed [42].

1.2   Literature Survey

The extensive growth of wireless communication devices offers an escalation to the spectrum scarcity issues in the radio spectrum. Both spectrum scarcity issues and underutilization of spectrum led the FCC to develop CR which allows the unlicensed users to access the licensed band in an opportunistic manner. Before the CR deployment, the spectrum occupancy measurement is necessary to predict the PU activity on the different licensed bands allocated for several services. An effective quantitative measurement is essential to provide a detailed structure of the current spectrum usage and to identify the suitable and potential candidate bands for future CR access. To do this, various measurement campaigns were conducted worldwide in

different locations such as US, Europe, New Zealand, South Africa, China, Singapore, Vietnam etc. covering the wide frequency range in order to find out the suitable bands for the secondary usage in the context of CR. Most of the observations were conducted in the US and hence assess the American spectrum regulations and monitoring. National Telecommunications and Information Administration (NTIA) has performed first larger spectrum occupancy measurement [43]. The occupancy statistics vary with the location, time, space and the band of operation. Moreover, the spectrum usage in the nearby country also affects the occupancy statistics [44]. The research activities involve survey on TV band, cellular band, UHF band, and many more assigned to different services. Based on the derived solutions from these studies conducted in diverse locations and scenarios, CR should undertake the various possibilities and challenges in technological aspects.

The continuous measurement system enables the CR device to scan multiple bands with sufficient sensitivity and efficiency by rotating or switching the antenna. Again, the CR device can not perform both transmission or reception and sensing operation simultaneously. Additionally, efficiency in the CRN can be maximized by minimizing the energy consumption during sensing and data transmission. So, it is desirable to develop an optimized SS model to minimize both time and energy consumption ensuring maximum throughput. SS is the backbone of the CR technology. Accurate identification of the PU is the primary concern and one of the most challenging problems in the CRN. In real time environment, the detection performance may degrade due to the dynamic behavior of the channel that occurs due to fading, mobility of the SU or the PU, shadowing, the presence of other MUs, etc. Lee et al. acquired the time diversity gain by combining the time domain sensing results obtained from a single user at different instants to improve the detection performance in the presence of fading. The time-domain combing SS algorithm was based on Bayesian method and Neyman-Pearson theorem [45]. In the CRN, the SS algorithm needs to be designed to provide proper utilization of the available spectrum providing sufficient protection to the PU. Hence, false alarm probability and miss detection probability should be equally balanced which is not possible in the conventional single threshold-based SS. So, in [46], an interference-aware SS method was proposed in which the probability of identifying the spectrum hole was maximized considering the missed detection and probability of interference to the PU. Besides the channel impairments, the presence of other malicious SUs may obstruct the naive SUs from obtaining the accurate sensing results. In order to nullify the harmful effect and to improve the detection performance Li et al. evaluated the trust value by considering the spatial and temporal correlation among the received information [47]. But, when the PU is small-scale mobile user such as the wireless microphone, a novel framework called Sequential mOnte carLo

combined with shadow-faDing estimation (SOLID) was proposed to accurately track the PU by discarding the false sensing reports from the malicious users [48]. When the SUs are the mobile SUs, the detection performance metrics were evaluated by considering different parameters such as velocities, locations of the SUs and distances of the SUs from the PU [49, 50].

As most of the detection techniques are based on the energy detection method, selecting the decision threshold is an important aspect in measuring the spectrum occupancy. Selecting the high threshold leads to underestimation of the actual spectrum occupancy and may cause interference to the PU. Similarly, selecting the low threshold leads to overestimation of the actual spectrum occupancy, and results in high false alarm probability. Further, in the conventional single threshold based detection technique, missed detection decreases with increase of the false alarm probability. Hence, several methods have been proposed to find the optimum threshold. Either, the detection schemes used two or more thresholds to compare the energy values of the SUs [51] or the threshold was optimized to minimize the sensing error [52]. In double threshold-based detection, the two thresholds control the false alarm and missed detection. The decision is made when the energy value falls either side of the two thresholds. However, if the energy value lies in between the two thresholds called the confusion area, either the SUs do not send any information [53], or send their energy values to the central unit [54] or they perform more sensing rounds until they reach to any final decision [55].

While conducting the spectrum occupancy measurement in different bands in diverse locations worldwide by the research campaigns, selecting the appropriate threshold is one of the major issues. This can be evaluated considering different parameters such as the average noise floor [56] or the minimum value of signal level [57] or the false alarm probability [58].

In CSS, although the participation of the more SUs offer reliable detection performance, but it may lead to more energy consumption and sensing overhead. So, an optimum number of SUs and suitable SUs need to be chosen to make a balance between the detection performance and energy consumption. It is always desirable to choose the SUs with high detection performance. In [59], the authors proposed three types of methods such as simple counting, partial-agreement counting, and collision detection to select the SUs with the best detection performance. In order to reduce the sensing overhead and energy consumption, Godarzi et al. proposed Secant method to obtain the optimum number of SUs for improving the detection performance under false alarm constraint [60]. The effective number of SUs were obtained to improve both throughput and sensing performance [61]. In [62], energy based sensor selection algorithm was proposed to select appropriate SUs that balanced the energy

consumption among the sensors, so that each sensor could participate in CSS for long time. To maintain the trade-off between the sensing performance and energy efficiency (EE), Zahmati et al. proposed an energy-aware SUs selection algorithm to obtain suitable SUs providing better detection probability with minimum false alarm probability, and the eligible SUs were chosen based on the local sensing results, global decision and the energy consumption [63]. In the practical environment, the cooperation between the SUs cannot be guaranteed always because of the obstruction in the propagation path between the transmitter and receiver. This is called shadowing which tends to produce a weak and correlated signal, hence reduces the diversity gain. Further, as the number of users increases, there is a chance of more users present in the vicinity of the same obstruction. As a result, those users suffer from similar levels of fading and their SS results are similar. Hence, the detection probability can be improved significantly by exclusion of spatially correlated SUs and inclusion of selected SUs [64]. In order to select less spatial correlated SUs Ren et al. applied adaptive genetic algorithm under the constraints of false and miss detection probability in correlated log-normal shadowing environment [65].

The CR devices are low powered battery-driven terminal.Further, the SUs can access the licensed band as long as the interference to the PU remain below a certain threshold. Hence, power allocation to the SUs is one of the important aspects in the CRN to maximize EE while providing sufficient protection to the PU. So, the main objective must be either to maximize EE or to minimize the energy consumption. In [66], EE was maximized by jointly optimizing the sensing time and power allocation under the constraints of interference to the PU, minimum achievable data rate and the target detection probability. The EE maximization problem was formulated by using the fractional programming based on Dinkelbach method. The optimal sensing time was obtained by exhaustive search method for maximum EE. In OFDM-based CR system, EE was maximized by optimizing the power allocation under the constraints of interference to the PU, maximum transmission power and minimum achievable data rate [67]. The energy-efficient power allocation per sub-carrier was obtained by original water filling factors aided search (WFAC) method. Additionally, the authors proposed simplified-WFAC method which had much lower complexity than original WFAC. In [68], EE optimization problem was expressed by Energy per Goodbit (EPG) combined with soft sensing information. Power assignment with interference constraint was solved by channel inversion policy, and maximization of EE with power allocation problem was solved by applying Lagrangian duality theorem. In the TV band, EE was maximized with sub-channel assignment and power allocation under the constraints of interference to the PU, maximum transmission power and minimum achievable data rate. The EE

maximization problem was transferred to concave programming problem by using Charnes-Cooper transformation method. Then Karush-Kuhn-Tucker (KKT) condition was applied to obtain the optimal power allocation [69]. The aid of bisection search method with the Lagrangian dual decomposition method was used to obtain the power allocation for maximizing EE [70]. In [71], the authors proposed an efficient process associated with the Bisection search method to optimize the SUs for maximizing the system throughput, minimizing the energy consumption and maximizing the EE. In the cooperative CRNs, when the SUs act as relay, maximization of EE was obtained by jointly optimizing the power and SUs relay set under the constraints of interference to the PU and minimum achievable data rate [72]. There, a Greedy spectrum sharing algorithm was proposed to jointly optimize the power allocation to the relay and also the best set of relays. When the SUs were the small cells and the PUs were the macro-cells, the EE maximization problem was formulated by convex parametric approach in [73]. Two types of algorithms based on Newton method and minorization-maximization principle with Newton method were proposed for orthogonal and non-orthogonal secondary transmission, respectively. In [74], the energy consumption was minimized by optimizing the sensing time and power allocation under the constraints of maximum average interference and transmit power. The optimization problem was formulated by using the fractional programming, and the sensing time was obtained by performing the exhaustive search for minimizing the average energy consumption. The EE in the CRN can also be maximized by minimizing the energy consumption. The joint optimization of threshold and number of sensor nodes helped in minimizing the energy consumption in [75] where the power allocation was obtained by using the bisection search method. The aid of convex optimization algorithm with an efficient iterative method was used to obtain suitable range of threshold using maximum probability of detection algorithm (MPDA), and in addition, modified energy-efficient sensor selection (MEESS) was proposed to obtain the sensing nodes. In [76], the total energy consumption was minimized by optimizing the amplifying gain and relay power allocation under the constraints of interference to the PU, minimum achievable throughput, detection and false alarm probability.

Hence, an energy-efficient CRN design with reliable spectrum detection depends on various parameters which need perfect optimization and evaluation.

1.3 Research Motivation

From the above discussion, it is apparently studied that the system parameters are directly influencing the designing of the energy-efficient CRN with balanced sensing performance. The sensing time and the selection of SUs are the two common

parameters which influence the detection performance and EE. Further, EE depends on the system throughput and the total power consumption.

Most of the existing SU's selection method are based on the estimation of the number of SUs that improve the detection probability. Apart from the number of SUs, the eligible SUs have also equal importance in improving the system performance. The SUs suitable for SS may not be effective for data transmission with least interference to the PU. Hence, proper selection of the SUs imparts similar performance towards the detection performance and system throughput.

Another parameter related to both SS performance and throughput is the sensing time. The longer sensing time gives accurate sensing result leaving very short duration for data transmission. Similarly, longer transmission period may not be reliable in giving proper knowledge about the PU due to the shorter sensing duration. Based on these arguments, it is necessary to incorporate the sensing time optimization for enhancing the system throughput while achieving the good detection performance. Therefore, it is required to include sensing time in designing of the energy-efficient CRN model.

Another important aspect is power allocation to the SUs so that the interference to the PU is kept under a certain limit as well as all the SUs achieve their minimum throughput intending for EE maximization. When the SUs are present at different distances from the PU, traditional same power allocation technique either leads to more transmission outage or the PU is affected by nearby secondary transmission. Hence, distance dependent power allocation policy needs to be adopted for designing an interference-aware energy-efficient CRN.

The PUE attacker always tends to prevent the secondary transmission by transmitting a similar signal that of the PU. Though, the SUs are intelligent enough to detect the attacker and start transmitting their data, but superimposition of the attacker's signal tends to reduce the signal-to-interference-plus-noise ratio (SINR), thereby decreasing the throughput. The SUs need to transmit with more power to achieve the minimum throughput in the presence of the attacker than without the attacker. In this scenario, the restriction in the transmission power regrowth needs to be imposed to protect the PU. This concept motivates us to design suitable power allocation algorithms that improve EE while giving adequate protection to the PU by controlling the transmission power of SUs.

Due to the exponential rise of consumer market for emerging vehicular applications and services, the deployment of CR enabled VANET is envisioned for efficient spectrum management and also for enhancing the communication efficiency in the dynamic vehicular environment. Application of CR in VANET provides

additional spectrum opportunities in TV bands. In CR-VANET, the channel characteristics between the SU and the PU vary due to the motion of the vehicles resulting spatial correlation between the local decisions of the vehicular SUs (VSUs) in cooperative scenario. The data transmission period is longer than the sensing period and the distance of the vehicle continuously changes with the time. Hence, fixed power allocation to the VSUs over the transmission period may increase the VSU's outage which introduces interference to the PU. Considering the time-varying channel gains in vehicular framework, appropriate dynamic power allocation to the vehicular CRs is an open research issue.

Most of the existing work on energy-efficient power allocation considered the hard decision fusion (HDF)- based SS and focused only on the optimization of the power allocation. The appearance of the PU during the data transmission period was not taken into consideration. Hence, an extensive study and development of interference-aware resource allocation algorithms in soft decision fusion (SDF)-based CSS satisfying required constraint is necessary. Further, the idea of CR deployment in the unlicensed band like industrial, scientific and medical (ISM) band need to be explored and development of adaptive power allocation algorithm are required so that other coexisting devices remain unaffected during the CR operation.

1.4   Research Contributions

The main objective of this research is to propose intelligent approaches for energy-efficient resource allocation in the CRN. SDF-based SS framework is chosen for implementation of our proposed schemes. The key contributions of this thesis are summarized below and are also concisely illustrated in Figure 1.4.

- The energy-efficient SDF-based CRN is designed for both the single and double threshold-based detection schemes satisfying the constraints of interference power to the PR, minimum achievable throughput, maximum transmission power and secondary outage probability. The total interference on the PR is derived analytically considering the exponential transition probability of the PU. The solution approaches towards the EE maximization problem start with the suitable SUs' selection algorithm to decide minimum number of SUs to achieve minimum sensing rounds in double threshold-based detection scheme. This is substantiated by selecting eligible SUs for both SS and data transmission. An iterative Dinkelbach method (IDM) algorithm is proposed to jointly optimize the sensing time and power allocation to the SUs. Accurate power assignment to the SUs is achieved through the proposed exact power allocation (EPA) algorithm. The efficacy of the proposed algorithms is verified by comparing with the

existing algorithms.

- The energy-efficient CRN system model is proposed for both single and double threshold-based detection schemes considering the presence of the PUE attacker. Mathematical expressions for the performance metrics are derived in the presence of the attacker. The negative impact of the attacker on the secondary transmission is analyzed and is considered as constraint in the formulation of the EE maximization problem. The detection performance and the system throughput are improvised by the proposed suitable SUs selection algorithm for SS and data transmission based on their channel gains. A novel iterative resource allocation (NIRA) algorithm is propsed to jointly optimize the sensing time and power allocation to the SUs. Dual decomposition and Difference of convex (DC) programming methods are applied to solve the non-convex constraints. A novel adaptive resource allocation (NARA) scheme is proposed based on Normalized least mean square (NLMS) algorithm to reduce the complexity and to improve the EE further.

- The energy-efficient SDF-based CR-VANET system model is proposed for a typical vehicular network scenario in the absence and presence of the PUE attacker. The spatial correlation between the local decisions of the vehicular SUs (VSUs) is considered as the weight coefficient while deriving the performance metrics. The EE maximization problem is formulated under the constraints of interference to the PR, minimum achievable throughput and maximum transmission power. In the presence of the attacker, an extra constraint is added to the optimization problem to control the excessive increase of the secondary transmission power. Two adaptive power allocation schemes based on NLMS and genetic algorithm (GA) are proposed to maximize EE considering the non-convex and time varying channel responses in the absence and presence of the attacker, respectively. The efficacy of our proposed intelligent resource allocation techniques is verified over different CR network parameters.

- For implementation of CR technology considering underlay spectrum sharing mechanism with the co-existing devices in the unlicensed band, an attempt is made in this research work to collect real time data through a practical measurement campaign using standard measurement setup. The spectrum occupancy is evaluated in the frequency range 2.4-2.5 GHz ISM band. A spectrum prediction algorithm based on functional link artificial neural network (FLANN) is proposed to forecast the future spectrum usage profile from the history of occupancy statistics. Using the proposed double threshold-based suitable band selection scheme with proper power allocation to the CR users

(CRUs), throughput is maximized by avoiding interference to the co-existing electronic devices operating in this band. The performance of the proposed approach is validated using the measurement data and their efficacies are verified.

1.5 Thesis Outline

This chapter provided a brief introduction to CR, its working principle and research challenges. Our research motivations and contributions are also discussed. The remainder of the thesis is structured as follows. In Chapter 2, different SS techniques are presented. The performances of both HDF and SDF-based CSS schemes are illustrated through the simulation results. In Chapter 3, the SDF-based model is introduced which is considered as the principal framework for the system model design in the next chapters. The EE maximization problem formulation both in the single and double threshold-based detection schemes under different constraints by optimizing both the sensing time and power allocation with selecting suitable number and eligible SUs are analyzed. Further, the concept of interference-aware power allocation in the adverse domain is explored and a novel energy-efficient CRN for both single and double threshold-based schemes considering the presence of PUEA is presented in Chapter 4. Along with the power optimization, EE maximization problem is solved by considering the eligible SUs and sensing time providing better sensing performance and system throughput. In Chapter 5, intelligent resource allocation techniques in the CR-VANET are introduced considering the absence and presence of the PUEA. Instead of allocating fixed power to all the vehicular SUs (VSUs), adaptive power assignment schemes are provided considering the time-varying behavior of the channel due to the velocity of the vehicle. Chapter 6 discusses the application of CR technology in the ISM band in the frequency range 2.4-2.5 GHz. The effect of threshold selection on the spectrum occupancy is examined taking the real-time data collected through practical indoor measurement campaign. A future occupancy prediction algorithm based on FLANN is proposed. A power allocation algorithm is provided in double threshold-based spectrum occupancy measurement to enhance the probability of spectrum utilization with adequately protecting the coexisting devices . Finally, in Chapter7, the thesis is concluded summarizing the major outcome, and some scopes towards future work.
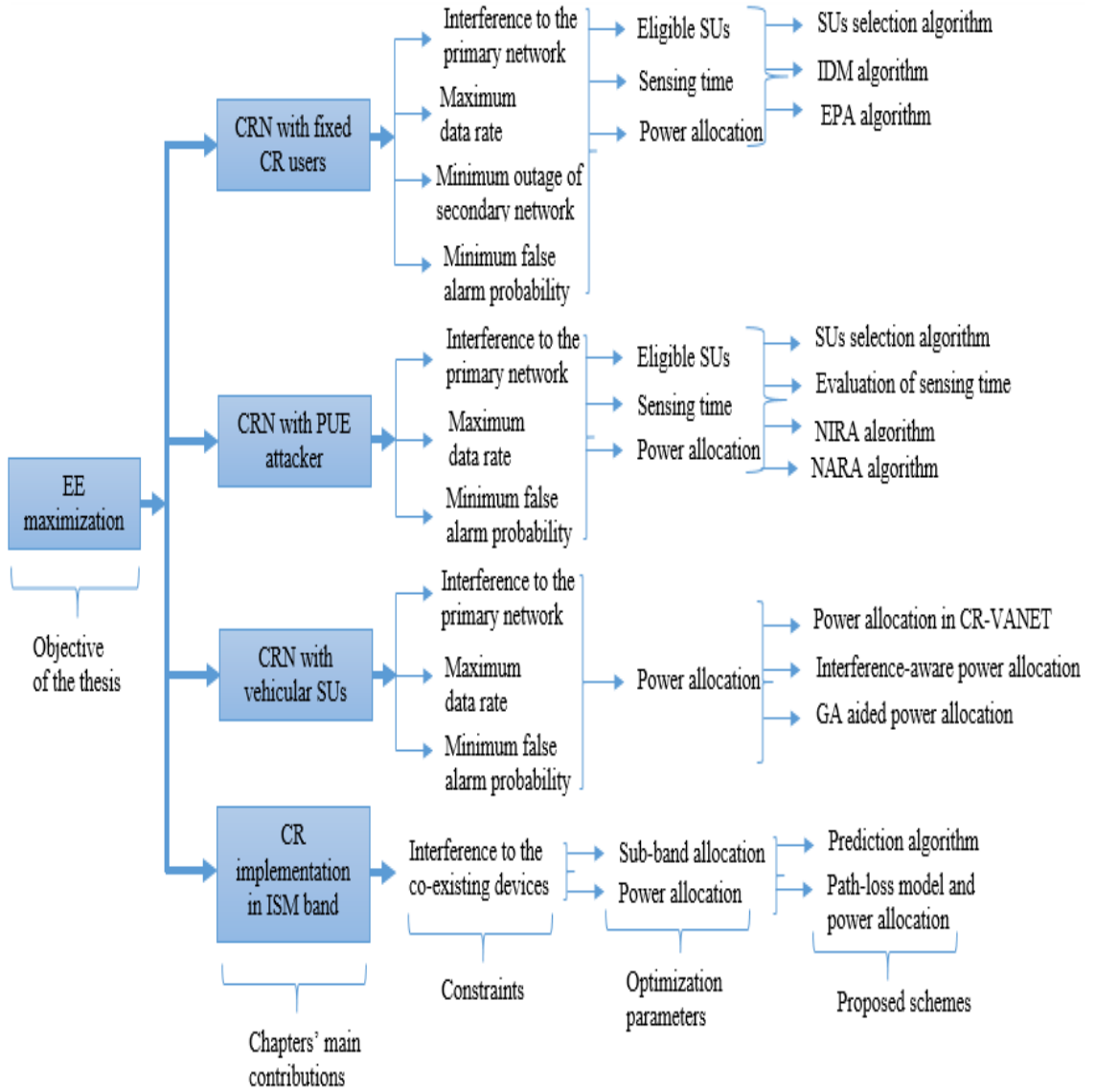
Figure 1.4: Illustration of Research contributions.

Chapter 2

Overview of Spectrum Sensing Techniques in the Cognitive Radio Network

This chapter discusses the conventional SS techniques with the detailed analysis of the decision fusion schemes. The highlights of the chapter are

- The conventional SS techniques are discussed in detail with their pros and cons.

- The probability of detection and false alarm are derived for both HDF and SDF-based SS tecniques.

2.1 Introduction

SPECTRUM sensing is the primary task in the CRN for effective utilization of the spectrum band. It enables the capability of CR to find the best underutilized licensed band. In the real-time wireless environment, availability of the spectrum varies with the time of performing SS, operating frequency and the location of measurement. The SUs are allowed to access the available licensed band in an opportunistic manner. Even in the harsh environmental condition, the SUs have the capability to frequently identify the idle spectrum for making the spectrum handoff without restraining the continuous data transmission. Additionally, while using the licensed band, the SUs have to periodically perform SS to know about the sudden appearance of the PU. If it happens, the SUs need to vacate the band quickly or reduce their transmission power level, so that the interference power level to the PU is maintained below a certain threshold. This is the most important feature of the SS which ensures the effective utilization of the available spectrum band while providing sufficient protection to the PU. Some recent studies on SS are discussed in [77, 78].

The rest of the chapter is organized as follows. Section 2.2 presents the hypothesis testing principal used in SS techniques. Different conventional PU detection techniques are discussed in Section 2.3. CSS with detail analysis of the different fusion schemes is provided in Section 2.4. The system performance analyses of the most commonly used fusion schemes are given in Section 2.5. Finally, Section 2.6 provides a brief summary of the chapter.

2.2 Hypothesis Testing

Hypothesis testing is the principal task in the SS techniques. It is used to identify the availbility of the PU in the licensed band. Most commonly used hypothesis testing is binary hypothesis testing. For example, if $s(n)$ represents the PU's transmitted signal at nth instant, then the SS problem is formulated by two hypothesis tests which are defined as [16]

$$x(n) = \begin{cases} \eta(n), & (H_0) \\ s(n) h_{ps} + \eta(n), & (H_1) \quad n = \{1, 2, ..., N\} \end{cases} \quad (2.1)$$

where $x(n)$ represents the received signal at the SU and N is the number of samples. h_{ps} is the propagation channel coefficient between the PU and the SU. The two hypotheses H_0 and H_1 correspond to the absence and presence of the PU, respectively. The null hypothesis H_0 represents idle state of the licensed band and only noise is received at the SU. Similarly, the hypothesis H_1 represents the busy state of the licensed band and the SU receives the PU's signal along with the noise. $\eta(n)$ is the additive white Gaussian

noise with mean zero and variance $\sigma_\eta{}^2$. It is not only important for the SU to decide the idle or busy state of the spectrum but also to identify whether the signal is from the PU or from other sources under the hypothesis H_1. Hence, the performance metrics of the CRN are measured by probability of detection P_d and proability of false alarm P_f. P_d is defined as the probability of correctly identifying the PU's signal in the sensing band and is expressed as

$$P_d = P_r\left(\hat{H}_1 | H_1\right) \tag{2.2}$$

where $\hat{H}_1$ denotes the decision made by the SU i.e., the PU's signal is detected. Similarly, P_f is defined as the probability of falsely identifying the vacant band to be occupied by the PU. In terms of hypothesis, it is expressed as

$$P_f = P_r\left(\hat{H}_1 | H_0\right) \tag{2.3}$$

Similar to the (2.2), $\hat{H}_1$ is the decision made by the SU about the PU's presence. More often the performance metric is characterized by the parameter called miss detection probability P_{md} which is just the complement of P_d. So, P_{md} is the probability of identifying the occupied band to be vacant which can be expressed as

$$P_{md} = 1 - P_d = P_r\left(\hat{H}_0 | H_1\right) \tag{2.4}$$

where $\hat{H}_0$ denotes the decision of the SU about the absence of the PU. Hence, the key challenge of the spectrum detection is to keep both P_f and P_{md} under certain threshold. High value of P_f leads to inefficient utilization of the available spectrum band by preventing the SUs from accessing that vacant band and high P_{md} results interference to the legitimate user. So, the total probability of sensing error P_e i.e. the probability of making wrong decision about the PU's status on the licensed band is the weighted sum of P_f and P_{md}. In general, it is expressed as

$$P_e = P_{H0}P_f + P_{H1}P_{md} \tag{2.5}$$

where P_{H0} and P_{H1} represent the probabilities of PU's absence and presence, respectively. So, both P_f and P_{md} can be decreased by minimizing P_e,.

The other two commonly known hypothesis testings are the Neyman-Pearson (N-P) test [79, 80] and the Bayes test [16, 81]. The N-P test maximizes P_d keeping P_f under the constraint. Following (2.1), the N-P detector is equivalent to the likelihood ratio test (LRT) which is given by

$$\Lambda_{LRT} = \prod_{n=1}^{N} \frac{P_r\left(x(n) | H_1\right)}{P_r\left(x(n) | H_0\right)} \overset{H_1}{\underset{H_0}{\gtrless}} \lambda_{LRT} \tag{2.6}$$

where Λ_{LRT} and λ_{LRT} denote the test statistic and the decision threshold, respectively.

The Bayes test can be represented as

$$\prod_{n=1}^{N} \frac{P_r\left(x\left(n\right)|H_1\right)}{P_r\left(x\left(n\right)|H_0\right)} \underset{H_0}{\overset{H_1}{\underset{<}{>}}} \frac{P_{H0}\left(C_{1,0}-C_{0,0}\right)}{P_{H1}\left(C_{0,1}-C_{1,1}\right)} = \lambda_B \qquad (2.7)$$

where λ_B is the decision threshold. $C_{i,j}$ is known as the cost which represents the decision of hypothesis H_i when H_j actually occurs, $(i,j \in \{0,1\})$. However, when distributions of the received signal under hypothesis H_0 and H_1 consist of the unknown parameters, then the hypothesis testing is known as composite hypothesis testing. Generalized likelihood ratio test (GLRT) is one of the approaches to solve this hypothesis testing problem where the unknown parameters are determined by the maximum likelihood estimates (MLE) [18]. The GLRT is expressed as

$$\prod_{n=1}^{N} \frac{\max\limits_{\emptyset_1} P_r\left(x\left(n\right)|\emptyset_1,H_1\right)}{\max\limits_{\emptyset_0} P_r\left(x\left(n\right)|\emptyset_0,H_0\right)} \underset{H_0}{\overset{H_1}{\underset{<}{>}}} \lambda_{GLRT} \qquad (2.8)$$

where $\emptyset_1$ and $\emptyset_0$ are the unknown parameters and λ_{GLRT} is the decision threshold.

2.3 Spectrum Sensing Techniques

In this section, we discuss some of the commonly used SS techniques. Each SU can use one of these techniques to find out the PU's activity. If the PU is absent, then the band is declared as the vacant band. SS techiques are the most important priliminary methods for making accurate decision about the spectrum occupancy.

2.3.1 Matched filter detection

Matched filter (MF) is an optimum detector which maximizes the received SNR, provided that some information about the PU's signal such as operating frequency, signal bandwidth, modulation type, pulse shaping, etc, are known a priori to the receiver [82]. The output of the MF is compared with the decision threshold to detect the presence or absence of the PU on the licensed band [20]. If Y and λ represent the output and the decision threshold, respectively, then P_d and P_f are given by

$$P_d = P_r\left(Y \geq \lambda | H_1\right) \qquad (2.9)$$

and

$$P_f = P_r\left(Y \geq \lambda | H_0\right), \qquad (2.10)$$

respectively. This detection scheme requires less time to provide the sensing result, as only $O\left(1/SNR\right)$ samples are required [82]. Besides having some of the benefits, it has

also lots of limitations. The advantages and disadvantages of the matched filtering are discussed below.

Advantages

- Coherent detection.

- Fast sensing.

- Less number of samples are required.

Disadvantages

- Requires a priori information about the PU's signal characteristics.

- Needs proper synchronization.

- Highly computational complex.

- Large power consumption.

- Needs dedicated receiver.

- Impractical to implement.

2.3.2 Energy detection

It is a non-coherent and semi-blind detection technique, in which the energy of the received PU's signal is compared with the threshold to obtain the information about the spectrum occupancy. Hence, accurate detection depends on the selection of appropriate threshold i.e. depends on the noise floor [21]. This detection process requires $O\left(1/_{SNR^2}\right)$ samples to provide SS decision [82]. However, the detection performance degrades under noise uncertainty and SNR wall [83]. Advantages and disadvantages of the energy detector (ED) are discussed below.

Advantages

- Easy implementation and low complexity.

- No priori information about the PU's signal.

- Optimal for independent identically distributed (i.i.d) PU signal.

Disadvantages

- Highly susceptible to noise uncertainty.

- Unable to differentiate the PU signal and the signal from the other sources.

- Can not detect spread spectrum signal.

- Poor performance in low SNR condition.

- Longer sensing time than MF.

2.3.3 Cyclostationary feature detection

The feature based detection method is based on extracting the specific features of the PU signal such as cyclic prefix, pilot signals, modulation types or spreading codes. These factors induce periodicity in the modulated signal. The cyclostationary characteristic of the PU signal shows the repetition of the mean and correlation after regular time interval. This introduces cyclic correlation between the widely separated frequency components of the modulated signal. This feature is ideal in differentiating the noise from the modulated signal [82]. It is more robust to the noise uncertainty. Besides its advantages, it has also some limitations which are discussed below.

Advantages

- Robustness to noise uncertainty.

- Better performance under low SNR condition.

- Ability to distinguish between the PU's signal and the signal from other sources.

- Synchronization is not required.

Disadvantages

- Requires a priori information about the cyclic features of the PU's signal.

- Longer sensing time.

- Computationally complex.

2.3.4 Waveform-based detection

Generally, a known pattern of the sequence is required for synchronization in the wireless system. These patterns include regularly transmitted pilot patterns, preambles, spreading sequences, etc. If the PU's transmitted signal pattern is known a priori, then waveform-based SS is performed by correlating the received signal at the SU with its own copy [23]. The pros and cons of this detection technique are

Advantages

- Faster sensing time than energy detection.

- Lesser complex than MF.

- Less susceptible to noise uncertainty.

Disadvantages

- Requires a priori information about the PU's signal pattern.

- Needs proper synchronization.

2.3.5 Covariance-based detection

The detection scheme is based on the spatial correlation characteristics of the PU's signal resulted due to the dynamically dispersive wireless channel [25]. The main advantage is that it does not require any information about the PU signal, channel or noise power. Different benefits and limitations of this SS technique are

Advantages

- Good for highly spatially-correlated signal.

- Blind (does not require any prior information).

- Low computational complexity.

Disadvantages

- Not suitable for uncorrelated PU's signal.

Comparing these conventional SS techniques, ED is found to be less complex and easier to implement. Hence, it is the most commonly used SS technique in the CRN. So, in this thesis, we prefer to use ED technique at each SU for performing SS. The SUs are able to find their local statistics without requiring any information about the PU's signal.

2.4 Cooperative Spectrum Sensing

Although the non-cooperative SS techniques have the advantages of avoiding sensing overhead, low computational complexity and easy implementation, still there are lots of shortcomings. The single SU may fail to make a correct decision regarding the PU's presence due to the multipath fading and shadowing [84]. Even, instead of residing within the PU's transmission range, it can not detect the actual state of the PU. This

problem leads to the concept of CSS, where more SUs cooperatively take the decision regarding the spectrum occupancy. By exploiting the spatial diversity and multiuser diversity, cooperative detection is a solution to combat the adversarial effect of the real time environment. Hence, it helps in increasing the detection performance and decreasing the false alarm probability. The final decision regarding the PU's presence depends on the combined decision of all the SUs. So, participation of more SUs improves the detection performance by lowering the effect of noise uncertainty, fading and shadowing on the wireless environment. However, CSS experiences cooperation overhead which increases delay and energy consumption. Therefore, in CSS the SUs should maintain the trade-off between the detection performance and energy consumption. The cooperative network is implemented in three different ways as shown in Figure 2.1. This shows the different methods of obtaining the global decision by sharing the information among the SUs. The classification of CSS is also discussed in [12, 16, 85].

- Centralized CSS:In centralized CSS, the SUs first perform SS through their sensing channels and then, report their results to the FC through the reporting channels. The central unit called the FC collects all the local information from the SUs, and makes the global decision about the availability of the spectrum band. Then, it either broadcasts the final SS decision to all the SUs or directly controls the CR traffic.

- Distributed CSS:Instead of using the central unit, the SUs share their information among themselves and make their own decision about the availability of spectrum hole. The global decision is made by conversing the information from the SUs. Based on the distributed algorithm, each SU sends its sensing decision to the other SU. The other SU combines the received data with its own sensing decision. Then by using the local criterion, it decides the presence of the PU on the licensed band. If this criterion is not satisfied, the SUs send their combined decisions to the other SUs. This process is repeated until the algorithm is converged or the SUs reach to a final decision.

- Relay assisted CSS:The SUs with strong sensing channels but weak reporting channels forward their information to the FC through the SUs with strong reporting channels but weak sensing channels. The SUs with weak sensing channels act as relays. These relays assist the other SUs to forward their sensing decisions to the FC. Since, the individual decision is forwarded to the FC by multiple hop, hence it is also called multi-hop CSS.
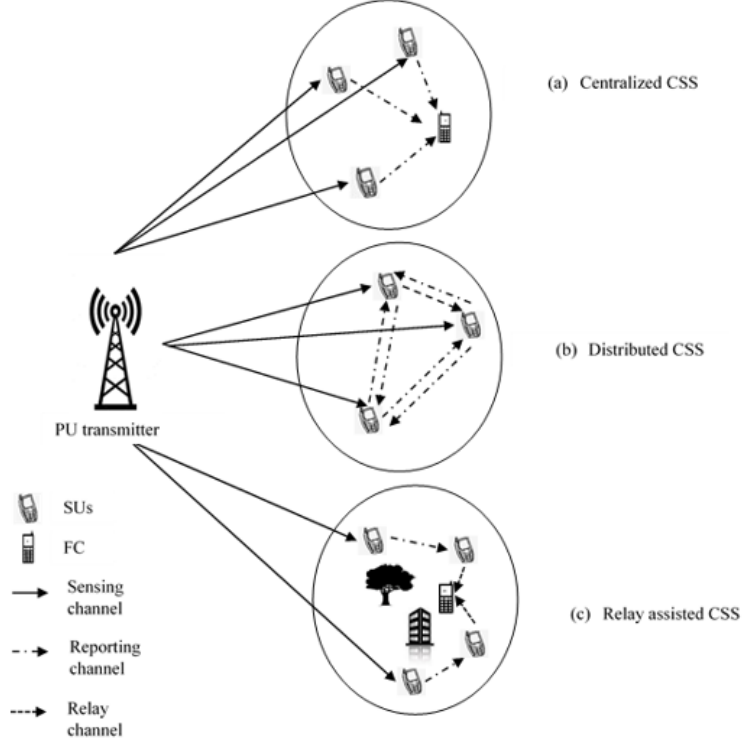
Figure 2.1: Classification of CSS.

2.5   System Model for Cooperative Spectrum Sensing

We consider a system model consisting of M SUs each with single ED. Each SU receives the signal from the PU and sends its local decision to the FC as shown in Figure 2.1. Let $s(n)$ represents the signal from the PU which is i.i.d of zero mean and variance σ_s^2. $x_m(n)$ be the received signal at mth SU at nth instant. Then, the SS is formulated by simply two binary hypothesis tests which are expressed as

$$x_m(n) = \begin{cases} \eta_m(n), & (H_0) \\ s(n)h_{psm} + \eta_m(n), & (H_1) \end{cases} \tag{2.11}$$

where h_{psm} is the channel coefficient between the PU and the mth SU. $\eta_m(n)$ denotes AWGN with mean zero and variance $\sigma_{\eta_m}^2$. N denotes the number of sample which is the product of sensing time τ_s and the sampling frequency f_s. Each SU measures the received power over N number of samples during the sensing interval and makes the local decision as follows

$$Y_m = \frac{1}{N} \sum_{n=0}^{N-1} |x_m(n)|^2 \tag{2.12}$$

According to the central limit theorem, for large value of N the local test statistic is approximately represented as the Gaussian distribution. If PU's signal is a binary phase shift keying (BPSK) signal and noise is real, then Y_m for the two hypotheses H_0 and H_1

is distributed as [86]

$$E\left[Y_m\right] = \begin{cases} \sigma_{\eta m}{}^2, & (H_0) \\ \sigma_{\eta m}{}^2\left(1+\gamma_m\right), & (H_1) \end{cases} \tag{2.13}$$

$$Var\left[Y_m\right] = \begin{cases} \frac{2\sigma_{\eta m}{}^4}{N}, & (H_0) \\ \frac{2\sigma_{\eta m}{}^4}{N}\left(1+2\gamma_m\right), & (H_1) \end{cases} \tag{2.14}$$

where γ_m is the received SNR at the mth SU and is given by $\gamma_m = \frac{\sigma_s{}^2\left|h_{psm}\right|^2}{\left|\sigma_{\eta m}\right|^2}$. If λ is the decision threshold, then, the probability of detection is evaluated by comparing Y_m with the λ. Mathematically, the probability of detection $P_{d,m}$ and false alarm probability $P_{f,m}$ of the mth SU are expressed as

$$P_{d,m} = Q\left(\frac{\lambda - \sigma_{\eta m}{}^2\left(1+\gamma_m\right)}{\sigma_{\eta m}{}^2\sqrt{2\left(1+2\gamma_m\right)}}\sqrt{N}\right) \tag{2.15}$$

and

$$P_{f,m} = Q\left(\frac{\lambda - \sigma_{\eta m}{}^2}{\sigma_{\eta m}{}^2\sqrt{2}}\sqrt{N}\right), \tag{2.16}$$

respectively. The decision threshold λ is calculated from the given value of $P_{f,m}$. Then, the value of $P_{d,m}$ in terms of $P_{f,m}$ is given by

$$P_{d,m} = Q\left(\frac{Q^{-1}\left(P_{f,m}\right)\sqrt{2}\sigma_{\eta m}{}^2 - \sigma_{\eta m}{}^2\gamma_m\sqrt{N}}{\sigma_{\eta m}{}^2\sqrt{2\left(1+2\gamma_m\right)}}\right) \tag{2.17}$$

So, $P_{d,m}$ is the individual decision of the SU. The local decisions are sent to the FC. The FC employs different fusion schemes for obtaining the global decision regarding the presence of the PU.

2.6   Fusion Schemes

In CSS, fusion schemes are the process of combining individual SU's sensing data. There are two types of fusion schemes depending on the local observation sent to the FC. One is HDF scheme in which the SUs send binary information to the FC in terms of "0" and "1" representing the absence and presence of the PU, respectively. Another fusion scheme is known as SDF scheme in which the test statistics of all the SUs are combined at the FC. The HDF-based and SDF-based CSS system models are shown in Figure 2.2 and Figure 2.3, respectively.
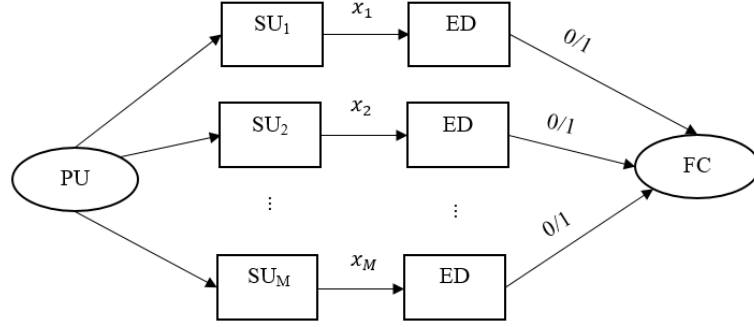
Figure 2.2: HDF-based CSS system model.

2.6.1 Hard decision fusion scheme

In the HDF scheme, each SU sends its binary decision regarding the presence of the PU to the FC. Specifically, the SU sends "1", if $P_r(Y_m \geq \lambda)$, indicating the presence of the PU. Similarly, if $P_r(Y_m < \lambda)$, each SU sends "0" indicating the absence of the PU. The FC employs three types of fundamental fusion rules to obtain the global sensing result. This fusion process reduces the communication overhead. The HDF- based fusion schemes are discussed in [87–89].

- **K-out-of-M rule**: The global decision is "1" if K SUs or more than K SUs out of the total M SUs result "1" where $K \in [1, M]$. Therefore, the FC decides the presence of the PU, if K SUs or more decide the same. Then, the global detection and false alarm probabilities are given by

$$Q_d = \sum_{k=0}^{M-K} \binom{M}{K+k} \left(1 - P_{d,k}\right)^{M-K-k} \left(P_{d,k}\right)^{K+k} \tag{2.18}$$

and

$$Q_f = \sum_{k=0}^{M-K} \binom{M}{K+k} \left(1 - P_{f,k}\right)^{M-K-k} \left(P_{f,k}\right)^{K+k}, \tag{2.19}$$

respectively. $P_{d,k}$ and $P_{f,k}$ represent the detection and false alarm probability of the kth SU, respectively. The special case of this K-out-of-M rule is known as majority voting rule or half voting rule. In this case, final decision at the FC depends on the local decisions obtained from the half or more than half SUs. For this case, $K = \lceil \frac{M}{2} \rceil$, where $\lceil \frac{M}{2} \rceil$ is the smallest integer not less than $\frac{M}{2}$. Substituting this value of K in (2.18) and (2.19), Q_d qnd Q_f are calculated for half voting rule.

- **Logical OR rule**: The global decision is "1" if any one of the SUs decides "1". So, the FC declares H_1, if a single SU reports "1". Substituting $K = 1$ in (2.18)

and (2.19), the Q_d and Q_f are calculated as

$$Q_d = 1 - \prod_{k=1}^{M} \left(1 - P_{d,k}\right) \tag{2.20}$$

and

$$Q_f = 1 - \prod_{k=1}^{M} \left(1 - P_{f,k}\right), \tag{2.21}$$

respectively. Since, the SUs tend to utilize the licensed band during the absence of the PU, possibility of interference to the PU can be minimized by employing logical OR rule at the FC.

- **Logical AND rule**: The global decision is the combination of all the local decisions. If all the SUs go in favor of H_1, then the FC declares H_1. For this scheme, $K = M$. Substituting the value of K in (2.18) and (2.19), Q_d and Q_f are derived as

$$Q_d = \prod_{k=1}^{M} \left(1 - P_{d,k}\right) \tag{2.22}$$

and

$$Q_f = \prod_{k=1}^{M} \left(1 - P_{f,k}\right), \tag{2.23}$$

respectively. As the sensing decision depends on all the SUs, the possibility of interference to the PU is more for logical AND decision fusion scheme.

2.6.2 Soft decision fusion scheme

In the SDF-based scheme, the energy values of the SUs are linearly combined with the corresponding weight coefficients at the FC. So, it is also called linear weight combining scheme. It improves the sensing performance by exploiting the diversity gains of all the cooperative SUs. Hence, the global test statistic Y_G at the FC is given by

$$Y_G = \sum_{m=1}^{M} w_m Y_m \tag{2.24}$$

where w_m is the weight coefficient assigned to mth SU. An external constraint is added to the weight vector $w = [w_1, w_2, \ldots, w_M]^T$ such that $\|w\| = 1$. These weight coefficients need to be optimized to improve the detection performance. For large value of N, Y_G can be approximated using the central limit theorem which is given as follows [86]

$$Y_G \sim \begin{cases} \aleph \left(\sum_{m=1}^{M} w_m \sigma_{\eta m}^2, \frac{2}{N} \sum_{m=1}^{M} w_m^2 \sigma_{\eta m}^4 \right), H_0 \\ \aleph \left(\sum_{m=1}^{M} w_m \sigma_{\eta m}^2 \left(1 + \gamma_m\right), \frac{2}{N} \sum_{m=1}^{M} w_m^2 \sigma_{\eta m}^4 \left(1 + 2\gamma_m\right) \right), H_1 \end{cases} \tag{2.25}$$

Then, global probability of detection Q_d is evaluated by comparing Y_G with the global threshold λ_g. Mathematically, the performance metrics are expressed as follows

$$Q_d = Q\left(\frac{\lambda_g - \sum_{m=1}^{M} \sigma_{\eta m}^2 (1+\gamma_m) w_m}{\sqrt{2\sum_{m=1}^{M} \sigma_{\eta m}^4 w_m^2 (1+2\gamma_m)}} \sqrt{N}\right) \tag{2.26}$$

and

$$Q_f = Q\left(\frac{\lambda_g - \sum_{m=1}^{M} \sigma_{\eta m}^2 w_m}{\sqrt{2\sum_{m=1}^{M} \sigma_{\eta m}^4 w_m^2}} \sqrt{N}\right) \tag{2.27}$$

If λ_g is calculated from the given Q_f, then Q_d is calculated as

$$Q_d = Q\left(\frac{Q^{-1}(Q_f) \sqrt{2\sum_{m=1}^{M} \sigma_{\eta m}^4 w_m^2} - \sum_{m=1}^{M} \sigma_{\eta m}^2 w_m \gamma_m \sqrt{N}}{\sqrt{2\sum_{m=1}^{M} \sigma_{\eta m}^4 w_m^2 (1+2\gamma_m)}}\right) \tag{2.28}$$

So, the detection performance can be improved by optimizing the weight coefficients. However, the weight optimization is further divided into single-objective optimization and multi-objective optimization scheme.
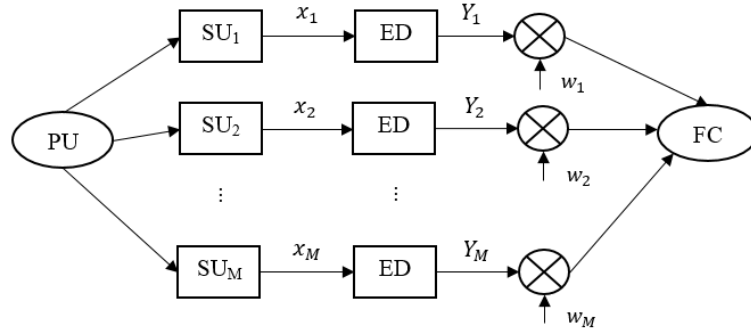
Figure 2.3: SDF-based CSS system model.

Single-objective optimization

Single-objective optimization schemes evaluate the optimal weight vector by maximizing the detection probability. There are several conventional schemes such as equal gain combining (EGC) [90], maximal ratio combining (MRC) [90], modified deflection coefficient (MDC) [91],etc that are proposed in the literature to find the optimal weight coefficients. The optimal weight can also be obtained by using some evolutionary algorithms such as GA, particle swarm optimization (PSO),etc.

- **EGC scheme** [92]: In EGC scheme, same weight is assigned to all the SUs. If M SUs are present in the CRN, then the weight coefficient w_m assigned to mth SU is given by

$$w_m = \sqrt{\frac{1}{M}} \tag{2.29}$$

This scheme is very simple and it does not require any channel state information.

- **MRC scheme** [92]: In the CRN, usually the SUs are distributed randomly and are present at different distances from the PU. Accordingly, their received SNRs vary and they offer different decisions regarding the PU's presence. Generally, the SU with high received SNR gives correct decision about the PU. In the SDF-based fusion scheme, the weight coefficient is linearly combined with the energy value. So, the detection performance can be improved by assigning high weight value to the SU with high received SNR. In this way, performance degradation can be minimized by assigning low value of weight coefficient to the poor SUs. Thus, the MRC-based weight coefficient w_m depends on the received SNR at the mth SU which is given by

$$w_m = \sqrt{\frac{\gamma_m}{\sum_{m=1}^{M} \gamma_m}} \qquad (2.30)$$

- **MDC maximization scheme** [91]: The detection performance is further enhanced by optimizing MDC for obtaining the optimal weight coefficients [91]. MDC is formulated based on variance-normalized distance between the centers of two conditional probability distribution functions (PDFs). It shows the effect of PDF on the detection performance. MDC is defined as

$$d_m{}^2(m) = \frac{[E(Y_G|H_1) - E(Y_G|H_0)]^2}{Var(Y_G|H_1)}$$
$$= \frac{[w^T \psi]^2}{w^T \sum_{H_1} w}. \qquad (2.31)$$

where $\psi = diag(\gamma) diag(\sigma_\eta{}^2)$, $\gamma = [\gamma_1, \gamma_2, \ldots, \gamma_M]^T$ and $\sigma_\eta{}^2 = [\sigma_{\eta 1}{}^2, \sigma_{\eta 2}{}^2, \ldots, \sigma_{\eta M}{}^2]^T$. $\sum_{H_1}$ is the covariance matrix for the hypothesis H_1 which is given by

$$\sum_{H_1} = \frac{2}{N} diag^2(\sigma_\eta{}^2) + \frac{4}{N} diag\left(|h_{ps}|^2\right) diag(\sigma_\eta{}^2) \qquad (2.32)$$

Here, $|h_{ps}|^2 = \left[|h_{ps1}|^2, |h_{ps2}|^2, \ldots, |h_{psM}|^2\right]^T$. The optimal weight vector is found by maximizing $d_m{}^2$ as

$$w_{MDC} = \underset{w}{argmax} \ d_m{}^2(w) \qquad (2.33)$$

By solving (2.33), the weight coefficient w_{MDC} is obtained by

$$w_{MDC} = \sum_{H_1}^{-1} \psi \qquad (2.34)$$

- **Evolutionary algorithms based weight optimization schemes**: In the literature, the authors adopted evolutionary algorithms like GA [93], binary GA [92], PSO [94,95], Population adaptive Gbest-guided artificial bee colony (PA-GABC) [96], etc, for optimizing the weight vector w to improve the detection probability Q_d. In [97], PSO was used to optimize w for minimizing the sensing error.

Multi-objective optimization problem

The single objective optimization techniques maximize the detection probability for the given value of false alarm probability. However, in the conventional SS techniques, these two objectives probability of detection and false alarm probability are conflicting in nature. Increasing the probability of detection increases the false alarm probability. Hence, the system performance can be maximized by simultaneously increasing the detection probability and decreasing the false alarm probability. To overcome the shortcomings of single-objective optimization technique, P.Pradhan et al. proposed multi-objective cat swarm optimization (MOCSO) in [98].

Motivated from the advantages of multi-objective algorithm, we propose multi-objective hybrid invasive weed optimization and particle swarm optimization (MO hybrid IWOPSO) for simultaneously maximizing the detection probability and minimizing the false alarm probability. The interaction between the dispersion property of the IWO algorithm and the updating velocity of PSO are combined to form the hybrid IWOPSO optimization [99]. PSO was developed by Kennedy and Eberhart in 1995 [100], and IWO was proposed by A.R.Mehrabian and C.Lucas in 2006 [101]. PSO is inspired from the flock movement behavior of birds whereas IWO is drawn from the colonization of weeds. The interaction between the dispersion method of the IWO algorithm and the velocity of the PSO controls the balance between local exploitation and global exploration in the search space. So, hybrid IWOPSO algorithm can be implemented as faster convergence and global optimization method. Single objective IWO was extended to nondominated sorting (NSIWO) for solving the optimization problems with two or more conflicting objectives [102]. In multi-objective optimization, instead of getting a single solution, a number of solutions are obtained which are superior to the other solutions. These solutions are called the nondominated fronts or Pareto optimal solution. Nondominated sorting genetic algorithm-II (NSGA-II) and multi-objective particle swarm optimization (MOPSO) were studied in [103] and [104] respectively The integration of PSO with the NSIWO in MO hybrid IWOPSO helps in finding the better nondominated fronts by exploring the search space. The steps for MO hybrid IWOPSO are summarized as follows

Step 1: Randomly initialize the position of each plant over the search space i.e. the position of the pth plant is $X_p = \left[X_{p1}, X_{p2}, \ldots, X_{pM} \right]$.

Step 2: Initialize the velocity of each plant to zero.

Step 3: Evaluate the objective function of each plant. Store the nondominated solutions, and assign the rank and crowding distance to each plant.

Step 4: Compute the weakness of each plant according to its rank and crowding distance using the following formula [102].

$$weakness(p) = rank(p) + \frac{1}{CD(p) + 2} \tag{2.35}$$

where $rank(p)$ and $CD(p)$ are the rank and crowding distance of the pth plant, respectively.

Step 5: In each iteration, binary tournament selection is done to select suitable plants from the current population.

Step 6: Find the maximum and minimum weakness values from the population. The member having minimum weakness value has got its position X_{gbest} and the pth member has its corresponding position X_{pbestp}.

Step 7: Each member generates seeds depending on their corresponding weakness value. The number of seeds varies from maximum seed S_{max} for the minimum weakness member to the minimum seed S_{min} for the maximum weakness member.

Step 8: For each seed calculate the velocity and position as per

$$\begin{aligned} V_p(t+1) = & V_p(t) + C_1 * rand * (X_{pbestp} - X_p(t)) \\ & + C_2 * rand * (X_{gbest} - X_p(t)) \end{aligned} \tag{2.36}$$

$$X_p(t+1) = X_p(t) + V_p(t+1) \tag{2.37}$$

where t is the current iteration and V_p is the velocity of the pth plant. C_1 and C_2 are the cognitive and social coefficient, respectively.

Step 9: Then the seeds are dispread over the problem space by normally distributed random number with zero mean and varying standard deviation. The standard deviation is expressed as

$$\sigma_t = \left(\frac{t_{max} - t}{t_{max}}\right)^\kappa (\sigma_{initial} - \sigma_{final}) + \sigma_{final} \tag{2.38}$$

where t_{max} is the maximum iteration. $\sigma_{initial}$ and σ_{final} are the initial and final standard deviation, respectively. κ is the non-linear modulation index. Then the new position is updated as

$$X_p(t+1) = X_p(t+1) + rand * \sigma_t \tag{2.39}$$

Step 10: When all the seeds find their positions, evaluate the fitness values of all the plants and their seeds. Then, arrange them according to the nondominated sorting, and assign rank and crowding distance to each individual.

Step 11: Compute the weakness of each individual as per (2.35).

Step 12: Finally, the individuals with lower fitness values are eliminated and a new population is formed for next iteration. This process is repeated until the termination condition is satisfied.

While calculating the fitness value, the position of each plant and seed has to satisfy the constraint $\|w\| = 1$. In multi-objective optimization problem, there are a set of nondominated solutions providing almost equal contributions in obtaining the optimized result. Hence, fuzzy decision making is used to find the compromised

solution providing reliability to these two optimized functions (probability of detection and false alarm) [98].

2.7   Simulation Results and Discussion

The system models shown in Figure 2.2 and Figure 2.3 are considered for the analysis of HDF and SDF-based CSS. The number of SUs M is set 10 and the number of samples N is 100. The propagation channels between the PU and the SUs are assumed to be Rayleigh distributed. The average SNR of the PU received at the SUs are $\gamma_1 = \gamma_2 = \ldots = \gamma_M = $-10 dB. We set σ_s^2=1. The Monte Carlo simulation goes through 10,000 iterations.

Figure 2.4 shows probability of detection Q_d vs probability of false alarm P_f comparing the HDF-based fusion schemes. For the half voting rule K=5. It is observed that fusion scheme employing the logical OR rule outperforms the other fusion schemes whereas the logical AND rule performs worst among all the schemes. Hence, it is clear that detection probability is high by considering the positive decision of at least a single SU regarding the PU's presence. Figure 2.5 shows Q_d vs Q_f comparing the conventional SDF-based fusion schemes. It is observed that both EGC and MRC schemes show similar performance for the given parameters. The MDC scheme performs better than EGC and MRC schemes.
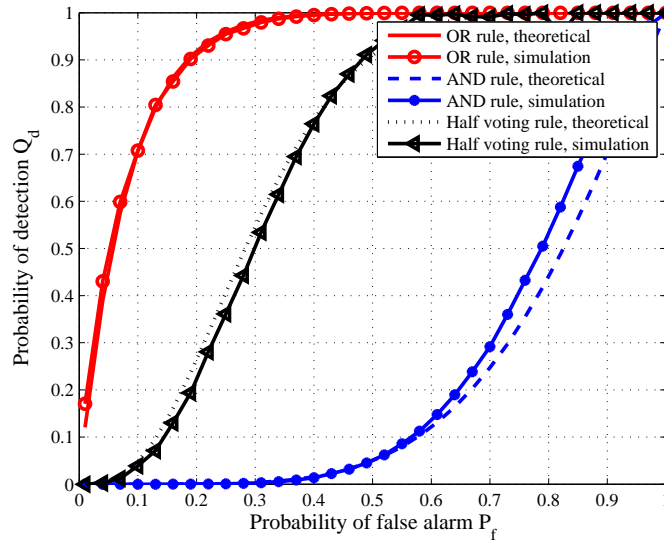
Figure 2.4: Q_d vs P_f for different HDF-based fusion schemes.

Figure 2.6 compares the convergence performance of GA, PSO, IWO and hybrid IWOPSO for the targated Q_f=0.1. The probability of detection is evaluated over 100 iterations for these four methods. The hybrid IWOPSO and IWO are converged at 3

and 2 iterations giving the values 0.8812 and 0.714, respectively. While PSO and GA are converged at 10 and 31 iterations giving the values 0.7017 and 0.6964, respectively. The computational time requirements for one run with 100 iterations of hybrid IWOPSO, IWO, PSO and GA are 0.20749, 0.17887, 0.43990 and 5.40167 secs, respectively. So, it is clearly observed that hybrid IWOPSO performs better than the other algorithms in terms of obtaining best global optimization result at the cost of slightly higher computational time as compared to IWO. Table 2.1 shows the control parameter values for single objective and multi-objective evolutionay algorithms.
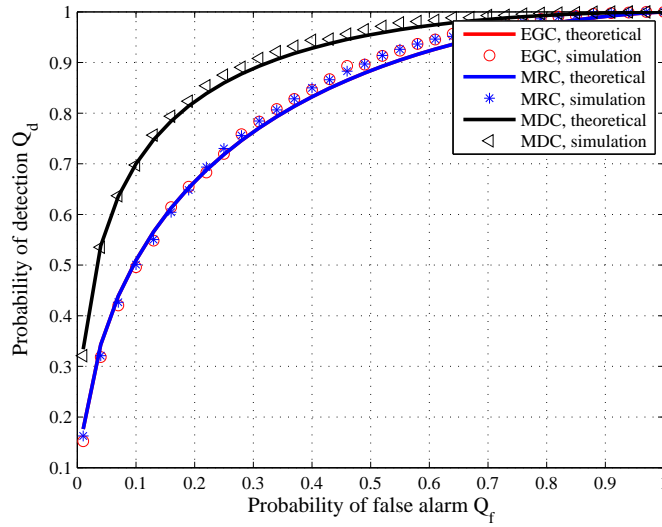
Figure 2.5: Q_d vs Q_f for EGC, MRC and MDC fusion schemes.
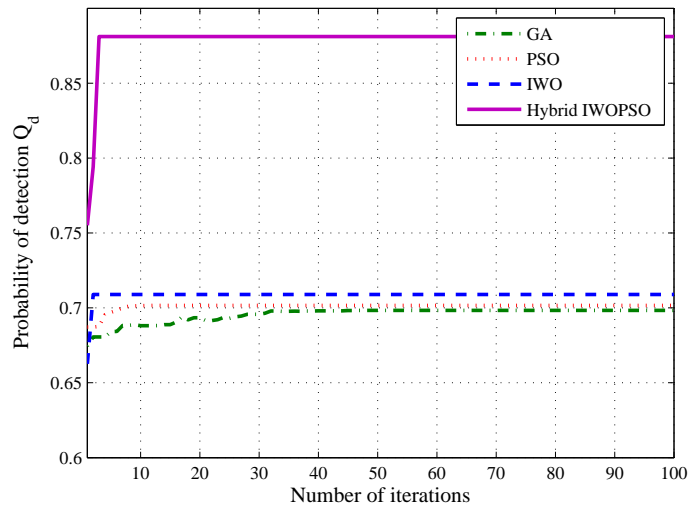
Figure 2.6: Convergence comparison over 100 iterations.

Table 2.1: Control parameters of GA/NSGA-II, PSO/MOPSO, IWO/NSIWO and hybrid IWOPSO/MO hybrid IWOPSO.

Symbols	Quantity	GA	PSO	IWO	Hybrid IWOPSO
t_{max}	Maximum iterations	100	100	100	100
dim	Dimension	M	M	M	M
P_{max}	Population number	80	80	80	80
S_{max}	Maximum seeds	–	–	5	5
S_{min}	Minimum seeds	–	–	0	0
κ	Non-linear modulation index	–	–	3	3
$\sigma_{initial}$	Initial value of SD	–	–	0.1	0.1
σ_{final}	Final value of SD	–		1e-6	1e-6
C_1	Cognitive coefficient	–	2	–	2
C_2	Social coefficient	–	2	–	2
P_c	Crossover distribution index	20	–	–	–
P_m	Mutation distribution index	20	–	–	–
tour	Tournament size	2	–	2	2

Figure 2.7 demonstrates the efficacy of hybrid IWOPSO over different values of probability of false alarm by comparing its performance with GA, PSO, IWO and MDC schemes. It is clearly observed that hybrid IWOPSO-based SDF scheme performs better than the other schemes. The efficiency of hybrid IWOPSO in obtaining the best global optimization solution in the single objective domain motivates us to propose the MO hybrid IWOPSO to solve the optimization problem in the multi-objective domain. Following the steps **Step 1** to **Step 12** of subsection 2.6.2, we evaluate the nondominated fronts of the MO hybrid IWOPSO. Its performance is compared with the other multi-objective algorithms NSGA-II, MOPSO and NSIWO in Figure 2.8. It is clearly observed that MO hybrid IWOPSO based method outperforms the other algorithms, and obtains a better quality of nondominated solutions.
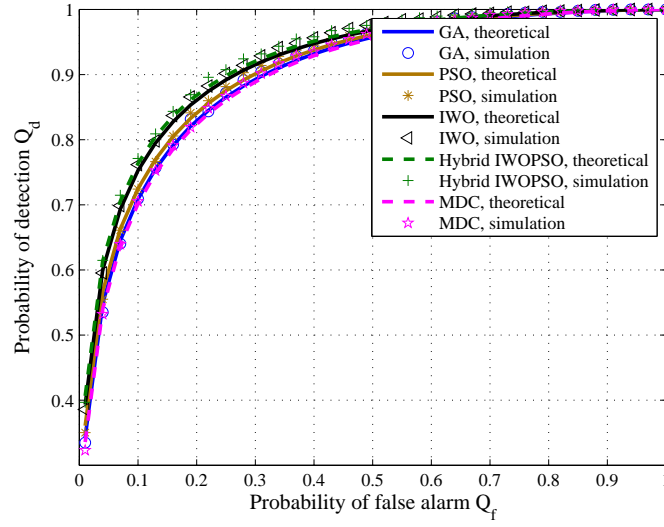
Figure 2.7: Performance comparison of different evolutionary algorithms.
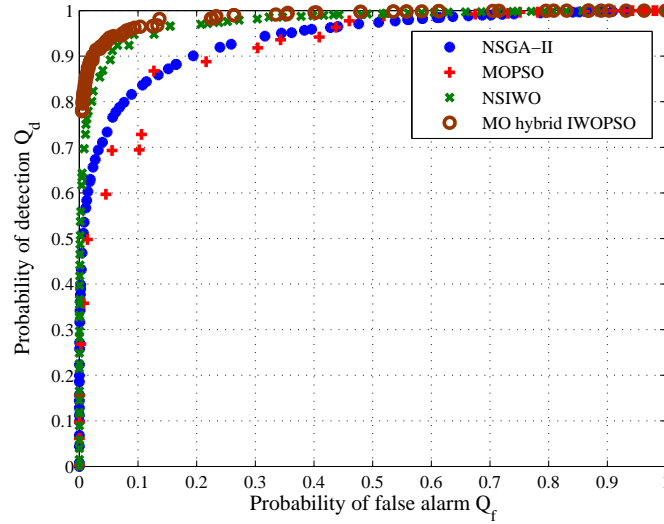
Figure 2.8: Comparison of approximate Pareto fronts obtained using the four multi-objective algorithms.

Figure 2.4 - Figure 2.8 show the performance analysis of both HDF and SDF-based schemes. MRC scheme is used for weight optimization in further analysis. It is simple and easy to implement, and also suitable for low SNR conditions. Hence, to avoid more complexity by employing evolutionary algorithms for weight optimization, MRC scheme is used in the subsequent chapters. Therefore, performance of the MRC scheme over different system parameters is analyzed. Figure 2.9 shows the probability of detection over different SNR conditions for different number of SUs. It is illustrated that Q_d gradually increases with increase in SNR. Further, the detection probability can be improved by participation of more number of SUs. We set Q_f is 0.1 for Figure

2.9 and Figure 2.10. Figure 2.10 shows Q_d vs M for different received SNR values. The received SNRs of M SUs are generated randomly within the ranges given in Figure 2.10. From Figure 2.9 and Figure 2.10 , it is concluded that probability of detection can be improved by involving more number of SUs in SS.
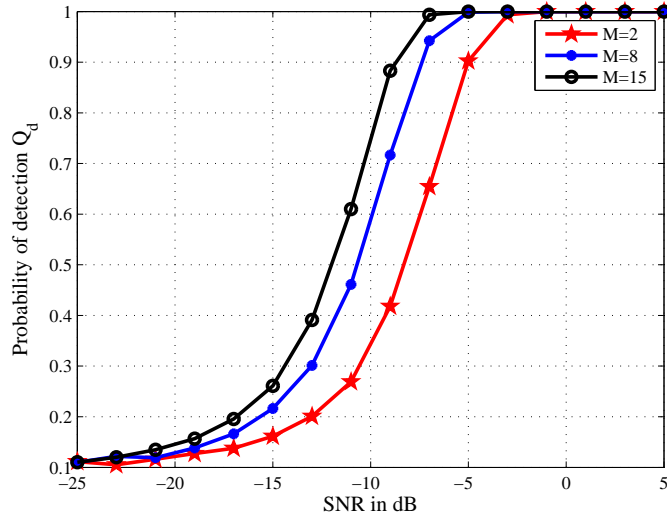
Figure 2.9: Q_d vs SNR for different values of M.
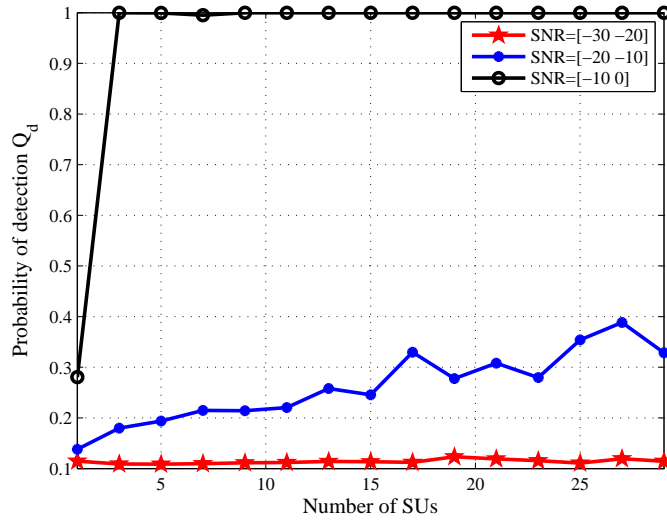
Figure 2.10: Q_d vs M for different ranges of SNR.

2.8   Summary

This chapter provided a brief overview of the SS techniques. It discussed the concept of the hypothesis testing used to identify the PU's activity on the desired band. Further, this chapter provided the knowledge about different conventional SS

techniques along with their pros and cons. Energy detection method is found to be the most commonly used spectrum detection method by the CR node due to its low complexity and implementation cost. This chapter also discussed different CSS CRN architectures. In CSS, global decision regarding the PU's presence is decided by the FC. The SUs' local decisions are combined at the FC and the final decision is obtained by employing different fusion schemes. A brief classification of the fusion schemes was presented. The multi-objective optimization algorithms were adopted to overcome the limitations of the single objective optimization schemes in SDF-based fusion method. Simulation results demonstrated the performances of the HDF and SDF-based CSS system models employing different fusion schemes. Evolutionary algorithms for weight optimization in SDF-based CSS framework performed better than the conventional schemes in terms of detection probability. This thesis focuses on proposing novel approaches to design the energy-efficient SDF-based CRN model for different scenarios. Specifically, evolutional algorithms need more computation and are complex than the conventional schemes. Further, among the three conventional schemes in SDF-based CSS model, MRC scheme is very simple and also depends on the average received SNR at each SU, and, hence, applicable to low SNR conditions. It is lesser complex in comparison to the MDC and evolutionary algorithms used for weight optimization. Therefore, MRC scheme is chosen for our CRN system model in the subsequent chapters.

Chapter 3

Proposed Approaches for Energy-Efficient Resource Allocation in the Cognitive Radio Network

This chapter focuses on solving the EE maximization problem both in the single and double threshold-based SDF CSS by jointly optimizing the sensing time and the power allocation to the SUs with suitably selecting SUs. The highlights of the chapter are

- The mathematical expression of the total interference that might occur to the PR is derived.

- Channel gain based SUs' selection method is proposed for both SS and data transmission.

- Energy-efficient algorithms are proposed to obtain the optimal sensing time and power allocation to the SUs.

3.1   Introduction

THE tremendous growth of wireless application devices is leading to an insatiable demand for more spectrum. Traditionally adopted fixed frequency allocation policy is not able to meet this requirement rather it results in spectrum congestion problem. CR is evolved to provide opportunistic access of the licensed spectrum to the unlicensed users [6]. SS is a key technology for ensuring reliable communication between the primary and secondary networks. But, accurate detection of the PU is not always guaranteed due to presence of fading or shadowing in the practical wireless environment. Further, in the single threshold-based CSS, false alarm probability increases with the detection probability which ultimately reduces the spectrum usage opportunities [55]. This problem can be overcome by employing double threshold-based CSS. In this scheme, either the detection probability or the false alarm probability is kept constant, then by varying the threshold difference, either the false alarm probability or the detection probability is minimized or maximized. The area between the two thresholds is called the confusion region or the fuzzy region [54, 105, 106]. When the energy of the SU falls within this area, there are three possibilities; It decides to send either no information [53, 107] or its corresponding energy value [54, 108] to the FC. The third possibility is that the SU performs more sensing rounds until the energy value falls on either side of the thresholds and a final decision is made [55]. In this chapter, we employ double threshold technique at the FC. So, all the SUs need to perform additional sensing rounds until the FC gives any final decision.

One of the main challenging issues in the CRN is EE maximization at low-battery-powered wireless terminals. EE depends on both system throughput and energy consumption made by the sensing devices. It is defined as the ratio of overall system throughput and the total power consumption at the secondary network. In CSS network, each frame consists of one sensing slot, reporting slot and one data transmission slot [86]. During the sensing slot, all the SUs cooperatively sense the availability of the licensed band and then transmit their data during the data transmission slot. Hence, accurate detection of the PU is necessary for effective spectrum usage and for avoiding collision between the PU and SUs. This depends on the sensing length of a frame. Longer sensing length provides more detection

---

Part of the contributions in this chapter are published in:
Deepa Das and Susmita Das,"Optimal Resource Allocation for Soft Decision Fusion-Based Cooperative Spectrum Sensing in Cognitive Radio Networks," Computers & Electrical Engineering, Elsevier, vol. 52, pp.362-378, 2016.
Deepa Das and Susmita Das, "A Novel Approach for Energy-Efficient Resource Allocation in Double Threshold-Based Cognitive Radio Network,"International Journal of Communication Systems, Wiley, 2016.

accuracy. On the other hand, it reduces the system throughput. Similarly, longer data transmission duration improves the system throughput at the cost of unreliability in sensing accuracy. Thus, an essential trade-off must be made in between the sensing time and the data rate to enhance the system throughput achieving detection accuracy [109]. Further, the SUs consume more energy during the data transmission than the SS. Hence, an efficient power allocation algorithm needs to be developed to restrict the transmission power to avoid serious interference to the primary network. So, this chapter mainly discusses the joint optimization of sensing time and transmission power under the different constraints associated with interference and outage of the CRNs. The outage constraint limits the data transmission outage of the SU below a prescribed threshold. Specifically, the constraints considered in this chapter offer minimum interference, achieve throughput more than throughput threshold, minimum outage with the optimal sensing time and power allocation.

3.1.1 Related works

The power allocation algorithms preserve EE by controlling the battery energy at the wireless terminals of the system. An overview of the existing resource allocation techniques with the associated challenges in the CRN design were discussed in [110, 111]. In [112], an energy-efficient resource allocation under PU's interference constraint was discussed for orthogonal frequency division multiplexing (OFDM)-based CR system. Bernstein approximation was used to tackle the interference constraint, and the power allocation to the sub-channels was done through the fast power allocation algorithm based on barrier method. Sun et al. introduced cooperative relays nodes with amplify-and-forward (AF) protocol in the OFDM network for maximizing EE [113]. Here, the optimization problem was formulated as convex optimization via its equivalent hypograph form, where the computational complexity was reduced by employing fast barrier algorithm. In [114], EE maximization problem was formulated in single PU and single SU CRN scenario, where the optimal sensing time and power allocation were obtained by using Bi-Section method under the constraints of interference to the PU and transmission delay. EE was evaluated in a CR system considering the Rayleigh fading both in the sensing and reporting channels [115]. Hasan et al. proposed a novel distributive heuristic channel assignment (DHCA) approach to maximize the throughput under the constraint of minimum queuing delay in [116]. In [117], EE in the centralized CRN was maximized by using PSO algorithm considering the spectrum switching delay and minimum rate requirement. In [118], the optimal power allocation was obtained by using fractional programming approach in green CRN under the PU's interference constraint. Then, the same method was implemented in decode-and-forward (DF)

relaying based green CR for optimal power allocation under the interference and outage constraints in [119]. In [120], SS, reporting, and data transmission times were optimized to minimize the energy consumption under the constraints of minimum achievable throughput, probability of detection and false alarm. To improve EE with limited interference to the PU, a clustered relay based CRN was designed in [121]. In [122], the aid of fractional programming with the Lagrangian duality theorem was applied to find the optimal power allocation for maximization of mean EE in fading channel scenarios consisting of multiple PUs and SUs under the constraints of outage probability of the PUs and peak transmit power of the SUs. Wu et al. maximized the EE in CSS by optimizing both sensing time and power allocation with detection parameters and interference constraint to the PU [123].

However, none of these methods considered the probability of PU's appearance during the data transmission duration while calculating the interference constraint. Moreover, most of the schemes were based on the single threshold-based HDF CSS. Hence, designing an energy-efficient model in both single and double threshold-based SDF cooperative network needs to considered. In the next subsection, a brief description of the contributions of this chapter is provided.

3.1.2   Chapter contributions and organization

The contributions of this chapter are mentioned below.

- An interference-aware CRN model for SDF CSS framework is proposed. Interference to the PR is evaluated considering the exponential transition probabilities of PU during the data transmission period.

- The EE maximization problem is formulated under the constraints of interference power to the PR, minimum achievable data rate and outage of SUs.

- An efficient algorithm is proposed to select suitable SUs for both SS and data transmission. The minimum number of SUs is chosen based on the sensing rounds in double threshold-based CSS model. Then, a IDM algorithm is proposed for joint optimization of sensing time and power allocation, in which the sensing time is obtained by applying golden section search method for maximum throughput and the power allocation to the SUs is derived by using our proposed EPA algorithm. Further, the complexity of the proposed algorithm is analyzed.

- The performance of our proposed algorithm is presented and compared with the previously existing techniques for both single threshold and double threshold-

based schemes. Further, the impact of the different network parameters on the system performance is studied.

The Chapter is structured as follows. Section 3.2 describes the system model illustrating the distribution of the SUs in the CRN with the detailed derivations of the performance metrics. The total interference to the PR calculation is given in Section 3.3. The optimization problem formulation is presented in Section 3.4. Our proposed solution approaches are discussed in Section 3.5. The detailed performance analysis is given and discussed in Section 3.6. Finally, summary of this chapter is presented in Section 3.7.

3.2 System Model

A CRN is considered consisting of M SUs which are uniformly distributed around the centrally located PU. It is assumed that the SUs collaboratively perform SS on the entire licensed band. During data transmission, the licensed band is divided into M sub-bands so as to allow each SU to transmit its data separately in one of these sub-bands to the corresponding secondary receiver (SR). Otherwise, the SUs continuously search for the vacant spectrum band. Let Q number of frames are allotted to a CR system each of length Γ as shown in Figure 3.1. Each frame consists of one sensing slot of duration τ_s, reporting slot of duration $\tau_r = \sum_{m=1}^{M} \tau_m$ and one data transmission slot of duration $\tau_d = \Gamma - \tau_r - \tau_s$. τ_m is the reporting duration of the mth SU. During τ_s, the SUs detect the availability of spectrum band, in τ_r they send their sensing reports to the FC and during the last slot τ_d the SUs transmit their data to SRs.
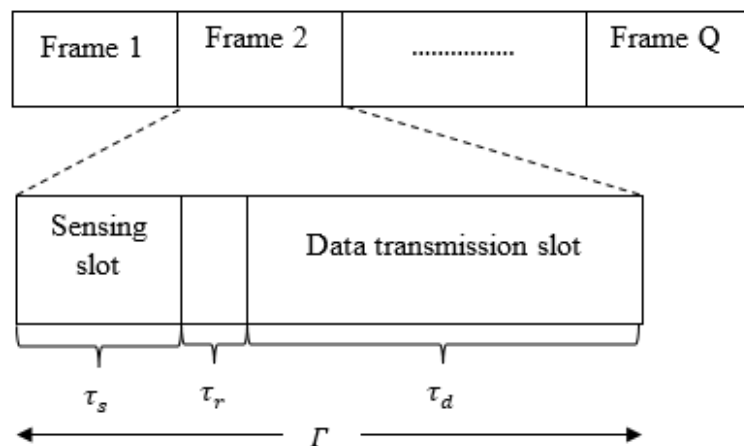
Figure 3.1: Frame structure in the CRN.

The SDF-based CSS system model is same as shown in the Figure 2.3. But, in the double threshold-based case, the FC in the system model employs double threshold

based decision scheme. The channel coefficient between the PU and the mth SU is distance dependent Rayleigh distributed, and is calculated as $h_{psm} \sim \aleph \left(0, \frac{1}{d_m{}^\alpha} \right)$, where d_m is the distance between the PU and the mth SU, and α is the path-loss exponent. The double threshold-based decision metric is shown in Figure 3.2. So, when Y_G falls in between two thresholds λ_{g1} and λ_{g2}, all the SUs need to perform sensing rounds until the FC achieves any final decision.
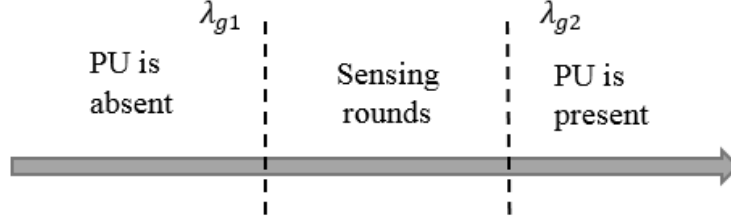
Figure 3.2: Double threshold-based FC's decision metric.

For the single threshold-based CSS system framework, Q_d and Q_f are same as (2.26) and (2.27), respectively. MRC fusion scheme given in (2.30) is used for the weight generation. In the double threshold-based energy detection scheme, let λ_{g1} and λ_{g2} be the two controlling thresholds for the missed detection and false alarm probability, respectively. When $Y_G \geq \lambda_{g2}$, the frequency band is occupied by the PU, and $Y_G \leq \lambda_{g1}$ shows the absence of the PU in the spectrum band. When Y_G lies in between λ_{g1} and λ_{g2}, the SUs need to do more sensing rounds before making any final decision. So, the target miss detection probability $\bar{Q}_{md}$ at λ_{g1} and the probability of false alarm Q_f at λ_{g2} are given by

$$\bar{Q}_{md}\left(\tau_s, \lambda_{g1}\right) = 1 - Q\left(\frac{\lambda_{g1} - \sum_{m=1}^{M} \sigma_{\eta m}{}^2 \left(1 + \gamma_m\right) w_m}{\sqrt{2 \sum_{m=1}^{M} \sigma_{\eta m}{}^4 \left(1 + 2\gamma_m\right) w_m{}^2}} \sqrt{\tau_s f_s}\right) = 1 - \bar{Q}_d\left(\tau_s, \lambda_{g1}\right) \tag{3.1}$$

where $\bar{Q}_d$ is the target detection probability. Similarly,

$$Q_f\left(\tau_s, \lambda_{g2}\right) = Q\left(\frac{\lambda_{g2} - \sum_{m=1}^{M} \sigma_{\eta m}{}^2 w_m}{\sqrt{2 \sum_{m=1}^{M} \sigma_{\eta m}{}^4 w_m{}^2}} \sqrt{\tau_s f_s}\right) \tag{3.2}$$

Then, the false alarm probability $\tilde{Q}_f$ for the given target detection probability $\bar{Q}_d$ is given by

$$\tilde{Q}_f\left(\tau_s, \lambda_{g1}\right) = Q\left(\frac{Q^{-1}\left(\bar{Q}_d\left(\tau_s, \lambda_{g1}\right)\right) \sqrt{2 \sum_{m=1}^{M} \sigma_{\eta m}{}^4 \left(1 + 2\gamma_m\right) w_m{}^2} + \sum_{m=1}^{M} \sigma_{\eta m}{}^2 \gamma_m w_m \sqrt{\tau_s f_s}}{\sqrt{2 \sum_{m=1}^{M} \sigma_{\eta m}{}^4 w_m{}^2}}\right) \tag{3.3}$$

λ_{g2} is calculated from the given value of δ such that $\delta = P_r\left(\lambda_{g1} < Y_G < \lambda_{g2} | H_1\right) = P_r\left(\lambda_{g1} < Y_G < \lambda_{g2} | H_0\right)$ and usually, $0 \leq \delta < 1$. If $\Delta = \lambda_{g2} - \lambda_{g1}$, then at λ_{g2} threshold,

$Q_f\left(\tau_s, \lambda_{g2}\right)$ is modified as

$$Q_f\left(\tau_s, \lambda_{g2}\right) = Q\left[a + \left(\Delta' + b\right)\sqrt{\tau_s f_s}\right] \tag{3.4}$$

where $\quad a = \dfrac{Q^{-1}\left(\bar{Q}_d\right)\sqrt{2\sum_{m=1}^{M}\sigma_{\eta m}^{4}\left(1+2\gamma_m\right)w_m^{2}}}{\sqrt{2\sum_{m=1}^{M}\sigma_{\eta m}^{4}w_m^{2}}}, \quad \Delta' = \dfrac{\Delta}{\sqrt{2\sum_{m=1}^{M}\sigma_{\eta m}^{4}w_m^{2}}} \quad$ and

$b = \dfrac{\sum_{m=1}^{M}\sigma_{\eta m}^{2}w_m\gamma_m}{\sqrt{2\sum_{m=1}^{M}\sigma_{\eta m}^{4}w_m^{2}}}.$

In the double threshold-based SS scheme, the probability that Y_G falls in between λ_{g1} and λ_{g2} is given by [55]

$$\rho = \left[\bar{Q}_d\left(\lambda_{g1}\right) - Q_d\left(\lambda_{g2}\right)\right]P_{H1} + \left[\tilde{Q}_f\left(\lambda_{g1}\right) - Q_f\left(\lambda_{g2}\right)\right]P_{H0} \tag{3.5}$$

Then, the average number of sensing rounds is $S_R = \frac{1}{1-\rho}$. So, S_R increases with increase in ρ as well as δ. Hence, $Q_f\left(\tau_s, \lambda_{g2}\right)$ can be reduced by varying δ keeping the probability of detection upper bounded $\bar{Q}_d\left(\tau_s, \lambda_{g1}\right)$. So, for double threshold-based FC scheme, $\tau_d = \Gamma - \tau_s S_R - \tau_r$.

From the next sections, all the mathematical expressions will be for the double threshold-based system model. For single threshold FC, $\lambda_{g1} = \lambda_{g2} = \lambda$ and $S_R = 1$.

3.3 Total Interference Analysis to the PR

Interference to the PR occurs when the PU is accessing the licensed band, but the SUs can not identify its presence during τ_s and start transmitting their data. So, during the data transmission period interference may be expected in two possible scenarios. In the first scenario, the SUs correctly detect the absence of the PU during sensing period but the PU makes a transition in the data transmission period. In the second scenario, SUs are unable to identify the presence of PU correctly during the sensing time and start transmitting their data.

The activity of the PU signal is modeled as an exponentially distributed ON-OFF process which alternates between ON and OFF state. If u and v represent the busy and idle rates, respectively, then the probability that the channel is being occupied by the PU is $P_{H1} = \frac{u}{u+v}$, and the probability that PU is absent on the licensed band is $P_{H0} = \frac{v}{u+v}$. In the exponentially distributed ON-OFF process, the transition probability $I_{ij}\left(\tau\right)$ of PU is defined as the probability that the PU will move from ith state to jth state after time τ. For the first scenario, the possibility of the PU being present during τ_d is given by [124]

$$I_{01}\left(\tau_d\right) = \frac{v}{u+v}\left(\tau_d + \frac{\left(exp\left(-\left(u+v\right)\tau_d\right)-1\right)}{u+v}\right) \tag{3.6}$$

So, for the given value of δ, interference for this scenario when the PU is priliminary in OFF state is calculated as

$$I_{OFF} = \left(1 - Q_f\left(\lambda_{g2}\right)\right)I_{01}\left(\tau_d\right) \tag{3.7}$$

In the second scenario, the probability of expected period when the PU exists during τ_d

is expressed as

$$I_{11}(\tau_d) = \tau_d - \frac{u}{u+v}\left(\tau_d + \frac{(exp(-(u+v)\tau_d)-1)}{u+v}\right) \qquad (3.8)$$

So, the interference in this busy state of the PU is determined by

$$I_{ON} = \bar{Q}_{md}(\lambda_{g1})I_{11}(\tau_d) \qquad (3.9)$$

The average interference introduced to the PR is defined as the ratio of total interference occurs during τ_d with the persistence of PU signal during the entire frame period.

$$I_{total} = \frac{I_{OFF} + I_{ON}}{P_{H1}\Gamma} \qquad (3.10)$$

3.4 Optimization Problem Formulation

3.4.1 Outage analysis

Based on the FC's final decision, there are two possible scenarios when the SUs intend to transmit their data to the SRs. In the first scenario, the PU is correctly detected to be absent on the desired band. So, the channel capacity achieved due to the data transmission from mth SU is given by

$$C_{0m} = log_2\left(1 + \frac{|h_{srm}|^2 P_{tm}}{N_p}\right) \qquad (3.11)$$

where h_{srm} is the sub-channel coefficient between the mth SU and the corresponding SR which is calculated as $h_{srm} \sim \aleph\left(0, \frac{1}{d_{srm}{}^\alpha}\right)$. d_{srm} is the distance between the mth SU and the corresponding SR. P_{tm} represents the transmission power from the mth SU and N_p denotes the noise power. In the second scenario, the PU is active on the channel, but SUs are unable to identify such weak PU signal and start transmitting their data. The channel capacity achieved due to this case is expressed as

$$C_{1m} = log_2\left(1 + \frac{|h_{srm}|^2 P_{tm}}{|h_{prm}|^2 P_p + N_p}\right) \qquad (3.12)$$

where P_p is the interference power received at the secondary network due to the presence of the PU and h_{prm} is the sub-channel coefficient between the PU and the mth SR. This interference mainly occurs due to the miss detection probability Q_{md} made by the SUs. P_p can be calculated as

$$P_p = \left(\frac{P_{H1}\bar{Q}_{md}(\lambda_{g1})}{P(\overline{H}_0)}\right)\sigma_s{}^2 \qquad (3.13)$$

where $P(\overline{H}_0)$ denotes the total probability of event $\overline{H}_0$ which is given by $P(\overline{H}_0) = P_{H0}(1 - Q_f(\lambda_{g2})) + P_{H1}\bar{Q}_{md}(\lambda_{g1})$. Comparing these two scenarios, it is obvious that

$C_{0m} > C_{1m}$, hence the average throughput of the secondary CRN is given by [86]

$$R(\tau_s, P_t) = \sum_{m=1}^{M} R_{1m}(\tau_s, P_{tm}) + \sum_{m=1}^{M} R_{2m}(\tau_s, P_{tm}) \cong \sum_{m=1}^{M} R_{1m}(\tau_s, P_t) \qquad (3.14)$$

where $R(\tau_s, P_t)$ is the function of sensing time τ_s and transmission power P_t, and

$$R_{1m}(\tau_s, P_{tm}) = \frac{\tau_d}{\Gamma}\left(1 - Q_f(\tau_s, \lambda_{g2})\right) P_{H0} C_{0m} \qquad (3.15)$$

$$R_{2m}(\tau_s, P_{tm}) = \frac{\tau_d}{\Gamma}\left(1 - \bar{Q}_d(\tau_s, \lambda_{g1})\right) P_{H1} C_{1m} \qquad (3.16)$$

From (3.14), it is obvious that longer sensing time reduces the system throughput. On the other hand, false alarm probability for the given value of Q_d is a decreasing function of τ_s. Hence, by increasing the sensing time, spectrum accessibility possibility can be maximized. If R_{th} denotes the minimum achievable data rate for each SU, then the minimum transmission power of that SU is represented as

$$P_{tm} \geq \frac{\left(2^{R_{th}} - 1\right) N_p}{|h_{srm}|^2} \qquad (3.17)$$

Then, we analyze the overall outage performance to examine the effect of interference on the system throughput. An outage occurs when the channel capacity of the SU falls below the threshold R_{th}. So, from **APPENDIX A**, the outage at mth SU is calculated as

$$P_{outm} = \frac{\tau_d}{\Gamma}\left[P_{H0}\left(1 - Q_f(\lambda_{g2})\right)\left\{1 - exp\left(-\frac{\gamma_{th}}{\sigma_{srm}^2}\right)\right\} + \right.$$

$$\left. P_{H1}\bar{Q}_{md}(\lambda_{g1})\left\{1 - \frac{\sigma_{srm}^2}{\sigma_{prm}^2 \gamma_p \gamma_{th} + \sigma_{srm}^2} exp\left(-\frac{\gamma_{th}}{\sigma_{srm}^2}\right)\right\}\right] \qquad (3.18)$$

where $\gamma_p = \frac{P_p}{N_p}$ and $\gamma_{th} = \frac{\left(2^{R_{th}}-1\right)N_p}{P_{tm}}$. σ_{srm}^2 and σ_{prm}^2 are the variances of the channel gains $|h_{srm}|^2$ and $|h_{prm}|^2$, respectively. Then the outage probability constraint of the mth SU is expressed as

$$P_{outm} \leq O_{th} \qquad (3.19)$$

where O_{th} is the outage threshold.

3.4.2 Problem formulation

EE is maximized by jointly optimizing the sensing time and power allocation $P_t = [P_{t1}, P_{t2}, \ldots, P_{tM}]$ in the CRN. So, we divide the joint optimization problem into two sub-optimization problems. Firstly, the sensing time is evaluated for maximum system throughput. Secondly, the exact power allocation to the SUs is evaluated. The first sub-optimization problem is formulated as

$$maximize \qquad : \qquad R(\tau_s) \qquad (3.20)$$

$$Subject \quad to \qquad : \qquad Q_d\left(\tau_s, \lambda_{g1}\right) = \bar{Q}_d \qquad (3.20\ a)$$

$$: \qquad Q_f\left(\tau_s, \lambda_{g2}\right) \leq \bar{Q}_f \qquad (3.20\ b)$$

$$: \qquad 0 \leq \tau_s \leq \Gamma \qquad (3.20\ c)$$

$$: \qquad (3.17) \text{ and } (3.19) \qquad (3.20\ d)$$

For any value of P_t, $R\left(\tau_s\right)$ is a unimodal function of τ_s. It increases monotonically from $0 \leq \tau_s < \tau_s{}^*$ and decreases from $\tau_s{}^* < \tau_s \leq \Gamma$. So, there exist a local maximum sensing time $\tau_s{}^*$ at which $R\left(\tau_s\right)$ is maximum.

Theorem 1. *$R\left(\tau_s\right)$ is a concave function of τ_s, where $\tau_s{}^*$ gives the maximum average throughput.*

Proof. Proof of this theorem is given in **Appendix B**. □

So, it is proved that $R\left(\tau_s\right)$ is a unimodal function in the range $0 \leq \tau_s \leq \Gamma$. Hence, golden section search algorithm is employed to get optimal sensing time for maximum throughput [125]. The second optimization problem is the main concern i.e. to maximize EE. Energy consumption depends on the SUs' decision on the PU's availability on the licensed band. If the PU is present or the SUs falsely detect the presence of the PU, no data transmission takes place. In this case, energy consumption occurs only due to the SS. Data transmission is possible in two scenarios; when the PU is absent on the licensed band and missed detection occurs. So, the total power consumption in the CR system is given by (neglecting the circuit power consumption)

$$P_T\left(\tau_s, P_t\right) = S_R \tau_s M P_s + \tau_d P\left(\overline{H}_0\right) \sum_{m=1}^{M} P_{tm} \qquad (3.21)$$

where P_s is the sensing power and assumed to be same for all the SUs. Then, EE (bit/s/joule) of the CRN is defined as the ratio of average throughput given in (3.14) and the total power consumed by the secondary network given in (3.21) which is expressed as

$$EE\left(\tau_s, P_t\right) = \frac{R\left(\tau_s, P_t\right)}{P_T\left(\tau_s, P_t\right)} \qquad (3.22)$$

Then, the EE maximization problem is formulated under the constraints of the following parameters

$$\begin{array}{c} Maximize \\ \tau_s,\ P_t \end{array} \qquad : \qquad \frac{R\left(\tau_s, P_t\right)}{P_T\left(\tau_s, P_t\right)} \qquad (3.23)$$

$$Subject \quad to \quad : \quad P_{tmax} - \sum_{m=1}^{M} P_{tm} \geq 0 \qquad (3.23 \text{ a})$$

$$: \quad I_{th} - I_{total} \sum_{m=1}^{M} |h_{sdm}|^2 P_{tm} \geq 0 \qquad (3.23 \text{ b})$$

$$: \quad O_{th} - P_{outm} \geq 0 \qquad (3.23 \text{ c})$$

$$: \quad C_{0m} \geq R_{th} \qquad (3.23 \text{ d})$$

$$: \quad P_{tm} \geq \frac{\left(2^{R_{th}} - 1\right) N_p}{|h_{srm}|^2} \qquad (3.23 \text{ e})$$

$$: \quad 0 \leq \tau_s \leq \Gamma \qquad (3.23 \text{ f})$$

P_{tmax} is the maximum allowable transmission power from SUs and I_{th} represents the interference power threshold. The total interference power below I_{th} will not affect the PR. Here, h_{sdm} is the sub-channel coefficient between the *m*th SU and the PR.

3.5 Proposed Solution Approaches

This section includes the selection of suitable SUs for both SS and data transmission. Further, an efficient algorithm called IDM is proposed for joint optimization of sensing time and transmission power within which the sub-problem associated with the exact power allocation is solved by the aid of Lagrangian dual problem using KKT condition.

3.5.1 Selection of suitable SUs

From (3.21), it is observed that power consumption increases with the sensing rounds. But the number of sensing rounds decreases with increase in the number of SUs; the proof is given in **APPENDIX C**. However, after a certain number of SUs the decrease rate is so negligible that it does not show any significant change though the number of SUs increases. Let total *K* SUs are present in the CRN, then the suitable number of SUs $M < K$ after which decrease in S_R is negligible. By doing this the number of sensing rounds and the number of SUs can be decreased simultaneously. Meanwhile, it helps in increasing the data transmission duration. Hence, both $R(\tau_s, P_t)$ and $EE(\tau_s, P_t)$ can be improved by selecting suitable *M* SUs with minimum sensing rounds S_{Rmin}. Here, we divide the **Algorithm** 3.1 into three Steps. In the first Step, suitable number of SUs *M* is selected based on the sensing rounds. In the subsequent steps, eligible *M* SUs are selected to maximize the detection probability and system throughput. During the sensing period, the problem of finding the suitable *M* SUs is based on the MDC

algorithm which is given as follows [91].

$$\begin{array}{lcl} \underset{w}{Maximize} & : & d_m{}^2\,(m) \\[2mm] Subject \quad to & : & \|w\| = 1 \end{array} \qquad (3.24)$$

where $d^2\,(w) = \dfrac{[E(Y_G|H_1) - E(Y_G|H_0)]^2}{Var(Y_G|H_1)} = \dfrac{\left(\sum_{m=1}^{M} \sigma_{\eta m}{}^2 \gamma_m w_m\right)^2}{\frac{2}{N}\sum_{m=1}^{M} \sigma_{\eta m}{}^4 (1+2\gamma_m) w_m{}^2}.$ If the average SNR received at each SU is same, then $d^2\,(w)$ is modified as

$$d^2\,(w) = \frac{\left(\sum_{m=1}^{M} \left|h_{psm}\right|^2 \sigma_s{}^2 w_m\right)^2}{\frac{2}{N}\sum_{m=1}^{M} \sigma_{\eta m}{}^2 \left(\sigma_{\eta m}{}^2 + \left|h_{psm}\right|^2 \sigma_s{}^2\right) w_m{}^2} \qquad (3.25)$$

From (3.25), it is found that M SUs with larger channel gains produce accurate detection performance as compared to the randomly selected M SUs. It is observed from (3.14) that throughput increases with channel gain between the SU and SR. Similarly, for the given value of I_{th} and I_{total} in (3.23 b), the total transmission power depends on the channel gain between the SU and the PR. Hence, the SUs closer to the SR in relative to the PR are selected for the data transmission. The proposed SUs' selection algorithm is described as follows. m represents the number of users and $m \in [1, K]$ and $u = 50$ (it is chosen based on the maximum sensing rounds possible considering both low and high SNR).So, K SUs are arranged in the descending order of their profit to loss ratio $\dfrac{|h_{srm}|^2}{|h_{sdm}|^2}$, and first M SUs are chosen for data transmission.

Algorithm 3.1 Selection of suitable SUs.

Input:
    $K \leftarrow$ total number of SUs.
    $m \leftarrow 1, z \leftarrow 50, Diff \leftarrow 1, \varepsilon \leftarrow 0.01$
Output:
    Eligible M

 1: **while** $(Diff > \varepsilon)$ **do**
 2:     $J \leftarrow z$;
 3:     find $S_R\,(m)$;
 4:     $z \leftarrow S_R\,(m)$;
 5:     $Diff \leftarrow J - z$;
 6:     $m \leftarrow m + 1$;
 7: **end while**
 8: $M \leftarrow m - 1$.
 9: For SS, select M SUs such that $m = \underset{m \in K}{\arg\max} \left|h_{psm}\right|^2.$

10: For data transmission, select M SUs such that $m = \underset{m \in K}{\arg\max} \dfrac{|h_{srm}|^2}{|h_{sdm}|^2}.$

3.5.2   Iterative Dinkelbach Method (IDM) for resource allocation

This subsection presents a novel iterative resource allocation algorithm using the Dinkelbach method which is based on the parametric transformation.   As per parametric programming, if $f_1(s)$ and $f_2(s)$ are continuous and real valued functions and $s \in S$, where S is a subset containg all possible values of s, then, $\max\limits_{s \in S} \left\{ \frac{f_1(s)}{f_2(s)} \right\}$ can be transformed to $\max\limits_{s \in S} \{ f_1(s) - \Upsilon f_2(s) \}$.   This transformation relies on the following theorem.

Theorem 2. *If S is the feasible set, then there exists an optimal objective function such that*

$$\Upsilon^* = \frac{f_1(s^*)}{f_2(s^*)} = \max_{s \in S} \left\{ \frac{f_1(s)}{f_2(s)} \right\} \tag{3.26}$$

If and only if

$$\max_{s \in S} \{ f_1(s) - \Upsilon^* f_2(s) \} = f_1(s^*) - \Upsilon^* f_2(s^*) = 0 \tag{3.27}$$

Proof.   Proof of this theorem is given in [126].   □

As per this theorem, our optimization problem is formulated as; $\Upsilon^* = \frac{R(\tau_s{}^*, P_t{}^*)}{P_T(\tau_s{}^*, P_t{}^*)} = \max\limits_{P_t \in P} \left\{ \frac{R(\tau_s, P_t)}{P_T(\tau_s, P_t)} \right\}$ and $\max\limits_{P_t \in P} \{ R(\tau_s, P_t) - \Upsilon^* P_T(\tau_s, P_t) \} = R(\tau_s{}^*, P_t{}^*) - \Upsilon^* P_T(\tau_s{}^*, P_t{}^*) = 0$ Here, $\tau_s{}^*$ and $P_t{}^*$ represent the optimal sensing time and power allocation, respectively. Our proposed IDM algorithm presents the steps for joint optimization of sensing time and power allocation with suitable SUs from **Algorithm** 3.1.

Algorithm 3.2 IDM algorithm for resource allocation.

Input:
   P_t satisfying the constraints (3.23 a - 3.23 f) and find out τ_s using golden section search method.
   Dinkelbach parameter$(\Upsilon) \leftarrow 0$;
   Acceptance tolerance value $\xi \leq 10^{-5}$;
   Current iteration $t \leftarrow 1$;
Output:
   Optimal sensing time $\tau_s{}^*$ and transmission power $P_t{}^*$.

1: **while** $|\Upsilon(t) - \Upsilon(t-1)| \geq \xi$ **do**
2:     For the given value of τ_s, evaluate power $P_t(t)$from EPA algorithm such that;

$$P_t = \arg\max_{P_t} \{ R(\tau_s, P_t) - \Upsilon(t) P_T(\tau_s, P_t) \}$$

3:     For the given $P_t(t)$, find corresponding sensing time τ_s;
4:     $t \leftarrow t+1$;
5:     $\Upsilon(t) \leftarrow \left\{ \frac{R(\tau_s, P_t)}{P_T(\tau_s, P_t)} \right\}$;
6: **end while**

According to **Algorithm** 3.2, at each iteration t, $P_t(t)$ is calculated from the subproblems associated with the convex optimization which is given in the next subsection. Then, for the given transmission power, corresponding sensing time is found out by using golden section search method for maximum throughput. The proposed algorithm is terminated when $\Upsilon(t)$ converges. In **Appendix D**, we prove the convergence of such type of fractional programming transformation algorithm.

3.5.3 Exact power allocation to the SUs

The main objective of this subsection is to maximize step 2 of **Algorithm** 3.2 meeting all the constraints (3.23 a-3.23 f). In (3.22), it is seen that $R(\tau_s, P_t)$ is a concave and $P_T(\tau_s, P_t)$ is an affine function of SUs' transmitting power P_t. Also the constraints given in the optimization problem (3.23) are either linear or convex. Hence, for the given τ_s, the optimal power allocation problem $\{R(\tau_s, P_t) - \Upsilon(t) P_T(\tau_s, P_t)\}$ can be formulated using the convex theory subject to the (3.23 a), (3.23 b) and (3.23 d) constraints. Then, this suboptimization problem is solved by Lagrangian duality theorem which is expressed as

$$
L(\theta, \mu, \vartheta) = C' \sum_{m=1}^{M} log_2 \left(1 + \frac{|h_{srm}|^2 P_{tm}}{N_p} \right) - \Upsilon(t) \left(S_R M \tau_s P_s + \tau_d P(\overline{H}_0) \sum_{m=1}^{M} P_{tm} \right)
$$
$$
+ \theta \left(P_{tmax} - \sum_{m=1}^{M} P_{tm} \right) + \mu \left(I_{th} - I_{total} \sum_{m=1}^{M} |h_{sdm}|^2 P_{tm} \right)
$$
$$
+ \vartheta_m \left(log_2 (1 + v_m P_{tm}) - R_{th} \right) \quad (3.28)
$$

$$
Subject\ to \qquad : \qquad P_{tmax} - \sum_{m=1}^{M} P_{tm} \geq 0 \qquad (3.28\ a)
$$

$$
: \qquad I_{th} - I_{total} \sum_{m=1}^{M} |h_{sdm}|^2 P_{tm} \geq 0 \qquad (3.28\ b)
$$

$$
: \qquad log_2 (1 + v_m P_{tm}) - R_{th} \geq 0 \qquad (3.28\ c)
$$

where θ, μ and $\vartheta = [\vartheta_1, \vartheta_2, ..., \vartheta_M]$ are the non-negative Lagrangian multipliers, $v_m = \frac{|h_{srm}|^2}{N_p}$ and $C' = \frac{\tau_d}{\Gamma} \left(1 - Q_f(\lambda_{g2}) \right) P_{H0}$. In each iteration t of **Algorithm** 3.2, the Lagrangian dual problem is solved such that $\min_{\theta, \mu, \vartheta} \max_{\tau_s, P_t} L(\theta, \mu, \vartheta)$. Then by applying KKT condition to this dual problem we have [127]

$$
\frac{C' v_m}{(1 + v_m P_{tm})(ln2)} - \Upsilon(t) \tau_d P(\overline{H}_0) - \theta - \mu I_{total} \sum_{m=1}^{M} |h_{sdm}|^2 + \vartheta_m C_{0m}' = 0 \quad (3.29)
$$

$$\theta \left(P_{tmax} - \sum_{m=1}^{M} P_{tm} \right) = 0 \qquad \text{(3.29 a)}$$

$$\mu \left(I_{th} - I_{total} \sum_{m=1}^{M} |h_{sdm}|^2 P_{tm} \right) = 0 \qquad \text{(3.29 b)}$$

$$\vartheta_m \left(log_2 \left(1 + v_m P_{tm} \right) - R_{th} \right) = 0 \qquad \text{(3.29 c)}$$

where $C_{0m}' = \frac{v_m}{(1+v_m P_{tm})ln2}$. It is clearly noticed from (3.29 a), (3.29 b) and (3.29 c) that each condition generates two cases; either the dual variable is zero or the corresponding constraint is zero. So, we have summarized these possibilities into four cases, and accordingly calculate $P_t(t)$ for the current iteration t of **Algorithm** 3.2.

Case-1: $\theta = \mu = 0$ and $\vartheta_m = 0$ for all $m \in M$. So, (3.29) reduces to

$$\frac{C' v_m}{(1+v_m P_{tm})(ln2)} - \Upsilon(t) \tau_d P(\overline{H}_0) = 0 \qquad \text{(3.30)}$$

$$Subject \ to \qquad : \qquad P_{tmax} - \sum_{m=1}^{M} P_{tm} \geq 0 \qquad \text{(3.30 a)}$$

$$: \qquad I_{th} - I_{total} \sum_{m=1}^{M} |h_{sdm}|^2 P_{tm} \geq 0 \qquad \text{(3.30 b)}$$

$$: \qquad log_2 \left(1 + v_m P_{tm} \right) - R_{th} \geq 0 \qquad \text{(3.30 c)}$$

The power solution of the mth SU of (3.30) is obtained by using water filling solution which is expressed as

$$P_{tm}^{\ 1} = \left[\frac{C'}{\Upsilon(t) \tau_d P(\overline{H}_0) ln2} - \frac{1}{v_m} \right]^+ \qquad \text{(3.31)}$$

where $[.]^+ = max[0,.]$. Then, by substituting the value of (3.31) in (3.30 a), (3.30 b) and (3.30 c), following three conditions (3.32 a), (3.32 b) and (3.32 c) are evaluated, respectively, which are as follows

$$\frac{C'}{\Upsilon(t) \tau_d P(\overline{H}_0) ln2} \leq \frac{P_{tmax}}{M} + \frac{1}{M} \sum_{m=1}^{M} \frac{1}{v_m} \qquad \text{(3.32a)}$$

$$\frac{C'}{\Upsilon(t) \tau_d P(\overline{H}_0) ln2} \leq \frac{I^* + \sum_{m=1}^{M} \frac{|h_{sdm}|^2}{v_m}}{\sum_{m=1}^{M} |h_{sdm}|^2} \qquad \text{(3.32b)}$$

$$\frac{C'}{\Upsilon(t) \tau_d P(\overline{H}_0) ln2} \geq \frac{\left(2^{R_{th}} \right)}{v_m} \qquad \text{(3.32c)}$$

where $I^* = \frac{I_{th}}{I_{total}}$. If (3.32 a), (3.32 b) and (3.32 c) are satisfied, then (3.31) is the power allocation solution.

Case-2: $\theta \neq 0, \mu = 0$ and $\vartheta_m = 0$ for all $m \in M$. Similar to the **Case-1**, (3.29) reduces to

$$\frac{C' v_m}{(1+v_m P_{tm})(ln2)} - \Upsilon(t) \tau_d P(\overline{H}_0) - \theta = 0 \qquad \text{(3.33)}$$

$$Subject\ to \qquad : \qquad \sum_{m=1}^{M} P_{tm} = P_{tmax} \qquad \text{(3.33 a)}$$

$$: \qquad (3.30b) \text{and} (3.30c) \qquad \text{(3.33 b)}$$

For this case, the exact solution for power allocation is obtained as

$$P_{tm}^{2} = \left[\frac{C'}{\left(\theta + \Upsilon(t)\,\tau_d P\left(\overline{H}_0\right)\right) ln2} - \frac{1}{v_m} \right]^{+} \qquad \text{(3.34)}$$

When (3.32 b) and (3.32 c) are satisfied, and (3.32 a) is reduced to equality constraint which is given by

$$\frac{C'}{\Upsilon(t)\,\tau_d P\left(\overline{H}_0\right) ln2} = \frac{P_{tmax}}{M} + \frac{1}{M} \sum_{m=1}^{M} \frac{1}{v_m} \qquad \text{(3.35)}$$

The water filling solution given in (3.34) consists of the dual variable θ in the denominator which is updated by sub-gradient method as per the following expression [127]

$$\theta(it+1) = \left[\theta(it) - \psi(it) \left(P_{tmax} - \sum_{m=1}^{M} P_{tm} \right) \right]^{+} \qquad \text{(3.36)}$$

where $\psi(it)$ is non-negative step size for the current iteration it and is set at $\frac{1}{\sqrt{it}}$. So, $\psi(it)$ decreases with the number of iterations and θ converges to the optimal value when $\psi(it)$ is sufficiently small.

Case-3: $\theta = 0, \mu \neq 0,\ \vartheta_m = 0$ for all $m \in M$. Then the KKT condition given in (3.29) is reduced to

$$\frac{C' v_m}{(1 + v_m P_{tm})(ln2)} - \Upsilon(t)\,\tau_d P\left(\overline{H}_0\right) - \mu I_{total} \sum_{m=1}^{M} |h_{sdm}|^2 = 0 \qquad \text{(3.37)}$$

$$Subject\ to \qquad : \qquad (3.30a) \text{and} (3.30c) \qquad \text{(3.37 a)}$$

$$: \qquad I_{th} = I_{total} \sum_{m=1}^{M} |h_{sdm}|^2 P_{tm} \qquad \text{(3.37 b)}$$

After solving (3.37), the power allocation solution is given by

$$P_{tm}^{3} = \left[\frac{C'}{\left(\Upsilon(t)\tau_d P\left(\overline{H}_0\right) + \mu I_{total} \sum_{m=1}^{M} |h_{sdm}|^2 \right) ln2} - \frac{1}{v_m} \right]^{+} \qquad \text{(3.38)}$$

With the conditions (3.32 a) and (3.32 c) are satisfied, and (3.32 b) is given with equality

$$\frac{C'}{\Upsilon(t)\,\tau_d P\left(\overline{H}_0\right) ln2} = \frac{I^* + \sum_{m=1}^{M} \frac{|h_{sdm}|^2}{v_m}}{\sum_{m=1}^{M} |h_{sdm}|^2} \qquad \text{(3.39)}$$

Similar to **Case-2**, the solution (3.38) consists of the dual variable μ in the denominator which is updated by sub-gradient method as per the following expression

$$\mu(it+1) = \left[\mu(it) - \psi(it) \left(I_{th} - I_{total} \sum_{m=1}^{M} |h_{sdm}|^2 P_{tm} \right) \right]^{+} \qquad \text{(3.40)}$$

So, μ converges to the optimal value when $\psi(it)$ is sufficiently small.

Case-4: $\vartheta_m \neq 0$ for all $m \in M$, $\theta = 0$ and $\mu = 0$. For this case, (3.29) reduces to

$$\frac{C'v_m}{(1+v_mP_{tm})\,ln2} - \Upsilon(t)\,\tau_d P(\overline{H}_0) + \vartheta_m C_{0m}{}' = 0 \qquad (3.41)$$

$$Subject \;\; to \qquad : \qquad (3.30a) \text{and}(3.30b) \qquad (3.41\;a)$$

$$: \qquad log_2(1+v_mP_{tm}) = R_{th} \qquad (3.41\;b)$$

After Solving (3.41), we have the water filling solution

$$P_{tm}{}^4 = \left[\frac{C'}{\left(\Upsilon(t)\,\tau_d P(\overline{H}_0) - \vartheta_m C_{0m}{}'\right)ln2} - \frac{1}{v_m}\right]^+ \qquad (3.42)$$

So, $P_{tm}{}^4$ in (3.42) consists of the dual variable ϑ_m in the denominator. But it is clear that there is no common water level for this solution. However, we have approached this solution in a clever way. In this case, the optimal solution occurs on the plane in (3.41 b) which is equivalent to

$$P_{tm}{}^4 = \left[\frac{C'}{\Upsilon(t)\,\tau_d P(\overline{H}_0)\,ln2} - \frac{1}{v_m}\right]^+ \quad or \quad P_{tm}{}^4 = \left[\frac{\left(2^{R_{th}}\right)}{v_m} - \frac{1}{v_m}\right]^+ \qquad (3.43)$$

We have checked all the inequalities conditions given in (3.32 a), (3.32 b) and (3.32 c). Also, we have evaluated the exact power allocations for the four cases. Then, we incorporate these four cases into a single **Algorithm** 3.3 to decide transmission power P_t for **Algorithm** 3.2. For convenience, we consider that $P_1 = \frac{C'}{\Upsilon(t)\tau_d P(\overline{H}_0)ln2}$,

$P_2 = \frac{P_{tmax}}{M} + \frac{1}{M}\sum_{m=1}^{M}\frac{1}{v_m}$, $P_3 = \frac{I^* + \sum_{m=1}^{M}\frac{|h_{sdm}|^2}{v_m}}{\sum_{m=1}^{M}|h_{sdm}|^2}$, $P_4 = \frac{\left(2^{R_{th}}\right)}{v_m}$. **Algorithm** 3.3 defines the power allocation to the mth SU. By following the same steps the power allocations to all the M SUs are calculated. A flowchart is given in Figure 3.3 that summarizes our proposed approaches for optimal resource allocation in designing the energy-efficient CRN.

Algorithm 3.3 EPA algorithm.

Input:

 $\Upsilon(t)$ from **Algorithm** 3.2.

Output:

 Power allocated to the mth SU $P_{tm}(t)$.

1: Evaluate $\left(\frac{C'}{\Upsilon(t)\tau_d P(\overline{H}_0)ln2} \right)$.

2: **if** $((P_1 < P_2)\&\&(P_1 < P_3)\&\&(P_1 > P_4)) \parallel ((P_1 == P_2)\&\&(P_1 == P_3))$ **then** ▷
 (Here, the condition (3.32c) is excluded because ϑ_m for all $m \in M$ does not satisfy
 the water level solution.)

3: $P_{tm} = P_{tm}{}^1$;

4: **else**

5: **if** $(P_1 = P_2) \&\& (P_1 < P_3)\&\&(P_1 > P_4)$ **then**

6: $P_{tm} = P_{tm}{}^2$;

7: **else**

8: **if** $(P_1 < P_2) \&\& (P_1 = P_3)\&\&(P_1 > P_4)$ **then**

9: $P_{tm} = P_{tm}{}^3$;

10: **else**

11: $P_{tm} = \left[\frac{C'}{(\Upsilon(t)\tau_d P(\overline{H}_0)+\theta+\mu I_{total}\sum_{m=1}^{M}|h_{sdm}|^2)ln2} - \frac{1}{v_m} \right]^+$;

12: **end if**

13: **end if**

14: **end if**

3.5.4 Complexity analysis

In IDM algorithm, let N_A and N_B be the number of iterations required to converge the fractional programming based on Dinkelbach method and to update the Lagrangian multipliers θ and μ, respectively. Therefore, the overall complexity is $O(N_A N_B log_2 \left| \frac{\Delta\tau}{\phi} \right|)$, where $\Delta\tau$ is the difference between lower and upper bound of the sensing time and $\phi = 10^{-6}$ is a small integer representing the minimum accuracy allowed in golden section search algorithm. The joint optimization through exhaustive search method has polynomial time complexity. Further, at each iteration of IDM algorithm, complexity may vary depending upon the Cases in **Algorithm** 3.3. If $P_{tm} = P_{tm}{}^1$, then $N_B = 0$. So, the complexity is reduced to $O(N_A log_2 \left| \frac{\Delta\tau}{\phi} \right|)$. Hence, the aid of **Algorithm** 3.3 in **Algorithm** 3.2 can be employed for solving EE maximization problem with considerably low complexity.
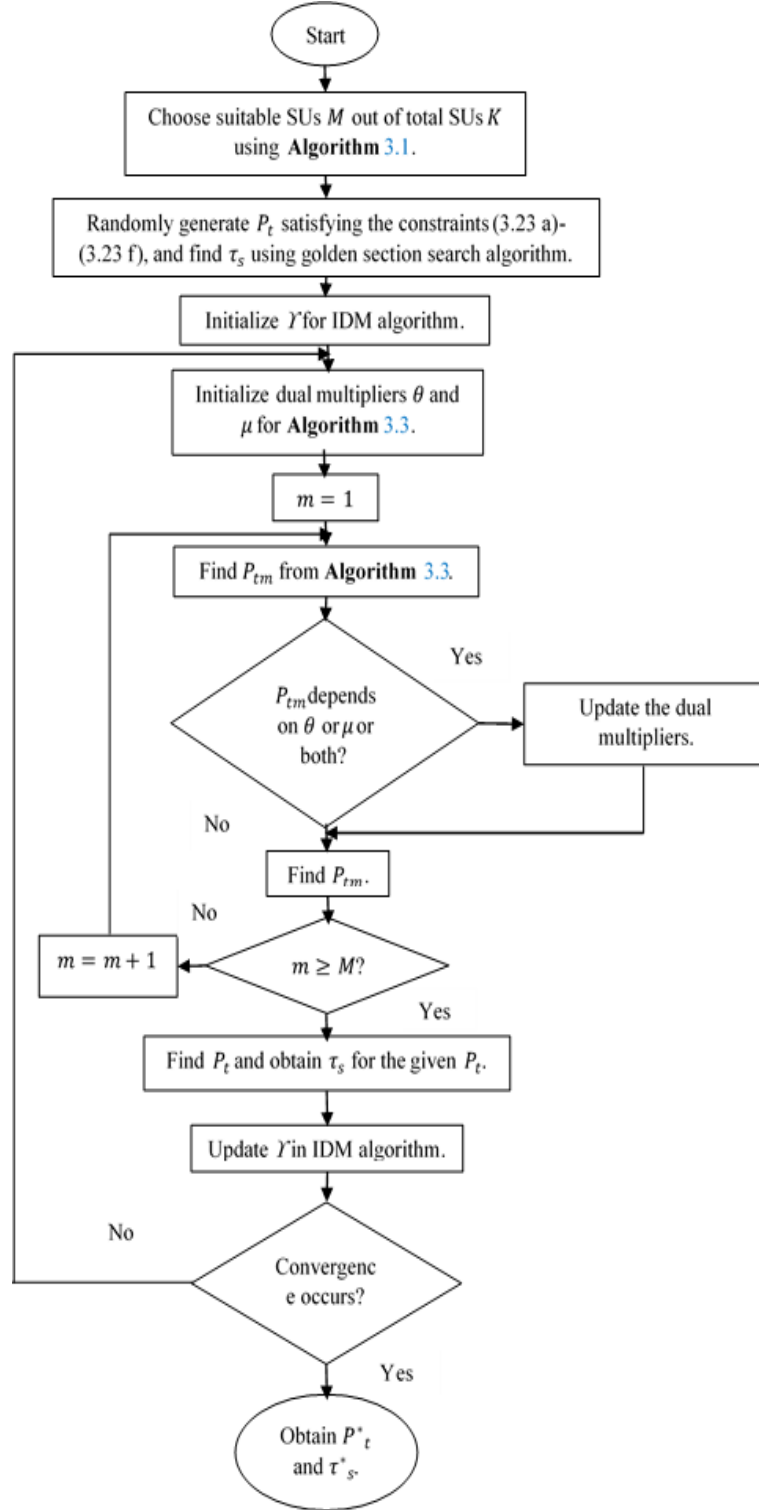
Figure 3.3: Flowchart that summarizes our proposed approach.

3.6   Simulation Results and Discussion

In this section, we present the extensive simulation results to evaluate the performance of our proposed algorithm over different system key parameters. We consider a CRN, where K=20 SUs are distributed around the centrally located PU in a circular area of

radius 1000m. Out of this K SUs suitable M SUs are chosen. The PR is present within the circular radius of 200m. The SRs are distributed randomly around the PU over the circular ring of radius in between 1000m to 1500m. We assume that σ_s^2=1. In the simulation results, some common parameters are used which are summarized in Table 3.1.

Table 3.1: Simulation Parameters

Simulation Parameters	Value
Noise power N_p	-80 dBm
Sensing power P_s	-20 dBm
Path-loss coefficient α	3
u	0.5
v	0.5
Frame duration Γ	0.01sec
Reporting duration τ_r	5μs
Target detection probability $\bar{Q}_d$	0.9
$\gamma_m \forall \in M$	-20dB
Sampling frequency f_s	6MHz

Figure 3.4 illustrates the benefits of selecting suitable SUs for improving the detection performance. Based on the channel gains between the PU and the SUs, here, M=6 SUs are chosen out of the total 20 SUs by employing step-9 of **Algorithm** 3.1. Further, the comparisons of double threshold-based SDF scheme (Scheme-I) with the existing single threshold-based SDF scheme [91] (Scheme-II), double threshold-based OR fusion HDF scheme [128] (Scheme-III) and double threshold-based AND fusion HDF scheme [128] (Scheme-IV) are demonstrated. Though at the low SNR condition, OR fusion-based SS scheme performs better than the other techniques but after SNR=-20 dB double threshold-based SDF scheme outperforms the other schemes. At SNR=-18 dB, Scheme-I offers approximately 7% improvement in detection performance over Scheme-II. Further, in Scheme-I, Q_d is improved by 14% at SNR=-18 dB by the inclusion of suitable SUs. However, the selected SUs based on their channel gains provide better detection performance in all the schemes. For this plot, we set target false alarm probability $\bar{Q}_f(\lambda_{g2})$=0.001 and δ=0.5.

For rest of the figures, we set $\bar{Q}_d(\lambda_{g1})$=0.9 from which $\tilde{Q}_f(\lambda_{g1})$ and $Q_f(\lambda_{g2})$ are calculated. Figure 3.5 shows optimal M and S_{Rmin} for different SNR conditions at δ=0.05, δ=0.1 and δ=0.5. It is clearly observed that by employing Step 1-8 of **Algorithm** 3.1, M and S_{Rmin} decrease as SNR increases. When SNR is increased by 20 dB (-30 dB to -10 dB), M and S_{Rmin} are reduced by 66% and 36%, respectively. So, for the given value of SNR, the unnecessary involvement of all K SUs can be avoided by choosing only M SUs. At the high SNR, the PU can easily be detected, hence the number of SUs requirement is very less.
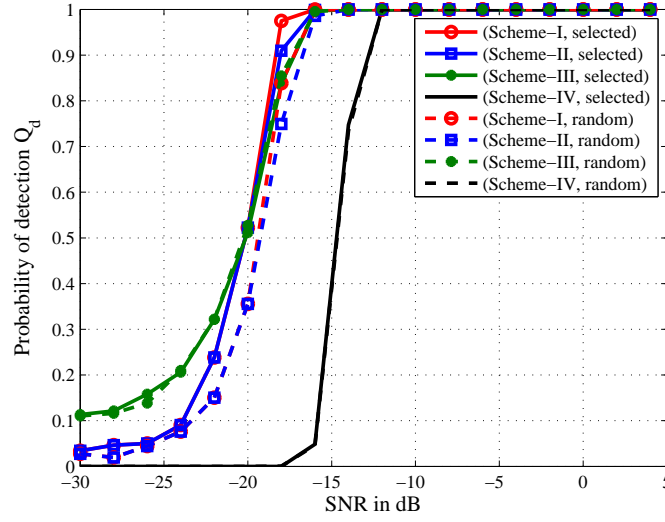
Figure 3.4: Q_d vs SNR for selected and random SUs.
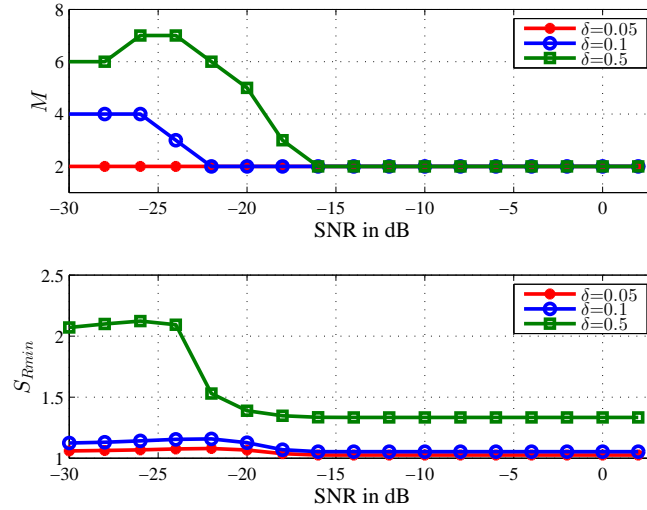
Figure 3.5: Variation of optimal number of SUs and minimum sensing rounds S_{Rmin} against SNR.

Figure 3.6 illustrates the optimal sensing time versus SNR for M=6 and M=15 considering δ=0 and $\delta = 0.5$. The M SUs are chosen randomly from the total K SUs. It is clearly noticed that at higher SNR more number of SUs require less sensing time. Further, at SNR= -24 dB nearly 3.4 msec out of 10 msec is spent for SS, hence at low SNR larger portion of the total frame period has been allocated for SS than at high SNR. So, system throughput is less at low SNR condition. Further, it is noticed that both single and double threshold-based FC decision making schemes show similar performance.
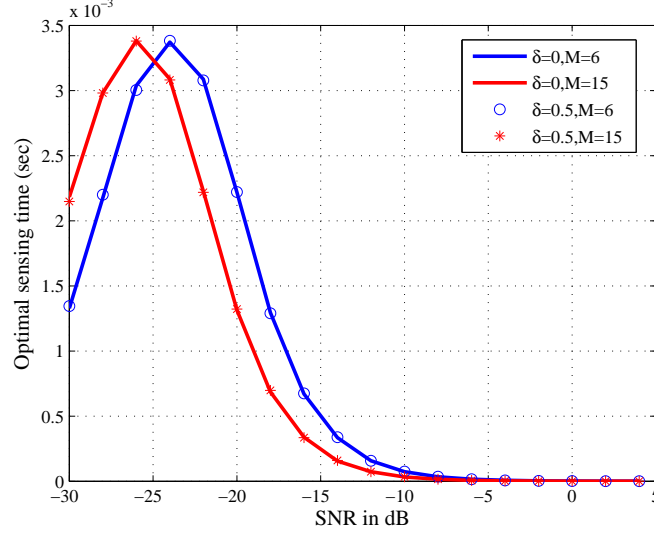
Figure 3.6: Optimum sensing time vs SNR for *M*=6 and *M*=15.

Figure 3.7 shows the convergence comparison of our proposed scheme with the other existing schemes. In Scheme I, the iterative process discussed in [119] is used for optimizing both sensing time and power allocation. In Scheme II, IDM algorithm is used for joint optimization of sensing time and transmission power but the exact power allocation for step-2 of **Algorithm** 3.2 is calculated directly from the water filling solution given in step 11 of **Algorithm** 3.3. In Scheme III, PSO algorithm is used for evaluating the optimal power allocation as in [117]. In Scheme IV, the method of optimizing both sensing time and transmission power allocation is obtained by employing Bi-Section search method as discussed in [114] . In our proposed scheme, both **Algorithm** 3.2 and **Algorithm** 3.3 are used. For this simulation, we set SNR = -20 dB, I_{th} = -70 dBm, R_{th} = 2 bits/s/Hz and O_{th} =0.05. For double threshold-based scheme we take δ=0.5. We set *M*=6 for both single and double threshold-based detection. It is clearly noticed that our proposed scheme outperforms the other existing schemes. After convergence in the proposed scheme, for double threshold method, EE is improved by 27% compared to the single threshold-based detection method. Further, EE obtained by the proposed scheme is improved by 3% with respect to Scheme II in single threshold-based detection scheme.

Though our proposed scheme performs almost same as Scheme II, but the complexity of our proposed algorithm lies between Scheme I and Scheme II. The resource allocation procedure in Scheme II has a constant complexity of $O(N_A N_B log_2 \left| \frac{\Delta \tau}{\phi} \right|)$. But the complexity of our proposed scheme may be same or less than Scheme II depending upon the conditions given in **Algorithm** 3.3. Though the complexity of our proposed method is more than Scheme I which is $O\left(N_A log_2 \left| \frac{\Delta \tau}{\phi} \right|\right)$ but in terms of performance our method gives significant improvement in EE with the

same simulation parameters. Hence, both **Algorithm** 3.2 and **Algorithm** 3.3 jointly provides better performance with considerably less complexity.
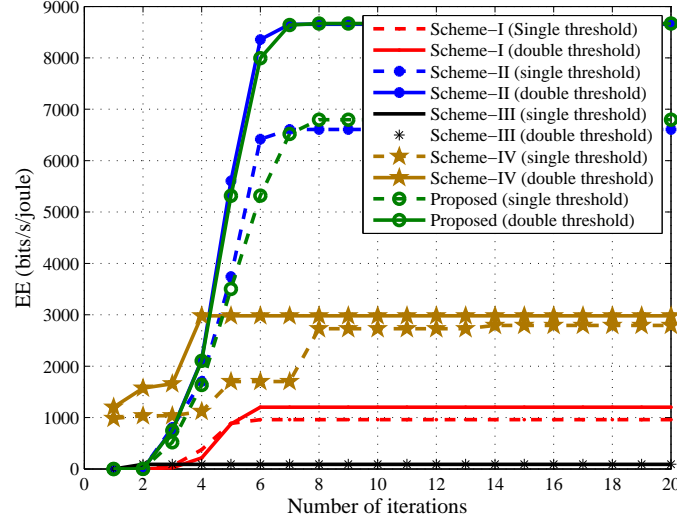
Figure 3.7: Convergence comparison of our proposed scheme with the other existing schemes.

Figure 3.8 demonstrates the benefit of selecting suitable SUs employing step 10 of **Algorithm** 3.1. In Scheme-I and in Scheme-II, the SUs are distributed in a circular area of radius 1000m and 500m, respectively. It is reasonable that the SUs present nearear to the PU consume less power because the minimum and maximum allowable powers are inversely proportional to the channel gains which ultimately depend on the distance between the terminals. So, when distance between the PU and the SU decreases, its corresponding channel gain increases, hence power assigned to the SU decreases which decreases the system throughput. Therefore, system throughput is decreased by 24% in Scheme-II at SNR=-11 dB. Further, it is observed that at SNR=-11 dB, system throughput using selected SUs is increased approximately by 8% when compared to the randomly selected SUs in Scheme-I.
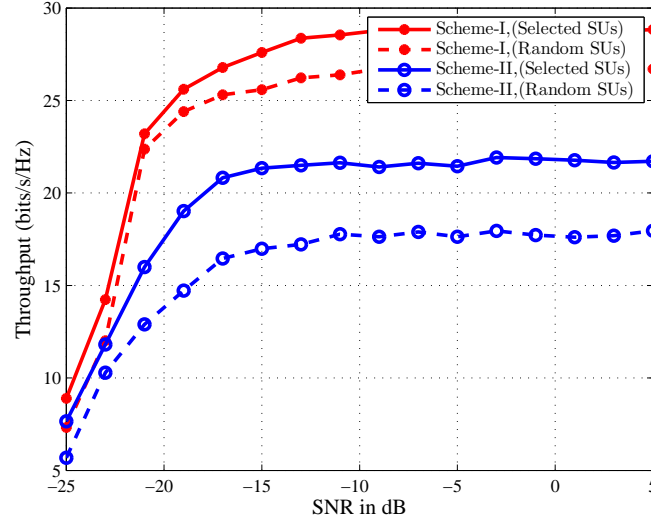
Figure 3.8: Effect of SNR on $R(\tau_s, P_t)$ for selected and randomly chosen SUs.

Figure 3.9 illustrates the impact of interference threshold I_{th} on the maximum EE and maximum system throughput for two different SNR conditions in both double and single threshold-based FC decision making schemes. It is observed that as I_{th} increases, $EE(\tau_s, P_t)$ decreases but $R(\tau_s, P_t)$ increases. This indicates that with the increase in I_{th}, maximum allowable transmission power increases as per (3.23 b), so EE decreases but throughput increases as transmission power increases. From Figure 3.9a, it is observed that the $R(\tau_s, P_t)$ is slightly higher in SNR= -20 dB than the SNR= -10 dB. This is because by employing **Algorithm** 3.1 for double threshold scheme, the number of SUs decreases with increase in SNR as shown in Figure 3.5. More SUs consume more power, hence throughput increases. But, in Figure 3.9b, we set M=6, and it shows the actual impact of SNR on system throughout. So, with rise in I_{th} by 4 dBm i.e from -60 dBm to -56 dBm, EE is reduced by 6% but throughput is increased by 8% for SNR=-10 dB. For, Figure 3.9, we take N_p=-100 dBm.
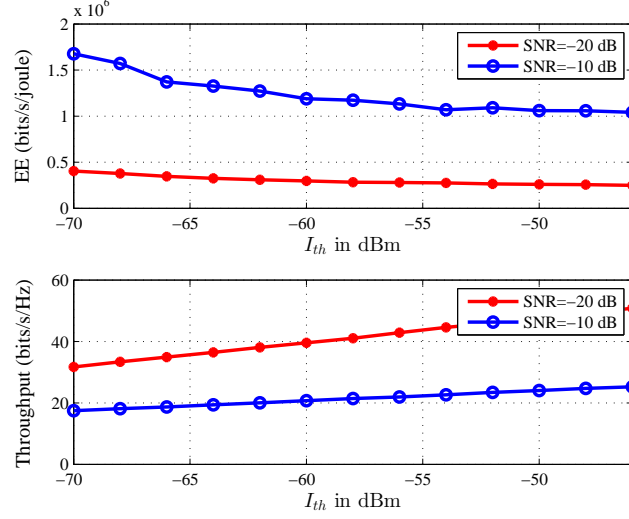
(a) Double threshold-based FC decision making scheme employing **Algorithm** 3.1.
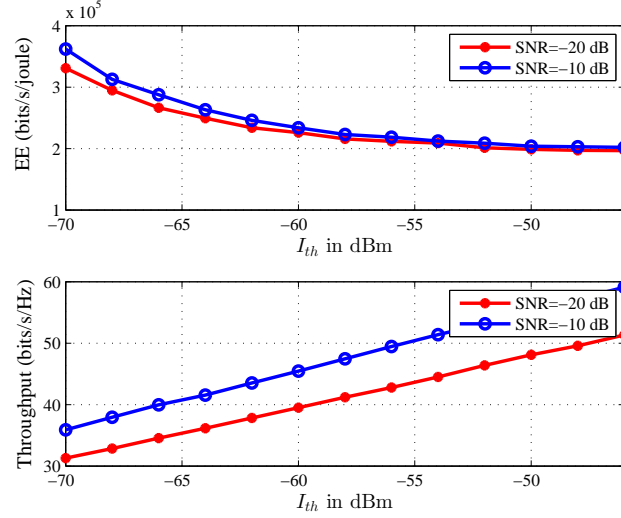
(b) Single threshold-based FC decision making scheme *M*=6.

Figure 3.9: Variation of $EE(\tau_s, P_t)$ and $R(\tau_s, P_t)$ against the interference threshold I_{th} for SNR=-20 dB and -10 dB.

Figure 3.10 shows the effect of R_{th} on the maximum EE and system throughput for δ=0.3 and δ=0.8. It is observed that EE decreases with increase in R_{th}. This is because as R_{th} increases, minimum required transmission power increases which leads to minimization of EE. So, at δ=0.8, when R_{th} is increased by 0.4 bits/s/Hz from 1.1 bits/s/Hz to 1.5 bits/s/Hz, EE is reduced by approximately 13%. Meanwhile, system throughput shows very gradual increase with R_{th}. Further, as δ increases both $EE(\tau_s, P_t)$ and $R(\tau_s, P_t)$ increase. Hence, when δ is raised from 0.3 to 0.8 at R_{th}=1.5 bits/s/Hz, both EE and system throughput are improved by 8% and 84%, respectively.
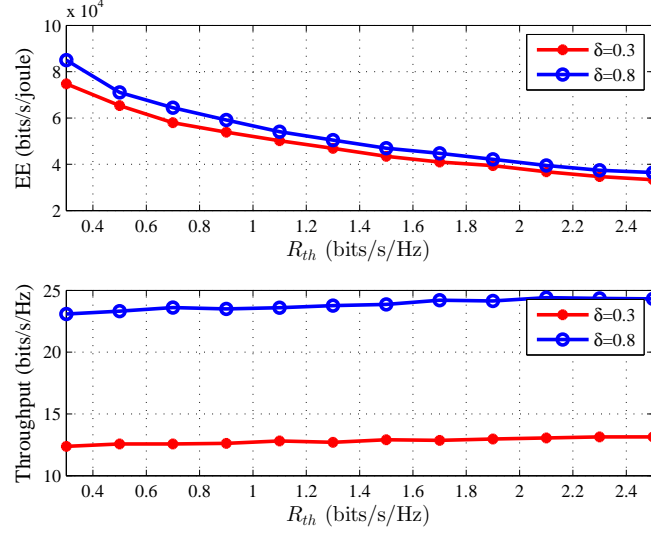
Figure 3.10: Effect of R_{th} on $EE\left(\tau_s, P_t\right)$ and $R\left(\tau_s, P_t\right)$ for different values of δ.

Figure 3.11 presents the effect of the number of cooperative SUs on maximum EE, system throughput and total power consumption for I_{th}=-70 dBm and -40 dBm considering the single threshold-based detection scheme. It is obvious that $EE\left(\tau_s, P_t\right)$ decreases with increase in the number of SUs but both $R\left(\tau_s, P_t\right)$ and $P_T\left(\tau_s, P_t\right)$ increase. This is reasonable because more SUs lead to more power consumption. However, the rate of decrease in EE does not change significantly after a certain number of SU though the transmission power increases. It is observed that when number of SUs increases from 5 to 10 at I_{th}=-70 dBm, EE decreases by only approximately 11% but both system throughput and power consumption increase by 44% and 73%, respectively. Hence, an energy-efficient model can be designed by selecting suitable number of SUs to avoid unnecessary power consumption. For this figure, the SUs are chosen randomly from the total SUs. We set N_p=-100 dBm.

Figure 3.12 presents the variation of EE and system throughput for different values of $\bar{Q}_d$ comparing the single and double threshold-based fusion schemes. We set M=6. It is clearly observed from (3.14) and (3.21) that both $R\left(\tau_s, P_t\right)$ and $P_T\left(\tau_s, P_t\right)$ are decreasing functions of $\bar{Q}_d$. This is because as $\bar{Q}_d$ increases, Q_f also increases for the given value of δ. Hence, $\left(1 - Q_f\right)$ decreases, so both throughput and total power consumption decrease. As EE is the ratio of $R\left(\tau_s, P_t\right)$ and $P_T\left(\tau_s, P_t\right)$, hence variation of EE with respect to $\bar{Q}_d$ depends on the rate of decrease of these parameters. Further, we can have 10% and 17% improvements in EE and throughput by employing double threshold-based detection scheme if we set $\bar{Q}_d$=0.9.
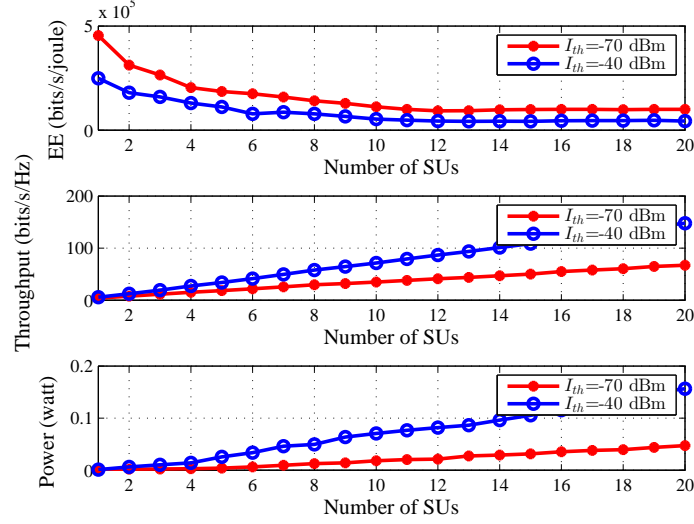
Figure 3.11: Variation of $EE\left(\tau_s, P_t\right)$, $R\left(\tau_s, P_t\right)$ and total sum of transmitting power w.r.t the number of SUs.
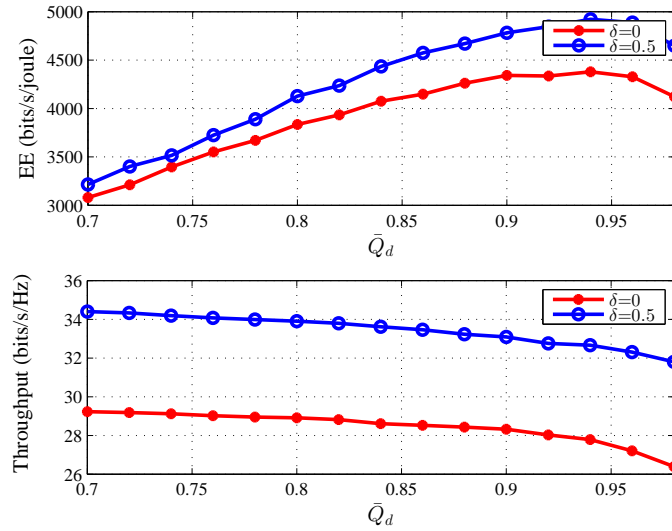
Figure 3.12: Variation of $EE\left(\tau_s, P_t\right)$ and $R\left(\tau_s, P_t\right)$ w.r.t $\bar{Q}_d$.

3.7 Summary

This chapter focused on maximization of EE for single and double threshold based CSS schemes satisfying the constraints of interference to the primary network, outage to the secondary network, maximum secondary transmission power and minimum achievable data rate considering the target detection probability. In double threshold-based detection scheme, the final decision was obtained at the cost of more sensing rounds made by the SUs. An efficient algorithm was proposed to select the suitable number of SUs based on the sensing rounds. The eligible SUs both for SS and

data transmission were selected based on their channel gains. The non-linear and non-convex EE maximization problem was solved by parametric transformation based on Dinkelbach method. A novel IDM algorithm was proposed for joint optimization of sensing time and power allocation. The exact power allocation to the SUs for the given sensing time was obtained by our proposed EPA algorithm. Further, the performances of our proposed schemes were validated by comparing with the other existing schemes, and it is observed that our scheme can solve the EE maximization problem with less complexity. Thus, it can be concluded that EE increases with SNR and threshold difference, and the system throughput increases with throughput threshold, number of SUs, SNR, threshold difference and interference threshold. So, with the proper selection of the system parameters a trade-off between EE and throughput could be obtained in the CRN. In this chapter, the system model did not consider any effect of the MUs in the CR environment. The characteristics of CR allow more active attackers in the CRN. Those attackers either degrade the CR performance or use the spectrum by deception for their own purposes. The attacker signal may cause interference to the secondary transmission. Hence, power allocation to the SUs considering the negative impacts of the attacker is one of the challenging issues which needs to be addressed.

Chapter 4

Proposed Approaches for Energy-Efficient Resource Allocation in the CRN with the Primary User Emulation Attack

This chapter focuses on solving the EE maximization problem both in the single and double threshold-based SDF CSS CRN considering the presence of PUEA. The highlights of the chapter are

- The negetive impact of the attacker on the secondary transmission is investigated.

- A suitable SUs' selection algorithm is proposed for both SS and data transmission.

- An efficient algorithm is proposed to obtain the sensing time maintaining the trade-off between throughput, transmission delay and false alarm probability.

- A novel iterative method is proposed for joint optimization of sensing time and power allocation to the SUs.

4.1 Introduction

I N the DSA environment, the PU always uses the authorized frequency band, and the SUs can utilize this spectrum band when the PU is not using it. So, SS process facilitates the SUs to identify the unoccupied bands and vacate the bands as the PU returns. However, correct decision of the SUs can not be guaranteed in the hostile wireless environment always. One of the serious attacks in the CRN is PUEA. In PUEA, the attacker generates the similar type of signal as the PU to make an error in the frequency band and to confuse the SU. So that the SUs erroneously identify the attacker as the PU, and vacate the spectrum band immediately. PUEA can produce serious interference to the SS and significantly reduces the available channel resources. It also imposes an excessive interference to the SUs transmission, thus forcing the SUs to transmit with high power thereby causing interference to the PU. Mainly, the attack is characterized as malicious/obstructive attack and selfish/greedy attack [36].

- Malicious Attack:- The attacker only launches PUEA on the spectrum band.

- Selfish Attack:- The attacker prevents other SUs from using the idle spectrum band by launching PUEA and reserves those bands for its own profit.

In the multi-hop channel environment, if PUEA is launched and there is no idle channel for SU, then the call is dropped or delayed [129]. A dropped call results in unreliable communication and the delayed call degrades the QoS. In the adverse environment, almost all the channels are affected by both MUs and greedy users [130]. Prevention of PUEA is vital in CRNs. On the other hand, complete elimination of these attacks is impossible in the real-time wireless environment. Another important aspect in CR system is the EE maximization for enhancing the battery life of low-powered cognitive terminals. So, for reliable data transmission with sensing accuracy, proper resource allocation in the presence of MUs is not only an important task but also is very difficult to solve. These can be achieved by carefully chosing the sensing time and eligible SUs for enhancing both EE and detection probability.

4.1.1 Related works

As far as the reliability is concerned, it is a challenging task to detect the PU accurately in the event of a PUEA [131]. So, several methods have been proposed in the literature to differentiate the PUEA and the PU signal. In [132], detection probability of the PU was maximized by optimally combining the weights with the received signal under the constraint of false alarm probability. The performance metrics for the CSS considering the presence of smart PUEA were derived in [133] and an optimal weight combining scheme was proposed to improve the detection performance in the same scenario in [134]. In [135], the authors presented an analytical model to detect the attacker. Here, Fenton's approximation was used to calculate the mean and variance of the received signal at the SUs from both PU and the attacker, and Wald's sequential probability ratio test (WSPRT) was used to detect PUEA. A location verification scheme was proposed in [136], where the Time Difference of Arrival (TDoA) method was used to detect the difference of time of arrival of the signals at the receiving terminals. However, this method required the deployment of extra anchor nodes. When the attacker was present nearer to the PU, Dang et al. proposed a new two-phase detection algorithm in [137], which distinguished between the PU and the attacker from the characteristics of the transmitted signal from the PU and difference of received power in the presence of attacker and noise. Further, in the presence of multiple PUE attackers, the authors proposed optimal weight combining scheme to improve the detection performance [138]. It is obvious that spurious signal from the PUEA increases the probability of error in the CRN. This can be minimized by obtaining the optimal threshold [139].

For power allocation in the presence of the attacker, Haghighat et al. in [140] and Du et al. in [141] proposed an optimal power allocation scheme in OFDM based CR for maximizing system throughput under the constraint of interference power to the PU. In [142], the detection performance and the system throughput were maximized in the multiband CSS scenario under the constraint of interference to the primary network. For the soft combination scheme, the detection performance was improved by optimizing the decision threshold and the weight coefficients. In the hard combination scheme, probability of detection was maximized by the optimal number of SUs and the decision threshold. Then, the system throughput was improved by considering the optimized parameters. In order to effectively distinguish between the PU and PUEA, the authors proposed an advanced encryption standard (AES) algorithm in the OFDM-based CRN, and the transmission rate was maximized through the suboptimal energy harvesting technique [143].

However, none of these methods discussed joint optimization of sensing time and

power allocation for EE maximization considering the attacker's presence. Further, delay in data transmission is not considered anywhere. Hence, energy-efficient resource allocation schemes in the presence of PUEA need to be explored to meet the challenges of successful deployment of CR in the adversarial environment.

4.1.2 Chapter contributions and organization

The main contributions are summarized below.

- The SDF-based system model is designed in the presence of an attacker for single and double threshold-based sensing schemes.

- Different constraints are evaluated considering different issues arise in the presence of the attacker.

- The solution approach to the EE maximization problem is started with the selection of eligible SUs for SS and data transmission.

- The non-linear optimization problem with non-convex constraints are solved by the novel iterative algorithm called NIRA in which the sensing time is obtained for maximum throughput, minimum false alarm probability, and minimum delay. The power allocation is obtained from an efficient algorithm which is the combination of fractional programming, dual decomposition method, and DC programming.

- To further reduce the complexity, the EE maximization problem with the associated constraints is solved by NARA algorithm which is based on well-established NLMS algorithm.

- The performances of our proposed algorithms are validated through the simulation results. The impact of different system parameters on EE and throughput is studied in detail for both single and double threshold-based SS schemes.

The chapter is structured as follows. Section 4.2 describes the system model with the detailed analysis of the performance metrics for both single and double threshold-based decision-making schemes. The problem formulation along with the different constraints is given in Section 4.3. Section 4.4 presents our proposed solution approaches. Comparative study and simulations results are demonstrated in Section 4.5. A summary of the chapter is presented in Section 4.6.

4.2   System Model

Let K SUs are distributed randomly in the CRN, out of which only M SUs are chosen. The attacker coexists with the other users and tries to emulate the PU's characteristics. So, it is present nearer to the PU. The CSS is performed by the M SUs each consisting of single ED for deriving individual decision regarding the presence of the PU. The PUE attacker purposely follows the same distribution as PU to prevent the SUs from accessing the licensed band. Each SU receives the signal from the PU and the PUE attacker.

4.2.1   Single threshold-based SS scheme

The CSS system model employing single threshold-based FC decision making scheme is shown in Figure 4.1. Let $s_a(n)$ be the transmitted signal from the attacker at nth instant. The received signal at each mth SU is expressed as four hypothesis tests which are as follows

$$x_m(n) = \begin{cases} s(n)h_{psm} + \beta s_a(n)h_{asm} + \eta_m(n), & (H_1, A_1) \\ s(n)h_{psm} + \eta_m(n), & (H_1, A_0) \\ \beta s_a(n)h_{asm} + \eta_m(n), & (H_0, A_1) \\ \eta_m(n), & (H_0, A_0) \end{cases} \tag{4.1}$$
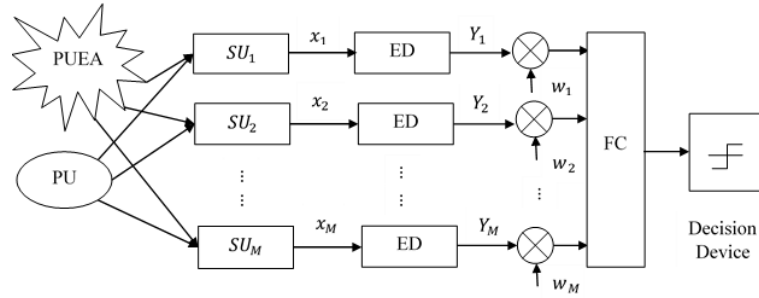
Figure 4.1: SDF-based detection scheme in the presence of PUEA.

A_0 and A_1 represent the absence and presence of the attacker, respectively. β is the probability of attacker's presence in the licensed band. The attacker tends to follow the similar type of signal as PU with zero mean and variance σ_a^2. h_{asm} is the sub-channel coefficient between the attacker and the mth SU. The sub-channel between the terminal is assumed to follow the Rayleigh fading distribution and is given by $h_{asm} \sim \aleph\left(0, \frac{1}{d_m^\alpha}\right)$. The summary statistic of each SU is same as (2.12). The SNR of the PU received at mth SU in the absence of the attacker is given by γ_m. However, γ_m gets reduced due to superimposition of the PUE attacker signal on the licensed band, and the attacker's

signal acts as the noise to the received signal. So, the SINR γ_{am} is given by

$$\gamma_{am} = \frac{\sigma_s^2 |h_{psm}|^2}{\sigma_{\eta m}^2 + \beta |h_{asm}|^2 \sigma_a^2} \tag{4.2}$$

According to the central limit theorem, for the large value of N the local test statistic is approximated by the Gaussian distribution. So, mean and variance of the test statistic for the four possible hypotheses are given by

$$E[Y_m] = \begin{cases} \sigma_{a\eta m}^2 (1 + \gamma_{am}), & (H_1, A_1) \\ \sigma_{\eta m}^2 (1 + \gamma_m), & (H_1, A_0) \\ \sigma_{a\eta m}^2, & (H_0, A_1) \\ \sigma_{\eta m}^2, & (H_0, A_0) \end{cases} \tag{4.3}$$

and

$$Var[Y_m] = \begin{cases} \frac{2\sigma_{a\eta m}^4}{N}(1 + 2\gamma_{am}), & (H_1, A_1) \\ \frac{2\sigma_{\eta m}^4}{N}(1 + 2\gamma_m), & (H_1, A_0) \\ \frac{2\sigma_{a\eta m}^4}{N}, & (H_0, A_1) \\ \frac{2\sigma_{\eta m}^4}{N}, & (H_0, A_0), \end{cases} \tag{4.4}$$

respectively. Here, $\sigma_{a\eta m}^2 = \sigma_{\eta m}^2 + \beta |h_{asm}|^2 \sigma_a^2$. It is assumed that the distances of the PU and the attacker from the SUs are known to the SUs. Thereby full channel state information is known to the SUs prior to the SS and data transmission. It is assumed that the attacker is present all the time during the SS and data transmission. So, the Q_d and Q_f are represented by (2.26) and (2.27), respectively but γ_m and $\sigma_{\eta m}^2$ are replaced by γ_{am} and $\sigma_{a\eta m}^2$, respectively.

4.2.2 Double threshold-based SS scheme

In Chapter 3, double threshold was employed at the FC. Accordingly, all the SUs perform sensing round, and the final decision is made. To further improve the detection performance, double threshold-based ED is employed at each CR. Let there are total K SUs are present in the CRN and if the test statistic of the kth SU Y_k lies on either side of the thresholds, it sends "0" or "1" depending on its decision to the OR-logical FC. But, when Y_k lies in the confusion area, the kth SU sends its corresponding Y_k to the SDF-based FC. In constrat to [144], here, double threshold is applied in the SDF-based FC to make the final decision in term of "0" or "1". Finally, all the binary decisions are combined through the OR-logic. So, this technique is termed as Hybrid MRC-OR double threshold technique which is shown in Figure 4.2.
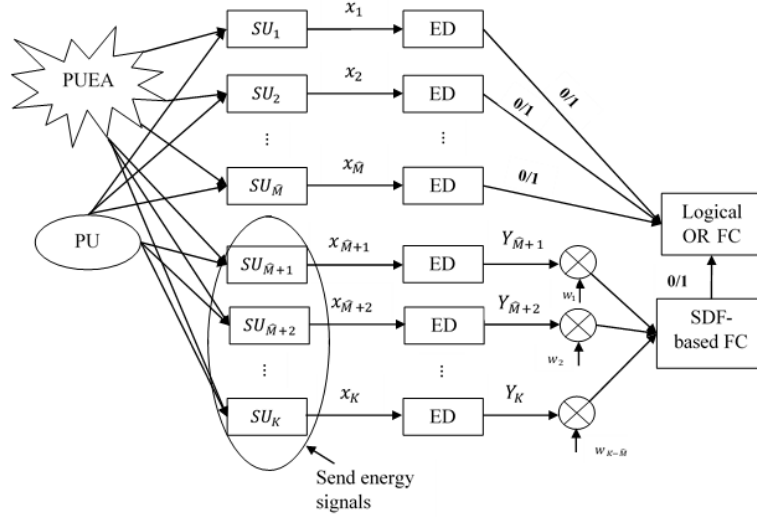
Figure 4.2: Double threshold-based CSS scheme in the presence of PUEA.

If λ_1 and λ_2 be the two local thresholds, then, $Y_k \leq \lambda_1$ and $Y_k \geq \lambda_2$ represent the idle and busy state of the licensed band, respectively. So, the detection probability and false alarm probability of the kth SU are given by

$$P_{d,k} = Q\left(\frac{\lambda_1 - \sigma_{a\eta k}{}^2(1+\gamma_{ak})}{\sigma_{a\eta k}{}^2\sqrt{2(1+2\gamma_{ak})}}\sqrt{N}\right) \tag{4.5}$$

and

$$P_{f,k} = Q\left(\frac{\lambda_2 - \sigma_{a\eta k}{}^2}{\sigma_{a\eta k}{}^2\sqrt{2}}\sqrt{N}\right), \tag{4.6}$$

respectively. λ_2 is evaluated to keep $P_{f,k} < 0.5$. When $\lambda_1 < Y_k < \lambda_2$, the kth SU confuses between the signal and noise and sends Y_k to the FC. If H_k represents the decision statistic of each SU, then

$$H_k = \begin{cases} 0, & Y_k \leq \lambda_1 \\ 1, & Y_k \geq \lambda_2 \\ Y_k, & \lambda_1 < Y_k < \lambda_2 \end{cases} \tag{4.7}$$

Let $\hat{M}$ SUs send hard decision bits, then, the energy values of the $K - \hat{M}$ SUs are linearly combined with the respective weight coefficients to evaluate the global test statistic Y_G. At the single threshold SDF-based FC, the detection probability Q_{SD} for $K - \hat{M}$ SUs is given by

$$Q_{SD} = Q\left(\frac{\lambda_g - \sum_{k=1}^{K-\hat{M}}\sigma_{a\eta k}{}^2(1+\gamma_{ak})w_k}{\sqrt{2\sum_{k=1}^{K-\hat{M}}\sigma_{a\eta k}{}^4 w_k{}^2(1+2\gamma_{ak})}}\sqrt{N}\right) \tag{4.8}$$

where w_k is the weight coefficient assigned to the kth SU. λ_g is calculated by taking Q_{SD}=0.9. Hence the corresponding false alarm probability Q_{FD} is given by

$$Q_{FD} = Q\left[a + b\sqrt{\tau_s f_s}\right] \tag{4.9}$$

where $a = \dfrac{Q^{-1}(\bar{Q}_{SD})\sqrt{2\sum_{k=1}^{K-\hat{M}}\sigma_{a\eta k}{}^4(1+2\gamma_{ak})w_k{}^2}}{\sqrt{2\sum_{k=1}^{K-\hat{M}}\sigma_{a\eta k}{}^4 w_k{}^2}}$ and $b = \dfrac{\sum_{k=1}^{K-\hat{M}}\sigma_{a\eta k}{}^2 w_k \gamma_{ak}}{\sqrt{2\sum_{k=1}^{K-\hat{M}}\sigma_{a\eta k}{}^4 w_k{}^2}}$. To further improve the SS efficiency, the SDF-based FC employs double threshold-based detection technique. So, if Y_G lies between the two thresholds λ_{g1} and λ_{g2}, the $K - \hat{M}$ SUs need to perform more sensing rounds until they reach to any final decision "0" or "1". So, SDF-based FC shows

$$D_I = \begin{cases} 0, & Y_G \leq \lambda_{g1} \\ 1, & Y_G \geq \lambda_{g2} \\ sensing\,rounds, & \lambda_{g1} < Y_G < \lambda_{g2} \end{cases} \quad (4.10)$$

Let, $\delta_{0k} = P_r\{\lambda_1 < Y_k < \lambda_2 | H_0\}$ and $\delta_{1k} = P_r\{\lambda_1 < Y_k < \lambda_2 | H_1\}$ be the probabilities that Y_k lies between λ_1 and λ_2 in the absence and presence of the PU, respectively. Similarly, $\delta_{g0} = P_r\{\lambda_{g1} < Y_G < \lambda_{g2} | H_0\}$ and $\delta_{g1} = P_r\{\lambda_{g1} < Y_G < \lambda_{g2} | H_1\}$ represent the probabilities that Y_G lies between the two global thresholds at SDF-based FC. Then, the overall detection probability Q_d is given by

$$Q_d = 1 - \left[\sum_{\hat{M}=0}^{K}\binom{K}{\hat{M}}\prod_{k=1}^{\hat{M}}(1-P_{d,k})\prod_{k=1}^{K-\hat{M}}\delta_{1k}\left(1-Q_{SD(K-\hat{M})}\right)\right] \quad or$$

$$Q_d = 1 - \left[\sum_{\hat{M}=0}^{K}\binom{K}{\hat{M}}\prod_{k=1}^{\hat{M}}(1-P_{d,k})\prod_{k=1}^{K-\hat{M}}\delta_{1k}\delta_{g1}\left(1-Q_{SD(K-\hat{M})}\right)\right] \quad (4.11)$$

Similarly, the overall false alarm probability Q_f is given by

$$Q_f = 1 - \left[\sum_{\hat{M}=0}^{K}\binom{K}{\hat{M}}\prod_{k=1}^{\hat{M}}(1-\delta_{0k}-P_{f,k})\prod_{k=1}^{K-\hat{M}}\delta_{0k}\left(1-Q_{FD(K-\hat{M})}\right)\right] \quad or$$

$$Q_f = 1 - \left[\sum_{\hat{M}=0}^{K}\binom{K}{\hat{M}}\prod_{k=1}^{\hat{M}}(1-\delta_{0k}-P_{f,k})\prod_{k=1}^{K-\hat{M}}\delta_{0k}\delta_{g0}\left(1-Q_{FD(K-\hat{M})}\right)\right] \quad (4.12)$$

So, the final test statistic is evaluated from the number of reporting bits from the $\hat{M}$ out of the K SUs and from the decision of the SDF-based FC. Hence, the global decision is obtained by employing the OR logic at the FC. This indicates the presence of the PU if any one of the SUs gives "1" i.e

$$G_D = \begin{cases} 1, & \left(D_I + \sum_{k=1}^{\hat{M}} H_k\right) \geq 1 \\ 0, & otherwise \end{cases} \quad (4.13)$$

4.3 Problem Formulation

Similar to Chapter 3, EE of the secondary network is given by (3.22). But, the secondary transmissions are interrupted due to the fake signal transmitted by the attacker. The presence of PUEA signal acts as an interference to the secondary

network, hence average system throughput decreases. We choose *M* SUs out of the *K* SUs for data transmission. For the given value of β, there are two possible scenarios when the SUs intend to transmit their data.

- If the PU is absent, and β=0 or $\beta = c \, (0 < c \leq 1)$: Data transmission takes place when the SUs correctly identify the absence of the PU but the constant presence of the attacker introduces interference to the SRs.

$$R_1 \left(\tau_s, P_t \right) = \frac{\tau_d}{\Gamma} P_{H0} \left(1 - Q_f \right) \sum_{m=1}^{M} log_2 \left(1 + \frac{|h_{srm}|^2 P_{tm}}{N_p + \beta |h_{arm}|^2 \sigma_a{}^2} \right) \qquad (4.14)$$

- If the PU is present, and β=0 or $\beta = c \, (0 < c \leq 1)$: Data transmission takes place when the SUs fail to identify the PU on the licensed band. So, system throughput obtained due to this missed detection Q_{md} is given by

$$R_2 \left(\tau_s, P_t \right) = \frac{\tau_d}{\Gamma} P_{H1} \left(Q_{md} \right) \sum_{m=1}^{M} log_2 \left(1 + \frac{|h_{srm}|^2 P_{tm}}{N_p + \beta |h_{arm}|^2 \sigma_a{}^2 + |h_{prm}|^2 \sigma_s{}^2} \right)$$
$$(4.15)$$

where h_{arm} is the sub-channel coefficient between the attacker and the *m*th SR. Due to presence of both the PU and the attacker, SINR gets reduced in (4.15), hence the system throughput $R \left(\tau_s, P_t \right)$ can be represented as

$$R \left(\tau_s, P_t \right) = R_1 \left(\tau_s, P_t \right) + R_2 \left(\tau_s, P_t \right) \approx R_1 \left(\tau_s, P_t \right) \qquad (4.16)$$

$P_T \left(\tau_s, P_t \right)$ is different for single and double threshold based system model shown in Figure 4.1 and Figure 4.2, respectively. For single threshold-based system model,

$$P_T \left(\tau_s, P_t \right) = \tau_s M P_s + \tau_d P \left(\overline{H}_0 \right) \sum_{m=1}^{M} P_{tm} \qquad (4.17)$$

For double threshold-based system model,

$$P_T \left(\tau_s, P_t \right) = P_s \left(\hat{M} \tau_s + S_R \tau_s \left(K - \hat{M} \right) \right) + \tau_d P \left(\overline{H}_0 \right) \sum_{m=1}^{M} P_{tm} \qquad (4.18)$$

Since the attacker always follows the PU, the secure EE maximization in the presence of potential attacker is very crucial. If the SUs have to achieve the minimum data rate threshold R_{th} both in the presence and absence of the attacker, then it is obvious that in the presence of the attacker, the SUs need to transmit with high power. This may induce interference to the primary network. So, in the next sub-sections, the adverse effects of the attacker during the data transmission are analyzed and accordingly the constraints are formulated while designing the optimization problem.

4.3.1 Total interference constraint

If I_{th} represents the interference power threshold to the PR, then the transmitted power assigned to the M SUs in such a manner that

$$I_{th} - I_{total} \sum_{m=1}^{M} |h_{sdm}|^2 P_{tm} \geq 0 \tag{4.19}$$

where I_{total} is given in (3.10).

4.3.2 Transmission delay constraint

Delay refers to the transmission delay of the SUs which mainly occurs due to the longer sensing time or incorrect identification of PU. Here, an effective delay D_{eff} is calculated which measures the excess delay caused by the SUs in the presence of the attacker. Based on D_{eff}, τ_s is evaluated to minimize D_{eff}. The transmission delay occurs in the following cases.

- D_1: SUs need to perform SS before their data transmission thereby requires τ_s/Γ of duration.

- D_2 and D_3: In the absence of the attacker, delay in data transmission takes place in two possible scenarios. When the PU is absent but falsely detected to be present, the corresponding delay is $P_r(Y_G \geq \lambda_g | H_0, E_0)\, \tau_d/\Gamma$. Similarly, when the PU is present and correctly detected by the SUs, the corresponding delay is $P_r(Y_G \geq \lambda_g | H_1, E_0)\, \tau_d/\Gamma$.

- D_4 and D_5: In the presence of the attacker, delay in transmission occurs when the PU is absent but SUs falsely classifies the attacker signal as PU signal and no data transmission takes place. So, the corresponding delay is $P_r(Y_G \geq \lambda_g | H_0, E_1)\, \tau_d/\Gamma$. Similarly, when both the PU and the attacker are present, and are correctly detected by the SUs; then the corresponding delay is $P_r(Y_G \geq \lambda_g | H_1, E_1)\, \tau_d/\Gamma$.

Hence, the effective delay due to the presence of the attacker is given by

$$D_{eff}(\tau_s) = D_P(\tau_s) - D_A(\tau_s) \tag{4.20}$$

where $D_P(\tau_s) = D_1 + D_2 + D_3$ and $D_A(\tau_s) = D_1 + D_4 + D_5$ represent the delay occurred in the absence and presence of the attacker, respectively. The main objective is to choose τ_s such that sensing duration is same as if there is no attacker present in the CRN. From (4.20), it is clear that $D_{eff}(\tau_s)$ is neither a concave nor convex function of τ_s. Hence, we analyze each part with respect to τ_s to find an effective solution (4.20).

Theorem 3. *For the given target detection probability Q_d, $D_P(\tau_s)$ and $D_A(\tau_s)$ are the convex function of τ_s.*

Proof. Proof of this theorem is given in **Appendix E**. □

So, the purpose is to evaluate sensing time so as to meet

$$\tau_{optP} \approx \tau_{optA} \tag{4.21}$$

where $\tau_{optP} = \underset{\tau_s}{argmin}\ D_P(\tau_s)$ and $\tau_{optA} = \underset{\tau_s}{argmin}\ D_A(\tau_s)$. The detail evaluation procedure is discussed in **Algorithm 4.6**.

4.3.3 Throughput balancing power allocation constraint

The system throughput is reduced due to presence of the attacker's signal. So, the SUs need to transmit with more power to achieve the minimum R_{th} in the presence of the attacker. Hence, we add an extra constraint to the EE maximization problem which balances between the throughput achieved in the absence and presence of an attacker. Let $R_{PA}(\tau_s, P_t)$ and $R_{AA}(\tau_s, \tilde{P}_t)$ represent the throughput obtained in the presence and absence of an attacker, respectively. $\tilde{P}_t$ is the power assigned to the SUs in the absence of an attacker. If same power is assigned to the SUs under these two conditions, then, it is obvious that $R_{AA}(\tau_s, \tilde{P}_t) > R_{PA}(\tau_s, P_t)$. The SUs need to transmit with more power to make $R_{AA}(\tau_s, \tilde{P}_t) \approx R_{PA}(\tau_s, P_t)$. Hence, we employ an adaptive power assignment scheme which not only balances $R_{PA}(\tau_s, P_t)$ and $R_{AA}(\tau_s, \tilde{P}_t)$ but also controls the excessive growth of transmission power. Then, the power balance equation is expressed as

$$C_{Am}(\tau_s, \tilde{P}_t) \approx C_{Pm}(\tau_s, P_t) \tag{4.22}$$

where $C_{Am}(\tau_s, \tilde{P}_t) = log_2\left(1 + \frac{|h_{srm}|^2 \tilde{P}_{tm}}{N_p}\right)$ and $C_{Pm}(\tau_s, P_t) = log_2\left(1 + \frac{|h_{srm}|^2 P_{tm}}{N_p + \beta |h_{arm}|^2 \sigma_a^2}\right)$.

4.4 Proposed Solution Approaches Towards the Secure EE Maximization

In this Section, we discuss the solution approaches towards the problems arise in the presence of an attacker discussed in Section 4.3. There are several factors that directly affect the EE such as the SUs, the sensing time and the transmission power. Furthermore, these SUs directly influence the detection probability and system throughput. Thus, we propose an efficient algorithm to evaluate the lower and upper bound of the number of SUs and also the eligible SUs that balance between the probability of detection and system throughput under the interference constraint. Further, we propose the resource allocation algorithms for maximizing EE satisfying the defined constraints.

4.4.1 SUs selection method

Let $\tilde{P}_{tmin}$ and P_{tmin} be the minimum transmission power of each SU in the absence and presence of the attacker, respectively, where $\tilde{P}_{tmin} = \frac{(2^{R_{th}}-1)N_p}{|h_{sr}|_{max}^2}$ and $P_{tmin} = \frac{(2^{R_{th}}-1)(N_p+\beta|h_{ar}|_{min}^2\sigma_a^2)}{|h_{sr}|_{max}^2}$. $|h_{sr}|_{max}^2 = max\left[|h_{sr1}|^2, |h_{sr2}|^2, \ldots, |h_{srM}|^2\right]$ and $|h_{ar}|_{min}^2 = min\left[|h_{ar1}|^2, |h_{ar2}|^2, \ldots, |h_{arM}|^2\right]$. Following the constraint (4.19), if the CRN consists of only a single SU, then the maximum transmission power is $P_{t\max} = \frac{I_{th}}{I_{total}|h_{sd}|^2}$, then the maximum channel capacity and the maximum power consumption are given by $T_{Rmax} = log_2\left(1+\frac{|h_{sr}|_{max}^2 P_{tmax}}{N_p+\beta|h_{ar}|_{min}^2\sigma_a^2}\right)$ and $T_{Pmax} = P_s\tau_s + \tau_d P\left(\overline{H}_0\right)P_{tmax}$, respectively. However, if we select M SUs, then the maximum allowed transmission power of each SU is $P_{t\max} = \frac{I_{th}}{MI_{total}|h_{sd}|_{min}^2}$, where $|h_{sd}|_{min}^2 = min\left[|h_{sd1}|^2, |h_{sd2}|^2, \ldots, |h_{sdM}|^2\right]$. The minimum required SUs M_L is evaluated so as to maintain a trade-off between the system throughput and EE. The EE and throughput tradeoff metric is given by

$$[T_R]^l \times [E_f]^{(1-l)} = \frac{[T_R]}{[T_P]^{(1-l)}} \tag{4.23}$$

where $l \in [0,1]$. Let M_L SUs participate in data transmission each with transmitting power P_{tmin}. We assume that all M_L SUs achieve R_{th}, then

$$\frac{M_L R_{th}}{[M_L]^{(1-l)}\left[P_s\tau_s + \tau_d P\left(\overline{H}_0\right)P_{tmin}\right]^{(1-l)}} >> \frac{T_{Rmax}}{T_{Pmax}} \tag{4.24}$$

$$M_L >> \left\lceil \left[\frac{T_{Rmax}\left[P_s\tau_s + \tau_d P\left(\overline{H}_0\right)P_{tmin}\right]^{(1-l)}}{T_{Pmax}R_{th}}\right]^{\frac{1}{l}} \right\rceil \tag{4.25}$$

If equal importance is given to the system throughput and EE, then l=0.5. Indeed, the SUs has straightforwardly affected on the spectrum detection and throughput. Since more SUs lead to more power consumption; spectral efficiency directly degrades with the number of SUs. The upper bound of SUs M_U is evaluated to find the maximum number of SUs required to achieve the scenario of without an attacker. Let M_L is calculated taking the equality (4.25), then M_U is calculated from

$$(M_U + M_L)R_{th} - M_L log_2\left(1+\frac{|h_{sr}|_{max}^2 P_{tmax}}{N_p}\right) \cong C_{out} \tag{4.26}$$

C_{out} is user defined integer variable. In the course of system design C_{out} can be varied so as to decide the maximum number of SUs. The purpose of (4.26) is to find the maximum number of SUs required in the presence of an attacker. We assume that $(M_U + M_L)$ SUs, each achieves with minimum throughput threshold R_{th} in the presence of the PUE attacker and M_L SUs each achieves with the maximum throughput in the absence of the attacker. Then, M_U is the maximum number of SUs

that balances between the minimum and maximum throughput achieved in the presence and absence of the attacker, respectively. Since, all the SUs do not transmit with exactly P_{tmin} or P_{tmax}, hence, (4.26) can be reformed as

$$M_U << \lfloor \frac{\bar{C}_{th}}{R_{th}} \rfloor \tag{4.27}$$

where $\bar{C}_{th} = C_{out} + M_L \left(log_2 \left(1 + \frac{|h_{sr}|_{max}^2 P_{tmax}}{N_p} \right) - R_{th} \right)$.

Specifically, the sensing accuracy and EE maximization depend on the locations of the SUs with respect to the PU, the attacker, the PR, and the SRs. So, a common approach is proposed which considers the conflicting scenarios of detection performance and maximum EE. It is obvious that the SUs with high SNR have to be chosen to nullify the effect of interference from the attacker. Hence, it is preferred to choose the SUs that are closer to the PU in relative to the attacker. Another important aspect is to maximize the system throughput with limited interference to the PR. From (4.16) and (4.19), it is clearly noticed that the SUs closer to the SR in relative to the PR enhance the system throughput causing minimum interference to the PR. So, a compromising factor b_k is introduced to measure the balancing efficiency Eff_k of the kth SU, where

$$Eff_k = \frac{b_k}{\sum_{k=1}^{K} b_k} \tag{4.28}$$

and $b_k = \left(\frac{\sigma_{\eta k}^2}{\sigma_{\eta k}^2 + \upsilon \frac{|h_{ask}|^2}{|h_{psk}|^2} + y \frac{|h_{sdk}|^2}{|h_{srk}|^2}} \right)$. Here, υ and y control the detection performance and the system throughput, respectively and $\upsilon + y = 1$. The pseudocode for the SUs selection is described in **Algorithm** 4.4 .

Algorithm 4.4 Eligible SUs selection method.

Input:
>   Decide M.
> $F = [1\ 2]$
> $1 \leftarrow$ during SS
> $2 \leftarrow$ during data transmission

Output:
>   Eligible M SUs.

1: **for** $f = 1 : length(F)$ **do**
2:      **for** $k = 1 : K$ **do**
3:          **if** $(f == 1)$ **then**
4:              $\upsilon > y$;
5:          **else**
6:              Check the values of υ and y;
7:          **end if**
8:          Evaluate b_k;
9:      **end for**
10:     Evaluate Eff_k from (4.28).
11:     Arrange K SUs in the descending order of their Eff_k and choose first M SUs.
12: **end for**

But, this algorithm does not consider the value of β in the compromising factor b_k, so, for double threshold-based scheme during the data transmission, we define Eff_k as per (4.28) where $b_k = \left(\dfrac{1}{1 + \beta \frac{|h_{ark}|^2}{|h_{srk}|^2} + \frac{|h_{sdk}|^2}{|h_{srk}|^2}} \right)$. The pseodocode is provided in **Algorithm 4.5**. This compromising factor b_k is meant for only data transmission.

Algorithm 4.5 Eligible SUs selection method considering the value of β.

Input:
>   Decide M between M_L and M_U.

Output:
>   Eligible M SUs.

1: **for** $k = 1 : K$ **do**
2:      Evaluate $b_k = \left(\dfrac{1}{1 + \beta \frac{|h_{ark}|^2}{|h_{srk}|^2} + \frac{|h_{sdk}|^2}{|h_{srk}|^2}} \right)$;
3: **end for**
4: Evaluate Eff_k from (4.28).
5: Arrange K SUs in the descending order of their Eff_k and choose first M SUs.

4.4.2 Resource allocation

The resource here indicates the obtaining of optimal sensing time and the power allocation to the SUs. The EE maximization problem for the single and double threshold-based detection schemes is solved by taking different constraints.

Single threshold-based detection

In accordance to the constraints discussed in Section 4.3, EE maximization problem is formulated as

$$\underset{\tau_s,\ P_t}{Maximize} \qquad : \qquad \frac{R\left(\tau_s, P_t\right)}{P_T\left(\tau_s, P_t\right)} \tag{4.29}$$

$$Subject \quad to \qquad : \qquad P_{tmax} - \sum_{m=1}^{M} P_{tm} \geq 0 \tag{4.29 a}$$

$$: \qquad I_{th} - I_{total} \sum_{m=1}^{M} |h_{sdm}|^2 P_{tm} \geq 0 \tag{4.29 b}$$

$$: \qquad C_{th} - \left(\tilde{R}\left(\tau_s, \tilde{P}_t\right) - \bar{R}\left(\tau_s, P_t\right)\right) \geq 0 \tag{4.29 c}$$

$$: \qquad \tau_{optP} \approx \tau_{optA} \tag{4.29 d}$$

$$: \qquad Q_f \leq 0.5 \tag{4.29 e}$$

$$: \qquad 0 \leq \tau_s \leq \Gamma \tag{4.29 f}$$

where C_{th} is the user defined integer variable. $\tilde{R}\left(\tau_s, \tilde{P}_t\right) = \sum_{m=1}^{M} C_{Am}\left(\tau_s, \tilde{P}_t\right)$ and $\bar{R}\left(\tau_s, P_t\right) = \sum_{m=1}^{M} C_{Pm}\left(\tau_s, P_t\right)$. EE is maximized by jointly optimizing the sensing time and transmission power. In the optimization problem (4.29), the numerator is concave and the denominator is an affine function of P_t. The combinatorial nature of the constraints makes the optimization problem little difficult to solve. Hence, we separate out the nondependent power constraints (4.29 d), (4.29 e) and (4.29 f) from the optimization problem. Further, it has already been proved from **Appendix B** that the system throughput is a concave function of τ_s, so there exists a unique value of sensing time at which throughput is maximum. Hence, an efficient algorithm is proposed to evaluate optimal sensing time for maximum throughput, minimum delay with lower value of false alarm probability. The pseudo-code for sensing time evaluation is described in **Algorithm 4.6**.

In the practical CR communication environment, $Q_f \leq 0.5$, hence $\left(\frac{a}{b}\right)^2 \frac{1}{f_s} \leq \tau_s$. So, the minimum sensing time is obtained from the equality constraint. This sensing time $t_{\bar{s}}$ is used in the further evaluation of the power allocation. The constraint (4.29 c) in the EE maximization problem (4.29) is neither a concave nor a convex function of P_t. So, we propose an efficient algorithm which is the combination of fractional programming based on parametric transformation, dual decomposition and DC programming for adaptive power allocation. Following the Theorem 2, the NIRA

algorithm is proposed for joint optimization of τ_s and P_t.

Algorithm 4.6 Evaluation of sensing time.

1: Select most eligible SUs M from **Algorithm** 4.4 taking f=2.
2: Randomly generate transmission power P_t satisfying the constraints (4.29 a) and (4.29 b).
3: $\tau_{\min 1} = \left(\frac{a}{b}\right)^2 \frac{1}{f_s}$.
4: Evaluate $\tau_{optA} = \underset{\tau_s}{argmin}\ D_A(\tau_s)$ by using golden section search method.
5: Evaluate $\tau_{opt} = \underset{\tau_s}{argmax}\ R(\tau_s, P_t)$ by using golden section search method.
6: Calculate $T_{\min} = \min\left\{\tau_{\min 1}, \tau_{opt}, \tau_{optA}\right\}$.
7: Calculate $T_{\max} = \max\left\{\tau_{\min 1}, \tau_{opt}, \tau_{optA}\right\}$.
8: Take $T_s = T_{\min} : \Delta_1 : T_{\max}$. ▷ ($\Delta_1$ is the small incremental factor depending on T_{min} and T_{max}.)
9: **for** $t_1 = T_{min} : \Delta_1 : T_{max}$ **do**
10:     Calculate $D_P(t_1)$;
11: **end for**
12: Find $\tau_{optP} = \underset{t_1}{argmin}\ D_P(t_1)$.
13: $[A, B] = min\left|T_s - \tau_{optP}\right|$.
14: Return $t_{\bar{s}} = T_s(B)$.

Algorithm 4.7 NIRA algorithm for joint optimization of sensing time and power allocation.

Input:
    Select suitable M SUs using **Algorithm** 4.4.
    Find out $t_{\bar{s}}$ using **Algorithm** 4.6.
    Dinkelbach parameter $\Upsilon \leftarrow 0$;
    Acceptance tolerance value $\xi \leq 10^{-5}$;
    Current iteration $t \leftarrow 1$;
Output:
    Optimal sensing time τ_s^* and transmission power P_t^*.

1: **while** $|\Upsilon(t) - \Upsilon(t-1)| \geq \xi$ **do**
2:     For the given value of $\Upsilon(t)$ and $t_{\bar{s}}$, find power $P_t(t)$ from **Algorithm** 4.8 .
3:     For the given $P_t(t)$, find corresponding sensing time τ_{opt}, then find $t_{\bar{s}}$ from **Algorithm** 4.6.
4:     $t \leftarrow t + 1$;
5:     $\Upsilon(t) \leftarrow \left\{\frac{R(t_{\bar{s}}, P_t)}{P_T(t_{\bar{s}}, P_t)}\right\}$;
6: **end while**

At each iteration t in **Algorithm** 4.7 , $P_t(t)$ is evaluated from the **Algorithm** 4.8. The while loop continues until $\Upsilon(t)$ converges to its optimal Υ^*. The summary of our proposed approaches is concisely presented in Figure 4.3 .
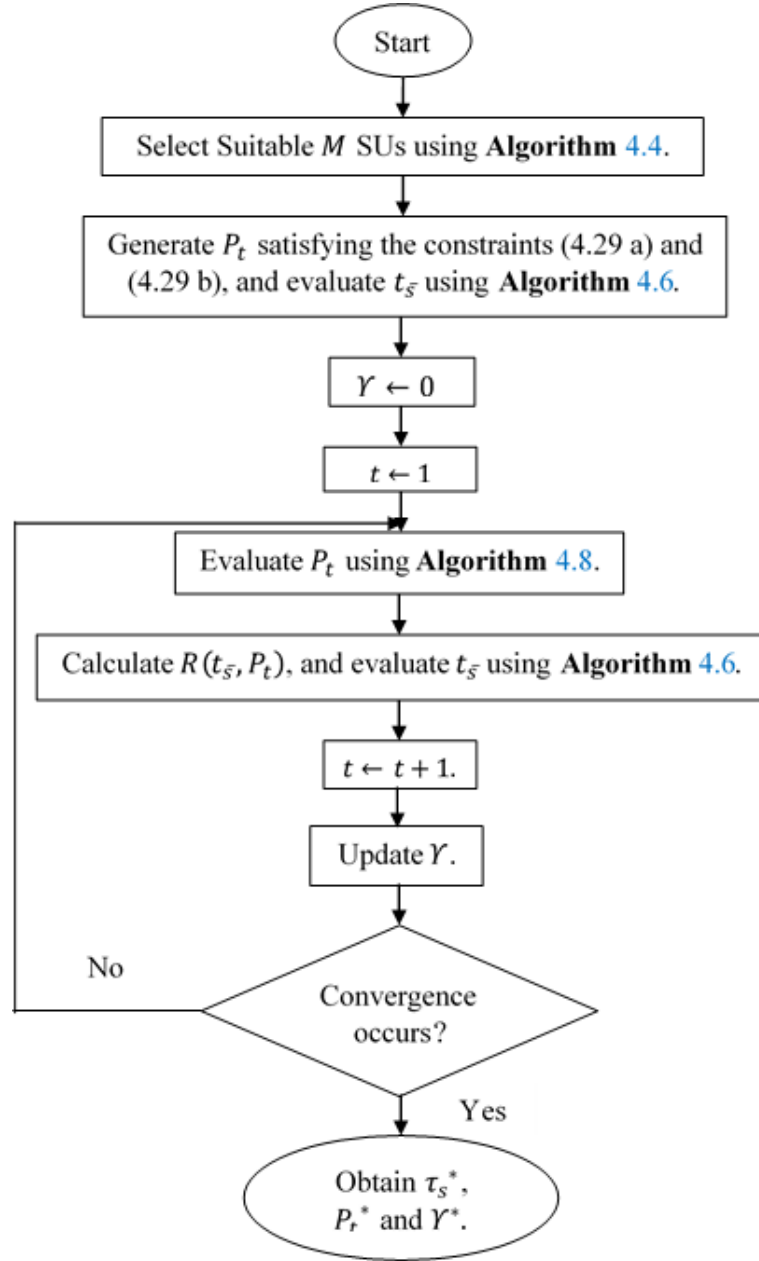
Figure 4.3: Representing the summary of our novel approaches for energy-efficient resource allocation in single threshold-based FC with the PUE attacker.

Dual decomposition and DC programming based power allocation

The optimization problem (4.29) consists of the constraint (4.29 c), which is neither convex nor concave w.r.t P_t. So, the optimization problem for Step 2 in **Algorithm** 4.7 is formulated as

$$\underset{P_t}{Maximize} \quad : \quad R\left(t_{\bar{s}}, P_t\right) - \Upsilon(t) P_T\left(t_{\bar{s}}, P_t\right) \tag{4.30}$$

$$Subject \quad to \qquad : \qquad \tilde{R}\left(\tau_s, \tilde{P}_t\right) - \bar{R}\left(\tau_s, P_t\right) \leq C_{th} \qquad (4.30\,a)$$

$$: \qquad I_{total} \sum_{m=1}^{M} |h_{sdm}|^2 P_{tm} \leq I_{th} \qquad (4.30\,b)$$

After applying Lagrangian duality theorem, the optimization problem (4.30) is expressed as

$$L(\theta, \vartheta) = R(t_{\bar{s}}, P_t) - \Upsilon(t) P_T(t_{\bar{s}}, P_t) + \theta \left(C_{th} - \tilde{R}\left(t_{\bar{s}}, \tilde{P}_t\right) + \bar{R}(t_{\bar{s}}, P_t)\right)$$
$$+ \vartheta \left(I_{th} - I_{total} \sum_{m=1}^{M} |h_{sdm}|^2 P_{tm}\right) \quad (4.31)$$

where θ and ϑ are the non-negative Lagrangian multipliers. So, the dual problem (4.31) is formulated as $\min\limits_{\theta \geq 0, \vartheta \geq 0} \max\limits_{P_t} L(\theta, \vartheta)$. The solution to (4.31) involves two steps. The first step involves the updations of θ and ϑ for the given P_t by using sub-gradient method which are expressed as

$$\theta_{i+1} = \left[\theta_i - \psi_i \left(C_{th} - \tilde{R}\left(t_{\bar{s}}, \tilde{P}_t\right) + \bar{R}(t_{\bar{s}}, P_t)\right)\right]^+ \qquad (4.32)$$

$$\vartheta_{j+1} = \left[\vartheta_j - \kappa_j \left(I_{th} - I_{total} \sum_{m=1}^{M} |h_{sdm}|^2 P_{tm}\right)\right]^+ \qquad (4.33)$$

where ψ_i and κ_j are the non-negative step sizes for the current iteration values i and j, respectively, and they are updated as $\psi_i = {}^1\!/_i$ and $\kappa_j = {}^1\!/_j$, respectively. So, θ and ϑ converge when ψ_i and κ_j are sufficiently small, respectively. The second step involves the evaluation of P_t for the given values of ψ_i and κ_j. So, (4.31) can be formulated as maximization of

$$L\left(\theta_i, \vartheta_j, P_t\right) = G\left(\theta_i, \vartheta_j, P_t\right) - H\left(\theta_i, \vartheta_j, P_t\right) \qquad (4.34)$$

where

$$G\left(\theta_i, \vartheta_j, P_t\right) = -\theta_i \tilde{R}\left(t_{\bar{s}}, \tilde{P}_t\right) - \Upsilon(t) P_T\left(t_{\bar{s}}, P_t\right) + \theta_i C_{th} - \vartheta_j I_{total} \sum_{m=1}^{M} |h_{sdm}|^2 P_{tm} \quad (4.35)$$

and

$$H\left(\theta_i, \vartheta_j, P_t\right) = -\left(\theta_i + \Omega\right) \bar{R}\left(t_{\bar{s}}, P_t\right) - \vartheta_j I_{th} \qquad (4.36)$$

where $\Omega = \frac{\tau_d}{\Gamma} P_{H0} \left(1 - Q_f\right)$. Both $\bar{R}\left(t_{\bar{s}}, P_t\right)$ and $\tilde{R}\left(t_{\bar{s}}, \tilde{P}_t\right)$ are the concave functions of P_t and $\tilde{P}_t$, respectively, hence $-\bar{R}\left(t_{\bar{s}}, P_t\right)$ and $-\tilde{R}\left(t_{\bar{s}}, \tilde{P}_t\right)$ are the convex functions of P_t and $\tilde{P}_t$, respectively. So, the optimization problem (4.34) is represented by the difference of two convex functions $G\left(\theta_i, \vartheta_j, P_t\right)$ and $H\left(\theta_i, \vartheta_j, P_t\right)$. The details of DC programming are given in [145]. In the previous literature, this DC programming was used for power allocation in [146], [147]. According to the DC programming, the optimization problem $\max\limits_{P_t} L\left(\theta_i, \vartheta_j, P_t\right)$ is solved by the following convex programming [146]

$$\max_{P_t} \left\{G\left(\theta_i, \vartheta_j, P_t\right) - H\left(\theta_i, \vartheta_j, P_t(q)\right) - \left\langle \nabla H\left(\theta_i, \vartheta_j, P_t(q)\right), P_t - P_t(q)\right\rangle\right\} \qquad (4.37)$$

where $P_t(q)$ is the power obtained at qth iteration. The Frank-and-Wold (FW) type procedure is used to generate the sequence of power P_t such that $L\left(\theta_i, \vartheta_j, P_t\right)$ always

converges [146]. $H\left(\theta_i, \vartheta_j, P_t\right)$ shows very gradual convexity w.r.t P_t , hence it is approximated by its first order gradient such as $H\left(\theta_i, \vartheta_j, P_t\left(q\right)\right) + \left\langle \nabla H\left(\theta_i, \vartheta_j, P_t\left(q\right)\right), P_t - P_t\left(q\right)\right\rangle$ for the power $P_t\left(q\right)$. Therefore,

$$H\left(\theta_i, \vartheta_j, P_t\left(q+1\right)\right) \geq H\left(\theta_i, \vartheta_j, P_t\left(q\right)\right) + \left\langle \nabla H\left(\theta_i, \vartheta_j, P_t\left(q\right)\right), P_t\left(q+1\right) - P_t\left(q\right)\right\rangle \tag{4.38}$$

As the convergence goes on, $P_t\left(q+1\right)$ is the optimal solution and $P_t\left(q\right)$ is the feasible solution of the power allocation at qth iteration. Therefore,

$$
\begin{aligned}
G\left(\theta_i, \vartheta_j, P_t\left(q+1\right)\right) &- H\left(\theta_i, \vartheta_j, P_t\left(q+1\right)\right) \tag{4.39}\\
&\geq \left[G\left(\theta_i, \vartheta_j, P_t\left(q+1\right)\right) - H\left(\theta_i, \vartheta_j, P_t\left(q\right)\right) - \left\langle \nabla H\left(\theta_i, \vartheta_j, P_t\left(q\right)\right), P_t\left(q+1\right) - P_t\left(q\right)\right\rangle\right]\\
&\geq G\left(\theta_i, \vartheta_j, P_t\left(q\right)\right) - H\left(\theta_i, \vartheta_j, P_t\left(q\right)\right)
\end{aligned}
$$

So, the optimal solution at the next iteration $q+1$, $P_t\left(q+1\right)$ is always better than the previous $P_t\left(q\right)$. Thus, the convergence of DC programming is proved. The pseudo-code for the power allocation algorithm is described in **Algorithm** 4.8.

Algorithm 4.8 Power allocation algorithm based on DC programming.

Input:

    Dinkelbach parameter $\Upsilon(t)$ at t th iteration.

    $\zeta \leftarrow$ non-improvement parameter of ϑ.

    $\varsigma \leftarrow$ non-improvement parameter of θ.

    $\iota \leftarrow$ non-improvement parameter of $L\left(\theta_i, \vartheta_j, P_t\right)$.

    $\zeta, \varsigma, \iota \leftarrow 10^{-4}$

Output:

    Return θ^*, ϑ^* and $P_t\left(\Upsilon(t)\right)$.

1: Initialize ϑ_0, κ_0 ;
2: $j \leftarrow 1$;
3: **while** $\left|\vartheta(j) - \vartheta(j-1)\right| \geq \zeta$ **do**
4:     Initialize θ_0, ψ_0;
5:     $i \leftarrow 1$;
6:     **while** $\left|\theta(i) - \theta(i-1)\right| \geq \varsigma$ **do**
7:         Initialize $P_t(0)$, $P_t(1)$. Find $L(P_t(0))$ and $L(P_t(1))$;
8:         $q \leftarrow 1$;
9:         **while** $\left|L\left(\theta_i, \vartheta_j, P_t(q)\right) - L\left(\theta_i, \vartheta_j, P_t(q-1)\right)\right| \geq \iota$ **do**
10:           Find $P_t(q)$ from (4.37) by using gradient method.
11:           $q \leftarrow q+1$;
12:           Calculate $L\left(\theta_i, \vartheta_j, P_t(q)\right)$;
13:         **end while**
14:         Update θ_i using (4.32);
15:         $i \leftarrow i+1$;
16:     **end while**
17:     Update ϑ_j using (4.33);
18:     $j \leftarrow j+1$;
19: **end while**

If we calculate the overall complexity, then, our proposed approach for single threshold-based detection scheme is mainly based on **Algorithm** 4.4, **Algorithm** 4.7 and **Algorithm** 4.8. In **Algorithm** 4.6, the sensing times τ_{optA}, τ_{opt} are obtained by employing golden section search method for minimum delay and maximum throughput, respectively. The computational complexity of the golden section search method is $O\left(\log_2\left|\frac{\Delta\tau}{\phi}\right|\right)$, where $\Delta\tau$ denotes the difference between the upper and lower bound of the sensing time and ϕ represents the non-improvement threshold. The computational complexity of **Algorithm** 4.7 and **Algorithm** 4.8 depends on the number of iterations required to converge the parameter in each layer. Let N_A, N_B, N_C, N_D and N_E are the number of iterations required to converge the convex programming (4.37), L, θ, ϑ and Υ respectively, then the computational complexity is roughly given by $O\left(N_E N_D N_C N_B\left(1/N_A\right)\log_2\left|\frac{\Delta\tau}{\phi}\right|\right)$.

However the aid of dual decomposition method with the DC programming requires more number of iterations. Hence, an adaptive method is proposed to maximize EE for

double threshold-based detection scheme. It maximizes EE by reducing the total energy consumption with lesser complexity than NIRA algorithm.

Double threshold-based detection scheme

As per the constraints discussed in Section 4.3, EE maximization problem is formulated as (transmission delay constraint is not considered)

$$
\begin{array}{ll}
\underset{\tau_s,\ P_t}{\textit{Maximize}} & : & \dfrac{R\left(\tau_s,P_t\right)}{P_T\left(\tau_s,P_t\right)} & (4.40)
\end{array}
$$

$$
\begin{array}{lll}
\textit{Subject\quad to} & : & P_{tmax} - \displaystyle\sum_{m=1}^{M} P_{tm} \geq 0 & (4.40\ a)
\end{array}
$$

$$
: \quad I_{th} - I_{total} \sum_{m=1}^{M} |h_{sdm}|^2 P_{tm} \geq 0 \qquad (4.40\ b)
$$

$$
: \quad C_{Pm}\left(\tau_s,P_t\right) \approx C_{Am}\left(\tau_s,\tilde{P}_t\right) \qquad (4.40\ c)
$$

$$
: \quad Q_f \leq 0.5 \qquad (4.40\ d)
$$

$$
: \quad 0 \leq \tau_s \leq \Gamma \qquad (4.40\ e)
$$

The constraints in (4.40 a-4.40 e) are the mixture of non-convex integer problem. This makes the EE maximization problem very difficult to solve. First, we minimize the search area of τ_s s.t. it ranges between $\tau_s \in \left(\tau_{smin}, \frac{\Gamma}{2}\right]$. The minimum sensing time τ_{smin} is calculated as per the following expression

$$
\tau_{smin} \geq \frac{1}{f_s}\left(\frac{\tilde{a}}{\tilde{b}}\right)^2 \qquad (4.41)
$$

where $\tilde{a} = \dfrac{Q^{-1}\left(\overline{P}_{d,k}\right)\sigma_{a\eta k}^2\sqrt{2(1+2\gamma_{ak})}}{\sqrt{2}\sigma_{a\eta k}^2}$ and $\tilde{b} = \dfrac{\left(\Delta+\gamma_{ak}\sigma_{a\eta k}^2\right)}{\sqrt{2}\sigma_{a\eta k}^2}$. The constraint (4.40 c) is neither a convex nor a linear function of P_t. So, we propose an adaptive power assignment scheme based on NLMS algorithm to solve this type of mixed integer problem. Here, the EE maximization problem is separated out into two parts; (a) minimizing $P_T\left(\tau_s,P_t\right)$ under the constraint of interference to the PR (b) maximizing $R\left(\tau_s,P_t\right)$ through the balancing power constraint. So, the objective problem (4.40) is transformed to the minimization of total power consumption $P_T\left(\tau_s,P_t\right)$ satisfying the constraints (4.40 b) and (4.40 c) which is represented as

$$
\begin{array}{lll}
\underset{P_t}{\textit{Minimize}} & : & P_T\left(\tau_s,P_t\right) & (4.42)
\end{array}
$$

$$
\begin{array}{lll}
\textit{Subject\quad to} & : & P_{tm}{}^{(j)}\left\{\hat{\Upsilon}_m\right\} \geq 2^{-C_m(j-1)} & (4.42\ a)
\end{array}
$$

$$
: \quad I_{total} \sum_{m=1}^{M} |h_{sdm}|^2 P_{tm}{}^{(j)} \leq I_{th} \qquad (4.42\ b)
$$

$$
\text{Here,} \qquad \hat{\Upsilon}_m \quad = \quad \left\{\frac{1}{\tilde{P}_{tm}}\left(\frac{N_p}{N_p+\beta|h_{arm}|^2\sigma_a^2}\right)\right\} \qquad \text{and}
$$

$C_m^{(j-1)} = log_2 \left(\frac{|h_{srm}|^2 \tilde{P}_{tm}}{N_p} \right) - log_2 \left(\frac{|h_{srm}|^2 P_{tm}^{(j-1)}}{N_p + \beta |h_{arm}|^2 \sigma_a^2} \right)$. These are obtained by assuming $log_2 (1 + x) \cong log_2 (x)$. The inequality nonlinear problems (4.42-4.42 b) are transferred to equivalent linear problem as

$$\sum_{m=1}^{M} P_{tm}^{(j)} + Z_U = \sum_{m=1}^{M} P_{tm}^{(j-1)} \tag{4.43}$$

$$P_{tm}^{(j)} \{ \hat{\Upsilon}_k \} + Z_H = 2^{-C_m(j-1)} \tag{4.44}$$

$$\sum_{m=1}^{M} |h_{sdm}|^2 P_{tm}^{(j)} + Z_L = \frac{I_{th}}{I_{total}} \tag{4.45}$$

Here, Z_U, Z_H and Z_L are the negative, positive and negative random numbers, respectively. The values are obtained from $Z_U \sim \aleph (0, 0.001)$, $Z_H \sim \aleph (0, 0.01)$ and $Z_L \sim \aleph (0, 0.01)$. If P_t is a sequence of dimension $[1 \times M]$, thereby we consider $\omega (i) = \left[P_{t1}^{(i)} \ P_{t2}^{(i)} \ P_{t3}^{(i)} ...... P_{tM}^{(i)} \right]$. If we represent (4.43-4.45) in their equivalent sequences, then

$$W (i) = \begin{cases} Q, & mod (M+2) \\ \bar{Q}_1, & mod (M+2) \\ \bar{Q}_2, & mod (M+2) \\ . \\ . \\ \bar{Q}_M, & mod (M+2) \\ \tilde{Q}, & mod (M+2) \end{cases} \tag{4.46}$$

where Q and $\tilde{Q}$ are matrices of dimension $[M \times M]$, and are give by

$$Q = \begin{pmatrix} 1 & 0 & \cdots & 0 \\ 0 & 1 & \cdots & 0 \\ \vdots & \vdots & \ddots & \vdots \\ 0 & 0 & \cdots & 1 \end{pmatrix} \tag{4.47}$$

and

$$\tilde{Q} = \begin{pmatrix} |h_{sd1}|^2 & 0 & \cdots & 0 \\ 0 & |h_{sd2}|^2 & \cdots & 0 \\ \vdots & \vdots & \ddots & \vdots \\ 0 & 0 & \cdots & |h_{sdM}|^2 \end{pmatrix} \tag{4.48}$$

$\bar{Q}_1 = \left[\hat{\Upsilon}_1 \ 0 \ 0 \ ... 0 \right]$, $\bar{Q}_2 = \left[0 \ \hat{\Upsilon}_2 \ 0 \ 0... 0 \right]$, and so on, each of dimension $[1 \times M]$. At ith

iteration, Z sequence is defined as

$$Z(i) = \begin{cases} Z_U, \\ Z_{H1}, \\ Z_{H2}, \\ . \\ . \\ Z_{HM}, \\ Z_L, \end{cases} \tag{4.49}$$

If $S(i)$ sequence is given by

$$S(i) = \begin{cases} \sum\limits_{m=1}^{M} P_{tm}^{(j-1)}, \\ 2^{-C_1(j-1)}, \\ 2^{-C_2(j-1)}, \\ . \\ . \\ 2^{-C_M(j-1)}, \\ \frac{I_{th}}{I_{total}}, \end{cases} \tag{4.50}$$

Then, following (4.43-4.50), we have

$$S(i) = \sum_{m=1}^{M} \omega_m^{(j)}(i) g_m(i)^T + Z(i) \tag{4.51}$$

$g_m(i)$ is the corresponding mth row of $W(i)$. If the proposed method is solved by using the NLMS algorithm, then the desired output of the system is given by [148].

$$d(i) = S(i) - \sum_{m=1}^{M} \omega_m^{(j)}(i-1) \hat{v}_m(i)^T \tag{4.52}$$

$V(i)$ is the random matrix of same size of $W(i)$ and its generation is similar to the mean and variance of Z_U, Z_H and Z_L. If $\hat{v}_k(i)$ is the mth vector of the matrix $\hat{V}(i) = W(i) - V(i)$, then the error is given by

$$e(i) = d(i) - \sum_{m=1}^{M} \omega_m^{(j)}(i-1) v_m(i)^T \tag{4.53}$$

where v_m is the corresponding mth vector of matrix $V(i)$. Here, $\omega^{(j)}(i)$ is the power allocation matrix, and is evaluated from

$$\omega_m^{(j)}(i) \leftarrow \omega_m^{(j)}(i-1) + \frac{\bar{\mu}}{\|v_m\|^2} v_m(i) e(i) \tag{4.54}$$

where $\bar{\mu}$ is the step size and its ranges between $0 < \bar{\mu} < 2$ for NLMS algorithm. The steps describing our proposed NARA algorithm are given below.

Algorithm 4.9 NARA algorithm.

Input:

    Find suitable M and eligible SUs using **Algorithm** 4.5.

    Decide τ_s in between $\tau_s \in \left(\tau_{smin}, \frac{\Gamma}{2} \right]$.

    $\xi \leftarrow$ minimum tolerence threshold.

    Randomly generate P_t satisfying the constraints (4.40 a) and (4.40 b) .

Output:

    Return optimal EE and optimal power $P_t^* = \omega^j$.

1: $j \leftarrow 1$;

2: **while** $|P_T(j) - P_T(j-1)| \geq \xi$ **do**

3:     $\omega^j \leftarrow \omega^{(j-1)}$;

4:     $i \leftarrow 1$;

5:     $A_1(i) \leftarrow \sum\limits_{m=1}^{M} \omega_m{}^{(j)}$;

6:     $B_1(i) \leftarrow I_{total} \sum\limits_{m=1}^{M} |h_{sdm}|^2 \omega_m{}^{(j)}$;

7:     $C_m(i) \leftarrow log_2 \left(\frac{|h_{srm}|^2 \tilde{P}_{tm}}{N_p} \right) - log_2 \left(\frac{|h_{srm}|^2 \omega_m{}^{(j)}}{N_p + \beta |h_{arm}|^2 \sigma_a{}^2} \right)$;

8:     **while** $(A_1(i) > A_1(i-1)) \,\&\&\, (B_1(i) > I_{th}) \,\&\&\, \left(\left(2^{-C_m(i)} < 2^{-C_m(i-1)} \right) \forall m \right)$
   do

9:         $d(i) \leftarrow S(i) - \sum\limits_{m=1}^{M} \omega_m{}^{(j)}(i-1) \hat{v}_m(i)^T$;

10:      $e(i) \leftarrow d(i) - \sum\limits_{m=1}^{M} \omega_m{}^{(j)}(i-1) v_m(i)^T$;

11:      **for** $m = 1 : M$ **do**

12:         $\omega_m{}^{(j)}(i) \leftarrow \omega_m{}^{(j)}(i-1) + \frac{\bar{\mu}}{\|v_m\|^2} v_m(i) e(i)$;

13:      **end for**;

14:      $i \leftarrow i+1$;

15:      Calculate $A_1(i)$, $B_1(i)$ and $C_m(i) \forall m$;

16:     **end while**

17:     $j \leftarrow j+1$;

18:     $\omega^j \leftarrow \omega^j(i)$;

19:     $P_T{}^{(j)} \leftarrow P_s \left(\hat{M}\tau_s + S_R \tau_s (K - \hat{M}) \right) + P\left(\overline{H}_0 \right) \sum\limits_{m=1}^{M} \omega_m{}^{(j)}$;

20: **end while**

21: $EE^* \leftarrow \frac{R^{(j)}(\tau_s, \omega^j)}{P_T{}^{(j)}(\tau_s, \omega^j)}$;

    If we analyze the computational complexity of our proposed algorithm, let N_A and N_B be the maximum number of iterations required for the inner while loop and the outer while loop of the NARA algorithm, respectively. Then, the overall complexity is $O(N_A N_B)$.

4.5   Simulation Results and Discussion

We consider the CRN consisting of *K*=20 SUs which are distributed around the centrally located PU in a circular area of radius 1000m. The PR and the attacker are present within the circular radius of 200m and 300m, respectively. The SRs are distributed randomly around the PU within the radius 1000m to 1500m. The system model given in Figure 4.1 and Figure 4.2 are used for the analysis of single and double threshold-based SDF CSS, respectively. To show the performances of the proposed approaches efficiently, separate algorithms are applied for single and double threshold-based methods. **Algorithm** 4.4, 4.6, 4.7 and 4.8 are used for single threshold-based SDF CSS model but by not employing (4.25) and (4.27) for deciding the value of *M* SUs. Similarly, **Algorithm** 4.5 and 4.9 are used for double threshold-based SDF model in which the number of SUs *M* is chosen from (4.25) and (4.27). For double threshold-based scheme we assume that $\delta_0 = \delta_1 = \delta_{g0} = \delta_{g1} = \delta$.The common simulation parameters are listed in Table 4.1.

Table 4.1: Simulation Parameters in the presence of an attacker.

Simulation Parameters	Value
N_p	-100 dBm
P_s	-20 dBm
α	3
Γ	0.01sec
τ_r	5μs
$\bar{Q}_d$	0.9
$\gamma_m \forall \in M$	-20dB
f_s	6MHz
$\sigma_s{}^2$	1

Figure 4.4 illustrates the variation of the probability of detection over different SNR values considering the system model Figure 4.1. The benefits of choosing suitable SUs using **Algorithm** 4.4 is clearly observed from this figure. We set *M*=8, υ=0.9 and *y*=0.1. In the absence of the attacker, *M* SUs present closer to the PU are chosen following step-9 of **Algorithm** 3.1 . Further, it is clearly observed that selected SUs show almost similar performance in the presence and absence of the attacker but provide 30% improvement in detection probability as compared to randomly selected SUs in the presence of an attacker at SNR=-15 dB. The detection performance is reduced by 22% in the presence of an attacker compared to in the absence of an attacker by selecting random SUs. So, the SUs present closer to the PU relative to the attacker perform better than the randomly selected SUs. β value is set 0.99. Similarly, Figure 4.5 shows the performance comparison of the schemes; Scheme-I, Scheme-II and Scheme-III at different SNR conditions. In Scheme-I, the CSS framework in Figure 4.2 consists of

a double threshold-based SDF FC. In Scheme-II, the CSS framework in Figure 4.2 consisting of a single threshold-based SDF FC [144]. In Scheme-III, each SU consists of a double threshold-based ED and the binary decisions of all K SUs converge at the FC using OR logic. It is observed that probability of detection increases with employing double threshold-based FC in Figure 4.2. So, for the given value of P_f and δ=0.05 at SNR=-23 dB, Scheme-I offers improvement in Q_d by 3 times and 6 times as compared to Scheme-II and Scheme-III, respectively.This shows that any information lost due to Δ_{g0} or Δ_{g0} can be avoided. Further, with increase in δ from 0.05 to 0.1, Q_d increases by 22% in Scheme-I at -23 dB SNR. The results are verified for P_f=0.1 and 0.001. It is reasonable that Q_d increase with increase in P_f.
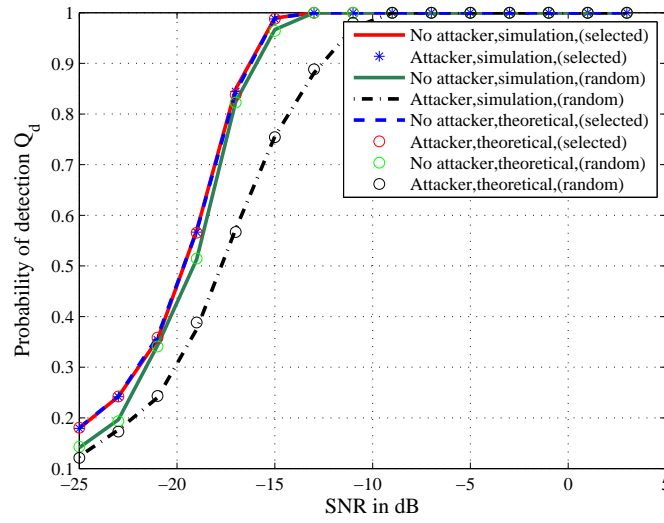
Figure 4.4: Effect of PUE attacker on the probability of detection.
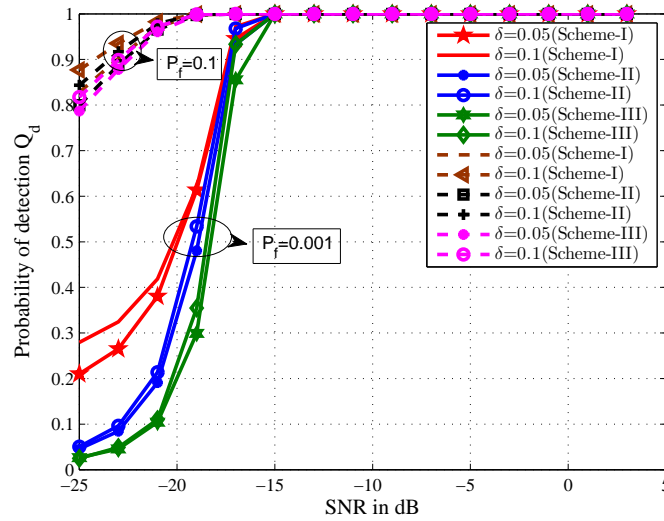
Figure 4.5: Probability of detection vs SNR for Figure 4.2.

Figure 4.6 shows the variation of sensing time over different values of SNR. The sensing times are $t_{\bar{s}}$, τ_{opt} and τ_{optA} from **Algorithm** 4.6. It is observed that our proposed sensing time $t_{\bar{s}}$ maintains a trade-off between minimum transmission delay and maximum throughput. But at high SNR conditions, these three sensing times coincide with each other. Furthermore, at low SNR conditions the sensing time is usually more leaving a very short period of data transmission. Hence,it can also be one of the reasons that system throughput is less at low SNR. We set M=8, I_{th}=-70 dBm, R_{th}=2 bits/s/Hz, β=0.99 and C_{th}=6 which are used for the analysis of Figures (4.6-4.11) based on single threshold-based FC.
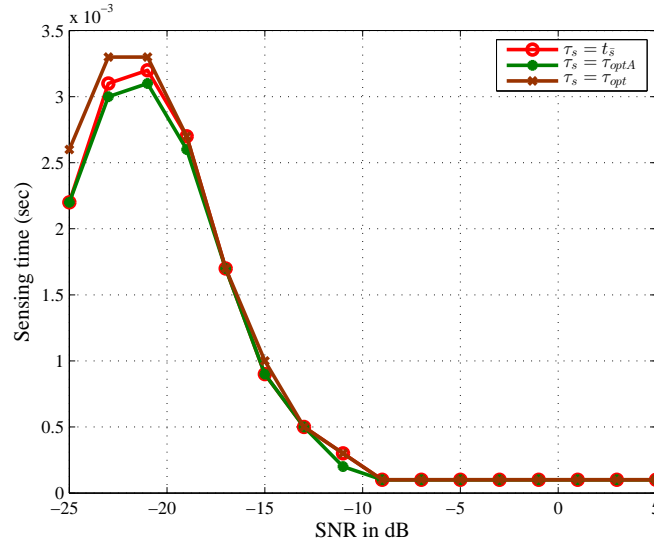
Figure 4.6: Variation of sensing times over different SNR values.

Figure 4.7 illustrates the convergence of maximum EE for different values of υ and *y*. These different values signify the dependance of EE on the channel gains between the PU and the SUs, between the SUs and the SRs, between the attacker and the SRs and also between the SUs and the PR. So, we evaluate EE for different values of υ and *y* to find the suitable value at which EE is maximum. It is found that EE with υ=0.9 and *y*=0.1 exhibits better result than the other combinations and is used in the further evaluation of simulation results. Further, the maximum EE is compared with the other existing scheme (Scheme-I) [142] in which power allocation was made on the basis of maximizing the system throughput without considering the power balancing constraint (4.29 c). It is obvious that data rate increases at the expense of power consumption, hence Scheme-I shows least EE for the same given parameters.

The benefit of selecting suitable SUs over randomly selected SUs for two different values of β is clearly observed in Figure 4.8. Further, it is observed that throughput is higher for the lower probability of attacker' presence. As β increases from 0.7 to 0.99, throughput is reduced by 6% at SNR=-11 dB. This is because the attacker's

interference power decreases the SINR of the secondary transmission. It is also verified that throughput can be improved approximately by more than 2 times by employing **Algorithm** 4.4 for selecting suitable SUs.
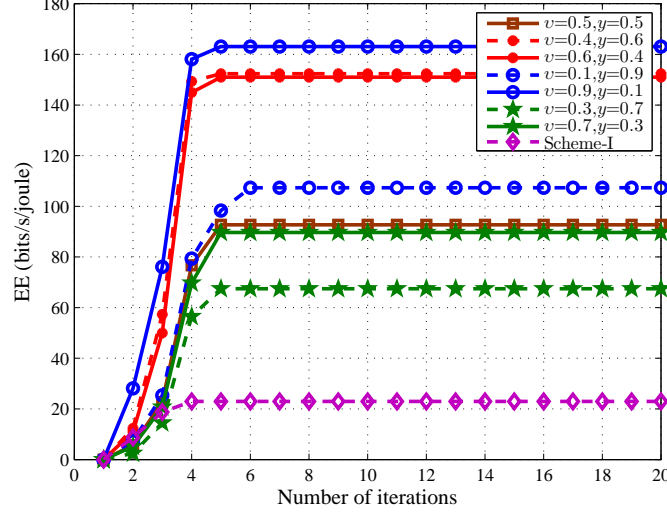
Figure 4.7: Convergence analysis of EE for different values of υ and y.
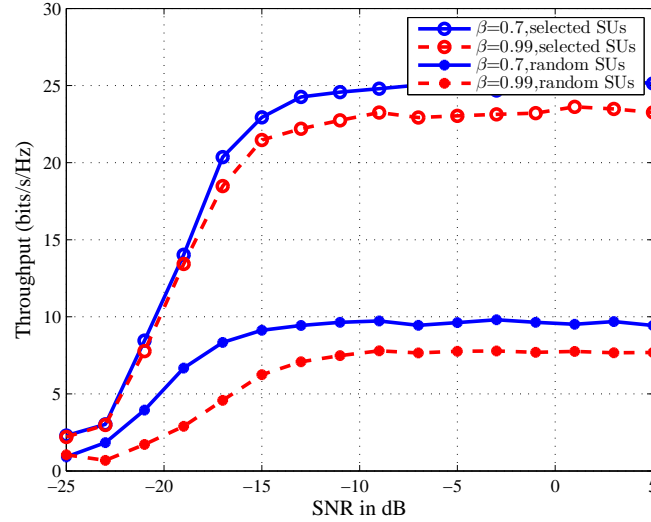
Figure 4.8: Validation of **Algorithm** 4.4 by showing $R\left(\tau_s, P_t\right)$ vs SNR.

The impact of I_{th} on EE and total power consumption for SNR=-20 dB and -10 dB is shown in Figure 4.9. It is obvious that increase in I_{th} increases the maximum allowable transmission power from the SUs. Hence, EE decreases but P_T increases. Figure 4.10 shows the variation of EE and throughput over different values of R_{th} for C_{th}=6 and 10. It is reasonable that EE decreases and throughput increases with increase in R_{th}, but here both of these parameters show very gradual changes. So, when R_{th} increases from

0.3 to 1.1 bits/s/Hz for C_{th}=10, EE is reduced by 4% but throughput remain unchanged. Further, large value of C_{th} helps in reducing the transmission power from SUs, thereby increases EE but throughput decreases.Comparing C_{th} at 10 and 6 for R_{th}=1.1 bits/s/Hz, the relative differences between EE values and throughputs are approximately 5% and 29%, respectively.
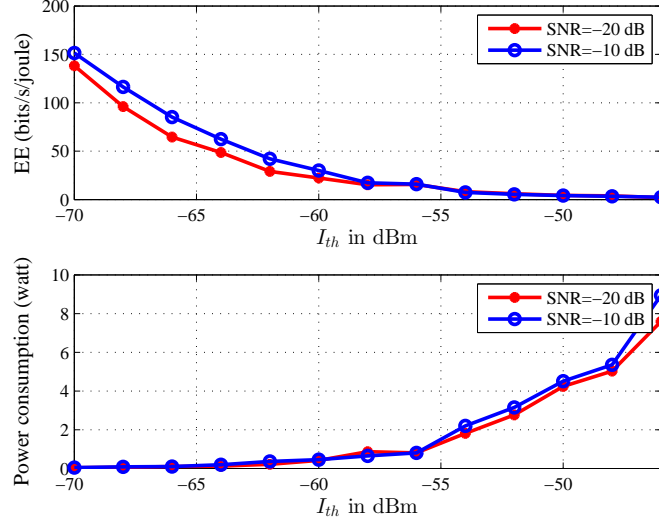
Figure 4.9: Impact of I_{th} on $EE\left(\tau_s, P_t\right)$ and $P_T\left(\tau_s, P_t\right)$.
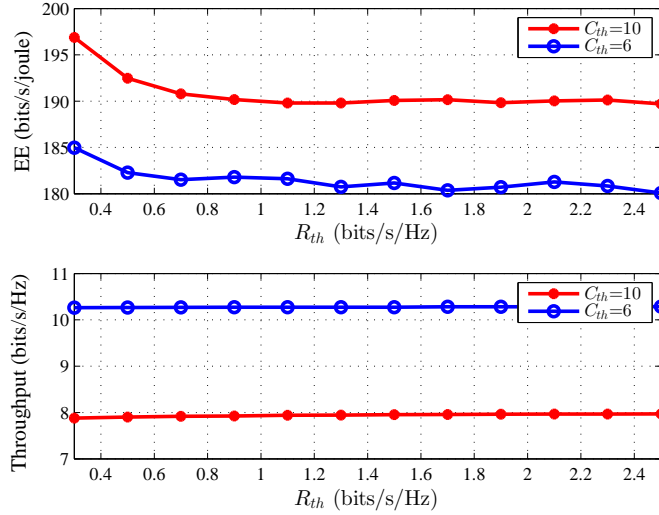
Figure 4.10: Impact of R_{th} on $EE\left(\tau_s, P_t\right)$ and $R\left(\tau_s, P_t\right)$ for C_{th}=6 and 10.

The variation of $R\left(\tau_s, P_t\right)$ and $P_T\left(\tau_s, P_t\right)$ over different values of $\bar{Q}_d$ considering the presence and absence of the attacker is analyzed in Figure 4.11. Both, system throughput and power consumption behave same as Figure 3.11. But, we observe that power consumption increases but the system throughput decreases in the presence of

the attacker. For $\bar{Q}_d$=0.9, the presence of an attacker reduces the system throughput by 76% but increases the power consumption by 15%. Hence, the attacker's interference power greatly affects the secondary network by increasing their power consumption.
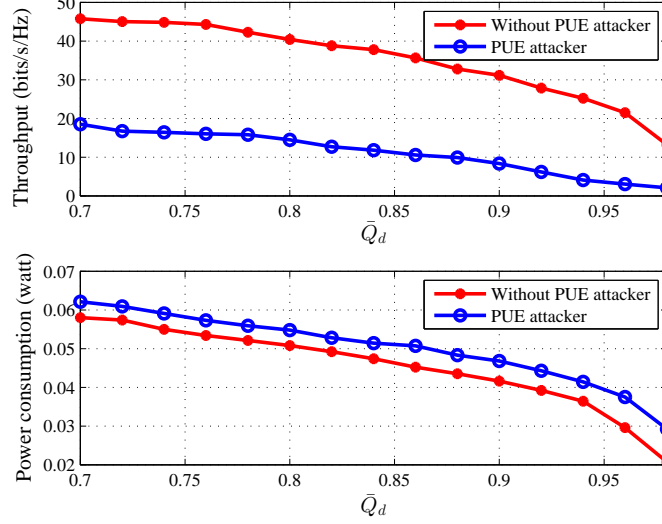
Figure 4.11: Variation of $R(\tau_s, P_t)$ and $P_T(\tau_s, P_t)$ w.r.t $\bar{Q}_d$.

While analyzing the double threshold-based detection scheme, we use (4.25) and (4.27) for selecting the suitable number of SUs. The eligible SUs for data transmission is selected by using **Algorithm** 4.5. The sensing time τ_s is calculated by using (4.41) and the power allocation to the SUs is obtained by the proposed NARA algorithm. For the given values of target detection probability and δ, Q_f is calculated.

Figure 4.12 illustrates the lower and upper bound of the number of SUs for different values of I_{th}, R_{th} and C_{out}. It is observed that M_U decreases with increase in R_{th}. This is due to the fact that when R_{th} increases, less SUs is required to achieve the maximum throughput as per (4.27). Further, M_U increases with increase in I_{th} and C_{out}. As I_{th} increases, the maximum allowed transmission power P_{tmax} increases, therefore as per (4.27) more SUs are required to achieve the given C_{out}. Similarly, M_U increases with C_{out}. As I_{th} rises from -71 dBm to -59 dBm, M_U increases from 11 to 13. Similarly, M_U reduces from 34 to 13 when R_{th} increases from 0.7 to 1.7. The increase in C_{out} from 1.7 to 3.8 increases M_U by 1 user i.e 11 to 12. For this figure, we set SNR=-20 dB, δ=0.01 and target detection probability=0.9.

Figure 4.13 illustrates the performance comparison of our proposed scheme with the DC programming. For DC programming analysis, we set C_{th}=6 and M=8. For NARA algorithm we set SNR=-20 dB, δ=0.01, target detection probability is 0.9, C_{out}=6, R_{th}=2 bits/s/Hz, I_{th}=-70 dBm and M=8. Further, this algorithm is evaluated for $\bar{\mu}$=0.1, 0.5 and 1. It is observed that NARA algorithm provides a significant improvement in EE even

in the presence of an attacker and obviously with lesser complexity. After convergence, it provides improvement approximately by 9 times at $\bar{\mu}$=0.1 when compared to DC programming method. $\bar{\mu}$=0.1 value will be used for further analysis.
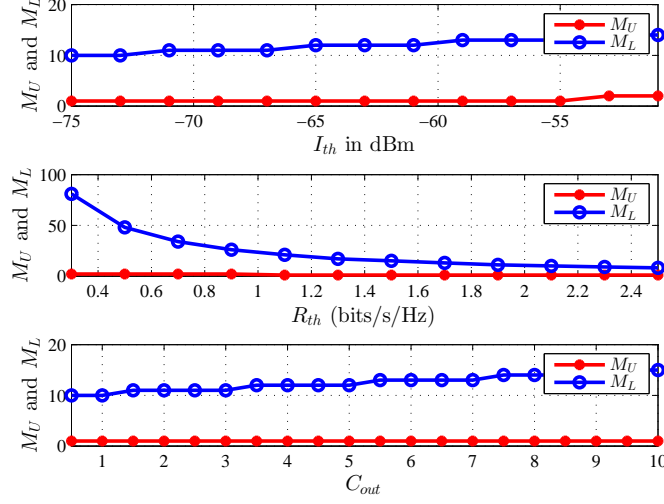
Figure 4.12: Variation of M_L and M_U against different values of I_{th}, R_{th} and C_{out}.
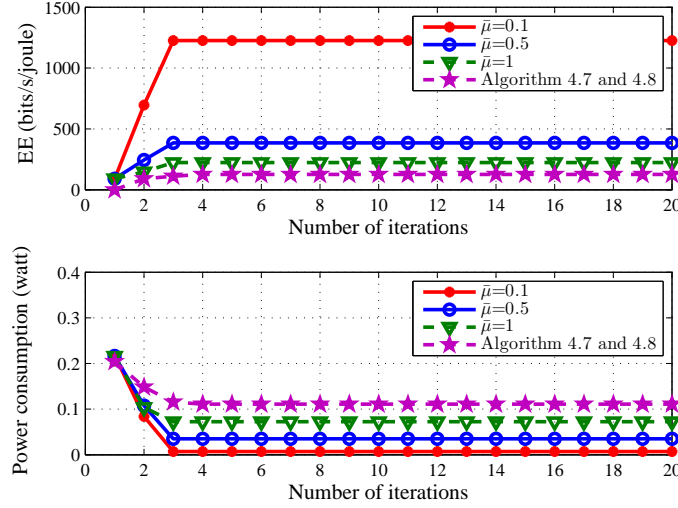
Figure 4.13: Convergence performance of NARA algorithm for different values of $\bar{\mu}$.

Figure 4.14 illustrates the benefit of employing **Algorithm** 4.5 for selecting suitable SUs for data transmission. Selected SUs provide better performance than the randomly chosen SUs. Further, system throughput is also analyzed for different values of δ. For δ=0.01 and SNR=-17 dB, we can have the improvement in throughput by 8% with the inclusion of suitable SUs.It is obvious that as δ increases Q_f decreases. So, $(1 - Q_f)$ increases which improves $R(\tau_s, P_t)$. It can be concluded that system throughput can be

maximized by employing double threshold-based scheme rather than single threshold-based scheme. The simulation parameters are same as Figure 4.13.
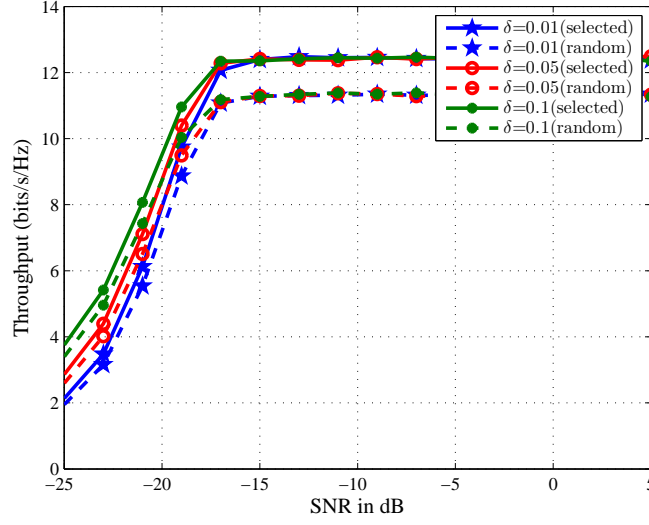
Figure 4.14: Variation of $R\left(\tau_s, P_t\right)$ against the SNR for different values of δ.

Figure 4.15 shows the effect of I_{th} on EE, system throughput and the total power consumption for C_{out}=2 and C_{out}=6. As discussed before, EE decreases, throughput and total power consumption increase with increase in I_{th}. As I_{th} decreases, EE shows better performance at C_{out}=2 than C_{out}=6 and is increased by 10% for I_{th}=-71 dBm. But C_{out} shows very least effect on the system throughput and power consumption. For this figure we set M=8 and other simulation parameters are same as Figure 4.13.

Figure 4.16 illustrates the characteristics of EE and system throughput towards the increased value of R_{th} for I_{th}=-70 dBm and -60 dBm. Both $EE\left(\tau_s, P_t\right)$ and $R\left(\tau_s, P_t\right)$ are analyzed taking M=8 and $M = M_U$. In different from the discussion for Figure 3.10, where throughput increases with increase in R_{th}, Figure 4.16 shows decrease in $R\left(\tau_s, P_t\right)$ after certain value of R_{th}. This is because the maximum number users M_U is dependent on I_{th} and R_{th} at the same time, which variations bring changes to the characteristics of EE and system throughput.

Figure 4.17 depicts the effect of target detection probability on the total power consumption $R\left(\tau_s, P_t\right)$ and $P_T\left(\tau_s, P_t\right)$ for δ=0.01 and 0.05. It is obvious that with increase in detection probability false alarm increases, which decreases both power consumption and system throughput. So, system throughput and total power are the decreasing functions of detection probability. Further, it is also observed that when δ reduces from 0.05 to 0.01, both system throughput and power consumption are reduced by 1.5% and 1.4%, respectively when target detection probability is set at 0.9. The simulation parameters are same as Figure 4.13.
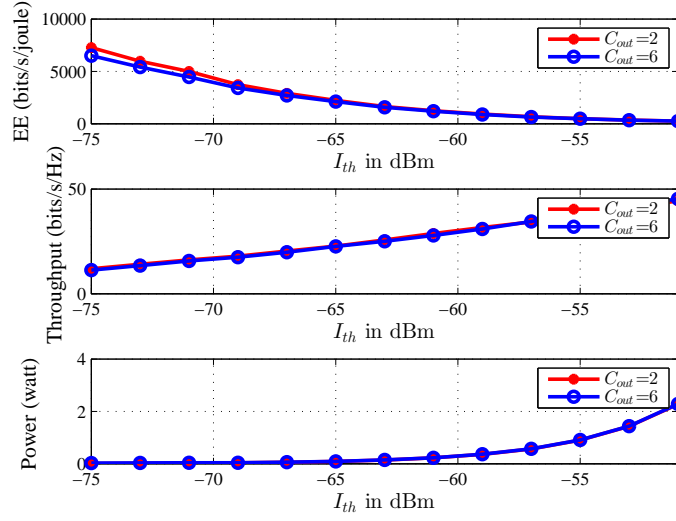
Figure 4.15: Effect of I_{th} on $EE(\tau_s, P_t)$, $R(\tau_s, P_t)$ and $P_T(\tau_s, P_t)$.
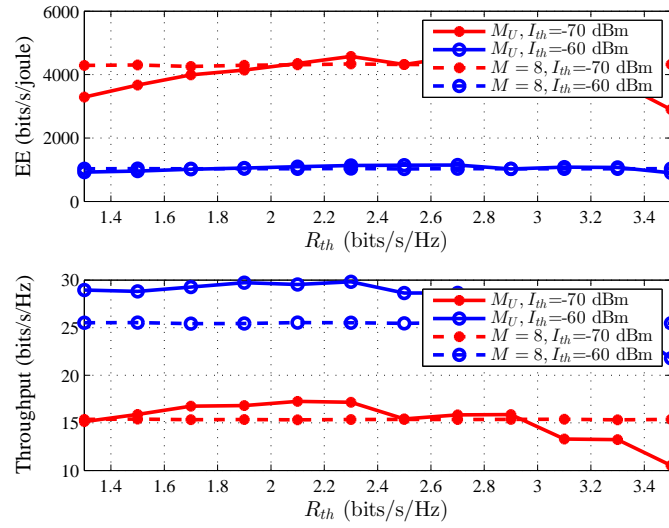
Figure 4.16: Effect of R_{th} on $EE(\tau_s, P_t)$ and $R(\tau_s, P_t)$ taking M=8 and $M = M_U$.
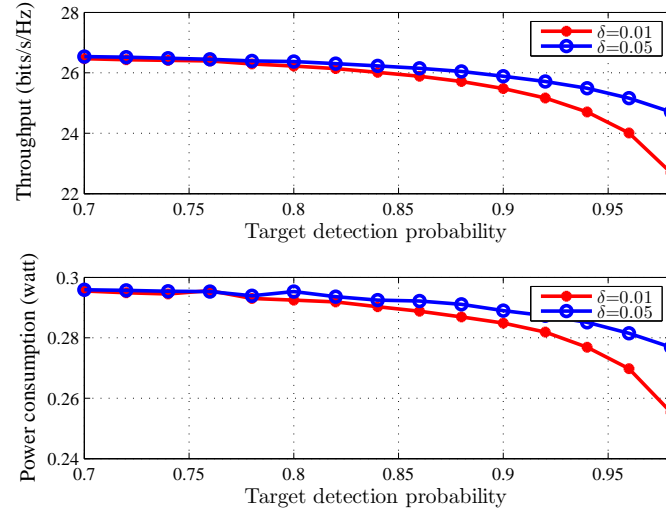
Figure 4.17: Effect of target detection probability on $R\left(\tau_s, P_t\right)$ and $P_T\left(\tau_s, P_t\right)$ for δ=0.01 and 0.05.

4.6 Summary

This chapter proposed the energy-efficient resource allocation technique in the CRN considering the presence of PUE attacker for both single and double threshold-based detection schemes. The interference, transmission delay and throughput balancing power allocation were considered as the constraints. The solution approach towards the EE maximization problem was achieved by optimizing the sensing time and power allocation with suitable SUs selection. For the single threshold-based detection technique, the EE maximization problem with non-convex constraints was solved by combining parametric transformation with the dual decomposition and DC programming method. As it was computationally complex requiring more iterations, an adaptive scheme based on NLMS algorithm was proposed which performed better than the DC programming method with lesser complexity. Further, with suitable algorithms eligible SUs were selected. It was observed that there was a significant enhancement in system throughput by employing both the proposed algorithms (**Algorithm** 4.4 and **Algorithm** 4.5) for data transmission purpose. The performances of all the algorithms were analyzed over different network parameters. It is concluded that NARA algorithm performed better than the NIRA algorithm with considerably lesser complexity and higher EE. In this chapter, it was assumed that the SUs are fixed, so the channel gains and the assigned power remain fixed for the entire data transmission duration. But in vehicular network, the constant power allocation to the moving SUs will not be valid due to the continuous change in distances of the VSUs from the PU, PR and the SRs with the vehicular motion. So, there is necessity of adaptive power allocation algorithms with time-varying channel gains.

Chapter 5

Proposed Approaches for Energy-Efficient Resource Allocation in the Cognitive Radio Vehicular Ad Hoc Network (without and with PUEA)

This chapter presents our novel proposed approaches for power allocation to the VSUs for maximizing EE in the SDF-based cooperative CR-VANET considering the absence and presence of PUEA. The highlights of the chapter are

- A new SDF-based cooperative CR-VANET is designed for a typical vehicular network scenario.

- The probability of detection and false alarm are derived considering the spatial correlation between the local decisions of the VSUs.

- Adaptive power allocation algorithms are proposed to solve the EE maximization problem associated with the non-convex and time-varying constraints.

5.1 Introduction

WITH the substantial rise in the number of moving vehicles on the road, the demand for employing new applications and services in the vehicular wireless communication has increased. Specifically, these applications are meant for the route selection, collision avoidance, road safety, data collection, vehicle-to-vehicle (V2V), infrastructure-to-vehicle (I2V), vehicle-to-infrastructure (V2I) communication, etc [37, 149]. Hence, VANET is introduced as an emerging technology to support these types of applications. As far as only the road safety is concerned, IEEE 1609 developed IEEE 802.11p standard and assigned 5.9 GHz band to support short-range communication in the time-varying vehicular environment. However, significant rise in the use of vehicular devices leads to spectrum congestion problem in this band resulting degradation of the vehicular communication efficiency. On the otherhand, FCC identified that nearly 15% to 85% of the licensed band is unutilized in temporal and spatial domain. Therefore, spectrum congestion problem in the vehicular communication can be solved partially by deploying VANET in TV licensed band. This enables the application of CR technology in VANET to exploit the unutilized licensed spectrum in an opportunistic manner for vehicular communications. Thus, the available bandwidth can be virtually broadened to achieve the QoS requirement for VANET without adding more spectral resources to the network. Due to the traffic intensity of the PUs and the mobility of the SUs, it is a challenging issue to find the under-utilized spectrum band, and to access that band without affecting the PUs. In VANET, data communication may occur either among the vehicles or between the vehicles and nearby APs. So, the communication is classified based on three such types of scenarios; V2I [150, 151], V2V [152, 153], and I2V [154] communications.

5.1.1 Related works

In the CR-VANET, the channel availability to the SUs dynamically varies with time and speed of the SUs. So, to enhance the detection performance, a variety of spectrum sensing techniques were proposed in the CR-VANET. In [155], the authors evaluated the miss detection probability considering the velocity of the SU, sensing range of the SU, and the protecting range of the PUs. The TV/WiMAX network users were considered as the PUs which were deployed on the roadside. Xu et al. used maximum likelihood ratio (MLR) detection scheme for local wideband SS in OFDM-based

---

CR-VANET. The global decision was made using the OR fusion rule with square-law selection (SLS) scheme [156]. However, this method did not consider the effect of the velocities of the SUs on the detection performance. A weighted CSS scheme in CR-VANET was proposed in [157], where the detection performance was evaluated considering the temporal and spatial diversity of the SUs and different weight coefficients were assigned to the different SUs to improve the detection probability. Also, the system performance was evaluated in terms of throughput and transmission delay. A CSS scheme using symmetry property of cyclic autocorrelation function (SP-CAF) method for each vehicle was proposed to detect the available channels in ISM band in [158]. The opportunistic spectrum access in the CR-VANET was formulated by using game theory, where the availability of the licensed band to the vehicles was based on the spatial and temporal behaviors of the primary transmitter [159]. Qian et al. used the most popular energy detection based SS for the evaluation of the miss detection probability under correlated Rayleigh fading sensing channel and binary symmetric reporting channel in [160].

Green CR has been introduced as an effective approach to meet the demands of high data rate traffic utilizing the limited energy resources. Further, in CR enhanced VANET, the CR nodes in vehicles being either electric-powered or powered by other sources, energy consumption minimization is one of the major challenges. Energy expenditure increases with the data rate. Since, the transmitted power affects both the system throughput and energy consumption, an adaptive power allocation scheme need to be designed to improve both spectral efficiency and EE. However, EE is an important aspect in battery-powered wireless terminals. Adapting energy harvesting techniques in CR transmitter not only prolongs life time of battery-powered terminals but also obviates the need of periodical battery replacement. An energy-efficient CR-VANET was introduced for the V2I uplink scenario in [150] . The overall energy consumption was minimized by jointly optimizing the sensing time and power allocation satisfying the minimum required throughput and interference power constraint to the PU. In [154], the throughput in the I2V scenario was maximized by selecting the route for both spectrum overlay and spectrum underlay model. The transmission power of the static vehicular base station was evaluated based on its distance from the VSUs and from the TV base station. The power allocation was also introduced for V2I scenario in [151] and for the I2V scenario in [161] in vehicular communications. Most of the existing works in the literature derived the system performance either in terms of detection probability or in terms of the system throughput. Even, those papers have not considered the presence of any malicious attack in the CR-VANET.

Though several resource allocation schemes are addressed in the existing literature

for the CRN, more exhaustive studies are required for designing the energy-efficient CR-VANETs. Hence, this chapter focuses on obtaining the interference-aware resource allocation in the CR-VANET model for V2I scenario in the spatial correlation environment both in the absence and presence of the PUE attacker.

5.1.2 Contributions and organization

The main contributions of this chapter are described as follows.

- Firstly, a new SDF-based CSS CR-VANET model is designed for a typical vehicular network scenario.

- Performance metrics are evaluated in the presence and absence of the PUEA considering the spatial correlation among the local decisions of the VSUs.

- The EE maximization problem is formulated under the constraints of total transmission power, interference to the PR and target detection probability.

- In the presence of PUEA, a power controlling constraint is added to control the transmitting power from the VSUs.

- In the absence of PUEA, the NLMS algorithm with the parametric transformation method is used to obtain the power allocation to the VSUs. In the presence of PUEA, the GA with the parametric transformation method is used to obtain the power allocation to the VSUs. The complexities of the proposed algorithms are also discussed.

- The detail simulation results based study are provided and compared with the existing scheme. The impact of different network parameters on the proposed algorithms is studied.

The chapter is organized as follows. Section 5.2 presents the CR-VANET system model and the detection performance is analyzed. The EE maximization problem formulation is discussed in Section 5.3. Our proposed solution approach is provided in Section 5.4. Simulation results are discussed in Section 5.5, followed by the conclusion in Section 5.6.

5.2 CR-VANET System Model

CR-VANET system model showing the distribution of the PU and the VSUs is given in Figure 5.1. The VSUs jointly perform SS on the entire licensed band but transmit their data on their respective sub-bands to the nearest SR deployed on the road side. The

sub-bands are assumed to be orthogonal to each other to avoid interference. We assume that the location of the PU and the SR are known to the VSUs. The PU is fixed, and let it be at the coordinate $[0,0]$. The VSUs are moving along the road. Let the coordinate of the mth VSU at τth instant be $[X_{m\tau}, Y_{m\tau}]$. The transmission range/protective range of the PU is denoted by D_R. Any vehicles fall inside the D_R are not allowed to transmit their data. The sensing range of the PU is denoted by D_S. S_T is the shortest distance between the PU and the edge of the road segment. It is obvious that $D_S > D_R$. The PUE attacker always tries to falsify the SUs, and prevents the SUs from transmitting their data. So, attacker is present in the sensing region on the road side. The PR is present in the protective region of the PU on the road side.
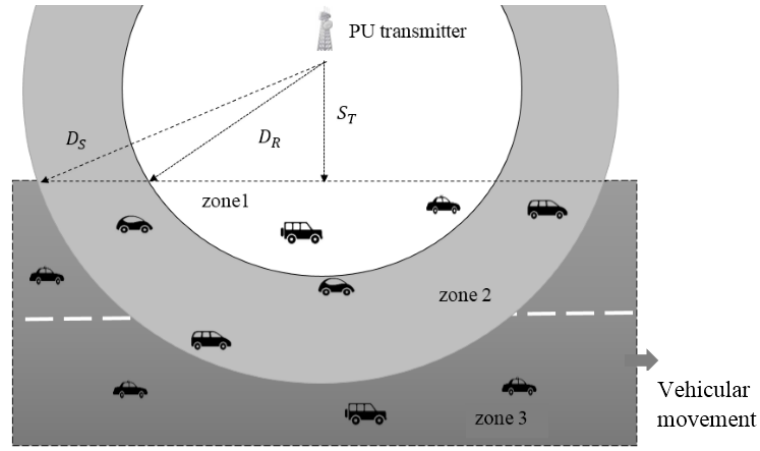
Figure 5.1: CR-VANET system model showing distribution of the CR users.

Let a_1 and a_2 be the average rates of arrival of the vehicles or the traffic flows in vehicles/sec into the sensing region and protective region, respectively. If the speed of the vehicle V is uniformly distributed between the minimum and maximum velocity V_{min} and V_{max}, respectively, then the PDF of V is given by

$$\mathscr{P}_V = \frac{1}{V_{max} - V_{min}} \tag{5.1}$$

Therefore, the expected velocity $E[V]$ is computed as $\left(\frac{V_{max} + V_{min}}{2}\right)$. Then the average vehicle densities v_{d1} and v_{d2} for the given a_1 and a_2 are given by $v_{d1} = \frac{a_1}{E[V]}$ and $v_{d2} = \frac{a_2}{E[V]}$, respectively. If **Area1** denotes the area of sensing region, then the number of VSUs expected in zone 2 can be computed as

$$M_1 = \left\lceil \frac{v_{d1}}{d_S} \textbf{Area1} \right\rceil \tag{5.2}$$

where d_S is the safety distance between the vehicles to avoid collision. Similarly, the number of vehicles expected only in the protective region is

$$M_2 = \left\lceil \frac{v_{d2}}{d_S} \textbf{Area2} \right\rceil \tag{5.3}$$

where **Area2** represents the area of zone 1. Therefore, total number of VSUs is $M =$

$M_1 + M_2$. Then, the binary hypotheses for the presence and absence of the attacker is same as (2.11), respectively. In SDF-based sensing scheme, the energy value of each SU is linearly combined with the respective weight coefficient to give the global decision as in Y_G. Here, the spatial correlation between the VSUs are represented in terms of weight coefficient. The spatial difference ρ_{mm_1} between the mth and m_1th vehicle is $\rho_{mm_1} = e^{-\varepsilon d_{mm_1}}$. Thus, the weight coefficient is calculated as

$$w_{mm_1} = \frac{\rho_{mm_1}}{\sum_{m_1=1}^{M} \rho_{mm_1}} \tag{5.4}$$

If the PU uses a BPSK signal, and the noise is real, then the global Q_d and global Q_f are evaluated taking the spatial correlation based weight coefficient which are given by

$$Q_d = \frac{1}{M} \sum_{m=1}^{M} Q \left(\frac{\lambda_g - \sum_{m_1=1}^{M} w_{mm_1} \left(1 + \gamma_m\right) \sigma_{\eta m}^2}{\sqrt{2 \sum_{m_1=1}^{M} w_{mm_1}^2 \left(1 + 2\gamma_m\right) \sigma_{\eta m}^4}} \sqrt{N} \right) \tag{5.5}$$

and

$$Q_f = \frac{1}{M} \sum_{m=1}^{M} Q \left(\frac{\lambda_g - \sum_{m_1=1}^{M} w_{mm_1} \sigma_{\eta m}^2}{\sqrt{2 \sum_{m_1=1}^{M} w_{mm_1}^2 \sigma_{\eta m}^4}} \sqrt{N} \right) \tag{5.6}$$

In the presence of the attacker, the probability of detection Q_d and the false alarm probability Q_f are obtained by replacing $\sigma_{\eta m}^2$ by $\left(\sigma_{\eta m}^2 + \beta |h_{asm}|^2 \sigma_a^2 \right)$ and γ_m by γ_{am} as in (4.2). The distance between the PU and the mth SU at time τ_s is given by $d_m(\tau_s) = \sqrt{X_{m\tau_s}^2 + Y_{m\tau_s}^2}$. If the initial velocity of the mth vehicle is V_{Im}, then the distance travelled by this vehicle in time τ_s is computed as (assuming that all the vehicles move in a straight path with moving angle zero)

$$X_{m\tau_s} = V_{Im} \tau_s + \frac{1}{2} v a_m \tau_s^2 \tag{5.7}$$

where a_m is acceleration of the mth vehicle, and v is uniformly distributed random number $v \in [-1, 1]$, provides acceleration or deceleration to the mth vehicle.

5.3   EE Maximization Problem Formulation

The VSUs present in zone 3 can transmit their data with peak power. They have no effect on the PU. Hence, the system performance is analyzed considering the vehicles present inside the sensing region. Each SU transmits its data as long as $d_m > D_R$. The location of each vehicle is recorded in the global positioning system (GPS) installed in it. It is obvious that $\tau_d > \tau_s$. So, the vehicles may not move with a same velocity during τ_d. Hence, we divide the τ_d into $\mathbb{K}$ slots, and at each kth instant, the velocity of the vehicle is assumed to be varied between V_{max} and V_{min}. Accordingly, the distances of the mth vehicle from the SR, PU and the PR are calculated.

In the absence of the attacker, the system throughput $R\left(\tilde{P}_t\right)$ is approximately given by

$$R\left(\tilde{P}_t\right) = \frac{P_{H0}}{\Gamma}\left(1 - Q_f\right) \sum_{k \in \Gamma_t} \sum_{m=1}^{M_1} log_2\left(1 + \frac{\tilde{P}_{tm}|h_{srm}(k)|^2}{N_p}\right) \tag{5.8}$$

Here, Q_f is the false alarm in the absence of the attacker. Similarly, in the presence of the attacker, (5.8) is modified as

$$R_A\left(P_t\right) = \frac{P_{H0}}{\Gamma}\left(1 - Q_f\right) \sum_{k \in \Gamma_t} \sum_{m=1}^{M_1} log_2\left(1 + \frac{P_{tm}|h_{srm}(k)|^2}{N_p + \beta|h_{ar}|^2\sigma_a^2}\right) \tag{5.9}$$

Here, Q_f is the false alarm in the presence of the attacker. $\Gamma_t \overset{\Delta}{=} \left\{\tau_s + \tau_r + \bar{\Delta}, \tau_s + \tau_r + 2\bar{\Delta}, ..., \tau_s + \tau_r + \mathbb{K}\bar{\Delta}\right\}$ and $\bar{\Delta} = \tau_d/\mathbb{K}$. $h_{srm}(k)$ is the distance dependent Rayleigh channel distributed sub-channel coefficient between the mth SU and the SR at kth instant. h_{ar} is the sub-channel coefficient between the attacker and the SR. Here, we denote $\tilde{P}_t$ and P_t as the transmitted power allocated to the SUs in the absence and presence of the attacker, respectively.

More specifically, energy consumption occurs during SS and data transmission. Data transmission takes place when the VSUs correctly identify the vacant band and when the occupied band is identified to be vacant. Further, we assume that the reporting channels between the VSUs and the FC are perfect, so, τ_r is taken very very less than Γ and τ_d. Therefore, energy consumption during the reporting is very very less, and hence it is neglected. The VSUs present in zone 1 and zone 2 that is M VSUs perform SS but the VSUs present only in zone 2 M_1 participate in data transmission. Hence, the average energy consumption can be evaluated without and with the attacker as

$$E_c\left(\tilde{P}_t\right) = P_s M \tau_s + \tau_d P\left(\overline{H}_0\right) \sum_{m=1}^{M_1} \tilde{P}_{tm} \tag{5.10}$$

and

$$E_{cA}\left(P_t\right) = P_s M \tau_s + \tau_d P\left(\overline{H}_0\right) \sum_{m=1}^{M_1} P_{tm}, \tag{5.11}$$

respectively. The propagation channel coefficient between any terminals is defined as $h \sim \aleph\left(0, d^{-\alpha}\right)$, d is the distance between the corresponding terminals. The overall system throughputs (5.8) and (5.9) consider the time-varying channel gains between the VSUs and the SR. The VSUs start transmitting their data just after τ_s and continue till the end of the frame period Γ (neglecting τ_r as $\tau_r << \tau_s$, so, distance moved by the VSUs during τ_r can be neglected). Hence, the average system throughputs are calculated by taking the distant dependent channel gains at the strating and ending time of the data transmission. If, we consider the average system throughput in the absence of the attacker, then $R\left(\tilde{P}_t\right)$ is rewritten as

$$R_V\left(\tilde{P}_t\right) = \frac{\tau_d}{\Gamma} P_{H0}\left(1 - Q_f\right) \sum_{m=1}^{M_1} log_2\left(1 + \frac{\tilde{P}_{tm}|h_{srm}|_{av}^2}{N_p}\right) \tag{5.12}$$

Similarly, average system throughput in the presence of the attacker is modified as

$$R_{VA}\left(P_t\right) = \frac{\tau_d}{\Gamma}P_{H0}\left(1 - Q_f\right)\sum_{m=1}^{M_1}log_2\left(1 + \frac{P_{tm}|h_{srm}|_{av}{}^2}{N_p + \beta|h_{ar}|^2\sigma_a{}^2}\right) \qquad (5.13)$$

where $|h_{srm}|_{av}^2 = \frac{|h_{srm}(\tau_s)|^2 + |h_{srm}(\Gamma)|^2}{2}$. Here, the EE is defined as the ratio of the average system throughput to the average power consumption. In the absence and presence of the attacker, the EE is denoted by $EE\left(\tilde{P}_t\right)$ and $EE_A\left(P_t\right)$, respectively which are given as follows

$$EE\left(\tilde{P}_t\right) = \frac{R_V\left(\tilde{P}_t\right)}{E_c\left(\tilde{P}_t\right)} \qquad (5.14)$$

and

$$EE_A\left(P_t\right) = \frac{R_{VA}\left(P_t\right)}{E_{cA}\left(P_t\right)} \qquad (5.15)$$

So, the optimization problem without PUEA is formulated as

$$\begin{array}{ll} \underset{\tilde{P}_t}{Maximize} & : \qquad \dfrac{R_V\left(\tilde{P}_t\right)}{E_c\left(\tilde{P}_t\right)} \end{array} \qquad (5.16)$$

$$Subject\quad to \qquad : \qquad \sum_{m=1}^{M_1}\tilde{P}_{tm} \leq P_{tmax} \qquad (5.16\ a)$$

$$: \qquad I_{total}\sum_{m=1}^{M_1}|h_{sdm}\left(k\right)|^2\tilde{P}_{tm} \leq I_{th} \qquad (5.16\ b)$$

$$: \qquad P_d \geq \bar{P}_d \qquad (5.16\ c)$$

$$: \qquad 0 \leq \tau_s \leq \Gamma \qquad (5.16\ d)$$

where $\bar{P}_d$ is the local target detection probability. $h_{sdm}\left(k\right)$ is the sub-channel coefficient between the mth SU and the PR at kth instant. If we compare the scenario of attacker's presence and absence with the given R_{th}, in the presence of the attacker, the VSUs need to transmit with more power to achieve the minimum throughput. Hence, a constraint is added to the EE maximization problem. So, our objective problem under the interference and power constraints considering the PUE attacker is formulated as

$$\begin{array}{ll} \underset{P_t}{Maximize} & : \qquad \dfrac{R_{VA}\left(P_t\right)}{E_{cA}\left(P_t\right)} \end{array} \qquad (5.17)$$

$$Subject\quad to \qquad : \qquad \sum_{m=1}^{M_1}P_{tm} \leq P_{tmax} \qquad (5.17\ a)$$

$$: \qquad I_{total}\sum_{m=1}^{M_1}|h_{sdm}\left(k\right)|^2P_{tm} \leq I_{th} \qquad (5.17\ b)$$

$$: \qquad \tilde{R}\left(k\right) - \bar{R}\left(k\right) \leq C_{th} \qquad (5.17\ c)$$

$$: \qquad P_d \geq \bar{P}_d \qquad (5.17\ d)$$

$$: \qquad 0 \leq \tau_s \leq \Gamma \qquad (5.17\ e)$$

where $\tilde{R}(k) = \sum\limits_{m=1}^{M_1} log_2 \left(1 + \frac{\tilde{P}_{tm}|h_{srm}(k)|^2}{N_p}\right)$ and $\bar{R}(k) = \sum\limits_{m=1}^{M_1} log_2 \left(1 + \frac{P_{tm}|h_{srm}(k)|^2}{N_p + \beta |h_{ar}|^2 \sigma_a^2}\right)$. The constraint (5.17 c) is added to control the power of secondary transmission, so that the effect of the attacker can be minimized to some extent. C_{th} is the user defined integer variable as mentioned in (4.29 c).

5.4 Solution Approach Towards the Designing of CR-VANET Without and With the PUEA

The variation of channel response with the movement of vehicular is considered in our optimization problem, which makes our proposed algorithms more comprehensive.The average system throughputs $R_V(\tilde{P}_t)$ and $R_{VA}(P_t)$ in the objective functions (5.16) and (5.17) are the approximation of the exact system throughputs (5.8) and (5.9), respectively . Further, the constraints (5.16 b) and (5.17 b) consist of the channel response $h_{sdm}(k)$ which varies with the time instant k. The constraint (5.17 c) also consists of the time-varying channel response $h_{srm}(k)$. Therefore, the proposed solution approaches to the objective fuctions (5.16) and (5.17) with these time-varying constraints are achieved by maximizing $EE(\tilde{P}_t)$ and $EE_A(P_t)$ in **Algorithm** 5.10 in which the adaptive power allocations for maximization of system throughputs satisfying the constraints are derived from **Algorithm** 5.11 and **Algorithm** 5.12 in the absence and presence of the attacker, respectively.

If R_{th} is the minimum threshold need to be achieved by each VSU, then the minimum transmission powers $\tilde{P}_{tmin}$ and P_{tmin} of the mth SU at the kth instant in the absence and presence of the attacker are represented as

$$\tilde{P}_{tminm}(k) \geq \frac{\left(2^{R_{th}} - 1\right) N_p}{|h_{srm}(k)|^2} \tag{5.18}$$

and

$$P_{tminmA}(k) \geq \frac{\left(2^{R_{th}} - 1\right) \left(N_p + \beta |h_{ar}|^2 \sigma_a^2\right)}{|h_{srm}(k)|^2}, \tag{5.19}$$

respectively. From (5.18) and (5.19), it is observed that $\tilde{P}_{tminm}(k)$ and $P_{tminmA}(k)$ vary with the VSUs and are different at different instants. Instead of taking different $\tilde{P}_{tmin}$ for different VSUs,$\tilde{P}_{tmin}(k)$ is decided by considering the farthest vehicle from the SR. The same concept is also applicable to P_{tminA}. Similarly, instead of generating different $\tilde{P}_{tmin}$ and P_{tminA} at different kth instants, we take $\tilde{P}_{tmin} = \frac{\tilde{P}_{tmin}(\tau_s) + \tilde{P}_{tmin}(\Gamma)}{2}$ and $P_{tminA} = \frac{P_{tminA}(\tau_s) + P_{tminA}(\Gamma)}{2}$. From (5.14), it is clear that $EE(\tilde{P}_t)$ is a non-convex function of $\tilde{P}_t$. Hence, this problem can be solved by using the parametric transformation based on Dinkelbach method, the way described in Theorem 2. Based on this theorem, our objective problem (5.16) is represented as

$$\Upsilon^* = \max_{\tilde{P}_t \in \tilde{P}} \left\{ \frac{R_V(\tilde{P}_t)}{E_c(\tilde{P}_t)} \right\} = \frac{R_V(\tilde{P}_t^*)}{E_c(\tilde{P}_t^*)} \quad \text{if} \quad \text{and} \quad \text{only} \quad \text{if}$$

$\max_{\tilde{P}_t \in \tilde{P}} \left\{ R_V \left(\tilde{P}_t \right) - \Upsilon^* E_c \left(\tilde{P}_t \right) \right\} = R_V \left(\tilde{P}_t^* \right) - \Upsilon^* E_c \left(\tilde{P}_t^* \right) = 0.$ $\tilde{P}_t^*$ denotes the optimal transmission power allocation to the SUs without the PUE attacker, and $\tilde{P}_t^* = \left[\tilde{P}_{t1}^*, \tilde{P}_{t2}^*, \ldots, \tilde{P}_{tM_1}^* \right]$. The solution approach to find the optimal power allocation is described in **Algorithm** 5.10.

Algorithm 5.10 Power allocation in CR-VANET.

Input:
    Randomly generate $\tilde{P}_t$ between $\tilde{P}_{tmin}$ and the constraint (5.16 a).
    Dinkelbach parameter$(\Upsilon) \leftarrow 0$;
    Acceptance tolerance value $\xi \leq 10^{-5}$;
    Current iteration $t \leftarrow 1$;
Output:
    Transmission power $\tilde{P}_t^*$.

1: **while** $|\Upsilon(t) - \Upsilon(t-1)| \geq \xi$ **do**
2:     For the given value of τ_s, evaluate power $\tilde{P}_t(t)$ from **Algorithm** 5.11 such that;

$$\tilde{P}_t = \arg\max_{\tilde{P}_t} \left\{ R_V \left(\tilde{P}_t \right) - \Upsilon(t) E_c \left(\tilde{P}_t \right) \right\}$$

3:     $t \leftarrow t+1$;
4:     $\Upsilon(t) \leftarrow \left\{ \frac{R_V(\tilde{P}_t)}{E_c(\tilde{P}_t)} \right\}$;
5: **end while**

The same **Algorithm** 5.10 is repeated for the EE maximization in the presence of the PUE attacker, where the power assigned to the VSUs in the step 2 is obtained from **Algorithm** 5.12.

5.4.1   Interference-aware power allocation without PUEA

Algorithm 5.10 describes the method of solving the EE maximization problem but the power allocation to the VSUs satisfying the constraints (5.16 b) with the maximization of $R_V \left(\tilde{P}_t \right)$ is obtained by our proposed adaptive scheme **Algorithm** 5.11. Maximization of the overall system throughput $R_V \left(\tilde{P}_t \right)$ of the CR-VANET is equivalent to the maximization of $\mathscr{R}_V(\tilde{P}_t) = \sum_{k \in \Gamma_t} \sum_{m=1}^{M_1} \log_2 \left(1 + \frac{\tilde{P}_{tm}|h_{srm}(k)|^2}{N_p} \right)$. $\mathscr{R}_V \left(\tilde{P}_t \right)$ can be approximately represented as $\mathscr{R}_V(\tilde{P}_t) \cong \sum_{m=1}^{M_1} \sum_{k \in \Gamma_t} log_2 \left(\frac{\tilde{P}_{tm}|h_{srm}(k)|^2}{N_p} \right)$. Hence, $R \left(\tilde{P}_t \right)$ can be maximized by improving $\mathscr{R}_V \left(\tilde{P}_t \right)$ which is equivalent to maximizing $\left\{ \sum_{m=1}^{M_1} \tilde{P}_{tm} R_{1m} \right\}$, where $R_{1m} = \sum_{k \in \Gamma_t} \frac{|h_{srm}(k)|^2}{N_p}$. So, the objective function for the power

allocation is expressed as

$$\underset{\tilde{P}_t}{Maximize} \quad : \quad \sum_{m=1}^{M_1} \tilde{P}_{tm}^{(j)} R_{1m} \geq S_{TH}^{(j-1)} \tag{5.20}$$

$$Subject \quad to \quad : \quad I_{total} \sum_{m=1}^{M_1} \tilde{P}_{tm}^{(j)} |h_{sdm}(k)|^2 \leq I_{th} \quad \forall k \in \Gamma_t \tag{5.20 a}$$

where $S_{TH}^{(j-1)} = \sum_{m=1}^{M_1} \tilde{P}_{tm}^{(j-1)} R_{1m}$. The objective function (5.20) with the constraint (5.20 a) is a mixed integer and non-linear problem. So, NLMS algorithm is applied to find the power allocation satisfying the time-varying constraint (5.20 a). The inequality constraints (5.20) and (5.20 a) can be converted to equality constraints as given below

$$\sum_{m=1}^{M_1} \tilde{P}_{tm}^{(j)} R_{1m} + Z_U = \sum_{m=1}^{M_1} \tilde{P}_{tm}^{(j-1)} R_{1m} \tag{5.21}$$

$$\sum_{m=1}^{M_1} \tilde{P}_{tm}^{(j)} |h_{sdm}(k)|^2 + Z_L = \frac{I_{th}}{I_{total}} \tag{5.22}$$

where Z_U and Z_L are positive and negative random variables, respectively with mean zero and their variances depends on R_{1m} and $|h_{sdm}(k)|^2$, respectively. Let us consider

$$U^{(j)}(i) = \begin{pmatrix} \tilde{P}_{t1}^{(j)} & 0 & \cdots & 0 \\ 0 & \tilde{P}_{t2}^{(j)} & \cdots & 0 \\ \vdots & \vdots & \ddots & \vdots \\ 0 & 0 & \cdots & \tilde{P}_{tM_1}^{(j)} \end{pmatrix} \tag{5.23}$$

Let $W(i)$ sequence at ith iteration is given by $W(i) = \begin{cases} Q_1 \\ Q_2 \end{cases}$, where

$$Q_1 = \begin{pmatrix} R_{11} & 0 & \cdots & 0 \\ 0 & R_{12} & \cdots & 0 \\ \vdots & \vdots & \ddots & \vdots \\ 0 & 0 & \cdots & R_{1M_1} \end{pmatrix} \tag{5.24}$$

and

$$Q_2 = \begin{pmatrix} |h_{sd1}|^2 & 0 & \cdots & 0 \\ 0 & |h_{sd2}|^2 & \cdots & 0 \\ \vdots & \vdots & \ddots & \vdots \\ 0 & 0 & \cdots & |h_{sdM_1}|^2 \end{pmatrix} \tag{5.25}$$

Z is a sequence consisting of Z_U and Z_L, and $Z = \begin{cases} Z_U \\ Z_L \end{cases}$. Similarly, for the ith iteration the right hand portions of the equality constraints (5.21) and (5.22) are represented as

$$S(i) = \begin{cases} S_{TH}^{(j-1)} \\ \frac{I_{th}}{I_{total}} \end{cases} \tag{5.26}$$

Hence, $S(i)$ can be expressed as

$$S(i) = \sum_{m=1}^{M_1} \omega_m{}^{(j)}(i) g_m(i)^T + Z(i) \tag{5.27}$$

$\omega^{(j)}(i)$ is the corresponding mth row for the ith and jth iteration of $U^{(j)}(i)$. $g_m(i)$ is the mth row of either Q_1 or Q_2 depending on the evaluation of (5.21) or (5.22). Applying NLMS algorithm, let the desired output is represented as

$$d(i) = S(i) - \sum_{m=1}^{M_1} \omega_m{}^{(j)}(i-1) \hat{v}_m(i)^T \tag{5.28}$$

$V(i)$ is the random matrix of same size of $W(i)$ and its generation is similar to $Z(i)$. So, $\hat{v}_k(i)$ is the mth vector of the matrix $\hat{V}(i) = W(i) - V(i)$. So, the error is given by

$$e(i) = d(i) - \sum_{m=1}^{M_1} \omega_m{}^{(j)}(i-1) v_m(i)^T \tag{5.29}$$

where v_m is the corresponding mth vector of matrix $V(i)$. Here, $\omega^{(j)}(i)$ is the power allocation matrix, and is evaluated from [148]

$$\omega_m{}^{(j)}(i) \leftarrow \omega_m{}^{(j)}(i-1) + \frac{\bar{\mu}}{\|v_m\|^2} v_m(i) e(i) \tag{5.30}$$

where $\bar{\mu}$ is the step size and it ranges between $0 < \bar{\mu} < 2$. The steps for interference-aware power allocation in the absence of the attacker are illustrated in **Algorithm** 5.11.

Algorithm 5.11 Interference-aware power allocation in CR-VANET.

Input:

$\xi \leftarrow$ minimum tolerence threshold.

Randomly generate $\tilde{P}_t$ between $\tilde{P}_{tmin}$ and the constraint (5.16 a).

Output:

Return power allocation $\tilde{P}_t = \tilde{P}_t^{(j)}$.

1: $\mathbb{A} \leftarrow infinity$;
2: $\mathbb{B} \leftarrow 0$;
3: $j \leftarrow j+1$;
4: **while** $\mathbb{A} \geq \mathbb{B}$ **do**
5:      $\mathbb{A} = \mathbb{B}$;
6:      $j \leftarrow j+1$;
7:      $\omega^{(j)} \leftarrow \omega^{(j-1)}$;
8:      **for** $k = 1 : length(\Gamma_t)$ **do**
9:          $\mathbb{C}^{(j)} \leftarrow I_{total} \sum\limits_{m=1}^{M_1} \tilde{P}_{tm}^{(j)} |h_{sdm}(k)|^2$;
10:          $i \leftarrow 1$;
11:          **while** $\mathbb{C}^{(j)} \geq I_{th}$ **do**
12:              Generate $W(i)$, $Z(i)$ and $V(i)$;
13:              $d(i) = S(i) - \sum\limits_{m=1}^{M_1} \omega_m^{(j)}(i-1)\hat{v}_m(i)^T$;
14:              $e(i) = d(i) - \sum\limits_{m=1}^{M_1} \omega_m^{(j)}(i-1)v_m(i)^T$;
15:              **for** $m = 1 : M_1$ **do**
16:                  $\omega_m^{(j)}(i) \leftarrow \omega_m^{(j)}(i-1) + \frac{\bar{\mu}}{\|v_m\|^2} v_m(i)e(i)$;
17:              **end for**;
18:              $i \leftarrow i+1$;
19:          **end while**
20:          $j \leftarrow j+1$;
21:          $\omega^j \leftarrow \omega^j(i)$;
22:          $\tilde{P}_t^{(j)}(k) \leftarrow \omega^{(j)}$;
23:      **end for**
24:      **for** $m = 1 : M_1$ **do**
25:          $\tilde{P}_t^{(j)}(1,m) = \frac{\sum\limits_{k \in \Gamma_t} \tilde{P}_{tm}^{(j)}(k)}{M_1}$;
26:      **end for**
27:      $\mathbb{B} = \sum\limits_{m=1}^{M_1} \tilde{P}_{tm}^{(j)} R_{1m}$;
28: **end while**

If we analyze the complexity, then the complexity of our proposed approach is calculated as $O(N_A N_B N_C)$, where N_A, N_B and N_C are the iterations required in the while loops in **Algorithm** 5.11 and in the while loop in **Algorithm** 5.10, respectively.

5.4.2 Interference-aware power allocation with PUEA

The main objective is to maximize $\{R_{VA}(P_t) - \Upsilon(t) E_{cA}(P_t)\}$ satisfying the constraints (5.17 b) and (5.17 c). Here, we apply heuristic algorithm for solving this type of non-convex combinatorial optimization problem. Previously, GA and PSO were used to solve the adaptive power allocation in [162] and [163], respectively. However, the scenarios and the methods of solving were different. Further, those papers did not consider any malicious attack in the CRN. The purpose of using an adaptive algorithm like GA is that, it can adaptively modify the population to handle a variety of optimization problems. The fitness function of our optimization problem is given by

$$\Lambda_1 = -\{R_{VA}(P_t) - \Upsilon(t) E_{cA}(P_t)\} \tag{5.31}$$

The negative sign indicates the minimization of the objective function. The constraints (5.17 b) and (5.17 c) are solved by employing our proposed rank assignment scheme in GA. As per the constraint (5.17 b),

$$I_{th} - \left(I_{total} \sum_{m=1}^{M_1} P_{tm} |h_{sdm}(k)|^2 \right) \geq 0 \tag{5.32}$$

Then, we consider a parameter to represent (5.32) as follows

$$\Lambda_2(k) = \begin{cases} 0, & \text{if } I_{th} \geq I_{total} \sum\limits_{m=1}^{M_1} |h_{sdm}(k)|^2 P_{tm} \\ 1, & \text{if } I_{th} < I_{total} \sum\limits_{m=1}^{M_1} |h_{sdm}(k)|^2 P_{tm} \end{cases} \tag{5.33}$$

The first outcome of each chromosome is evaluated as $O_1 = \sum\limits_{k \in \Gamma_t} \Lambda_2(k)$. Similarly, considering the constraint (5.17 c),

$$C_{th} - \left(\tilde{R}(k) - \bar{R}(k)^{(j)} \right) \geq 0 \tag{5.34}$$

where $C_{th} = \tilde{R}(k) - \bar{R}(k)^{(j-1)}$ and j is the current iteration. Representing the (5.34) with the following parameter as

$$\Lambda_3(k) = \begin{cases} 0, & \text{if } C_{th} \geq \left(\tilde{R}(k) - \bar{R}(k)^{(j)} \right) \\ 1, & \text{if } C_{th} < \left(\tilde{R}(k) - \bar{R}(k)^{(j)} \right) \end{cases} \tag{5.35}$$

Then the second outcome for each chromosome is evaluated as $O_2 = \sum\limits_{k \in \Gamma_t} \Lambda_3(k)$. We take the third outcome $O_3 = \Lambda_1$. The first priority is to provide sufficient protection to the PR. So, the individual with less O_1 is given rank 1. The detail steps for the adaptive power allocation algorithm employing GA are described in **Algorithm** 5.12. Our proposed approach is summarized in Figure 5.2.

Algorithm 5.12 Proposed GA aided power allocation algorithm.

1: Initialize the chromosomes randomly of size $\mathbb{D}$ and dimension M_1 over the search space. Each chromosome represents the transmitting power distribution to the M_1 VSUs.
2: Find out the fitness function Λ_1 of each chromosome.
3: $j \leftarrow 1$.
4: Repeat
5: Assign a rank to each chromosome as per the following steps.
6: **if** $(O_{1d} < O_{2d})$ **then**   ▷ O_{1d} is the first outcome of dth parent chromosome.
7:      Assign rank 1 to the dth individual;
8: **else**
9:      **if** $(O_{1d} == O_{2d})$ **then**
10:          Assign rank 2 to the dth chromosome;
11:      **else**
12:          **if** $(O_{2d} < O_{1d})$ **then**
13:              Assign rank 3 to the dth chromosome.
14:          **end if**
15:      **end if**
16: **end if**
17: For the chromosomes assigned with the same rank, one extra scaling factor is determined for each chromosome to select the best chromosome for offsprings reproduction. The scaling factors $B_d(1)$, $B_d(2)$ and $B_d(3)$ of the dth chromosome for the ranks 1, 2 and 3 are given by $B_d(1) = \frac{1}{1 + \frac{1}{O_{2d}} + \frac{1}{O_{3d}}}$, $B_d(2) = \frac{2}{2 + \frac{1}{O_{3d}}}$ and $B_d(3) = \frac{3}{3 + \frac{1}{O_{1d}} + \frac{1}{O_{3d}}}$, respectively.
18: The selection process is based on the tournament selection. The tour size is pre-decided by the user. The chromosome with lowest rank is selected, and if the rank of the chromosomes are same, then the chromosome with lowest scaling factor is selected.
19: Simulated binary crossover and polynomial mutation are used to generate the offspring chromosomes.
20: Add the offsprings with the parent chromosomes to generate the new parent chromosomes.
21: Calculate the fitness function (5.31) of each chromosome. Sort the chromosomes in ascending order of their fitness functions and choose first $\mathbb{D}$ chromosomes for the next generation.
22: $j \leftarrow j + 1$;
23: The process is continued until the maximum number of iterations is achieved.

Let N_A be the iterations required to converge the **Algorithm** 5.10. The computational complexity of the GA with tournament selection is $O(N_B \mathbb{D} M_1)$, where N_B is the number of generation required in GA. Hence, the overall complexity of our proposed algorithm is $O(N_A \mathbb{K} N_B \mathbb{D} M_1)$.
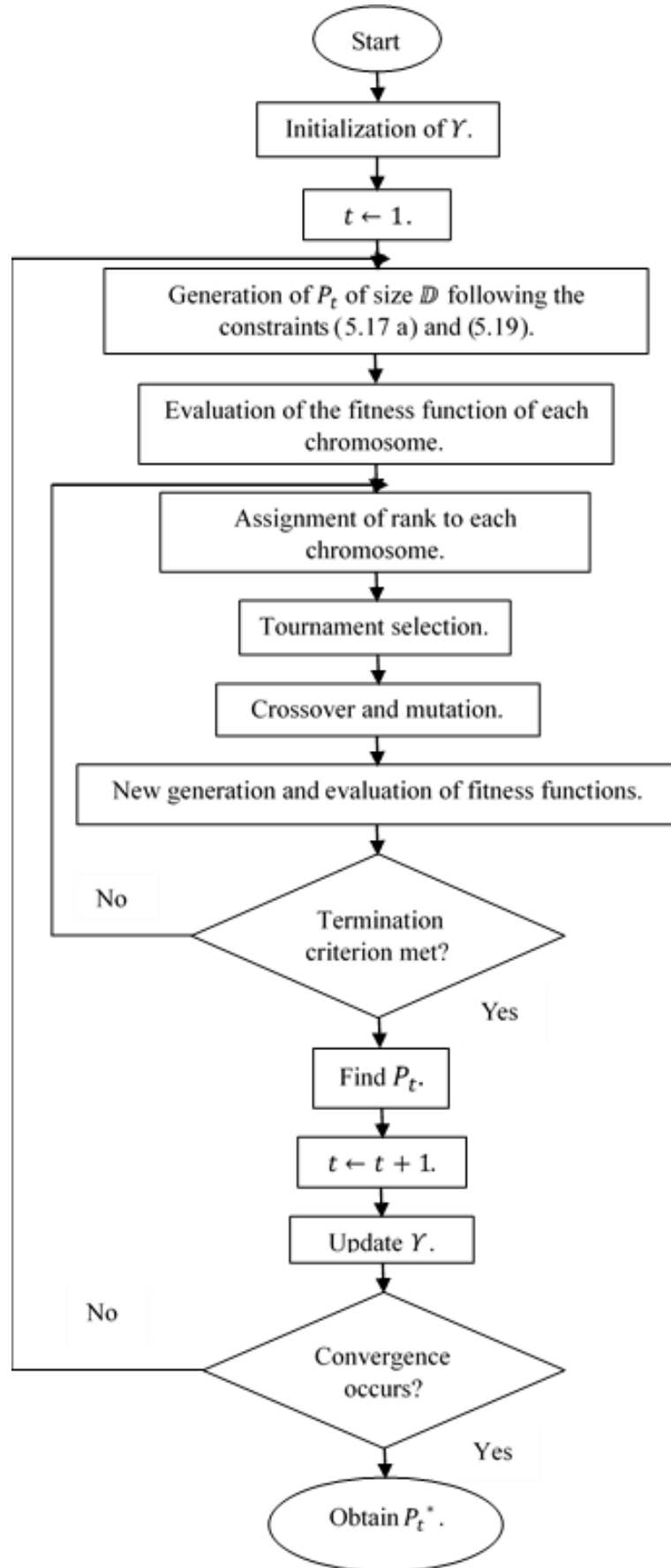
Figure 5.2: Schematic flow chart of our proposed approach for resource allocation.

5.5   Simulation Results and Discussion

The system model shown in Figure 5.1 is used as the main framework for doing the performance analysis. In GA aided power allocation algorithm, we set $\mathbb{D}$=80, tournament size is 2, and both crossover distribution index and mutation distribution index are 20. The maximum number of generation is 100. Some common parameters used in the simulation results are provided in Table 5.1.

Table 5.1: Simulation parameters for CR-VANET.

Parameter	Value	Parameter	Value
D_S	1000m	Γ	100ms
D_R	300m	τ_s	10%ofΓ
S_T	80m	τ_r	5μs
d_S	20m	P_{H0}	0.7
V_{min}	5 km/hr	P_{H1}	0.3
V_{max}	60 km/hr	α	3
f_s	6 MHz	$\sigma_s{}^2$	30 dBm
a_1	0.0025 vehicles/s	P_s	-20 dBm
a_2	0.001 vehicles/s	N_p	-100 dBm

Figure 5.3 shows effect of the attacker on the global probability of detection over different SNR conditions. We set β=0.99 for all the figures. It is observed that the presence of the attacker decreases Q_d. P_f is the local false alarm probability. Total M number of VSUs participate in SS.
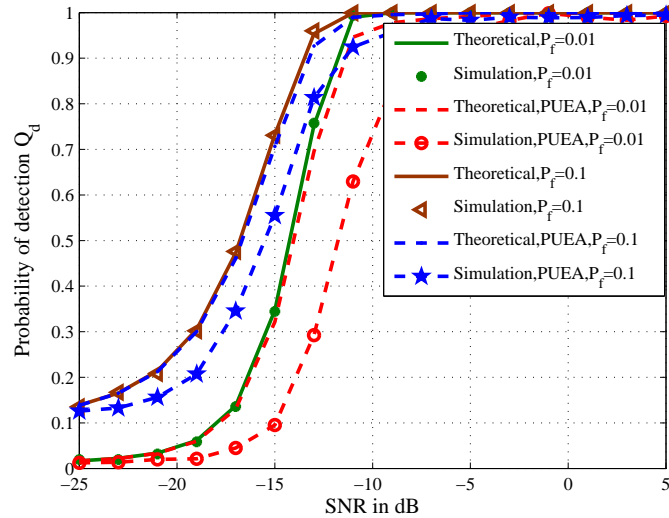

Figure 5.3: Q_d vs SNR for P_f=0.01 and 0.1 in absence and presence of the PUE attacker.

Figure 5.4a illustrates the convergence comparison of our proposed algorithm (the aid of **Algorithm** 5.10 and **Algorithm** 5.11) with the other existing schemes. In

Scheme-I, we adopt the Dinkelbach method for maximizing $EE(\tilde{P}_t)$ without considering any constraints. The iterative method is same as discussed in [119]. In Scheme-II, the iterative method discussed in [123] is adopted for power allocation to the VSUs. This scheme maximizes $EE(\tilde{P}_t)$ under the constraints (5.16 a) and (5.16 b) without considering the variations of channel gains with the velocity of the vehicles at different instances. For this scheme, we take average h_{sdm} considering the starting and ending transmission time τ_s and Γ, respectively. Therefore, $|h_{sdm}|^2$ for Scheme-II is replaced by $|h_{sdm}|^2_{av} = \frac{|h_{sdm}(\tau_s)|^2 + |h_{sdm}(\Gamma)|^2}{2}$. It is observed that EE increases by introducing the constraints into the optimization problem. This is because, the interference constraint controls the transmitting power of the VSUs. So, our proposed scheme with different values of $\bar{\mu}$ performs better than the Scheme-I. Though, Scheme-II performs better than our proposed scheme but it is not suitable for vehicular scenario. The simulation parameters used for this Figure 5.4a are SNR=-15 dB, P_f=0.01, R_{th}=2 bits/s/Hz, P_{tmax}=30 dBm and I_{th}=-70 dBm. Similarly, in the presence of the PUE attacker, Figure 5.4b illustrates the convergence comparison of our proposed algorithm (Scheme-I) with the existing schemes in the literature. But, those schemes did not consider the time-varying channel responses and the power balancing constraint which are newly introduced in our optimization problem formulation. In Scheme-II, we employ the iterative method used in [119] for maximization of $EE_A(P_t)$ (5.17) without considering any constraints. In Scheme-III and Scheme-IV, we adopt the methods used in [164] and [142], respectively for maximizing $EE_A(P_t)$ (5.17) satisfying the constraints (5.17 a) and (5.17 b). But, the time varying channel responses in (5.17 b) $I_{total} \sum_{m=1}^{M_1} |h_{sdm}(k)|^2 P_{tm} \leq I_{th}$ is replaced by $I_{total} \sum_{m=1}^{M_1} |h_{sdm}|^2_{av} P_{tm} \leq I_{th}$, where $|h_{sdm}|^2_{av} = \frac{|h_{sdm}(\tau_s)|^2 + |h_{sdm}(\Gamma)|^2}{2}$. It is obvious that EE can be maximized by including constraints into the optimization problem, hence Scheme-I and Scheme-III perform better that Scheme-II. Though Scheme-III performs better than our proposed algorithm but it provides the approximate solution to the optimization problem. In Scheme-IV, throughput is maximized to find the power allocation which is obtained by increasing the transmission power, hence, EE decreases. The exact solution for typical vehicular scenario in which the distances of the VSUs from the PU vary with the velocities and time, is obtained by our proposed approach Scheme-I. However, from these two figures it is observed that adding the constraints into the optimization problem, our proposed approaches offer improvement in EE approximately by 1.5 times for $\bar{\mu}$=0.01 and 14% compared to without taking any constraints in the absence and presence of PUEA, respectively. For Figure 5.4b, P_{tmax}=40 dBm and all other parameters remain same as Figure 5.4a .
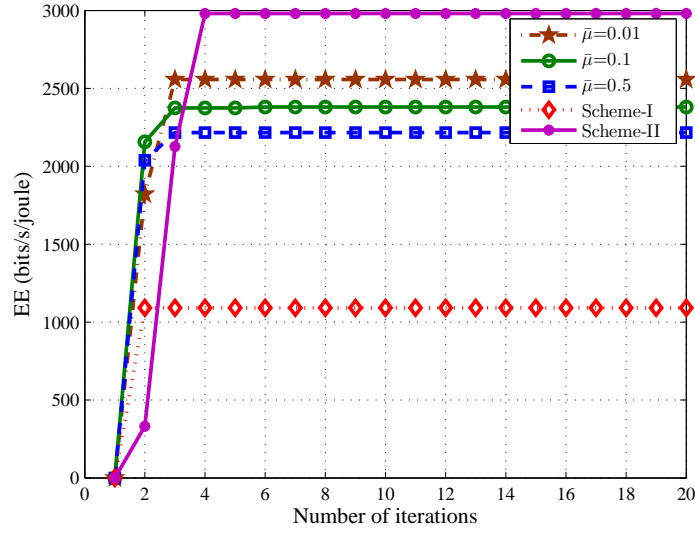
(a) Analysis of our proposed scheme in the absence of PUEA for $\bar{\mu}$=0.01, 0.1 and 0.5.
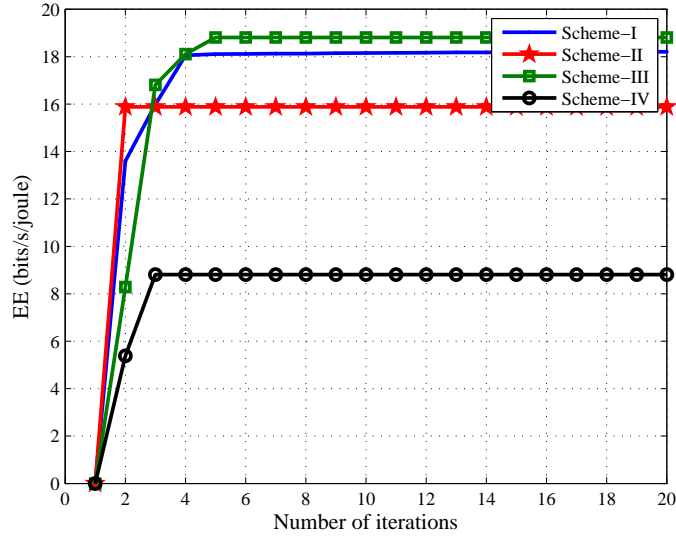
(b) Analysis of our proposed scheme in the presence of PUEA.

Figure 5.4: Convergence comparison of our proposed scheme with the iterative method discussed in **Algorithm** 5.10.

For rest of the figures, we set $\bar{P}_d$=0.9. P_{tmax} is 30 dBm and 40 dBm in the absence and presence of the attacker, respectively. Figure 5.5a and Figure 5.5b illustrate the effect of SNR on the average system throughput $R_V\left(\tilde{P}_t\right)$ and $R_{VA}\left(P_t\right)$, respectively for different values of τ_s. For Figure 5.5, we take I_{th}=-60 dBm. As SNR increases Q_f decreases with the given value of P_d. This increases $\left(1-Q_f\right)$, and hence throughput increases. Further, it is observed that at low SNR condition, longer sensing time produces less Q_f, but at high SNR when the PU can be easily detected shorter sensing time is required. Analyzing Figure 5.5a, it is observed that at low SNR i.e SNR=-23

dB, when τ_s=20% of Γ, throughput increases by 64% compared to when τ_s=5% of Γ but at high SNR i.e SNR=-9 dB, for τ_s=20% of Γ, throughput is decreased by 19% compared to τ_s=5% of Γ.
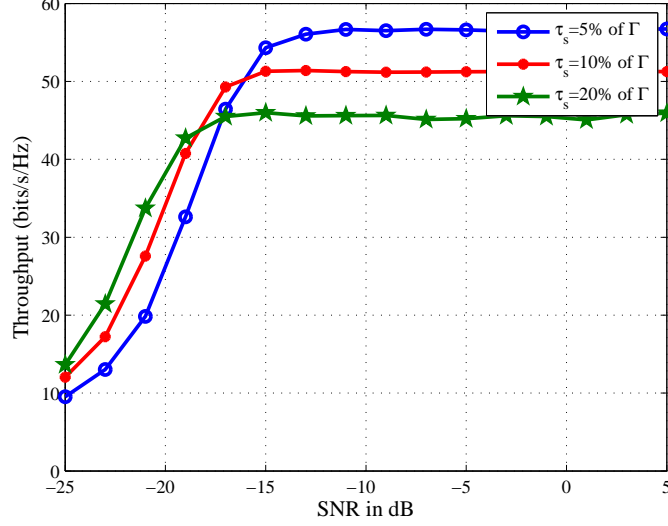
(a) In the absence of PUEA.
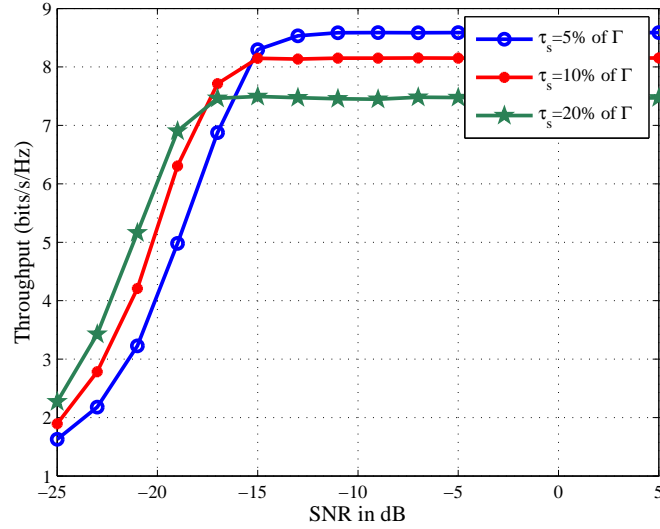
(b) In the presence of PUEA.

Figure 5.5: Average system throughput vs SNR for different values of τ_s.

Figure 5.6a and Figure 5.6b illustrate the effect of I_{th} on EE and the system throughput for different values of P_{tmax} in the absence and presence of the PUE attacker, respectively. As I_{th} increases, according to the constraints (5.16 b) and (5.17 b), the maximum allowable transmission power from the VSUs increases, accordingly, system throughput increases but EE reduces. Further, tightly bounded total transmission power P_{tmax} increases the EE but decreases the throughput. In Figure 5.6a, for I_{th}=-63 dBm, with increase in P_{tmax} by 4 dBm from 31 dBm to 35 dBm, EE

decreases by 40% but throughput increases by 39%. When I_{th} increases from -75 dBm to -51 dBm, for P_{tmax}=31 dBm, EE decreases by 78%. In Figure 5.6b, for I_{th}=-63 dBm when P_{tmax} increases from 40 dBm to 50 dBm, throughput increases by 0.05%, but EE does not show any significant changes.
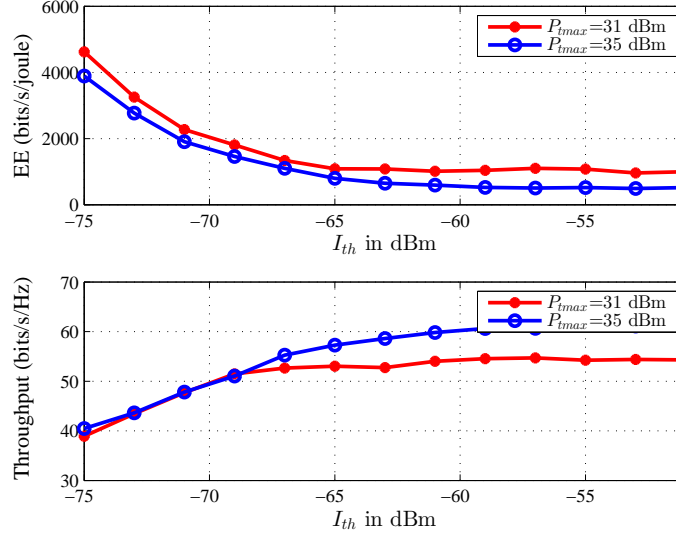
(a) In the absence of PUEA.
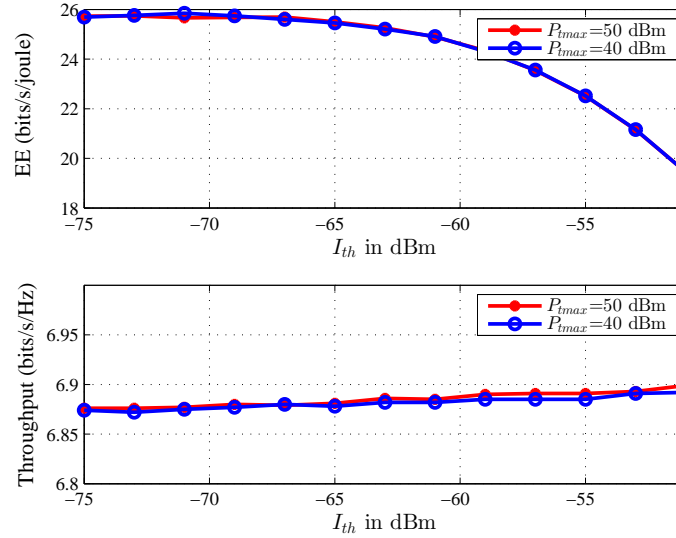
(b) In the presence of PUEA.

Figure 5.6: Effect of I_{th} on EE and average system throughput.

The impact of R_{th} on $EE\left(\tilde{P}_t\right)$ and $E_c\left(\tilde{P}_t\right)$, and on $EE_A\left(P_t\right)$ and $E_{cA}\left(P_t\right)$ are demonstrated in Figure 5.7a and Figure 5.7b , respectively. From (5.18) and (5.19), it is clearly observed that $\tilde{P}_{tmin}$ and P_{tminA} increase with increase in R_{th}, so EE decreases but total power consumption increases. Hence, analyzing Figure 5.7a, when R_{th} increases from 0.3 to 2.5 bits/s/Hz,EE decreases by 6% but power consumption

increases by 24% for SNR=-10 dB. In Figure 5.7b, it is verified that for R_{th}=2.1 bits/s/Hz, EE of the system model without PUEA is increased by 12 times over the system model with PUEA. This is because, power consumption with PUEA increases by 80% over the system model without PUEA for the same R_{th}. For Figure 5.7, I_{th} is set at -55 dBm.
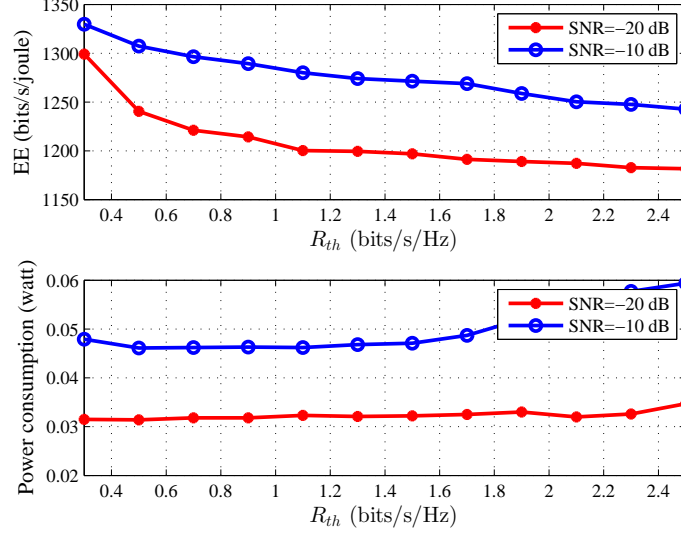
(a) Effect of R_{th} on $EE\left(\tilde{P}_t\right)$ and $E_c\left(\tilde{P}_t\right)$.
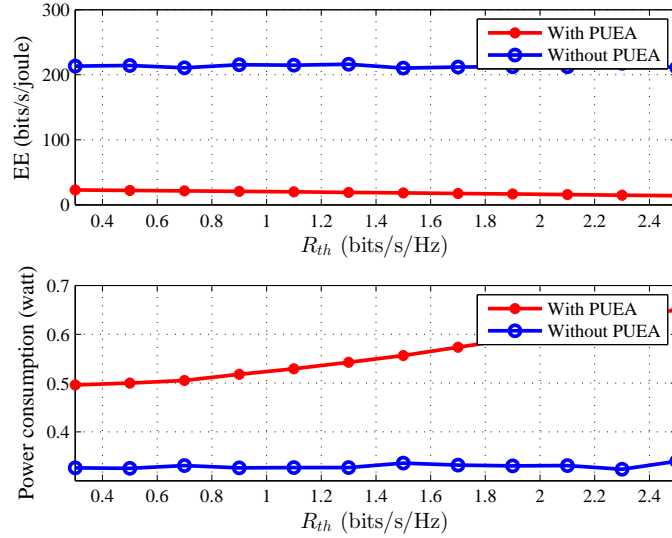
(b) Effect of R_{th} on $EE_A\left(P_t\right)$ and $E_{cA}\left(P_t\right)$.

Figure 5.7: Effect of R_{th} on EE and the total power consumption.

The variations of $R_V\left(\tilde{P}_t\right)$ and $E_c\left(\tilde{P}_t\right)$ for different target detection probability $\bar{P}_d$ values are shown in Figure 5.8a. Similarly, The variations of $R_{VA}\left(P_t\right)$ and $E_{cA}\left(P_t\right)$ for different target probability of detection $\bar{P}_d$ values are shown in Figure 5.8b. In the conventional SS technique, false alarm probability increases with increase in detection

probability. Hence, $\left(1 - Q_f\right)$ decreases with increase in $\bar{P}_d$. So, both system throughput and total power consumption decrease. In Figure 5.8b, it is clearly observed that power consumption will be more for higher value of β. For $\bar{P}_d$=0.9, throughput is reduced by 12% but power consumption increases by 3.5% when β is increased from 0.8 to 0.99.
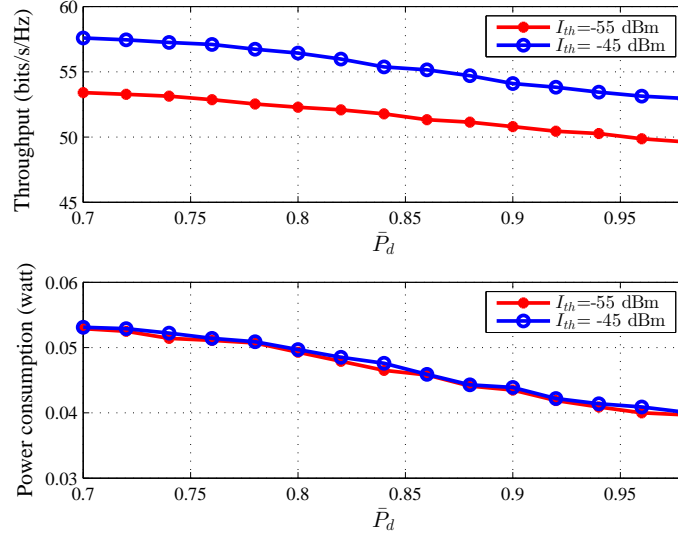
(a) Effect of $\bar{P}_d$ on $R_V\left(\tilde{P}_t\right)$ and $E_c\left(\tilde{P}_t\right)$.
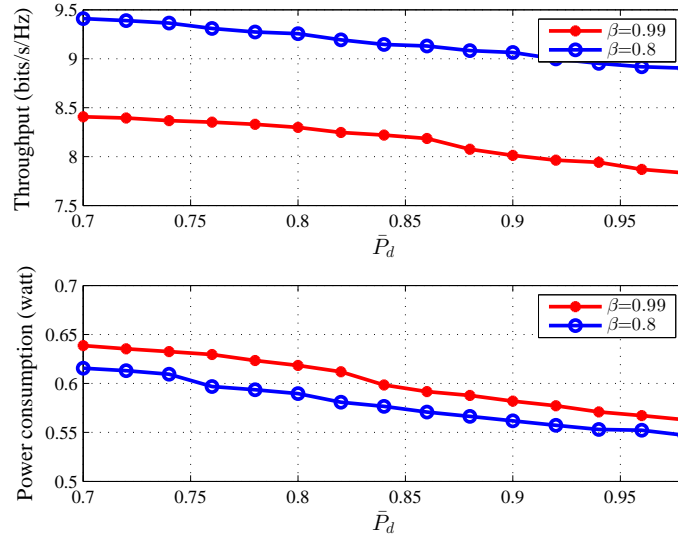
(b) Effect of $\bar{P}_d$ on $R_{VA}\left(P_t\right)$ and $E_{cA}\left(P_t\right)$.

Figure 5.8: Effect of $\bar{P}_d$ on the system throughput and the total power consumption.

5.6 Summary

This chapter proposed adaptive approaches for power allocation in the CR-VANET. A system model consisting of PU, PR, VSUs, SR and the attacker was designed for a typical vehicular scenario where the protective region of the PU and the sensing region

of the VSUs covered a small portion of the road segment and the vehicles were moving unidirectional. Accordingly, number of possible VSUs in different zones were evaluated. The EE maximization problem was formulated under the constraints of maximum transmission power, minimum achievable data rate, target probability of detection and interference to the PR. In the presence of PUEA, an extra constraint was added to control the additional increase of the transmitting power from the VSUs. The non-linear and non-convex optimization problem was solved by the well-known parametric transformation. The power allocation to the VSUs was achieved by the proposed adaptive algorithm based on NLMS. In the presence of PUEA, a GA based power allocation algorithm which maximized EE with the defined constraints was verified to be efficient. Performance assessment through simulation studies showed that the EE can be maximized by including power limiting constraints. The effects of interference threshold, throughput threshold, SNR and probability of PUEA presence on the performance parameters such as EE, throughput and power consumption were studied in detail. Upto this chapter, CR application in the licensed TV band was considered in the study. Recently, considering the limited spectrum availability due to heavily deployed wireless devices and applications, the unlicensed ISM band has attracted the researchers worldwide to consider the CR deployment in this band. As, there is no concept of PUs or SUs, the CR devices must operate in such a way so as to avoid interference or collision to other coexisting devices. With the concept of the CR user (CRU) occupying the underutilized sub-band and using that band for its data transmission without interrupting the coexisting devices, an extensive study and analysis is extended to the next chapter.

Chapter 6

Spectrum Occupancy Prediction and Optimal Power Allocation to the CRU-A Study in the 2.4 GHz ISM Band

This chapter presents the spectrum occupancy statistics of the ISM band evaluated from real measurement data. The highlights of the chapter are

- An occupancy prediction algorithm based on FLANN is proposed to forecast the future spectrum usage profile.

- A double threshold-based sub-band selection scheme is proposed for the CRU.

- An inference-aware power allocation technique is proposed for the CRU so that collision to the coexisting devices can be avoided.

6.1   Introduction

NOW-A-DAYS, an efficient spectrum utilization is one of the major issues, where the wireless technologies must compete to investigate the underutilized frequency band for their use. To make the CR deployment successful in the near future, an effective measurement in different bands assigned for several services is essential to provide detailed characteristics of the PU activity. Several measurement campaigns have been conducted in various locations worldwide, covering a wide frequency range, to assess the potential bands available for secondary usage in the context of CR. It has been observed that spectrum occupancy varies with the locations and duration of measurements taken, as well as with the type of licensed band. The increasing demands of more spectrum attract the researchers to incorporate the CR on the unlicensed band; where, the users can not be distinguished as PU and SUs, and all the devices have equal rights to use this spectrum band [165]. The unlicensed band includes ISM band and Unlicensed National Information Infrastructure (U-NII) band. The ISM band is often shared by various unlicensed electronic devices such as IEEE 802.11 standard WLAN, 802.15.1 standard Bluetooth devices, 802.15.4 standard ZigBee, cordless phones, microwave ovens (emits frequency mostly in 2.45 GHz), etc., with approximately no coordination amongst them. The operation of these devices in the same band increases the potential interference between them. Hence, it is worth to exploit the capability of CR i.e. to find the less occupied frequency bands which improve the spectral efficiency with limited unpredictable interference with the co-existing devices.

6.1.1   Related works

Most of the papers address spectrum occupancy in the licensed band for CR application but there are few papers which discuss the idea of CR implementation in ISM band by investigating the occupancy statistics in different locations and in different scenarios [166]. In Cambridge, UK, a measurement campaign was conducted in three different areas in the presence of different interfering devices. The results showed that the occupancy statistics varied with the measurement locations and types of interfering devices [167]. Another measurement was conducted in eight different

locations of Oulu, Finland each with one week of observation revealed the lower occupancy status i.e 0 - 3 % in ISM band [168]. Here, a novel method named transmission encapsulation based on the connected component labeling (TECCL) was proposed to find the number of free channels per time instant. A distributed and directional spectrum occupancy model was presented to study the impact of spatial dimension on the measurement system [169]. In that paper, two measurement devices each with 3 directional antennas were placed in the office to measure occupancy from all the directions. A dynamic channel selection algorithm was proposed in the coexistence of IEEE 802.11 WLAN and IEEE 802.15.4 sensor networks in [170]. A Wi-Fi Cognitive Radio Learning (CORAL) platform was conducted in downtown Ottawa to identify the spectrum holes, and also occupancies of all the channels and their transmission rate were investigated [171]. Most of the popular SS techniques employ EDs for simplicity, where the judgment of PU activity is based on a threshold value. During the spectrum occupancy measurement, the threshold value was chosen to be a certain number of dB above the noise floor [172], or was calculated from allowable false alarm probability [173] (with some underlying assumptions regarding noise and signal distributions). This chapter introduces an optimum threshold evaluation approach from the real data to enhance the efficiency of all the channels available in this band by avoiding interference to the coexisting devices in a particular channel.

Several spectrum occupancy prediction models mentioned in the existing literature were mostly based on multi-layer perceptron (MLP)-based neural networks [174] and hidden Markov models (HMM) [175]. In [174], hour long data records were divided into 60 intervals each consisting of 360 data samples, and these records were processed through a MLP predictor to show the prediction accuracy. A neural network based prediction model was developed to measure the cooperative spectrum occupancy in Abuja, Nigeria for different bands including the 875 MHz broadcasting band, a GSM downlink at 905 MHz, a 3G downlink at 1865 MHz, and a GSM uplink at 890 MHz band [176]. In that paper, the authors used two spectrum analyzers (SAs) for signal reception so as to improve the reliability of the prediction; also, the prediction accuracy was improved by employing GA for optimizing weights of the MLP model. The probability of incorrect prediction using the MLP predictor for busy and idle channel status were verified under different traffic characteristics of PU, and this was reduced to 4.07 % by taking perfect training and testing samples [177]. Further, the prediction error was reduced to 14% by employing multi-secondary users each having a channel status predictor [178].

In the literature, the spectrum occupancy measurement was based on the single threshold, and the detailed analysis regarding the CR deployment in ISM band was not

studied. This chapter introduces novel approaches for spectrum occupancy prediction and implementation of CR technology in ISM band utilizing the real time measurement data.

6.1.2 Chapter contributions and organization

The main contributions of the chapter are briefly discussed as follows.

- The spectrum occupancy is estimated using different thresholds in 2.4 GHz ISM band based on the real indoor measurement data.

- Furthermore, a novel forecasting algorithm using FLANN is proposed to predict the future occupancy statistics from previous data sets.

- This chapter further introduces a novel concept of deploying CR technology in the ISM band with least interference to the coexising electronic devices by selecting suitable sub-band and power allocation.

- This is achieved by double threshold-based sub-band selection method in which the CR will select the appropriate sub-band for its data transmission.

- Considering the maximum and minimum transmission power from the various devices in the ISM band, the lower and upper bound of the transmitting power of the CR node is decided.

- Further, an interference-aware power allocation scheme is proposed, so that the CRUs can communicate with each other without causing any interference to other existing devices.

- Experimental results are provided to validate our proposed schemes.

The rest of the chapter is structured as follows. The measurement setup is discussed in detail in Section 6.2. Section 6.3 explains the structure of FLANN and its application toward spectrum occupancy measurement. Different threshold adaptations for spectrum occupancy are evaluated in Section 6.4. Our proposed prediction algorithm is discussed in Section 6.5. The implementation CR technology in the ISM band based on double threshold-based sub-band selection scheme and proper power allocation considering the propagation channel model in the indoor environment are given in Section 6.6. The performances of our proposed approaches are evaluated and discussed in Section 6.7. Finally, Section 6.8 presents the chapter summary.

6.2 Measurement Setup

Our measurement campaign was conducted in different positions of four indoor hallways present in the first through third floors (mostly on the second and third floors) of the Swearingen Engineering Center, University of South Carolina, Columbia, SC, USA over 5 working days (Monday - Friday) from 9 AM to 5 PM during Fall 2014 semester from October 13th to October 17th in 2014. For our experiment, the measurement equipment consisted of an omnidirectional monopole antenna for the 2.4 GHz frequency band which received Wi-Fi signals from the APs installed behind the ceiling (spaced approximately 80-120 m apart from each other), from WLAN terminals, and from various electronic devices such as Bluetooth and microwave ovens, etc. The received signal was input to an Agilent N9342C portable SA. The SA stored the received signal power across the entire frequency range during the measurement periods. Finally, all the stored raw data was processed through MATLAB® to evaluate the spectrum occupancy statistics. Figure 6.1 shows the measurement setup diagram in the hallways of Swearingen Engineering building. The measurement setup parameters of the SA are listed in Table I.

The SA and antenna were placed on a movable plastic equipment cart, and the received power was continuously recorded and stored in the SA over the measurement periods of duration 8 hours, from 9 AM to 5 PM. The data was gathered over a time span T_{span}=8 hours for 5 working days and along a frequency span F_{span}=100 MHz. If N_{points} is the number of frequency points measured by the SA, then the discrete frequency point f_n in the range of F_{span} is given by

$$f_n = f_{start} + (n-1).f_r \tag{6.1}$$

where $n = [1, 2, \ldots, 461]$. f_{start} is the starting frequency. f_r is the frequency resolution and is determined by $f_r = \frac{F_{span}}{N_{points}}$. Here, F_{span} is 100 MHz and N_{points} is the number of sweep/trace points in the Agilent N9342C handheld SA, which is fixed at 461 (regardless of center frequency and span).

Figure 6.1: Measurement setup in the hallway of Swearingen Engineering Center.

Table 6.1: SA parameters used for spectrum occupancy measurements.

SA parameters	Values
Frequency range	2.4-2.5GHz
Number of trace points	461
Resolution bandwidth (RBW)	1MHz
Video bandwidth (VBW)	1MHz
Sweep time	18.103 msec(Auto selected)
Reference level	-5dBm
Impendance	50 ohms
Attenuation	0 dB
Preamplifier	OFF

6.3 Functional Link Artificial Neural Network Structure

Neural Networks have been good candidates for learning in the CRNs. There are different types of neural network models such as Feed-forward MLP, Recurrent MLP, radial basis function (RBF), etc., which perform the same function but with high computational cost and complexity due to the presence of a hidden layer. Hence, a better prediction model with lower complexity is desirable to make the SS faster in the

CRNs. FLANN may be a good solution to fulfill these objectives. This alternate ANN structure was first proposed by Pao [179] to replace MLP since FLANN has a faster convergence rate and lower complexity. It is a novel single layer ANN model which eliminates the need of a hidden layer. In contrast to MLP, FLANN acts on the entire input pattern by using a set of linearly dependent functional expansions [180], [181]. In this chapter, we consider Trigonometric and Chebyshev polynomials for functional expansions, and the output node is followed by the typical sigmoid transfer function that provides a nonlinear mapping between input and output.

The Trigonometric polynomial basis function comprises orthogonal sine and cosine functions and is given by the set $\{I_n, cos\,(\pi I_n), sin\,(\pi I_n), cos\,(2\pi I_n), sin\,(2\pi I_n), ..., cos\,(D\pi I_n), sin\,(D\pi I_n)\}$ for any arbitrary input I_n, and D depends on the dimension of the functional expansion [181]. The generalized structure of the Trigonometric functional expansion based on FLANN is presented in Figure 6.2.
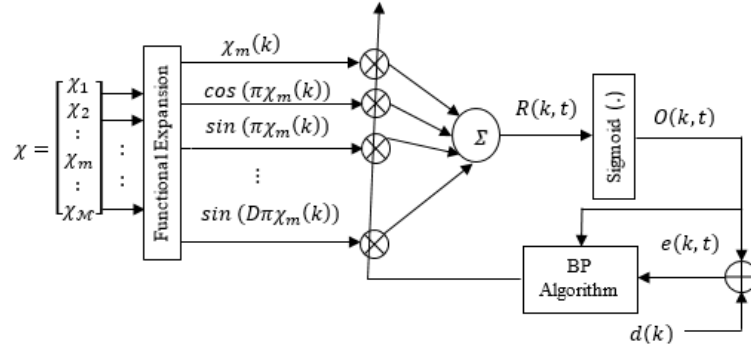
Figure 6.2: General structure of Trigonometric polynomial based on FLANN.

Another set of polynomials called Chebyshev polynomials, derived from the solution of the Chebyshev differential equation, offer less computation time than the Trigonometric expansions. These polynomials are generated by using this recursive formula [182]

$$T_{l+1}\,(I_n) = 2I_nT_l\,(I_n) - T_{l-1}\,(I_n) \tag{6.2}$$

where l is the order of the Chebyshev polynomial. For example, zero and first order polynomials are given by $T_0\,(I_n) = 1$ and $T_1\,(I_n) = I_n$ respectively, and higher order polynomials are given by $T_2\,(I_n) = 2I_n^2 - 1$, $T_3\,(I_n) = 4I_n^3 - 2I_n$ and so on. Let χ be an input vector consisting of $\mathcal{M}$ parameters $\chi = [\chi_1\chi_2...\chi_m...\chi_{\mathcal{M}}]^T$ where each parameter χ_m consists of K elements. Then, for the Trigonometric expansion, the kth element of the mth parameter of χ vector is expanded using D cosine terms, D sine terms plus the

sample $\chi_m(k)$ itself, yielding a vector of length $J = 2D+1$ which is given by

$$T(k) = \{\chi_m(k), \cos(\pi\chi_m(k)), \sin(\pi\chi_m(k)), \cos(2\pi\chi_m(k)), \sin(2\pi\chi_m(k)), \ldots$$
$$\ldots, \cos(D\pi\chi_m(k)), \sin(D\pi\chi_m(k)) \quad (6.3)$$

If the Chebyshev polynomial expansion is used, then the expanded pattern of the kth element of the mth parameter is expressed as

$$C(k) = \left\{ 1, \chi_m(k), 2\chi_m(k)^2 - 1, 4\chi_m(k)^3 - 3\chi_m(k), \ldots \right\} \quad (6.4)$$

of length $J = 2D+1$. For our experiment, the number of elements in the Trigonometric polynomial function is the same as that in the Chebyshev functional expansion. Hence, the total number of basis functions is $J = 2D+1$. In contrast to MLP, here the weight vector W is linearly combined with the expanded polynomial basis function. Let t be the current iteration number, then the weight vector W is represented as

$$W(t) = \left\{ w_1(t), w_2(t), \ldots, w_j(t), \ldots, w_J(t) \right\}^T \quad (6.5)$$

At the output, a logistic sigmoid function is used to provide a nonlinear mapping between the output and input. So, the predicted output of the FLANN model is calculated as

$$O(k,t) = \frac{1}{1 + \exp(R(k,t))} \quad (6.6)$$

where $R(k,t)$ represents the internal output of the kth element at iteration t, which is given by

$$R(k,t) = T(k)W \ \ or \ \ C(k)W \quad (6.7)$$

If $d(k) = \{d_1(k), d_2(k), \ldots, d_m(k), \ldots, d_{\mathscr{M}}(k)\}$ is the desired output, then the error for kth element at iteration t is calculated by subtracting the predicted output from the desired output;

$$e(k,t) = d(k) - O(k,t) \quad (6.8)$$

For the training process, weights are updated by using the back propagation algorithm as per the following expression [180]

$$W(t+1) = W(t) + \varphi\bar{\beta}(k,t)(T(k))^T \quad (6.9)$$

Here, φ is known as the learning rate and its range is $0 < \varphi < 1$ and $\bar{\beta}(k,t)$ is given by

$$\bar{\beta}(k,t) = \left(1 - O(k,t)^2\right)e(k,t) \quad (6.10)$$

6.4   Signal Detection and Spectrum Occupancy

The spectrum occupancy is calculated by separating out the information signal from the noise in the desired band. The information signal is detected by comparing its received signal energy with a predefined threshold λ. If P is the average power of the PU signal

received at the SU, then probability of detection and false alarm are given by

$$P_d = Q\left(\frac{\lambda - (P + \sigma_\eta^{\,2})}{(P + \sigma_\eta^{\,2})\sqrt{2/N}}\right) \tag{6.11}$$

and

$$P_f = Q\left(\frac{\lambda - \sigma_\eta^{\,2}}{\sigma_\eta^{\,2}\sqrt{2/N}}\right), \tag{6.12}$$

respectively. Here, false alarm probability means the probability that the noise samples are present above the selected threshold. Similarly, the probability of detection refers to the probability that the received samples present above the threshold.

6.4.1 Threshold evaluation

Selection of threshold is a critical aspect in separating the signal from the noise. A low value of threshold gives overestimation of the channel occupancy. Similarly, some of the weak signal samples cannot be detected if the threshold value is chosen too high, which results in underestimation of channel occupancy. In this paper, thresholds are evaluated by employing three different methods.

Fixed threshold-based evaluation

This threshold evaluation model relies on the calculation of probability distribution of received signal power and received noise power. Figure 6.3 shows the normalized probability distributions of both received signal power and noise power, and the intersecting line represents the fixed decision threshold which is found to be -85.2830 dBm.
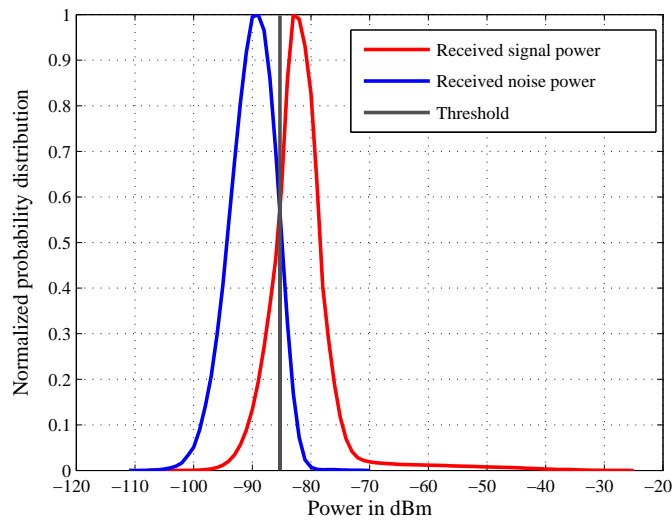

Figure 6.3: Probability distributions of received signal power and noise power with estimated threshold from measurement data.

Dynamic threshold-based evaluation

The SA collects the signal samples at 461 frequency points, and the average noise floor is different at each discrete frequency point. So, we employ different decision thresholds at different frequency points. To do so, a dynamic threshold value at each frequency point is calculated from the allowable false alarm probability. We know that $P_f < 0.5$ represents the aggressive CR system to attain more than 50% spectrum utilization with less than 50% interference to the PU [86]. Hence, for our experiment, we have chosen targeted P_f to be 0.1.

Optimum threshold-based evaluation

In a single threshold-based detection scheme, threshold value plays a major role in determining the system performance. Considering the CR system, both the probability of detection P_d and false alarm probability P_f decrease monotonically with respect to threshold λ, so, a trade-off must be maintained to achieve a target P_f with the minimization of P_{md}, where $P_{md} = 1 - P_d$ is the probability of missed detection. To achieve this, an optimum detection threshold λ^* must be chosen that will minimize the total sensing error (with optimum here defined as attaining the desired P_f with minimum P_{md}).In unlicensed bands like the ISM band, an optimum threshold is necessary to reduce the interference between the co-existing systems.

Proposition 4. *If we assume that λ_1 and λ_2 be the minimum and maximum threshold values selected from our received signal samples, then the total sensing error, defined as $P_e(\lambda) = zP_f(\lambda) + (1-z)P_{md}$, is a convex function of λ which monotonically decreases from $\lambda_1 \geq \lambda > \lambda^*$ and increases from $\lambda^* < \lambda \leq \lambda_2$. So, there necessarily exists an optimum threshold value λ^* which produces minimum sensing error.*

Proof. Proof of this proposition is given in **Appendix F** . □

Parameter z is known as a weighting factor which maintains the balance between false alarm probability and miss detection probability. Its range is $0 \leq z \leq 1$ and its value is chosen based on whether we give more importance to decreasing P_f or to decreasing P_{md}. Here, we consider that both play the same role, so, we set $z = 0.5$. Hence, minimization via golden section search algorithm can be employed to calculate the optimum threshold value λ^* [125]. For example, in Figure 6.4, one can observe that sensing error monotonically decreases from threshold value -89 dBm to λ^* dBm and then monotonically increases from λ^* to the threshold value -82 dBm. Hence, after applying the golden section search algorithm λ^* is calculated to be -84.7511 dBm for minimum sensing error 0.1463. Worth noting it that the sensing error is quite small over a range of ~ 1 dB or more, hence in practice threshold specification only requires this order of precision.
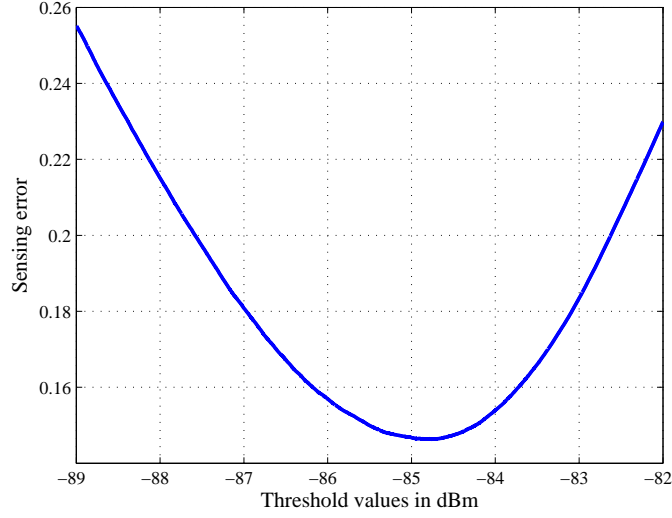
Figure 6.4: Convex characteristic of sensing error with respect to threshold at *z*=0.5.

6.4.2 Spectrum occupancy

Occupancy of a particular spectrum is calculated from the received sample values that exceed the predefined threshold. The data samples are collected over a time period T_{span} and over a frequency range F_{span}, then the data matrix is represented as

$$A = [A(\tau_i, f_j)] \tag{6.13}$$

where $i = [1, 2, ..., \mathbb{I}]$ and $j = [1, 2, ..., \mathbb{J}]$. Here, $\mathbb{I}$ represents the total number of discrete time instants and $\mathbb{J}$ represents the total number of frequency points. $A(\tau_i, f_j)$ represents the received signal power at the ith time instant and jth frequency point. For occupancy calculation, each component of the matrix is compared with the predefined threshold and a new matrix is computed, with elements are set to one if A exceeds the threshold, otherwise the elements are set to zero. Then the total number of ones is divided by the total number of measurement samples to obtain the fractional occupancy measure.

Fixed decision threshold-based spectrum occupancy evaluation

In this method, average threshold λ is calculated from the PDF of signal and noise components. Then, the decision metric element is represented as

$$D_M(\tau_i, f_j) = \begin{cases} 1 & \text{if } A(\tau_i, f_j) \geq \lambda \\ 0 & \text{if } A(\tau_i, f_j) < \lambda. \end{cases} \tag{6.14}$$

So, the spectrum occupancy at jth frequency point is computed as

$$Occupancy(1, f_j) = \frac{\sum_{i=1}^{\mathbb{I}} D_M(\tau_i, f_j)}{\mathbb{I}} \tag{6.15}$$

Similarly, the spectrum occupancy at ith time instant is computed as

$$Occupancy(1, \tau_i) = \frac{\sum_{j=1}^{\mathbb{J}} D_M(\tau_i, f_j)}{\mathbb{J}} \tag{6.16}$$

Dynamic decision threshold-based spectrum occupancy evaluation

In this method, P_f is set fixed for all the frequency points and then λ_j is computed such that only a targeted fraction of the noise samples at the jth frequency point lie above the threshold value. The decision metric is given by

$$D_M\left(\tau_i, f_j\right) = \begin{cases} 1 & \text{if } A\left(\tau_i, f_j\right) \geq \lambda_j \\ 0 & \text{if } A\left(\tau_i, f_j\right) < \lambda_j. \end{cases} \tag{6.17}$$

Then, the spectrum occupancy at each frequency point and time instant are calculated as per (6.15) and (6.16), respectively.

Optimal decision threshold-based spectrum occupancy evaluation

In this method, optimal threshold λ^* is calculated by using the golden section search algorithm on $P_e\left(\lambda\right)$ to get the minimum sensing error. For this case, the decision metric is given by

$$D_M\left(\tau_i, f_j\right) = \begin{cases} 1 & \text{if } A\left(\tau_i, f_j\right) \geq \lambda^* \\ 0 & \text{if } A\left(\tau_i, f_j\right) < \lambda^*. \end{cases} \tag{6.18}$$

The spectrum occupancy at each frequency point and time instant are calculated as per (6.15) and (6.16), respectively.

6.5 Proposed Prediction Algorithm Based on FLANN

Our main objective is to design the spectrum occupancy model for one day in advance using Trigonometric FLANN. As noted, we collected a set of data over 5 working days from Monday to Friday from 9 AM to 5 PM. The total length of time of observation is divided into 32 time slots of duration 15 minutes and the observation difference, i.e., the occupancy difference between any arbitrary selected days, taken at the exact same time instant τ_i which is computed at 15 minute intervals. This periodic evaluation is done to manage complexity and gain insight with initial results.

Let $O_M\left(\tau_1, \tau_2, .., \tau_{\mathbb{I}}\right)$, $O_T\left(\tau_1, \tau_2, .., \tau_{\mathbb{I}}\right)$, $O_W\left(\tau_1, \tau_2, .., \tau_{\mathbb{I}}\right)$, $O_{TH}\left(\tau_1, \tau_2, .., \tau_{\mathbb{I}}\right)$ and $O_F\left(\tau_1, \tau_2, .., \tau_{\mathbb{I}}\right)$ be the matrices each consisting of the 32 elements of measured spectrum occupancy at $\left(\tau_1, \tau_2, ..., \tau_{\mathbb{I}}\right)$ instants on days Monday through Friday, respectively, which are evaluated from (6.18) and (6.16). Here, the value of $\mathbb{I}$ is equal to 32. The final estimated occupancy statistics of 4 days are represented as $O_{TF}\left(\tau_1, \tau_2, .., \tau_{\mathbb{I}}\right)$, $O_{WF}\left(\tau_1, \tau_2, .., \tau_{\mathbb{I}}\right)$, $O_{THF}\left(\tau_1, \tau_2, .., \tau_{\mathbb{I}}\right)$ and $O_{FF}\left(\tau_1, \tau_2, .., \tau_{\mathbb{I}}\right)$ for Tuesday through Friday, respectively and are obtained by updating the weights of the FLANN to minimize the error between measured and predicted spectrum occupancy values. For our proposed model, the corresponding threshold values λ_2, λ_3 and λ_4 are evaluated from the final estimated occupancy results $O_{TF}\left(\tau_1, \tau_2, .., \tau_{\mathbb{I}}\right)$, $O_{WF}\left(\tau_1, \tau_2, .., \tau_{\mathbb{I}}\right)$ and $O_{THF}\left(\tau_1, \tau_2, .., \tau_{\mathbb{I}}\right)$, respectively. Let $\hat{O}_T\left(\tau_1, \tau_2, .., \tau_{\mathbb{I}}\right)$,

$\hat{O}_W(\tau_1, \tau_2, .., \tau_{\mathbb{I}})$, $\hat{O}_{TH}(\tau_1, \tau_2, .., \tau_{\mathbb{I}})$ and $\hat{O}_F(\tau_1, \tau_2, .., \tau_{\mathbb{I}})$ be the matrices consisting of predicted spectral occupancy values of Tuesday through Friday, respectively. As, our observation duration is the same for all the week days, occupancy statistics are calculated for the same 32 instants. Steps explaining the future prediction model are described as follows

Step-1: Calculate optimum threshold λ_1 for Monday and find $O_M(\tau_1, \tau_2, .., \tau_{\mathbb{I}})$.

Step-2: Find $O_T(\tau_1, \tau_2, .., \tau_{\mathbb{I}})$. Then, compare the received samples of Tuesday with λ_1 to predict $\hat{O}_T(\tau_1, \tau_2, .., \tau_{\mathbb{I}})$, and estimate $O_{TF}(\tau_1, \tau_2, .., \tau_{\mathbb{I}})$ by updating the weights of the Trigonometric FLANN to minimize the error between $\hat{O}_T(\tau_1, \tau_2, .., \tau_{\mathbb{I}})$ and $O_T(\tau_1, \tau_2, .., \tau_{\mathbb{I}})$. Evaluate λ_2 from $O_{TF}(\tau_1, \tau_2, .., \tau_{\mathbb{I}})$.

Step-3: Compare the spectrum occupancy statistics of $O_M(\tau_1, \tau_2, .., \tau_{\mathbb{I}})$ and $O_{TF}(\tau_1, \tau_2, .., \tau_{\mathbb{I}})$, and find the difference of the occupancy at the ith instant which is expressed as follows

$$diff(\tau_{\mathrm{i}}) = |O_{TF}(\tau_{\mathrm{i}}) - O_M(\tau_{\mathrm{i}})| \quad \mathrm{i} = [1, 2, ..., 32] \tag{6.19}$$

In a similar manner, evaluate the differences at all 32 instances.

Step-4: Add and subtract the observation difference $diff(\tau_{\mathrm{i}})$ from the final estimated occupancy $O_{TF}(\tau_{\mathrm{i}})$ to generate two new occupancy statistics $\mathbb{X}(\tau_{\mathrm{i}})$ and $\mathbb{Y}(\tau_{\mathrm{i}})$ at τ_{i} instant, respectively. If the probable occupancy statistics are known a priori, then the corresponding threshold value can be easily found from measurement data. Hence, we calculate the corresponding thresholds λ_x and λ_y from the matrices $\mathbb{X}(\tau_1, \tau_2, .., \tau_{\mathbb{I}})$ and $\mathbb{Y}(\tau_1, \tau_2, .., \tau_{\mathbb{I}})$, respectively. Mean value of λ_x and λ_y acts as the decision threshold for Wednesday. Thus, obtain $\hat{O}_W(\tau_1, \tau_2, .., \tau_{\mathbb{I}})$. Including these differences at all 32 instances enables us to account for first-order variation of day-to-day occupancy for the next day prediction.

Step-5: Evaluate $O_{WF}(\tau_1, \tau_2, .., \tau_{\mathbb{I}})$ by optimizing the weights of the FLANN to minimize the error between $O_W(\tau_1, \tau_2, .., \tau_{\mathbb{I}})$ and $\hat{O}_W(\tau_1, \tau_2, .., \tau_{\mathbb{I}})$, and find out λ_3 from $O_{WF}(\tau_1, \tau_2, .., \tau_{\mathbb{I}})$.

Step-6: Similarly, compare $O_M(\tau_1, \tau_2, .., \tau_{\mathbb{I}})$, $O_{TF}(\tau_1, \tau_2, .., \tau_{\mathbb{I}})$ and $O_{WF}(\tau_1, \tau_2, .., \tau_{\mathbb{I}})$ to calculate the observation difference which is given as follows

$$diff(\tau_{\mathrm{i}}) = \frac{1}{3}\{|O_{WF}(\tau_{\mathrm{i}}) - O_{TF}(\tau_{\mathrm{i}})| + |O_{WF}(\tau_{\mathrm{i}}) - O_M(\tau_{\mathrm{i}})| + |O_{TF}(\tau_{\mathrm{i}}) - O_M(\tau_{\mathrm{i}})|\} \tag{6.20}$$

Evaluate $O_{THF}(\tau_1, \tau_2, .., \tau_{\mathbb{I}})$ by using the procedures described in **Step-1** to **Step-5**. Find out λ_4 from $O_{THF}(\tau_1, \tau_2, .., \tau_{\mathbb{I}})$. Our underlying assumption in this work is that occupancy varies diurnally, but is essentially statistically stationary (wide sense) over our entire measurement/prediction period. Hence, each pairwise difference is equally weighted.

Step-7: Following the **Step-3** to **Step-6**, compute $diff(\tau_{\mathrm{i}})$ for Friday as per the

following expression

$$diff(\tau_i) = \frac{1}{6}[|O_{THF}(\tau_i) - O_{WF}(\tau_i)| + |O_{THF}(\tau_i) - O_{TF}(\tau_i)| + |O_{THF}(\tau_i) - O_M(\tau_i)|$$
$$+ |O_{WF}(\tau_i) - O_{TF}(\tau_i)| + |O_{WF}(\tau_i) - O_M(\tau_i)| + |O_{TF}(\tau_i) - O_M(\tau_i)|]$$
(6.21)

As per **Step-4**, predict $\hat{O}_F(\tau_1, \tau_2, .., \tau_{\mathbb{I}})$, and finally obtain $O_{FF}(\tau_1, \tau_2, .., \tau_{\mathbb{I}})$ by updating the FLANN weights to minimize the error between $O_F(\tau_1, \tau_2, .., \tau_{\mathbb{I}})$ and $\hat{O}_F(\tau_1, \tau_2, .., \tau_{\mathbb{I}})$.

In general, if we have a historical data set of $(\mathbb{N} - 1)$ days, then $diff(\tau_i)$ for $\mathbb{N}$th day is calculated as

$$diff(\tau_i) = \sum_{\mathfrak{a}=2}^{\mathbb{N}-1} \left[\frac{1}{\mathbb{N} - \mathfrak{a}} \sum_{\mathfrak{b}=1}^{\mathbb{N}-\mathfrak{a}} |O_{(\mathbb{N}-\mathfrak{a}+1)}(\tau_i) - O_{(\mathbb{N}-\mathfrak{a}+1-\mathfrak{b})}(\tau_i)| \right] \qquad (6.22)$$

which requires $\frac{(\mathbb{N}-2)(\mathbb{N}-1)}{2}$ additions. Again, for the occupancy prediction of one day, all the previous occupancy statistics have to be considered. So, mathematical complexity increases with an increase in the number of days before the prediction day.

Meanwhile, the accuracy of prediction gradually improves when the data of more days is averaged, up to a limit, of course. Hence, to get accurate future prediction a trade-off must be considered between mathematical complexity and prediction accuracy.

As our measurements were conducted during typical college semester days, the observation differences show very little changes. Of course, if long term measurements were conducted, either unusual college events (having significantly larger numbers of persons accessing the network) or inevitable long-term network usage pattern changes would occur, and the observation differences would show significant changes. The proposed method implementing the Trigonometric FLANN is described in **Appendix G**.

6.6 CR Implementation in 2.4 GHz Unlicensed Band

The 100 MHz ISM band is not always occupied by the electronic devices at all the time. So, the CR can be implemented by identifyining the least occupied sub-band for its data transmission. The maximum transmission power level of the CRU is decided not to cause any harm to other coexting devices.

6.6.1 Double threshold-based sub-band selection

For the sub-band selection, the frequency band ranges from 2.4 GHz to 2.4835 GHz is considered as the operating band of bandwidth 83.5 MHz which is then divided into $\mathcal{N}$

sub-bands each of bandwidth B_s. The CRU performs SS on $\mathscr{N}$ sub-bands to select the least occupied sub-band for its data transmission; so that the interference to the other co-existing devices can be minimized. If $s(n)$ represents the transmitted signal from the other coexisting devices, then the received signal of nth sample at CRU on $\mathfrak{n}$th sub-band is given by

$$x_\mathfrak{n}(n) = \begin{cases} \eta_\mathfrak{n}(n), & (H_0) \\ s(n)h + \eta_\mathfrak{n}(n), & (H_1) \end{cases} \tag{6.23}$$

where $n = [1, 2, ..., N]$ and $\mathfrak{n} = [1, 2, ..., \mathscr{N}]$. The two hypotheses H_0 and H_1 represent the idle and busy state of the $\mathfrak{n}$th sub-band, respectively. $\eta_\mathfrak{n}$ is the additive white Gaussian noise in the $\mathfrak{n}$th sub-band of mean zero and variance $\sigma_\eta{}^2$. Then, the sensing metric of the $\mathfrak{n}$th sub-band is given by

$$Y_\mathfrak{n} = \frac{1}{N} \sum_{n=0}^{N-1} |x_\mathfrak{n}(n)|^2 \tag{6.24}$$

Specifically, the spectrum occupancy statistic is measured by two parameters probability of detection P_d and the probability of false alarm P_f. In difference to the conventional SS techniques, here we define the performance metrics on the basis of channel vacancy. $P_{d\mathfrak{n}}$ is defined as the probability that the CRU correctly identifies the $\mathfrak{n}$th sub-band to be vacant. $P_{f\mathfrak{n}}$ is defined as the probability that the CRU identifies the occupied sub-band to be vacant. Similarly, the miss detection probability $P_{md\mathfrak{n}}$ represents the probability of identifying a vacant sub-band to be occupied. In a single threshold-based detection scheme, decrease in P_f leads to increase in P_{md}, this decreases the spectral usage. Hence, we address the double threshold-based measurement scheme to ensure the target miss detection probability with less P_f through two controlling thresholds λ_1 and λ_2. The main objective is to identify the vacant band correctly for data transmission. So, we keep P_{md} lower bounded and control P_f by varying Δ; where $\Delta = \lambda_1 - \lambda_2$. Figure 6.5 shows the double threshold-based spectrum detection scheme.
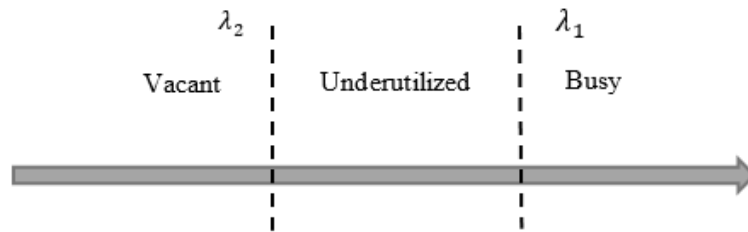

Figure 6.5: Double threshold-based spectrum availability metric.

In this experiment, the occupancy of the $\mathfrak{n}$th sub-band is evaluated from the received signal strength. Data is collected over the frequency span and time span, and make a matrix A of size $\mathbb{I} \times \mathbb{J}$. $\mathbb{I}$ and $\mathbb{J}$ represent the total number of discrete time instants and

total number of frequency points available in the $\mathfrak{n}$th sub-band, respectively. So, each component of the matrix is expressed as $A(\tau_i, f_j)$, where i represents the discrete time instant and j represents the frequency point. Accurate channel utilization is evaluated by comparing each sample that lies within the sub-band with the two thresholds. So, the decision metric is evaluated as

$$D_{M\mathfrak{n}}(\tau_i, f_j) = \begin{cases} 0 & \text{if } A(\tau_i, f_j) < \lambda_2 \\ Underutilized & \text{if } \lambda_2 \le A(\tau_i, f_j) \le \lambda_1 \\ 1 & \text{if } A(\tau_i, f_j) > \lambda_1. \end{cases} \tag{6.25}$$

The $\mathfrak{n}$th sub-band utilization is expressed as

$$C_{U\mathfrak{n}} = \frac{\sum_{i=1}^{\mathbb{I}} \sum_{j=1}^{\mathbb{J}} D_{M\mathfrak{n}}(\tau_i, f_i)}{\mathbb{I}\mathbb{J}} \tag{6.26}$$

In these conditions, $P_{d\mathfrak{n}}$, $P_{f\mathfrak{n}}$ and $P_{md\mathfrak{n}}$ are represented as

$$P_{d\mathfrak{n}} = P_r(Y_\mathfrak{n} < \lambda_2 | H_0) \tag{6.27}$$

$$P_{f\mathfrak{n}} = P_r(Y_\mathfrak{n} < \lambda_2 | H_1) \tag{6.28}$$

$$P_{md\mathfrak{n}} = 1 - P_r(Y_\mathfrak{n} < \lambda_1 | H_0) = P_r(Y_\mathfrak{n} > \lambda_1 | H_0) \tag{6.29}$$

$$P_{md\mathfrak{n}} = P_r(\lambda_2 \le Y_\mathfrak{n} \le \lambda_1 | H_0) \tag{6.30}$$

According to (6.29) and (6.30), $P_{md\mathfrak{n}}$ occurs when the noise samples exceed the decision threshold λ_1, and the CRU consider the vacant band to be occupied. However, the probability of (6.30) is less; so we consider (6.29) for deriving decision threshold λ_1 for the given $P_{md\mathfrak{n}}$. Hence, λ_1 for the $\mathfrak{n}$th sub-band is evaluated as

$$\lambda_1 = N_F(dBm) + Q^{-1}(P_{md\mathfrak{n}})\sigma_\eta^2 \tag{6.31}$$

where N_F (dBm) represents the CR noise floor, and is given by [183]

$$N_F = -154(dBm/Hz) + 10log(RBW) \tag{6.32}$$

The estimated noise power spectral density (PSD) for this specific frequency range with this SA is $\approx -154(dBm/Hz)$ and σ_η^2 represents the noise variance. The ideal thermal noise PSD is $\approx -174(dBm/Hz)$. So, the measured noise PSD is 20 dBm higher than the ideal thermal noise PSD. Before transmitting data, the CRU scans each sub-band for the total time duration T. If the signal is received at T_s interval then the signal strengths are averaged over the frequency points fall within the frequency range of a particular sub-band. If N number of samples are chosen during T, then the occupancy statistics of the $\mathfrak{n}$th sub-band evaluated from the (6.25) and (6.26) are expressed as

$$H_\mathfrak{n} = \left\{ H_\mathfrak{n}^1, H_\mathfrak{n}^2, H_\mathfrak{n}^3 \right\} \tag{6.33}$$

The three elements $H_\mathfrak{n}^1$, $H_\mathfrak{n}^2$ and $H_\mathfrak{n}^3$ represent the three states busy, idle, and underutilized of the $\mathfrak{n}$th sub-band, respectively. The final occupancy status of each

sub-band at kth instant is given by

$$\bar{O}_n(k) = max\left\{H_n{}^1, H_n{}^2, H_n{}^3\right\} \tag{6.34}$$

Then, each sub-band is experimented over K times to obtain the final occupancy statistic of the nth sub-band which is given by $\bar{O}_\mathfrak{n} = \frac{1}{K}\sum_{k=1}^{K}\bar{O}_\mathfrak{n}(k)$. So, all the $\mathscr{N}$ sub-bands are experimented over K times to get the final occupancy statistic which is given as

$$\bar{O} = \left[\bar{O}_1, \bar{O}_2, ..., \bar{O}_\mathscr{N}\right] \tag{6.35}$$

Let $\mathscr{J}$ number of sub-bands obtain $H_\mathfrak{n}{}^1$, hence, the CRU finds these sub-bands to be fully congested. So, it has to select from $\mathscr{N} - \mathscr{J}$ sub-bands for its data transmission. Then, the channel vacancy statistics of $\mathscr{N} - \mathscr{J}$ sub-bands are evaluated referring (6.26) for the first condition given in (6.25). Let it be expressed as

$$V = \left[V_1, V_2, ..., V_{\mathscr{N}-\mathscr{J}}\right] \tag{6.36}$$

Then, $V = \left[V_1, V_2, ..., V_{\mathscr{N}-\mathscr{J}}\right]$ is processed through the interference free communication index (IFCI) [184] which measure how long the CRU can transmit data without causing interference to the co-existing devices on that particular sub-band which is expressed as

$$Z_{\mathfrak{n}'} = e^{-V_{\mathfrak{n}'}} \quad \mathfrak{n}' = [1, 2, ..., \mathscr{N} - \mathscr{J}] \tag{6.37}$$

The values of $Z = \left[Z_1, Z_2, ..., Z_{\mathscr{N}-\mathscr{J}}\right]$ vary between 0 and 1. The least value of Z indicates the interference free nth sub-band which is used by the CRU for its data transmission. We assume that the CRU has to stay on the selected sub-band for the duration T. If the CRU intend to transmit its data in another duration, then it has to switch to that sub-band (sub-band is selected by employing (6.37)). In this way, interference introduced to the co-existing systems can be minimized to some extent.

6.6.2 Power allocation and path-loss model

The CRU transmitter employs OFDM scheme for data transmission. So, each sub-band of bandwidth B_s is divided into S orthogonal sub-carriers, each of bandwidth Δf. As, we have considered the underlay spectrum sharing mechanism in which the CRU co-exists with the other systems; the transmitting power should be adopted such that it would not cause any interference to other coexisting devices. Hence, the minimum allowable transmit power of the CRU in a sub-band can be expressed as [185]

$$P_{tmin}(dBm) = -61dBm/MHz + 10log_{10}(S \times \Delta f)\,dBm \tag{6.38}$$

If the PSD measured in 1 MHz does not exceed $\approx -61dBm$, it will not cause any interference to the other devices operating in this 2.4 GHz ISM band.

Most of the devices in 2.4 GHz ISM band operate in low power. For example, the transmitting power of Bluetooth ranges from 0 dBm (1mW) to 20 dBm (100 mW). The

minimum transmission power level for IEEE 802.15.4 is 6 dBm. The maximum output power of the operating devices is limited to 30 dBm. Hence, the transmitting power of the CRU on the sth sub-carrier is P_{ts} which is limited between minimum transmitting power $P_{tmins} = -40dBm$ and maximum transmitting power P_{tmaxs}. We assume P_{tmaxs} is -10 dBm. In the indoor environment, the transmitting signal from the CRU suffers from reflection and diffraction, and may also be interrupted due to the partition walls or due to motion of any objects or persons. The basic path loss model adopted in this chapter is

$$P_L(dB) = P_L(d_0) + \bar{\Omega} log_{10}\left(\frac{d}{d_0}\right) + L_f(\mathfrak{p})(dB) \tag{6.39}$$

where $\bar{\Omega}$: distance power loss coefficient, $L_f(\mathfrak{p})$: floor penetration loss factor (dB) where $\mathfrak{p}$ is number of floors between the two terminals, f: frequency (MHz), d: distance between the two CRUs ($d > 1m$) and d_0: reference distance ($1m$). The values of the parameters are obtained from the International telecommunication union (ITU) indoor propagation channel model [186] considering the office scenario.

6.6.3 Throughput analysis

The measurement was conducted in the office hour from 9 AM-5 PM. So, it is obvious that almost all the electronic devices are active during this period. Specifically, interference to the co-existing systems occurs due to the CRU's data transmission. So, the amount of interference introduced by the sth sub-carrier to the jth sub-band can be expressed as [67]

$$I_s{}^j = g_s \int\limits_{\Delta l_s - \Delta f/2}^{\Delta l_s + \Delta f/2} \Theta_s(f)\,df \tag{6.40}$$

where g_s is the channel gain, and $\Theta_s(f)$ represents the PSD of the sth sub-carrier which can be expressed as

$$\Theta_s(f) = T_o P_{ts}\left(\frac{sin\pi f T_o}{\pi f T_o}\right)^2 \tag{6.41}$$

where T_o is the OFDM symbol duration. Δ_{ls} represents the frequency separation between the sth sub-carrier of $\mathfrak{n}$th sub-band and the center frequency of the jth sub-band (highest occupied sub-band). Hence, the average interference introduced by the sth sub-carrier to all $\mathscr{J}$ sub-bands is given by

$$I_{avgs} = \sum_{j=1}^{\mathscr{J}} I_0{}^j \tag{6.42}$$

where $I_0{}^j = g_s T_o \int\limits_{\Delta l_s - \Delta f/2}^{\Delta l_s + \Delta f/2} \left(\frac{sin\pi f T_o}{\pi f T_o} \right)^2 df$. Data transmission always takes place on the

least occupied sub-band. Then, the overall throughput achieved is

$$R = P_{H0} \sum_{s=1}^{S} C_{0s} \tag{6.43}$$

Let N_1 be the number of samples lies below λ_2. Then, the absence rate is $P_{H0} = N_1/N$. Neglecting the interference from the co-existing systems on the selected sub-band, we assume that

$$C_{0s} = log_2 \left(1 + \frac{|h_{ss}|^2 P_{ts}}{N_p} \right) \tag{6.44}$$

Here, $|h_{ss}|^2$ represents the channel gain between the CRUs on sth sub-carrier and is calculated from the path-loss model (6.39), and N_p is the noise power. Then, the throughput maximization problem under the interference constraint can be formulated as

$$\begin{array}{c} Maximize \\ P_t \end{array} \quad : \quad R \tag{6.45}$$

$$Subject \quad to \quad : \quad \sum_{s=1}^{S} P_{ts} \le P_{tmax} \tag{6.45 a}$$

$$: \quad \sum_{s=1}^{S} P_{ts} I_{avgs} \le I_{th} \tag{6.45 b}$$

where $P_t = [P_{t1}, P_{t2}, ..., P_{tS}]$ and P_{tmax} is the maximum transmission power. I_{th} is the interference threshold below which the secondary transmission does not affect the co-existing systems. The optimization problem (6.45) is a standard convex optimization problem, hence it can be solved by the Lagrangian duality theorem which is expressed as

$$L(\mu, \theta) = R + \mu \left(I_{th} - \sum_{s=1}^{S} P_{ts} I_{avgs} \right) + \theta \left(P_{t\max} - \sum_{s=1}^{S} P_{ts} \right) \tag{6.46}$$

Then, P_{ts} is derived by using the KKT condition [127]

$$P_{ts} = \left[\frac{1}{(\theta + \mu \sum_{s=1}^{S} I_{avgs})ln2} - \frac{N_p}{|h_{ss}|^2} \right]^+ \tag{6.47}$$

where $[.]^+ = max[0, .]$. μ and θ are known as Lagrangian multipliers, and are updated by using the sub-gradient method as per the following expression

$$\mu(it + 1) = \left[\mu(it) - \psi(it) \left(I_{th} - \sum_{s=1}^{S} P_{ts} I_{avgs} \right) \right]^+ \tag{6.48}$$

$$\theta(it + 1) = \left[\theta(it) - \psi(it) \left(P_{t\max} - \sum_{s=1}^{S} P_{ts} \right) \right]^+ \tag{6.49}$$

where $\psi(it)$ is non-negative step size for the current iteration it and is set at $\frac{1}{\sqrt{it}}$. So, $\psi(it)$ decreases with the number of iteration. μ and θ converge to the optimal values when $\psi(it)$ is sufficiently small.

## 6.7 Performance Assessment and Discussion

The numerical computations are carried out in MATLAB environment with a Windows 8 based operating system, with a 3.4 GHz i7 CPU and 6 GB RAM specifications. In the experimental results, Feed-forward MLP, Recurrent MLP, Trigonometric based FLANN and Chebyshev based FLANN are represented by the legends F-MLP, R-MLP, TG-FLANN and CH-FLANN, respectively. Unlike the other models, ANN requires only one training process for adjustment of the interconnected processing parameters meant for a specific problem. During the training process, the weights are initialized randomly and then adjusted iteratively to minimize the normalized mean square error (MSE). If t be the current iteration number and $e(t)$ is the error at that iteration, then normalized MSE is calculated as $10log_{10}\left(\frac{e(t)}{\max(e(t))}\right)$. Training parameters are chosen after the trial and error process. All these four models employ the same training and testing samples. After the completion of training, weights are fixed and used for testing. The targeted P_f and weighting factor z are set 0.1 and 0.5, respectively.

For our experiment, the F-MLP and R-MLP models consist of a single hidden layer with 10 neurons. In FLANN, the input data is expanded using 9 polynomial functions that are either the Trigonometric or Chebyshev polynomial functional expansions. After the trial and error process, the learning rate for both ANN and FLANN is set 0.07. In all cases, the logistic sigmoid function is used as the nonlinear transfer function. The weights are updated for 8000 iterations. For training purposes, 10,000 samples are selected randomly at each frequency point and the normalized MSE is calculated by comparing the actual average spectrum occupancy value with the predicted average spectrum occupancy. The general convergence characteristics of the MLP and FLANN for predicting spectrum occupancy statistics are shown in Figure 6.6. The elapsed time required for the training process of F-MLP, R-MLP, CH-FLANN and TG-FLANN are 445.283 sec, 272.373 sec, 69.483 sec and 74.125 sec, respectively for 8000 iterations, and are 110.928 sec, 69.252 sec, 10.647 sec and 11.309 sec, respectively for 2000 iterations. Hence, FLANN outperforms the MLP in terms of less computational time and smaller normalized MSE. It is noticed that CH-FLANN has the lowest convergence time whereas F-MLP requires the highest time to converge. It is also observed that as iteration number increases, the normalized MSE of CH-FLANN gradually decreases but only very gradually. Further, a larger number of iterations implies greater complexity (and time) for these models. So, it

may be concluded that though TG-FLANN requires slightly more computational time than CH-FLANN, it outperforms the other models in terms of normalized MSE.
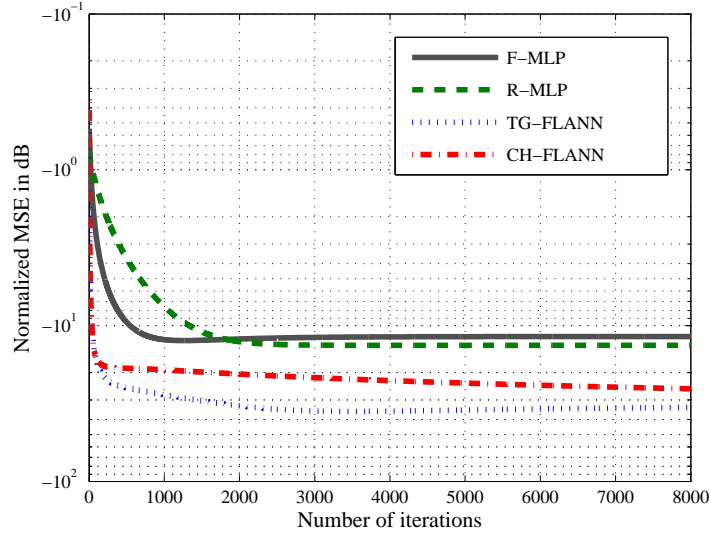
(a) 8000 iterations.
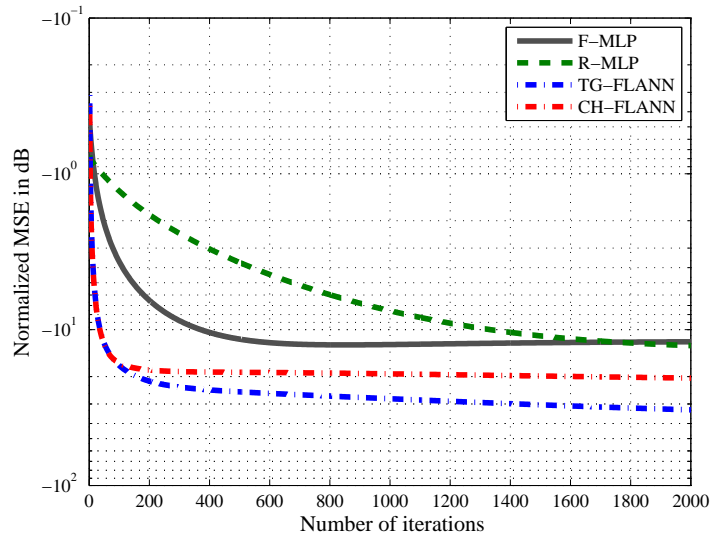
(b) 2000 iterations.

Figure 6.6: General convergence characteristics of ANN models.

The average received signal power over the frequency band and the time period for the entire days of measurements is shown in Figure 6.7. Figure 6.8 depicts the maximum, minimum and mean signal strength in dBm against frequency band. Considering the entire time period, the maximum values of received signal power, minimum values of signal power levels and mean values of received signal strength are calculated at each frequency point. So, it is observed that the overall received signal strength lies between -107.15 dBm and -24.55 dBm with mean value -80.874 dBm.
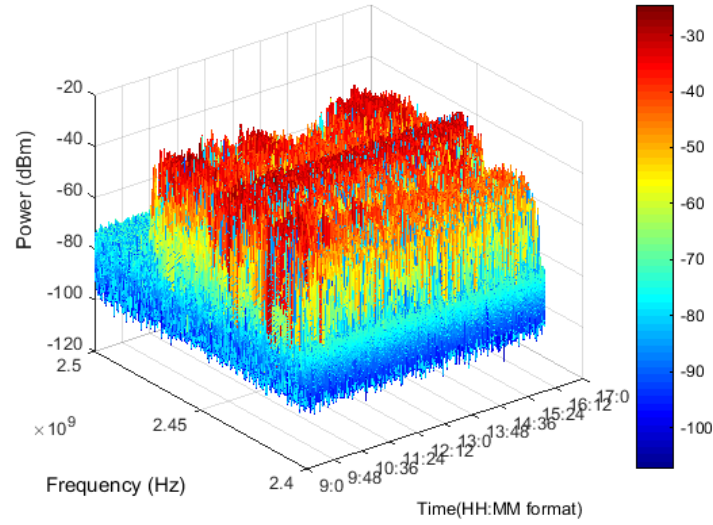
Figure 6.7: Received signal power for 2.4 GHz to 2.5 GHz over the days of observation. Frequency is shown in Hz and Time is in the format of hour: minute.
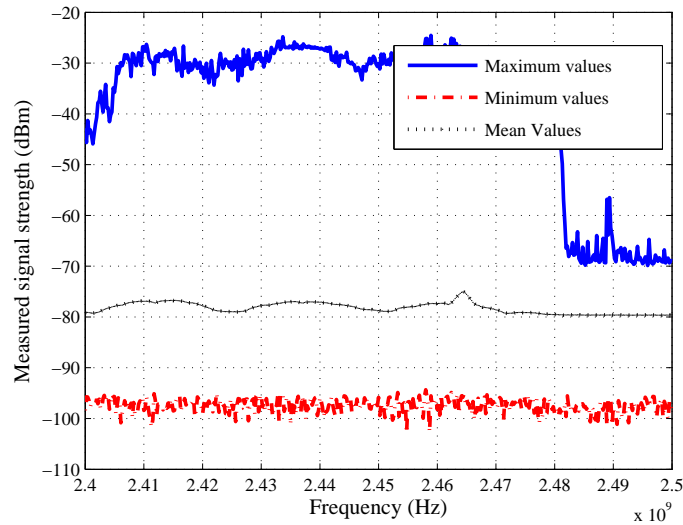

Figure 6.8: Statistics of signal level over the entire frequency range of measurement for the entire course of 5 working days (Monday-Friday).

For testing purposes, 80,000 data samples are selected at each frequency point and are used for evaluating the performance of four ANN models with the three different threshold selection methods. Figure 6.9 illustrates the performance of ANN models using the test data employing three different threshold methods. It is noted that all four ANN models are trained well to evaluate spectrum occupancy with high accuracy. Figure 6.10 illustrates the effect of decision thresholds on the spectrum occupancy prediction by TG-FLANN, and it is evidently observed that the detection performance is greatly influenced by the decision threshold.
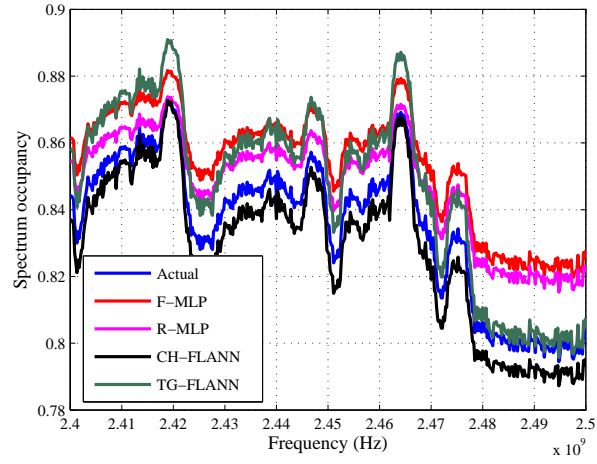
(a) Fixed threshold.
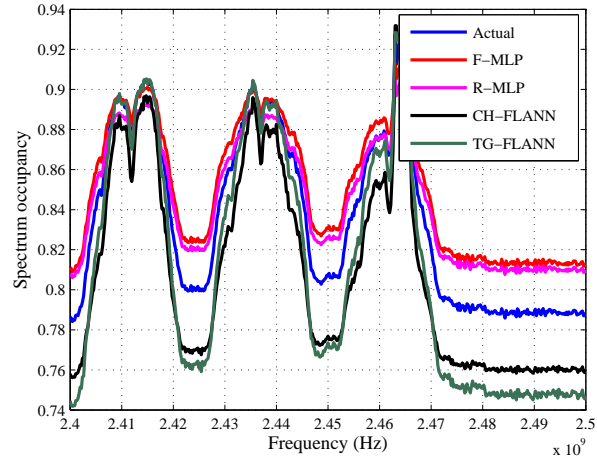
(b) Dynamic threshold.
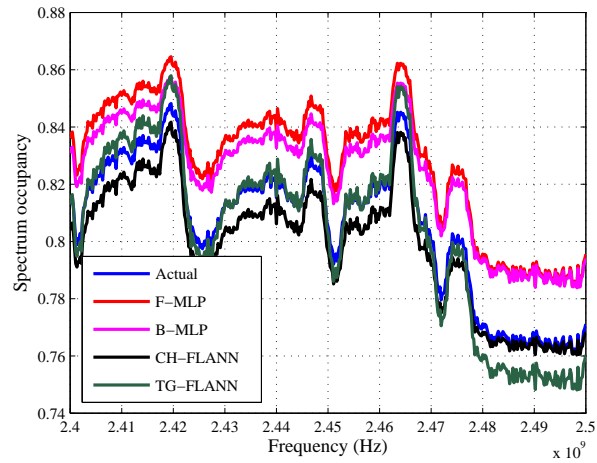
(c) Optimal threshold.

Figure 6.9: Illustration of spectrum occupancy results (over Monday- Friday) comparing the performance of ANN models.
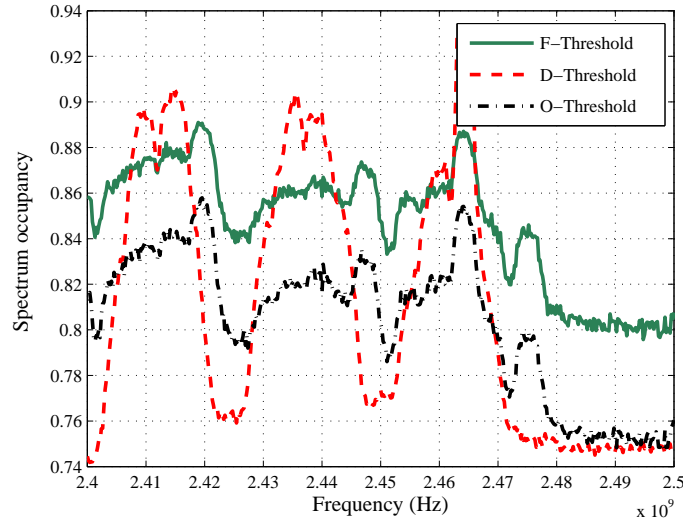
Figure 6.10: Illustration of the TG-FLANN results for the 3 different threshold methods; Fixed threshold (F-Threshold), Dynamic threshold (D-Threshold) and Optimum threshold (O-Threshold).

Table 6.2 summarizes the performance of all four ANN models for three different types of threshold evaluations. It is noted that fixed decision threshold based measurement shows a larger spectral occupancy but the optimal threshold yields minimum sensing error (with our chosen value of z). It is also observed that FLANN predicts more accurate spectrum occupancy. The main goal of our work is to improve CR learning schemes by introducing the FLANN model, which we have shown can learn and train its parameters from historical information.

Table 6.2: Performance comparison of ANN models in terms of accuracy.

Decision threshold	Actual Avg. occupancy%	Sensing error	ANN models	Predicted Avg. occupancy	Accuracy%
Fixed threshold	83.54	0.1479	F-MLP	85.38	97.8
			R-MLP	84.75	98.55
			CH-FLANN	82.76	99.06
			TG-FLANN	84.19	99.22
Dynamic threshold	81.18	0.1541(mean value)	F-MLP	83.08	97.65
			R-MLP	82.62	98.22
			CH-FLANN	80.93	99.69
			TG-FLANN	81.1	99.9
Optimum threshold	80.55	0.1463	F-MLP	82.81	97.19
			R-MLP	82.37	97.74
			CH-FLANN	79.86	99.14
			TG-FLANN	80.38	99.78

The received samples are organized to show the variation of spectrum occupancy

at different time periods over the entire frequency range. The result for the optimum threshold is shown in Figure 6.11. It is clearly noticed that the spectrum occupancy is distinctly high in 3 different WLAN channels in channel: 1, 6 and 11. As per the 802.11 WLAN group, only 11 channels are allowed in USA. Hence, the unused WLAN channels 12, 13 and 14 of center frequency 2.467, 2.472 and 2.484 GHz, respectively, are empty and contain no signal component. Out of the 3 distinct channels (1, 6 and 11), channel 6 is mostly occupied by WLAN and other electronics devices operating in this 2.4-2.5 GHz frequency range.
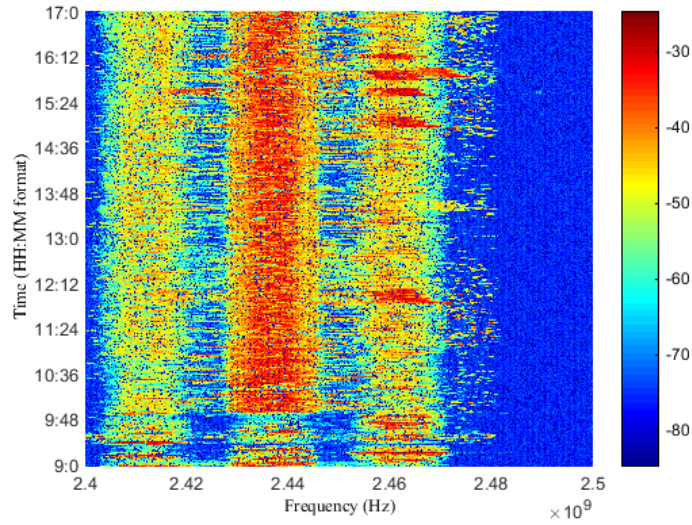

Figure 6.11: Illustration of spectrum occupancy over different time period for ISM band (over 5 days of observations).

Out of the four ANN models, the Trigonometric FLANN yields the most accurate spectrum occupancy statistics, although the Chebyshev FLANN results are essentially identical. We have observed from Table 6.2 that Chebyshev FLANN gives under estimation of spectrum occupancy which is more serious than over estimation of spectrum occupancy. Hence, our proposed forecasting prediction model is designed with the Trigonometric FLANN. Figure 6.12 illustrates the comparison between actual spectrum occupancy (spectrum occupancy obtained by comparing the received samples with the optimal threshold) and the predicted spectrum occupancy obtained by our proposed algorithm based on FLANN prediction model for the 4 working days (Tuesday through Friday). Average occupancy of the ISM band for five working days is illustrated in Figure 6.13. For Figure 6.13, the average predicted occupancies for Tuesday to Friday are evaluated by employing our proposed algorithm. It is observed that Friday shows slightly more occupancy than the other days. It may be concluded that the spectrum occupancy statistics are fairly constant over the week days Monday-Friday.

From Figure 6.14, it is evident that as the amount of averaged historical data increases over the week, our proposed model becomes more accurate. For Tuesday, the accuracy of prediction decreases slightly (as the algorithm has only one data set at that time), then increases and maintains a constant value for Wednesday, Thursday and Friday.

(a) Tuesday.

(b) Wednesday.
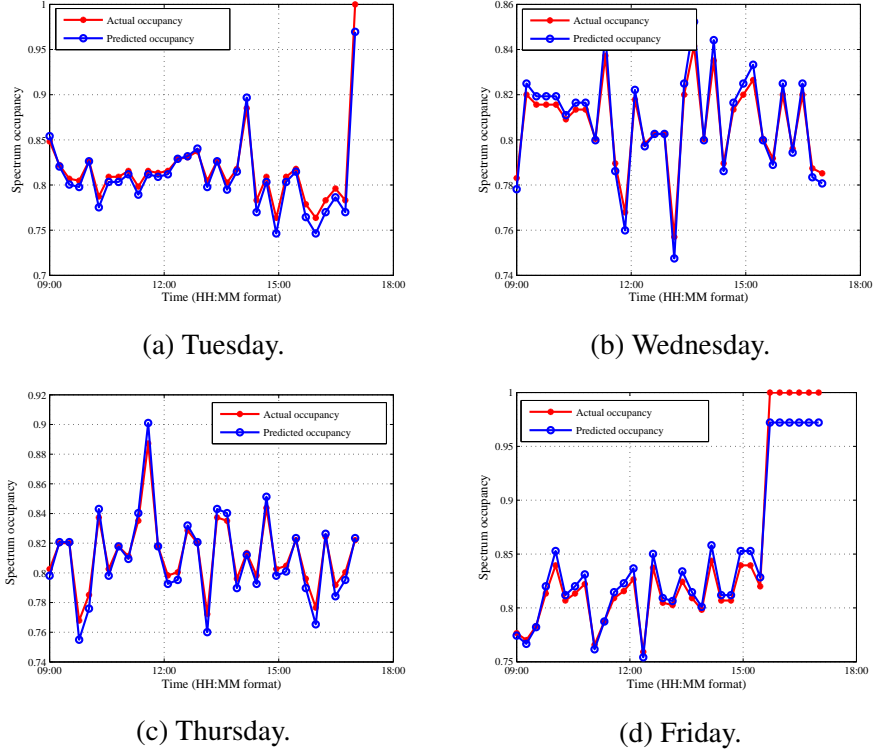
(c) Thursday.

(d) Friday.

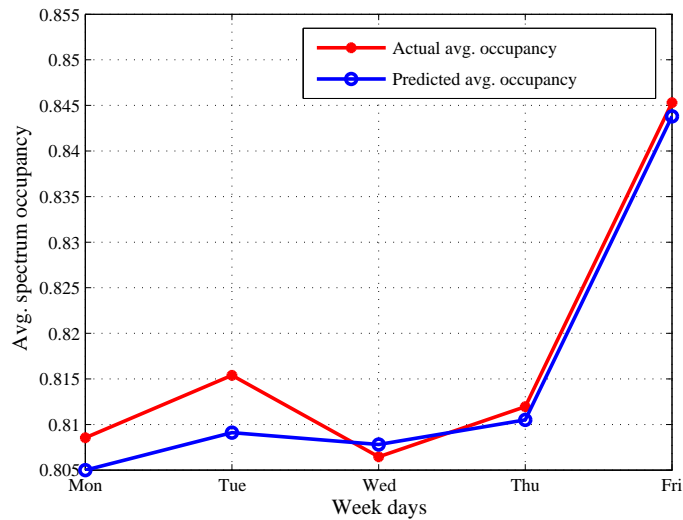Figure 6.12: Validation of the proposed method for future occupancy prediction.

Figure 6.13: Comparison of actual occupancy with predicted occupancy over 5 working days in a week.
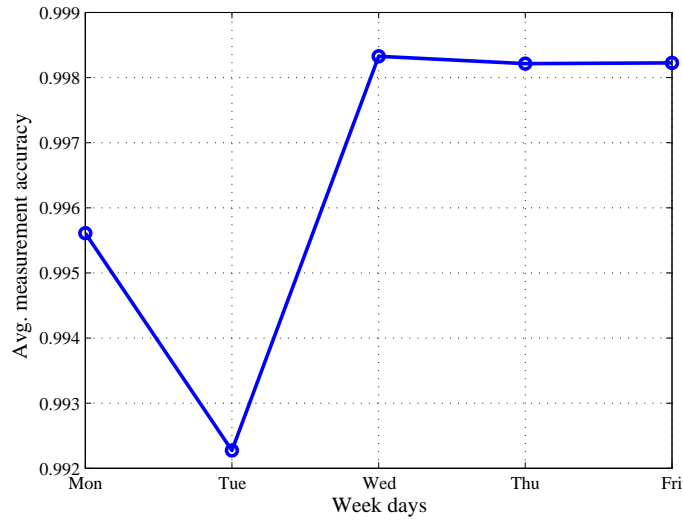
Figure 6.14: Depiction of accuracy achieved from forecasting model for 5 working days in a week.

In our experiment, the measurements were conducted during the usual college days. So, we achieve about 99% accuracy from our future prediction model. However, our proposed model can also be employed to predict the spectrum occupancy in any scenarios having different statistics (e.g., unusual college events) as long as the measurements/predictions take place during periods when the statistics are constant.

Implementing the CR technology, Figure 6.15 shows the average spectrum occupancy over the 5 days of observation. λ_1 is evaluated from (6.31) taking $P_{md} = 0.1$. λ_2 is calculated from the given value of $\Delta = 0.5$. The measurement was carried out during Fall 2014 semester in usual college days. Hence, the spectrum occupancies of those days are nearly same. However, Thursday shows the least occupied day. So, the measurement data of Thursday is used for implementing the CR application. Exactly, it would not be the practical case, because the CRU may choose any day for its data transmission. Specifically, we have chosen Thursday data set for further evaluation.

Figure 6.16 shows the impact of threshold difference Δ on the spectrum utilization. It is observed that with the increase in Δ, probability of underutilization increases but the probability that the information signal samples fall below λ_2 decreases. But, if we increase the value of Δ further, the vacancy probability and underutilization coincide. Figure 6.17 shows the impact of target miss detection probability on the false alarm probability for different values of Δ. It is observed that P_f decreases with increase in P_{md}. Hence, for targeted P_{md}, P_f can be controlled by varying the value of Δ.
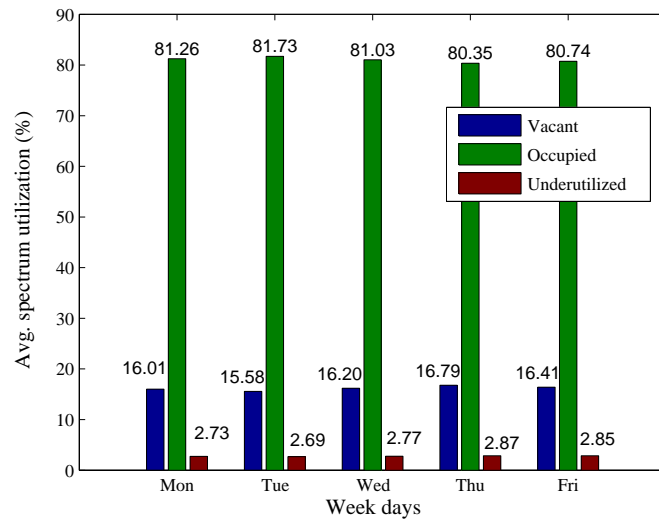
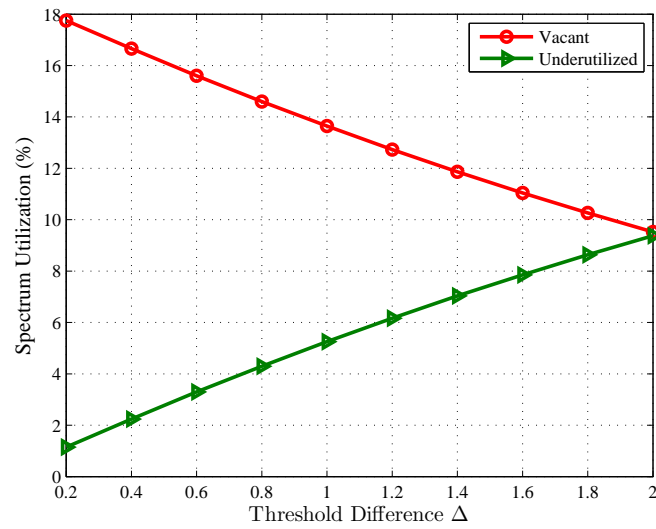Figure 6.15: Spectrum utilization over week days.

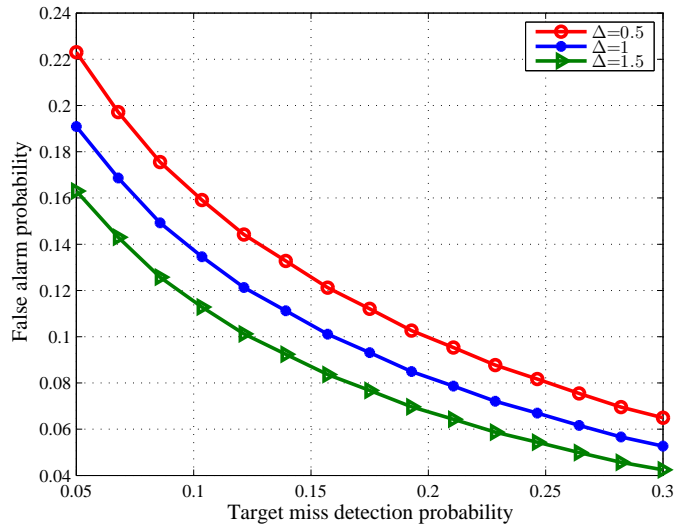Figure 6.16: Variation of spectrum utilization over Δ.

Figure 6.17: Impact of targeted P_{md} on P_f.

The channel availability is checked for the particular duration T before the CRU transmits its data. Let T_s be the interval between the two received signal strengths, and F_R is the number of frames have to be identified per sub-band. Specifically, there is a periodic beacon frame from Wi-Fi APs in every 100 msec. So, T_s must be chosen very carefully such that the received signals are not correlated, and $T_s \geq 150$ msec. For our experiment we have chosen T_s=10 sec, T=1 hr and F_R=300. Hence, 300 samples are selected at each frequency point for evaluating the channel utilization. 802.11 b/g/n Wi-Fi devices mostly transmit in the non-overlapping channels (Channel 1, Channel 6 and Channel 11) of center frequencies 2.412 GHz, 2.437 GHz and 2.462 GHz. Microwave oven operates around 2.45 GHz. So, all the sub-bands are not fully occupied at all the times. As the total number of frequency points in SA is 461, the discrete frequency point f_n in the frequency range 2.4 – 2.5 GHz is given by (6.1). The measurement was carried out in the frequency span of 100 MHz, but the sub-band selection is done within the bandwidth 83.5 MHz. Hence, 388 number of discrete frequency points out of 461 are processed for the evaluation of Figure 6.18 – Figure 6.21. We divide the entire licensed band into 14 sub-bands each of 5 MHz bandwidth and separated by guard bandwidth 0.4 MHz. So, 23 discrete frequency points are assigned to each sub-band maintaining a gap of 3 discrete frequency points between the sub-bands. The CRU has to select the appropriate sub-band for the data transmission using (6.37).

Figure 6.18 shows the occupancy status of all the sub-bands for 11 AM to 12 PM on Thursday. It is observed that sub-band 4 is highly congested, and sub-band 14 can be used for data transmission by the CRU. We set $P_{md\text{n}}$=0.1 and Δ=0.5. Figure 6.19 shows the variation of system throughput over 8 hours of observation (9 AM – 5 PM) on Thursday. We set P_{tmins}= -40 dBm, P_{tmaxs}=-10 dBm and P_{tmax}= 0 dBm. I_{th} is set at

-20 dBm. The OFDM symbol duration T_0= 25 μsec and N_p is assumed to be -90 dBm. Each sub-band is divided into 16 sub-carriers. From the figure it is depicted that system throughput decreases as time increases from 9 AM. This means as time approaches towards afternoon, the hallways in the Swearingen Engineering Center are getting busy showing the busy duration of the college campus. So, more active users are accessing the spectrum from 12 PM onwards, and the sub-band is highly occupied during 2 PM-4 PM. Thus, throughput is less during this period. Further, the throughput is higher for less value of Δ.
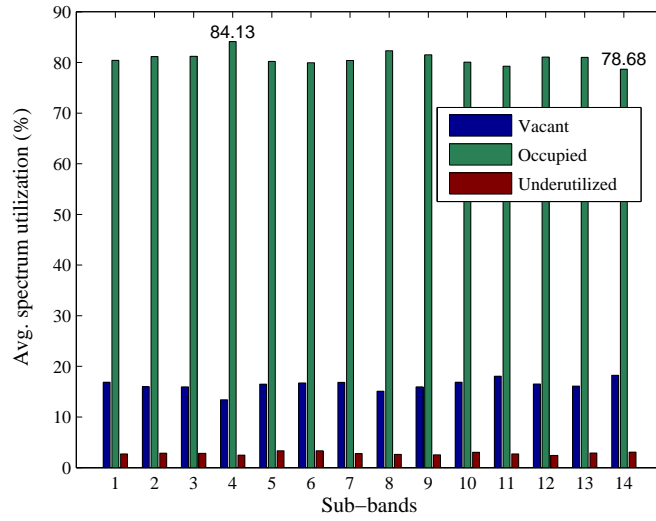

Figure 6.18: Spectrum utilization variation in different sub-bands.
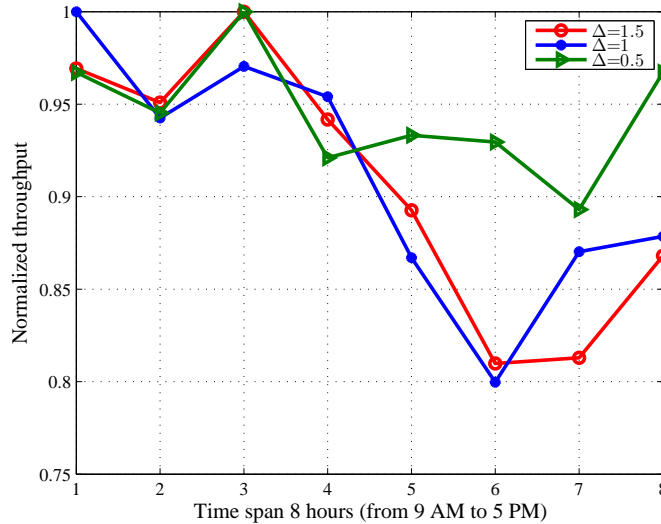
Figure 6.19: Variation of system throughput over different time periods.

Figure 6.20 shows the impact of distance difference between the CRUs on the system throughput for P_{tmaxs}= -10 dBm, -5 dBm and 0 dBm. P_{tmax} is set at 5 dBm. It is

obvious that path-loss increases when the distance increases, so throughput decreases. For P_{tmaxs}=-10 dBm, normalized throughput decreases by 32% when distance between the CRUs increases from 2 to 4 meter. With rise in maximum power P_{tmaxs} by 5 dBm and 10 dBm from -10 dBm, normalized throughput is increased by 3% and 5%, respectively, when the distance between the CRUs is 3meter.
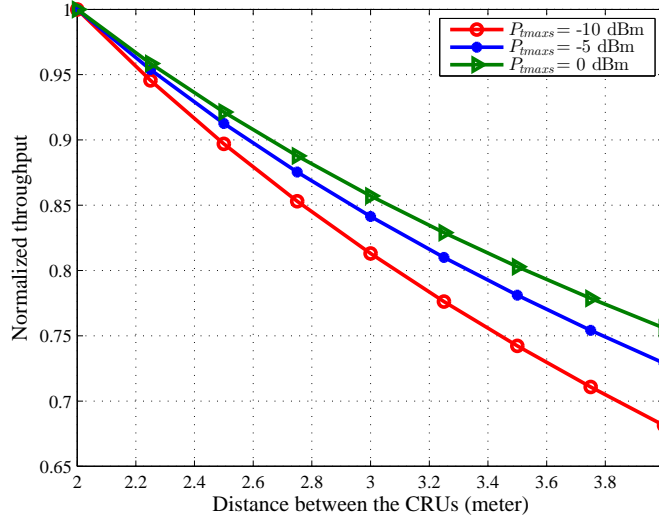
Figure 6.20: Impact of distance difference between the CRUs on throughput.

Figure 6.21 shows the impact of I_{th} on the system throughput taking the most vacant sub-band and the most congested sub-band. It is obvious that as interference threshold increases, the upper bound transmission power of each CRU increases as per (6.45 b), so, throughput increases. Further, P_{H0} is more in the vacant sub-band than the congested sub-band, so vacant sub-band shows more throughput. For I_{th}=-30 dBm vacant sub-band offers improvement in normalized throughput by 2% compared to the congested sub-band. When I_{th} increases by 40 dBm from -50 dBm to -10 dBm, normalized throughput in the vacant sub-band is improved by 39%.
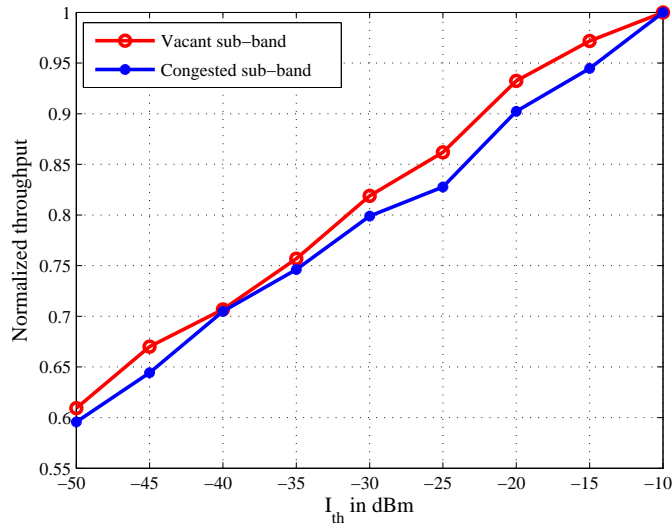
Figure 6.21: Impact of I_{th} on throughput.

6.8   Summary

The inclusion of recent advancements in learning schemes for ANNs can provide better models for forecasting future spectrum occupancy, which facilitates energy-efficient radio systems. This chapter proposed an optimum threshold based enhanced FLANN soft computing method into the CR application. Experimental results showed that this model gave better prediction accuracy and took less computational time compared to conventional ANN models. Furthermore, a prediction model was proposed to forecast the channel statistics by analyzing the previously observed data. FLANN provided a fairly accurate prediction of spectrum occupancy one day in advance. So, FLANN based spectrum occupancy prediction can be an effective approach towards improving the CR performance further. This research has attempted deployment of CR technology in 2.4 GHz ISM band. Double threshold-based detection scheme was used to find the exact status of the spectrum occupancy, which ultimately improved the spectral efficiency. The performance of the proposed scheme was investigated using the real data collected in 2.4-2.5 GHz spectrum band. In addition, an adaptive power allocation scheme was proposed for CRUs' data transmission with limited interference to the co-existing systems. Hence, it is concluded that by adaptive proper resource allocation with the suitable channel selection, CR can be successfully deployed in an unlicensed band, which can solve the spectrum scarcity issue to certain extent.

Chapter 7

Conclusions and Future Work

7.1 Introduction

THE demand for more spectral efficient wireless communication has led to the development of intelligent dynamic technologies for new wireless communication systems. CR is basically a set of technologies that can utilize the techniques of machine learning, game theory, and artificial intelligence properties to attain this dynamic behavior. However, CR is a complex system that must have the ability to perceive the radio channels, to learn and to adapt its parameters according to statistical variations of the surrounding environment. The inclusion of intelligent schemes for optimizing the resource parameters facilitates the energy-efficient radio systems. Hence, in this thesis, the proposed approaches aim for EE maximization considering different domain specific constraints defined for various scenarios.

7.2 Chapterwise Conclusions

This thesis focused on developing intelligent approaches for energy-efficient resource allocation in the CRN. The CRN system model is consisting of the PU, SUs, SRs and the PR. The SUs are distributed at different distances from the PU. So, their distance dependent channel gains are very important in choosing the appropriate SUs for SS and data transmission. The SUs chosen for SS may not improve the system throughput, but there are some common parameters on which both SS and EE depend. Hence, this dissertation addressed the EE maximization problem satisfying the constraints of interference to the PR, minimum achievable data rate of the SUs and target detection probability by selecting suitable SUs, optimizing sensing time and allocating appropriate power to the SUs.

Chapter 2 discussed different transmitter detection techniques and their advantages and disadvantages in detail. The two fusion schemes HDF and SDF were discussed and their performances were analyzed through the simulation results. It was observed from Figure 2.7 that Hybrid IWOPSO algorithm outperformed the other SDF-based weight combining schemes by improving the probability of detection. The detection performance was further improved by optimizing the weight coefficients at the FC using multi-objective optimization algorithms.

In Chapter 3, a circular grid consisting of the stationary SUs distributed around the centrally located PU was chosen to represent the system model. In the assumed scenario, the PR was present closer to the PU and the SRs were distributed around the PU maintaing slightly larger distances from the PU. The FC used both single and double threshold-based fusion schemes. Suitable SUs were chosen separately for SS and data transmission using the proposed algorithm. In double threshold-based

detection scheme, the minimum number of SUs was evaluated for minimum sensing rounds. The EE maximization problem was solved by the proposed IDM algorithm which jointly optimized the sensing time and power allocation. The sensing time optimization was evaluated by employing golden section search method which maximizes the system throughput. The power allocation to the SUs was optimized using EPA algorithm. From the simulation results, it was observed that the inclusion of suitable SUs improved the detection performance by 14% for SNR=-18 dB. Figure 3.5 showed minimum number of SUs and the sensing rounds required for the given SNR. The efficacy of our proposed approaches was illustrated in Figure 3.7 by comparing with the other existing schemes. Further, it was observed that the system throughput was increased by 8% for SNR=-11 dB by using 6 number of suitable SUs. It was verified that with increasing the interference and throughput threshold, EE reduces. Further, EE and throughput were maximized by 10% and 19%, respectively if the target detection probability is set at 0.9 in case of double threshold-based detection scheme.

In Chapter 4, we considered the presence of the PUE attacker closer to the PU in the CRN along with the SUs, PR and SRs. On this system model, EE maximization problem was formulated for both single and double threshold-based detection schemes at the FC. In addition to this, each SU used double threshold-based detection scheme to further enhance the detection probability. The global decision was made by the hybrid MRC-OR double threshold data fusion scheme. The negative impact of the attacker on the secondary network was considered as the constraints in terms of interference, transmission delay and throughput balancing power allocation while formulating the EE maximization problem. The eligible SUs for SS and data transmission were selected initially and the EE maximization problem was solved by our proposed NIRA algorithm. To overcome the high computational complexity of NIRA, an improved NARA algorithm was proposed. It was observed that NARA algorithm offered improvement in EE approximately by 9 times as shown in Figure 4.13 for the defined system parameters. It was clearly observed from Figure 4.11 that the attacker signal reduced the SINR, hence required more power consumption. For the given target detection probability 0.9, the presence of attacker decreased the system throughput by 76% but increased the power consumption by 15%. It was concluded that EE can be maximized by increasing SNR and threshold difference as shown in Figure 4.9 and Figure 4.14, respectively.

In extension to the work carried in Chapter 3 and Chapter 4, Chapter 5 introduced the intelligent resource allocation in the CR-VANET where the CRs were mounted on the moving vehicles. A typical vehicular network scenario in which the PU, PR, SR and the FC were present at certain distances from the road lane was considered in this

research. The protective region of the PU and the transmission region of the SUs were named as zone 1 and zone 2 which covered some portions of the road. Then, the expected number of vehicles were calculated for the zone 1 and zone 2. In this CR-VANET, the performance metrics were evaluated by considering the spatial correlation of each vehicle with the other vehicles. In the moving vehicular scenario, the time varying channel responses made the EE maximization problem more comprehensive. Hence, EE was maximized under the various constraints like interference to the PR, maximum transmission power and minimum achievable data rate. An adaptive algorithm based on NLMS was proposed to solve such type of time-varying optimization problem which showed 14% improvement in EE compared to the scheme without considering those constraints. Figure 5.5 illustrated that lower SNR required more sensing time than the higher SNR. It was also verified from Figure 5.7b that EE without considering the PUE attacker was increased by 12 times over the system model with PUE attacker. But power consumption in the presence of the attacker was increased by 80% without the attacker when the throughput threshold was set at 2.1 bits/s/Hz. The proposed approaches will be highly beneficial for CR-VANET even in an adversarial wireless environment.

Chapter 6 discussed our novel attempt of CR deployment in the ISM band. From the real measurement data in 2.4-2.5 GHZ spectrum band, spectrum occupancy was evaluated. Also, the proposed spectrum occupancy prediction algorithm based on FLANN was successful in predicting the occupancy of the ISM band prior to the observation day as 99% of accuracy from the prediction model was achieved. An interference-aware intelligent power allocation scheme was utilized for the CRU so that the transmitting power of the CRU would not cause any significant interference to the other co-existing devices.

7.3 Future Scope of Research

The CR technology explores itself to the multidisciplinary field which requires more robust and heuristic algorithms to support the adversarial wireless surroundings. Though the thesis contributed novel resource allocation schemes towards the energy-efficient CRN design satisfying different constraints, still it may be extended as our future work.

- ED-based SS techniques considered throughout the thesis are semi-blind. Therefore, in order to make the system more robust to noise uncertainty, blind SS based techniques may be used.

- In the thesis, the performance of our proposed algorithm was analyzed by

assuming that the PU is fixed and present at the center. Accordingly, the positions of all the SUs were determined. In a real time scenario, where the PUs are mobile and transmit with low power, the fixed power allocation may not be suitable. In that context, while designing the power allocation algorithm dependence on different channel parameters and the shadowing factor need to be incorporated.

- The algorithms in this research were proposed for a typical system model. Designing CRN models for a heterogeneous Two-Tier network consisting of picocells and femtocells may be attempted.

Appendix A

Derivation of (3.18)

The outage of mth SU is

$$P_{outm} = P_r \left\{ log_2 \left(1 + \frac{|h_{srm}|^2 P_{tm}}{N_p} \right) < R_{th} \right\} \qquad (A.1)$$

So, the overall outage probability of mth SU is given by

$$P_{outm} = \frac{\tau_d}{\Gamma} \left[P_{H0} \left(1 - Q_f \left(\lambda_{g2} \right) \right) P_r \left(log_2 \left(1 + \frac{|h_{srm}|^2 P_{tm}}{N_p} \right) < R_{th} \right) + \right.$$
$$\left. P_{H1} \bar{Q}_{md} \left(\lambda_{g1} \right) P_r \left(log_2 \left(1 + \frac{|h_{srm}|^2 P_{tm}}{N_p + P_p |h_{prm}|^2} \right) < R_{th} \right) \right] \qquad (A.2)$$

$$P_{outm} = \frac{\tau_d}{\Gamma} \left[P_{H0} \left(1 - Q_f \left(\lambda_{g2} \right) \right) P_r \left(|h_{srm}|^2 < \gamma_{th} \right) + \right.$$
$$\left. P_{H1} \bar{Q}_{md} \left(\lambda_{g1} \right) P_r \left(|h_{srm}|^2 - |h_{prm}|^2 \gamma_p \gamma_{th} < \gamma_{th} \right) \right] \qquad (A.3)$$

As $|h_{srm}|^2$ and $|h_{prm}|^2$ are Rayleigh distributed and independent of each other, so

$$P_r \left(|h_{srm}|^2 < \gamma_{th} \right) = 1 - exp \left(\frac{\gamma_{th}}{\sigma_{srm}^2} \right) \qquad (A.4)$$

$$P_r \left(|h_{srm}|^2 - |h_{prm}|^2 \gamma_p \gamma_{th} < \gamma_{th} \right) = \iint \frac{1}{\sigma_{srm}^2} exp \left(-\frac{x}{\sigma_{srm}^2} \right) \frac{1}{\sigma_{prm}^2} exp \left(-\frac{y}{\sigma_{prm}^2} \right) dxdy$$
$$= 1 - \frac{\sigma_{srm}^2}{\sigma_{prm}^2 \gamma_p \gamma_{th} + \sigma_{srm}^2} exp \left(-\frac{\gamma_{th}}{\sigma_{srm}^2} \right)$$
$$\qquad (A.5)$$

Substituting the solutions (A.4) and (A.5) in (A.2), (3.18) is obtained.

Appendix B

Proof of $R(\tau_s, P_t)$ is a unimodal function in the range $0 \le \tau_s \le T$.

Appendix B1 (Single threshold-based SDF model)

$$R'(\tau_s, P_t) = \frac{dR(\tau_s, P_t)}{d\tau_s} = \frac{C_0 P_{H0}}{\Gamma} \left[\left\{ \left(-Q_f'(\tau_s) \right) \tau_d \right\} - (1 - Q_f(\tau_s)) \right] \quad \text{(B.1)}$$

Solving (3.4) as single threshold, we have

$$Q'_f(\tau_s) = \frac{-b\sqrt{f_s}}{2\sqrt{2\pi}} \tau_s^{-\frac{1}{2}} exp\left(-\frac{\left(a + b\sqrt{\tau_s f_s} \right)^2}{2} \right) \quad \text{(B.2)}$$

where $C_0 = \sum_{m=1}^{M} C_{0m}$, At $\tau_s = 0$, since $Q'_f(0) = -\infty$. So $\lim_{\tau_s \to 0} R'(0) = \infty$ for all values of P_t. At $\tau_s = \Gamma$, since $0 \le Q_f(\Gamma) < 1$. So, $\lim_{\tau_s \to \infty} R'(\Gamma) < 0$. Hence, it is proved that $R'(\tau_s)$ is a unimodal function in the range $0 \le \tau_s \le \Gamma$.

Appendix B2(Double threshold-based SDF model)

$$R'(\tau_s) = \frac{1}{T} C_0 P_{H0} \left[\left\{ -\left(S_R'(\tau_s) \tau_s + S_R(\tau_s) \right) \right\} (1 - Q_f(\tau_s)) + \tau_d \left(-Q_f'(\tau_s) \right) \right] \quad \text{(B.3)}$$

From (3.3), (3.4) and (3.5)

$$Q_f'(\tau_s) = \frac{-\left(\Delta' + b \right) \sqrt{f_s}}{\sqrt{8\pi\tau_s}} exp\left\{ -\frac{\left(a + (\Delta' + b)\sqrt{\tau_s f_s} \right)^2}{2} \right\} \quad \text{(B.4)}$$

$$S_R'(\tau_s) = \frac{\left(\tilde{Q}_f'(\tau_s) - Q_f'(\tau_s) \right) P_{H0}}{\left(1 - \left((\bar{Q}_d - Q_d(\tau_s)) P_{H1} + (\tilde{Q}_f(\tau_s) - Q_f(\tau_s)) P_{H0} \right) \right)^2} \quad \text{(B.5)}$$

In deriving (B.5), we will see that $Q_f'(0) = \tilde{Q}_f'(0) = -\infty$ for any value of Δ. Similar to the condition given in Appendix B1, it is proved that $R'(\tau_s)$ is a unimodal function in the range $0 \le \tau_s \le \Gamma$.

Appendix C

Proof of S_R is a decreasing function of M.

Let δ is decided such that $Q_f(\lambda_{g2}) = \bar{Q}_f$. Then, taking the first partial derivative of S_R with respect to M

$$S_R{}' = \frac{-Q_d{}'(\lambda_{g2})P_{H1} + \tilde{Q}'_f(\lambda_{g1})P_{H0}}{(1-\rho)^2} \tag{C.1}$$

For the given target false alarm probability $\bar{Q}_f$, $Q_d(\lambda_{g2})$ is given by

$$Q_d(\lambda_{g2}) = Q\left(\frac{Q^{-1}(\bar{Q}_f)\sqrt{2\sum_{m=1}^{M}\sigma_{\eta m}^4 w_m^2} - \sum_{m=1}^{M}\sigma_{\eta m}^2 w_m \gamma_m \sqrt{\tau_s f_s}}{\sqrt{2\sum_{m=1}^{M}\sigma_{\eta m}^4(1+2\gamma_m)w_m^2}} \right) \tag{C.2}$$

From (3.3) and (C.2), it is proved that $\tilde{Q}_f(\lambda_{g1})$ and $Q_d(\lambda_{g2})$ are the decreasing and increasing function of M, respectively. Hence, $\frac{dS_R}{dK} < 0$. So, it is proved that S_R is a decreasing function of M.

Appendix D

Proof of convergence of $F\left(\Upsilon, \tau_s, P_t\right) = \left\{R\left(\tau_s, P_t\right) - \Upsilon P_T\left(\tau_s, P_t\right)\right\}.$

To prove this convergence, let S be the search subset, then $F\left(\Upsilon\right) = \max\limits_{\tau_s, P_t}\left\{R\left(\tau_s, P_t\right) - \Upsilon P_T\left(\tau_s, P_t\right)\right\}$ is a monotonically decreasing function and converges at each iteration.

Proof: Let t represents the current iteration. First, assume that $\Upsilon\left(t+1\right) > \Upsilon\left(t\right)$. Then

$$F\left(\Upsilon\left(t+1\right)\right) = \max\left\{R\left(\tau_s, P_t\right) - \Upsilon\left(t+1\right)P_T\left(\tau_s, P_t\right)\right\} \tag{D.1}$$
$$= R\left(\tau_s^*, P_t^*\right) - \Upsilon\left(t+1\right)P_T\left(\tau_s^*, P_t^*\right)$$
$$< R\left(\tau_s^*, P_t^*\right) - \Upsilon\left(t\right)P_T\left(\tau_s^*, P_t^*\right)$$
$$\leq \max\left\{R\left(\tau_s, P_t\right) - \Upsilon\left(t\right)P_T\left(\tau_s, P_t\right)\right\}$$
$$= F\left(\Upsilon\left(t\right)\right)$$

To prove the convergence of $F\left(\Upsilon, \tau_s, P_t\right)$, it is sufficient to show that $R\left(\tau_s, P_t\right) - \Upsilon\left(t\right)P_T\left(\tau_s, P_t\right)$ decreases with successive iterations. We know that

$$F\left(\Upsilon\left(t\right)\right) = R\left(\tau_s^*\left(t\right), P_t^*\left(t\right)\right) - \Upsilon\left(t\right)P_T\left(\tau_s^*\left(t\right), P_t^*\left(t\right)\right) \tag{D.2}$$
$$= \Upsilon\left(t+1\right)P_T\left(\tau_s^*\left(t\right), P_t^*\left(t\right)\right) - \Upsilon\left(t\right)P_T\left(\tau_s^*\left(t\right), P_t^*\left(t\right)\right)$$
$$= \left\{\Upsilon\left(t+1\right) - \Upsilon\left(t\right)\right\}P_T\left(\tau_s^*\left(t\right), P_t^*\left(t\right)\right)$$

As $F\left(\Upsilon\left(t\right)\right) > 0$, $\Upsilon\left(t+1\right)$ should be greater than $\Upsilon\left(t\right)$. Hence, $F\left(\Upsilon, \tau_s, P_t\right)$ goes on decreasing in successive iterations.

Appendix E

Proof of Theorem 3.

In the absence of an attacker, Q_f in terms of $\bar{Q}_d$ is expressed as (3.4) (considering the single threshold-based detection scheme). Taking the first derivative of $D_P(\tau_s)$ with respect to τ_s, we have

$$\frac{dD_P(\tau_s)}{d\tau_s} = \frac{1}{\Gamma} - \frac{1}{\Gamma}Q\left[a + b\sqrt{\tau_s f_s}\right] - \frac{(\tau_d)}{\Gamma}\frac{b\sqrt{f_s}}{\sqrt{8\pi\tau_s}}exp\left\{-\frac{\left(a + b\sqrt{\tau_s f_s}\right)^2}{2}\right\} - \frac{\bar{Q}_d}{\Gamma} \quad \text{(E.1)}$$

From (E.1), it is obvious that $\lim\limits_{\tau_s \to 0} \frac{dD_P(\tau_s)}{d\tau_s} = -\infty$ and $\lim\limits_{\tau_s \to \Gamma} \frac{dD_P(\tau_s)}{d\tau_s} > 0$. Hence, $D_P(\tau_s)$ decreases from τ_s to τ_s^*, and the increases from τ_s^* to Γ. Further differentiating (E.1), it is proved that $\frac{d^2 D_P(\tau_s)}{d\tau_s^2} > 0$. Hence, $D_P(\tau_s)$ is a convex function of τ_s. So, there exists a unique solution τ_s^* in the range $[0, \Gamma]$ at which $D_P(\tau_s)$ is minimum. Thus, Theorem 3 is proved.

Similarly, it can be proved that $D_A(\tau_s)$ is also a convex function of τ_s.

Appendix F

Proof of Proposition 4.

Given $P_e(\lambda) = zP_f(\lambda) + (1-z)P_{md}$. Differentiating both $P_f(\lambda)$ and $P_f(\lambda)$ with respect to λ we have

$$\frac{dP_f(\lambda)}{\lambda} = -\frac{\sqrt{N}}{2\sigma_\eta^2\sqrt{\pi}}exp\left\{-\frac{1}{2}\left(\frac{\lambda - \sigma_\eta^2}{\sigma_\eta^2\sqrt{2/N}}\right)^2\right\} \tag{F.1}$$

and

$$\frac{dP_d(\lambda)}{\lambda} = -\frac{\sqrt{N}}{2(P+\sigma_\eta^2)\sqrt{\pi}}exp\left\{-\frac{1}{2}\left(\frac{\lambda - (P+\sigma_\eta^2)}{(P+\sigma_\eta^2)\sqrt{2/N}}\right)^2\right\} \tag{F.2}$$

So,

$$\frac{dP_e(\lambda)}{\lambda} = z\frac{dP_f(\lambda)}{\lambda} - (1-z)\frac{dP_d(\lambda)}{\lambda} \tag{F.3}$$

Using (F.1) and (F.2), and further differentiating both the sides of (F.3), we obtain

$$\frac{d^2P_e(\lambda)}{d\lambda^2} = \frac{zN}{2\sigma_\eta^4\sqrt{2\pi}}Q^{-1}(P_f(\lambda))\,exp\left\{-\frac{1}{2}(Q^{-1}(P_f(\lambda)))^2\right\} -$$
$$\frac{(1-z)N}{2(P+\sigma_\eta^2)^2\sqrt{2\pi}}Q^{-1}(P_d(\lambda))\,exp\left\{-\frac{1}{2}(Q^{-1}(P_d(\lambda)))^2\right\} \tag{F.4}$$

In the practical wireless environment, P_f should be less than 0.5 and P_d should be greater than 0.5 are desirable to maximize the system throughput [86]. Hence, for $P_f \leq 0.5$ and $P_d \geq 0.5$, (F.4) is positive.

Thus $P_e(\lambda)$ is a convex function of λ.

Appendix G

Formulation of Proposed Method using the Trigonometric FLANN.

This describes the formulation of our proposed method implementating the FLANN to predict spectrum occupancy one day in advance. The FLANN model consists of the 4 dimensional input pattern $\chi = [O_T, O_W, O_{TH}, O_F]^T$. So, χ is a matrix composed of 4×32 elements. The procedure to implement FLANN is summarized below.

Step-1: Initialize the input matrix.

Step-2: Initialize τ_i and $i = 1$, then the ith element of O_T is expanded by the following functional expansion

$$\mathbb{Z}(\tau_i) = [O_T(\tau_i), \cos(\pi O_T(\tau_i)), \sin(\pi O_T(\tau_i)), \cos(2\pi O_T(\tau_i)), ..., \sin(4\pi O_T(\tau_i))] \tag{G.1}$$

Step-3: Initialize iteration $r = 1$ and the weight vector for $\mathbb{Z}(\tau_i)$ is $W_{\tau_i}(r) = \left[W_{\tau_i}{}^1(r), W_{\tau_i}{}^2(r), ..., W_{\tau_i}{}^J(r)\right]^T$ where J is the number of functional elements, and here $j = 9$.

Step-4: Compute the output of the ith element as

$$\bar{O}_{\tau_i}(r) = sigmoid\left(\mathbb{Z}(\tau_i) W_{\tau_i}(r)\right), \tag{G.2}$$

and compute the corresponding error as $e_{\tau_i}(r) = O_T(\tau_i) - \bar{O}_{\tau_i}(r)$.

Step-5: Update the weight as $W_{\tau_i}(r+1) = W_{\tau_i}(r) + \varphi \bar{\beta}_{\tau_i}(r) \mathbb{Z}(\tau_i)^T$, where $\bar{\beta}_{\tau_i}(r) = \left(1 - \left(\bar{O}_{\tau_i}(r)\right)^2\right) e_{\tau_i}(r)$.

Step-6: Repeat **Step-3** to **Step-5** until the convergence criteria is satisfied.

Step-7: Repeat **Step-2** to **Step-6** until spectrum occupancy statistics of all the 32 elements of O_T are evaluated.

Step-8: Thus, the final occupancy statistic of Tuesday $O_{TF}(\tau_1, \tau_2, .., \tau_{\mathbb{I}})$ is estimated and predict occupancy for Wednesday i.e. $\hat{O}_W(\tau_1, \tau_2, .., \tau_{\mathbb{I}})$. Then, follow **Step-2** to **Step-7** to predict the occupancy statistic for Thursday.

Dissemination

Journals

1. Deepa Das and Susmita Das,"Optimal Resource Allocation for Soft Decision Fusion-Based Cooperative Spectrum Sensing in Cognitive Radio Networks," Computers & Electrical Engineering, Elsevier,vol. 52, pp.362-378, 2016. http://dx.doi.org/10.1016/j.compeleceng.2016.02.001.

2. Deepa Das and Susmita Das, "A Survey on Spectrum Occupancy Measurement for Cognitive Radio," Wireless Personal Communications, Springer, vol. 85, no. 4,pp. 2581-2598,2015. doi:10.1007/s11277-015-2921-1.

3. Deepa Das and Susmita Das, "Primary user emulation attack in cognitive radio networks: A survey,"International Journal of Computer Networks and Wireless Communications, vol. 3, no. 3,pp. 312-318,2013.

4. Deepa Das and Susmita Das, "A Novel Approach for Cognitive Radio Application in 2.4 GHz ISM Band,"International Journal of Electronics,Taylor & Francis,2016. doi:10.1080/00207217.2016.1244865.

5. Deepa Das and Susmita Das, "A Novel Approach for Energy-Efficient Resource Allocation in Double Threshold-Based Cognitive Radio Network,"International Journal of Communication Systems, Wiley,2016. doi: 10.1002/dac.3198.

6. Deepa Das, David W. Matolak and Susmita Das, "Spectrum Occupancy Prediction Based on Functional Link Artificial Neural Network (FLANN) in ISM Band," Neural Computing and Applications, Springer, 2016. doi:10.1007/s00521-016-2653-5.

7. Deepa Das and Susmita Das, "An Adaptive Resource Allocation Scheme for Cognitive Radio Vehicular Ad Hoc Network in the Presence of Primary User Emulation Attack," IET Networks, 2016. doi: 10.1049/iet-net.2016.0033.

8. Deepa Das and Susmita Das, "An intelligent Approach for Resource Allocation in the Cognitive Radio Vehicular Ad Hoc Network," Transactions on Emerging Telecommunications Technologies, Wiley, 2017. doi =10.1002/ett.3159.

9. Deepa Das and Susmita Das, "An Intelligent Resource Management Scheme for SDF-Based Cooperative Spectrum Sensing in the Presence of Primary User Emulation Attack,"Computers & Electrical Engineering, Elsevier (Accepted).

10. Deepa Das and Susmita Das, "An Intelligent Resource Allocation Scheme for the Cognitive Radio Network in the presence of Primary User Emulation Attack," IET Communications (Provisionally accepted, revision submitted).

Conferences

1. Deepa Das and Susmita Das, "A novel resource allocation for energy-efficient Cognitive Radio," 2015 Annual IEEE India Conference (INDICON), New Delhi, 2015, pp. 1-6. doi: 10.1109/INDICON.2015.7443395.

2. Deepa Das and Susmita Das, "Cooperative spectrum sensing using hybrid IWOPSO algorithm in cognitive radio networks," 2015 IEEE 12th Malaysia International Conference on Communications (MICC), Kuching, Malaysia, 2015, pp. 59-63. doi: 10.1109/MICC.2015.7725407.

3. Deepa Das and Susmita Das, "Interference-aware power allocation in soft decision fusion (SDF) based cooperative spectrum sensing," 2014 Annual IEEE India Conference (INDICON), Pune, 2014, pp. 1-6. doi: 10.1109/INDICON.2014.7030618.

4. Deepa Das and Susmita Das, "A cooperative spectrum sensing scheme using multiobjective hybrid IWO/PSO algorithm in cognitive radio networks," Issues and Challenges in Intelligent Computing Techniques (ICICT), 2014 International Conference on, Ghaziabad, 2014, pp. 225-230. doi: 10.1109/ICICICT.2014.6781284.

5. Deepa Das and Susmita Das, "Eigenvalue detection based method to mitigate PUEA in cognitive radio networks," 2013 IEEE International Conference on Advanced Networks and Telecommunications Systems (ANTS), Kattankulathur, 2013, pp. 1-6. doi: 10.1109/ANTS.2013.6802854.

Bibliography

[1] I. F. Akyildiz, W.-Y. Lee, and K. R. Chowdhury, "Crahns: Cognitive radio ad hoc networks," *AD hoc networks*, vol. 7, no. 5, pp. 810–836, 2009.

[2] I. F. Akyildiz, W.-Y. Lee, M. C. Vuran, and S. Mohanty, "Next generation/dynamic spectrum access/cognitive radio wireless networks: a survey," *Computer networks*, vol. 50, no. 13, pp. 2127–2159, 2006.

[3] B. Wang and K. Liu, "Advances in cognitive radio networks: A survey," *Selected Topics in Signal Processing, IEEE Journal of*, vol. 5, no. 1, pp. 5–23, 2011.

[4] A. M. Wyglinski, M. Nekovee, and T. Hou, *Cognitive radio communications and networks: principles and practice*. Academic Press, 2009.

[5] L. Khalid and A. Anpalagan, "Emerging cognitive radio technology: Principles, challenges and opportunities," *Computers & electrical engineering*, vol. 36, no. 2, pp. 358–366, 2010.

[6] S. Haykin, "Cognitive radio: brain-empowered wireless communications," *Selected Areas in Communications, IEEE Journal on*, vol. 23, no. 2, pp. 201–220, 2005.

[7] M. Sherman, A. N. Mody, R. Martinez, C. Rodriguez, and R. Reddy, "Ieee standards supporting cognitive radio and networks, dynamic spectrum access, and coexistence," *Communications Magazine, IEEE*, vol. 46, no. 7, pp. 72–79, 2008.

[8] C. Cordeiro, K. Challapali, D. Birru, and N. Sai Shankar, "Ieee 802.22: the first worldwide wireless standard based on cognitive radios," in *New Frontiers in Dynamic Spectrum Access Networks, 2005. DySPAN 2005. 2005 First IEEE International Symposium on*. IEEE, 2005, pp. 328–337.

[9] J. Mitola III, "Software radios: Survey, critical evaluation and future directions," *Aerospace and Electronic Systems Magazine, IEEE*, vol. 8, no. 4, pp. 25–36, 1993.

[10] J. Mitola III and G. Q. Maguire Jr, "Cognitive radio: making software radios more personal," *Personal Communications, IEEE*, vol. 6, no. 4, pp. 13–18, 1999.

[11] F. C. Commission *et al.*, "Notice of proposed rule making and order: Facilitating opportunities for flexible, efficient, and reliable spectrum use employing cognitive radio technologies," *ET docket*, no. 03-108, p. 73, 2005.

[12] R. Umar and A. U. Sheikh, "A comparative study of spectrum awareness techniques for cognitive radio oriented wireless networks," *Physical Communication*, vol. 9, pp. 148–170, 2013.

[13] K.-C. Chen, Y.-J. Peng, N. Prasad, Y.-C. Liang, and S. Sun, "Cognitive radio network architecture: part i–general structure," in *Proceedings of the 2nd international conference on Ubiquitous information management and communication*. ACM, 2008, pp. 114–119.

[14] A. Ghasemi and E. S. Sousa, "Spectrum sensing in cognitive radio networks: requirements, challenges and design trade-offs," *Communications Magazine, IEEE*, vol. 46, no. 4, pp. 32–39, 2008.

[15] X. Chen, H.-H. Chen, and W. Meng, "Cooperative communications for cognitive radio networks—from theory to applications," *Communications Surveys & Tutorials, IEEE*, vol. 16, no. 3, pp. 1180–1192, 2014.

[16] I. F. Akyildiz, B. F. Lo, and R. Balakrishnan, "Cooperative spectrum sensing in cognitive radio networks: A survey," *Physical communication*, vol. 4, no. 1, pp. 40–62, 2011.

[17] S. K. Sharma, T. E. Bogale, S. Chatzinotas, B. Ottersten, L. B. Le, and X. Wang, "Cognitive radio techniques under practical imperfections: A survey," *Communications Surveys & Tutorials, IEEE*, vol. 17, no. 4, pp. 1858–1884, 2015.

[18] E. Axell, G. Leus, E. G. Larsson, and H. V. Poor, "Spectrum sensing for cognitive radio: State-of-the-art and recent advances," *Signal Processing Magazine, IEEE*, vol. 29, no. 3, pp. 101–116, 2012.

[19] T. Yücek and H. Arslan, "A survey of spectrum sensing algorithms for cognitive radio applications," *Communications Surveys & Tutorials, IEEE*, vol. 11, no. 1, pp. 116–130, 2009.

[20] J. Ma, G. Y. Li, and B. H. F. Juang, "Signal processing in cognitive radio," *Proceedings of the IEEE*, vol. 97, no. 5, pp. 805–823, 2009.

[21] F. F. Digham, M.-S. Alouini, and M. K. Simon, "On the energy detection of unknown signals over fading channels," *IEEE transactions on communications*, vol. 55, no. 1, pp. 21–24, 2007.

[22] A. Tani and R. Fantacci, "A low-complexity cyclostationary-based spectrum sensing for uwb and wimax coexistence with noise uncertainty," *Vehicular Technology, IEEE Transactions on*, vol. 59, no. 6, pp. 2940–2950, 2010.

[23] H. Tang, "Some physical layer issues of wide-band cognitive radio systems," in *New frontiers in dynamic spectrum access networks, 2005. DySPAN 2005. 2005 first IEEE international symposium on*.   IEEE, 2005, pp. 151–159.

[24] Y. Zeng and Y.-C. Liang, "Eigenvalue-based spectrum sensing algorithms for cognitive radio," *Communications, IEEE Transactions on*, vol. 57, no. 6, pp. 1784–1793, 2009.

[25] Y. Zeng and Y.-C. Liang, "Spectrum-sensing algorithms for cognitive radio based on statistical covariances," *Vehicular Technology, IEEE Transactions on*, vol. 58, no. 4, pp. 1804–1815, 2009.

[26] B. Farhang-Boroujeny, "Filter bank spectrum sensing for cognitive radios," *Signal Processing, IEEE Transactions on*, vol. 56, no. 5, pp. 1801–1811, 2008.

[27] Z. Tian and G. B. Giannakis, "A wavelet approach to wideband spectrum sensing for cognitive radios," in *Cognitive radio oriented wireless networks and communications, 2006. 1st international conference on*.   IEEE, 2006, pp. 1–5.

[28] D. J. Thomson, "Spectrum estimation and harmonic analysis," *Proceedings of the IEEE*, vol. 70, no. 9, pp. 1055–1096, 1982.

[29] Z. Tian and G. B. Giannakis, "Compressed sensing for wideband cognitive radios," in *Acoustics, Speech and Signal Processing, 2007. ICASSP 2007. IEEE International Conference on*, vol. 4.   IEEE, 2007, pp. IV–1357.

[30] S. S. Ivrigh, S. M.-S. Sadough, and S. A. Ghorashi, "A blind source separation technique for spectrum sensing in cognitive radio networks based on kurtosis metric," in *Computer and Knowledge Engineering (ICCKE), 2011 1st International eConference on*.   IEEE, 2011, pp. 333–337.

[31] G. Ganesan and Y. Li, "Agility improvement through cooperative diversity in cognitive radio," in *Global Telecommunications Conference, 2005. GLOBECOM'05. IEEE*, vol. 5.   IEEE, 2005, pp. 5–pp.

[32] I. F. Akyildiz, W.-Y. Lee, M. C. Vuran, and S. Mohanty, "A survey on spectrum management in cognitive radio networks," *Communications Magazine, IEEE*, vol. 46, no. 4, pp. 40–48, 2008.

[33] S. Parvin, F. K. Hussain, O. K. Hussain, S. Han, B. Tian, and E. Chang, "Cognitive radio network security: A survey," *Journal of Network and Computer Applications*, vol. 35, no. 6, pp. 1691–1708, 2012.

[34] D. Das and S. Das, "Primary user emulation attack in cognitive radio networks: A survey," *IRACST-International Journal of Computer Networks and Wireless Communications*, vol. 3, no. 3, pp. 312–318, 2013.

[35] S. Arkoulis, L. Kazatzopoulos, C. Delakouridis, and G. Marias, "Cognitive spectrum and its security issues," in *Next Generation Mobile Applications, Services and Technologies, 2008. NGMAST'08. The Second International Conference on*. IEEE, 2008, pp. 565–570.

[36] R. Chen and J.-M. Park, "Ensuring trustworthy spectrum sensing in cognitive radio networks," in *Networking Technologies for Software Defined Radio Networks, 2006. SDR'06.1 st IEEE Workshop on*. IEEE, 2006, pp. 110–119.

[37] K. D. Singh, P. Rawat, and J.-M. Bonnin, "Cognitive radio for vehicular ad hoc networks (cr-vanets): approaches and challenges," *EURASIP Journal on Wireless Communications and Networking*, vol. 2014, no. 1, pp. 1–22, 2014.

[38] D. B. Rawat, Y. Zhao, G. Yan, and M. Song, "Crave: Cognitive radio enabled vehicular communications in heterogeneous networks," in *Radio and Wireless Symposium (RWS), 2013 IEEE*. IEEE, 2013, pp. 190–192.

[39] A. A. Khan, M. H. Rehmani, and M. Reisslein, "Cognitive radio for smart grids: survey of architectures, spectrum sensing mechanisms, and networking protocols," 2015.

[40] A. R. Syed and K.-L. A. Yau, "On cognitive radio-based wireless body area networks for medical applications," in *Computational Intelligence in Healthcare and e-health (CICARE), 2013 IEEE Symposium on*. IEEE, 2013, pp. 51–57.

[41] G. P. Joshi, S. Y. Nam, and S. W. Kim, "Cognitive radio wireless sensor networks: applications, challenges and research trends," *Sensors*, vol. 13, no. 9, pp. 11 196–11 228, 2013.

[42] M. Hoyhtya, J. Kyrolainen, A. Hulkkonen, J. Ylitalo, and A. Roivainen, "Application of cognitive radio techniques to satellite communication," in *Dynamic Spectrum Access Networks (DYSPAN), 2012 IEEE International Symposium on*. IEEE, 2012, pp. 540–551.

[43] F. H. Sanders, "Broadband spectrum surveys in denver, co, san diego, ca, and los angeles, ca: methodology, analysis, and comparative results," in *Electromagnetic Compatibility, 1998. 1998 IEEE International Symposium on*, vol. 2. IEEE, 1998, pp. 988–993.

[44] M. H. Islam *et al.*, "Spectrum survey in singapore: Occupancy measurements and analyses," in *Cognitive Radio Oriented Wireless Networks and Communications, 2008. CrownCom 2008. 3rd International Conference on*. IEEE, 2008, pp. 1–7.

[45] S. Lee and S.-L. Kim, "Optimization of time-domain spectrum sensing for cognitive radio systems," *Vehicular Technology, IEEE Transactions on*, vol. 60, no. 4, pp. 1937–1943, 2011.

[46] Y.-E. Lin, K.-H. Liu, and H.-Y. Hsieh, "On using interference-aware spectrum sensing for dynamic spectrum access in cognitive radio networks," *Mobile Computing, IEEE Transactions on*, vol. 12, no. 3, pp. 461–474, 2013.

[47] H. Li, X. Cheng, K. Li, C. Hu, N. Zhang, and W. Xue, "Robust collaborative spectrum sensing schemes for cognitive radio networks," *Parallel and Distributed Systems, IEEE Transactions on*, vol. 25, no. 8, pp. 2190–2200, 2014.

[48] A. W. Min and K. G. Shin, "Robust tracking of small-scale mobile primary user in cognitive radio networks," *Parallel and Distributed Systems, IEEE Transactions on*, vol. 24, no. 4, pp. 778–788, 2013.

[49] Y. Zhao, P. Paul, C. Xin, and M. Song, "Performance analysis of spectrum sensing with mobile sus in cognitive radio networks," in *Communications (ICC), 2014 IEEE International Conference on*. IEEE, 2014, pp. 2761–2766.

[50] X. Wang, M. Jia, Q. Guo, and X. Gu, "Performance analysis of spectrum sensing for mobile cognitive radio networks," in *2015 IEEE Globecom Workshops (GC Wkshps)*. IEEE, 2015, pp. 1–6.

[51] X. Liu, G. Wang, H. Wang, B. Li, and G. Liu, "A signal-to-noise ratio based multiple thresholds cooperative spectrum sensing scheme," in *Biomedical Engineering and Informatics (BMEI), 2014 7th International Conference on.* IEEE, 2014, pp. 908–912.

[52] X. Tan, X. Liu, and A. A. Anghuwo, "Optimization algorithm for cooperative detection in cognitive radio," in *Wireless Communications and Networking Conference (WCNC), 2012 IEEE.* IEEE, 2012, pp. 2774–2779.

[53] L. Duan, L. Zhang, Y. Chu, and S. Liu, "Cooperative spectrum sensing with double threshold detection based on reputation in cognitive radio," in *Wireless Communications, Networking and Mobile Computing, 2009. WiCom'09. 5th International Conference on.* IEEE, 2009, pp. 1–4.

[54] F. Mohammed and M. Deriche, "A two-threshold cooperative spectrum sensing algorithm using swarm intelligence," in *Computing, Communications and IT Applications Conference (ComComAp), 2013.* IEEE, 2013, pp. 59–62.

[55] X. Zhang and H. Su, "Cream-mac: Cognitive radio-enabled multi-channel mac protocol over dynamic spectrum access networks," *Selected Topics in Signal Processing, IEEE Journal of*, vol. 5, no. 1, pp. 110–123, 2011.

[56] M. Mehdawi, N. Riley, K. Paulson, A. Fanan, and M. Ammar, "Spectrum occupancy survey in hull-uk for cognitive radio applications: measurement & analysis," *International Journal of Scientific & Technology Research*, vol. 2, no. 4, pp. 231–236, 2013.

[57] V. Valenta, R. Maršálek, G. Baudoin, M. Villegas, M. Suarez, and F. Robert, "Survey on spectrum utilization in europe: Measurements, analyses and observations," in *Cognitive Radio Oriented Wireless Networks & Communications (CROWNCOM), 2010 Proceedings of the Fifth International Conference on.* IEEE, 2010, pp. 1–5.

[58] M. López Benítez and F. J. Casadevall Palacio, "Spectrum occupancy in realistic scenarios and duty cycle model for cognitive radio," *Advances in Electronics and Telecommunications, Special Issue on Radio Communication Series: Recent Advances and Future Trends in Wireless Communication*, vol. 1, no. 1, pp. 1–9, 2010.

[59] Z. Khan, J. Lehtomäki, K. Umebayashi, and J. Vartiainen, "On the selection of the best detection performance sensors for cognitive radio networks," *Signal Processing Letters, IEEE*, vol. 17, no. 4, pp. 359–362, 2010.

[60] D. M. Godarzi, K. Arshad, Y. Ko, and K. Moessner, "Selecting users in energy-efficient collaborative spectrum sensing," in *Wireless Communications and Networking Conference (WCNC), 2012 IEEE.* IEEE, 2012, pp. 1029–1033.

[61] Y. Chen, K. Yang, and B. Zhao, "Collaborative user number selection based on saturation throughput and sensing performance," *Vehicular Technology, IEEE Transactions on*, vol. 60, no. 8, pp. 4019–4023, 2011.

[62] M. Monemian and M. Mahdavi, "Analysis of a new energy-based sensor selection method for cooperative spectrum sensing in cognitive radio networks," *Sensors Journal, IEEE*, vol. 14, no. 9, pp. 3021–3032, 2014.

[63] A. Sepasi Zahmati, X. Fernando, and A. Grami, "Energy-aware secondary user selection in cognitive sensor networks," *Wireless Sensor Systems, IET*, vol. 4, no. 2, pp. 86–96, 2014.

[64] A. S. Cacciapuoti, I. F. Akyildiz, and L. Paura, "Correlation-aware user selection for cooperative spectrum sensing in cognitive radio ad hoc networks," *Selected Areas in Communications, IEEE Journal on*, vol. 30, no. 2, pp. 297–306, 2012.

[65] D. Ren, J. Ge, and J. Li, "Secondary user selection scheme using adaptive genetic algorithms for cooperative spectrum sensing under correlated shadowing," *Wireless personal communications*, vol. 71, no. 1, pp. 769–788, 2013.

[66] X. Wu, J.-L. Xu, M. Chen, and J. Wang, "Joint optimization over sensing time and power allocation in cognitive radio networks based on energy efficiency," in *Communications and Networking in China (CHINACOM), 2014 9th International Conference on.* IEEE, 2014, pp. 545–549.

[67] J. Mao, G. Xie, J. Gao, and Y. Liu, "Energy efficiency optimization for ofdm-based cognitive radio systems: a water-filling factor aided search method," *Wireless Communications, IEEE Transactions on*, vol. 12, no. 5, pp. 2366–2375, 2013.

[68] A. Alabbasi, Z. Rezki, and B. Shihada, "Energy efficient scheme for cognitive radios utilizing soft sensing," in *Wireless Communications and Networking Conference (WCNC), 2014 IEEE*. IEEE, 2014, pp. 701–706.

[69] K. Illanko, M. Naeem, A. Anpalagan, and D. Androutsos, "Energy-efficient frequency and power allocation for cognitive radios in television systems."

[70] L. Dong and G. Ren, "Optimal and low complexity algorithm for energy efficient power allocation with sensing errors in cognitive radio networks," in *Wireless Communications and Signal Processing (WCSP), 2014 Sixth International Conference on*. IEEE, 2014, pp. 1–5.

[71] S. Althunibat, M. Di Renzo, and F. Granelli, "Cooperative spectrum sensing for cognitive radio networks under limited time constraints," *Computer Communications*, vol. 43, pp. 55–63, 2014.

[72] J. Chen, L. Lv, Y. Liu, Y. Kuo, and C. Ren, "Energy efficient relay selection and power allocation for cooperative cognitive radio networks," *Communications, IET*, vol. 9, no. 13, pp. 1661–1668, 2015.

[73] R. Ramamonjison and V. K. Bhargava, "Energy efficiency maximization framework in cognitive downlink two-tier networks," *Wireless Communications, IEEE Transactions on*, vol. 14, no. 3, pp. 1468–1479, 2015.

[74] Z. Shi, T. Tan, K. C. Teh, and K. H. Li, "Energy efficient cognitive radio network based on multiband sensing and spectrum sharing," *Communications, IET*, vol. 8, no. 9, pp. 1499–1507, 2014.

[75] A. Ebrahimzadeh, M. Najimi, S. M. H. Andargoli, and A. Fallahi, "Sensor selection and optimal energy detection threshold for efficient cooperative spectrum sensing," *Vehicular Technology, IEEE Transactions on*, vol. 64, no. 4, pp. 1565–1577, 2015.

[76] S. Chatterjee, S. P. Maity, and T. Acharya, "Energy efficient cognitive radio system for joint spectrum sensing and data transmission," *Emerging and Selected Topics in Circuits and Systems, IEEE Journal on*, vol. 4, no. 3, pp. 292–300, 2014.

[77] M. T. Masonta, M. Mzyece, and N. Ntlatlapa, "Spectrum decision in cognitive radio networks: A survey," *Communications Surveys & Tutorials, IEEE*, vol. 15, no. 3, pp. 1088–1107, 2013.

[78] H. Sun, A. Nallanathan, C.-X. Wang, and Y. Chen, "Wideband spectrum sensing for cognitive radio networks: a survey," *Wireless Communications, IEEE*, vol. 20, no. 2, pp. 74–81, 2013.

[79] E. Visotsky, S. Kuffner, and R. Peterson, "On collaborative detection of tv transmissions in support of dynamic spectrum sharing," in *New Frontiers in Dynamic Spectrum Access Networks, 2005. DySPAN 2005. 2005 First IEEE International Symposium on*. IEEE, 2005, pp. 338–345.

[80] A. Ghasemi and E. S. Sousa, "Asymptotic performance of collaborative spectrum sensing under correlated log-normal shadowing," *Communications Letters, IEEE*, vol. 11, no. 1, pp. 34–36, 2007.

[81] Q. Liu, J. Gao, and L. Chen, "Optimization of energy detection based cooperative spectrum sensing in cognitive radio networks," in *Wireless Communications and Signal Processing (WCSP), 2010 International Conference on*. IEEE, 2010, pp. 1–5.

[82] D. Cabric, S. M. Mishra, and R. W. Brodersen, "Implementation issues in spectrum sensing for cognitive radios," in *Signals, systems and computers, 2004. Conference record of the thirty-eighth Asilomar conference on*, vol. 1. IEEE, 2004, pp. 772–776.

[83] R. Tandra and A. Sahai, "Snr walls for signal detection," *Selected Topics in Signal Processing, IEEE Journal of*, vol. 2, no. 1, pp. 4–17, 2008.

[84] A. Ghasemi and E. S. Sousa, "Collaborative spectrum sensing for opportunistic access in fading environments," in *New Frontiers in Dynamic Spectrum Access Networks, 2005. DySPAN 2005. 2005 First IEEE International Symposium on*. IEEE, 2005, pp. 131–136.

[85] J. Unnikrishnan and V. V. Veeravalli, "Cooperative sensing for primary detection in cognitive radio," *Selected Topics in Signal Processing, IEEE Journal of*, vol. 2, no. 1, pp. 18–27, 2008.

[86] Y.-C. Liang, Y. Zeng, E. C. Peh, and A. T. Hoang, "Sensing-throughput tradeoff for cognitive radio networks," *Wireless Communications, IEEE Transactions on*, vol. 7, no. 4, pp. 1326–1337, 2008.

[87] E. Peh and Y.-C. Liang, "Optimization for cooperative sensing in cognitive radio networks," in *Wireless Communications and Networking Conference, 2007. WCNC 2007. IEEE*. IEEE, 2007, pp. 27–32.

[88] W. Zhang, R. K. Mallik, and K. B. Letaief, "Cooperative spectrum sensing optimization in cognitive radio networks," in *Communications, 2008. ICC'08. IEEE International Conference on*. IEEE, 2008, pp. 3411–3415.

[89] E. Hossain and V. K. Bhargava, *Cognitive wireless communication networks*. Springer Science & Business Media, 2007.

[90] J. Ma, G. Zhao, and Y. Li, "Soft combination and detection for cooperative spectrum sensing in cognitive radio networks," *Wireless Communications, IEEE Transactions on*, vol. 7, no. 11, pp. 4502–4507, 2008.

[91] Z. Quan, S. Cui, and A. H. Sayed, "Optimal linear cooperation for spectrum sensing in cognitive radio networks," *Selected Topics in Signal Processing, IEEE Journal of*, vol. 2, no. 1, pp. 28–40, 2008.

[92] M. Hossain, A. A. El-Saleh *et al.*, "Cognitive radio engine model utilizing soft fusion based genetic algorithm for cooperative spectrum optimization," *arXiv preprint arXiv:1304.3273*, 2013.

[93] K. Arshad, M. A. Imran, and K. Moessner, "Collaborative spectrum sensing optimisation algorithms for cognitive radio networks," *International Journal of Digital Multimedia Broadcasting*, vol. 2010, 2010.

[94] S. Zheng, C. Lou, and X. Yang, "Cooperative spectrum sensing using particle swarm optimisation," *Electronics letters*, vol. 46, no. 22, p. 1525, 2010.

[95] M. Akbari, M. R. Manesh, A. A. El-Saleh, and M. Ismail, "Improved soft fusion-based cooperative spectrum sensing using particle swarm optimization," *IEICE Electronics Express*, vol. 9, no. 6, pp. 436–442, 2012.

[96] X. Li and L. Liu, "Cooperative spectrum sensing for cognitive radios based on a pa-gabc algorithm," in *Electronics, Communications and Control (ICECC), 2011 International Conference on*. IEEE, 2011, pp. 2604–2607.

[97] A. A. El-Saleh, M. Ismail, M. Akbari, M. R. Manesh, and S. A. R. T. Zavareh, "Minimizing the detection error of cognitive radio networks using particle swarm optimization," in *Computer and Communication Engineering (ICCCE), 2012 International Conference on*. IEEE, 2012, pp. 877–881.

[98] P. M. Pradhan and G. Panda, "Cooperative spectrum sensing in cognitive radio network using multiobjective evolutionary algorithms and fuzzy decision making," *Ad Hoc Networks*, vol. 11, no. 3, pp. 1022–1036, 2013.

[99] H. Hajimirsadeghi and C. Lucas, "A hybrid iwo/pso algorithm for fast and global optimization," in *EUROCON 2009, EUROCON'09. IEEE*. IEEE, 2009, pp. 1964–1971.

[100] J. Kenndy and R. Eberhart, "Particle swarm optimization," in *Proceedings of IEEE International Conference on Neural Networks*, vol. 4, 1995, pp. 1942–1948.

[101] A. R. Mehrabian and C. Lucas, "A novel numerical optimization algorithm inspired from weed colonization," *Ecological informatics*, vol. 1, no. 4, pp. 355–366, 2006.

[102] A. H. Nikoofard, H. Hajimirsadeghi, A. Rahimi-Kian, and C. Lucas, "Multiobjective invasive weed optimization: Application to analysis of pareto improvement models in electricity markets," *Applied Soft Computing*, vol. 12, no. 1, pp. 100–112, 2012.

[103] K. Deb, A. Pratap, S. Agarwal, and T. Meyarivan, "A fast and elitist multiobjective genetic algorithm: Nsga-ii," *Evolutionary Computation, IEEE Transactions on*, vol. 6, no. 2, pp. 182–197, 2002.

[104] C. A. C. Coello, G. T. Pulido, and M. S. Lechuga, "Handling multiple objectives with particle swarm optimization," *Evolutionary Computation, IEEE Transactions on*, vol. 8, no. 3, pp. 256–279, 2004.

[105] A. Rauniyar and S. Y. Shin, "Adaptive double-threshold based energy and matched filter detector in cognitive radio networks."

[106] P. Verma and B. Singh, "Overcoming sensing failure problem in double threshold based cooperative spectrum sensing," *Optik-International Journal for Light and Electron Optics*, 2016.

[107] A. Bhowmick, S. Nallagonda, S. D. Roy, and S. Kundu, "Cooperative spectrum sensing with double threshold and censoring in rayleigh faded cognitive radio network," *Wireless Personal Communications*, vol. 84, no. 1, pp. 251–271, 2015.

[108] S.-Q. Liu, B.-J. Hu, and X.-Y. Wang, "Hierarchical cooperative spectrum sensing based on double thresholds energy detection," *Communications Letters, IEEE*, vol. 16, no. 7, pp. 1096–1099, 2012.

[109] E. C. Y. Peh, Y.-C. Liang, Y. L. Guan, and Y. Zeng, "Optimization of cooperative sensing in cognitive radio networks: a sensing-throughput tradeoff view," *Vehicular Technology, IEEE Transactions on*, vol. 58, no. 9, pp. 5294–5299, 2009.

[110] M. Naeem, A. Anpalagan, M. Jaseemuddin, and D. C. Lee, "Resource allocation techniques in cooperative cognitive radio networks," *Communications Surveys & Tutorials, IEEE*, vol. 16, no. 2, pp. 729–744, 2014.

[111] G. Tsiropoulos, O. A. Dobre, M. H. Ahmed, and K. E. Baddour, "Radio resource allocation techniques for efficient spectrum access in cognitive radio networks," 2015.

[112] S. Wang, W. Shi, and C. Wang, "Energy-efficient resource management in ofdm-based cognitive radio networks under channel uncertainty," *Communications, IEEE Transactions on*, vol. 63, no. 9, pp. 3092–3102, 2015.

[113] X. Sun and S. Wang, "Energy-efficient power allocation for cognitive radio networks with minimal rate requirements," *International Journal of Communication Systems*, 2015.

[114] H. Hu, H. Zhang, and H. Yu, "Energy-efficient sensing for delay-constrained cognitive radio systems via convex optimization," *Journal of Optimization Theory and Applications*, vol. 168, no. 1, pp. 310–331, 2016.

[115] A. Bhowmick, S. D. Roy, and S. Kundu, "Sensing throughput trade-off for an energy efficient cognitive radio network under faded sensing and reporting channel," *International Journal of Communication Systems*, 2015.

[116] N. Hasan and W. Tu, "On energy-efficient performance-guaranteed channel assignment in cognitive radio-based wireless mesh networks," *International Journal of Communication Systems*, vol. 28, no. 17, pp. 2197–2213, 2015.

[117] Y. Qu, M. Wang, and J. Hu, "A new energy-efficient scheduling algorithm based on particle swarm optimization for cognitive radio networks," in *Signal Processing, Communications and Computing (ICSPCC), 2014 IEEE International Conference on*. IEEE, 2014, pp. 467–472.

[118] M. Naeem, K. Illanko, A. Karmokar, A. Anpalagan, and M. Jaseemuddin, "Optimal power allocation for green cognitive radio: fractional programming approach," *Communications, IET*, vol. 7, no. 12, pp. 1279–1286, 2013.

[119] M. Naeem, K. Illanko, A. Karmokar, A. Anpalagan, and M. Jaseemuddin, "Decode and forward relaying for energy-efficient multiuser cooperative cognitive radio network with outage constraints," *Communications, IET*, vol. 8, no. 5, pp. 578–586, 2014.

[120] W. Ejaz, G. A. Shah, H. S. Kim *et al.*, "Energy and throughput efficient cooperative spectrum sensing in cognitive radio sensor networks," *Transactions on Emerging Telecommunications Technologies*, vol. 26, no. 7, pp. 1019–1030, 2015.

[121] N. Nouri and N. Noori, "Optimal power allocation for cognitive radio networks with relay-assisted directional transmission," *International Journal of Communication Systems*, vol. 27, no. 11, pp. 3488–3501, 2014.

[122] L. Wang, M. Sheng, X. Wang, Y. Zhang, and X. Ma, "Mean energy efficiency maximization in cognitive radio channels with pu outage constraint," *Communications Letters, IEEE*, vol. 19, no. 2, pp. 287–290, 2015.

[123] X. Wu, J.-L. Xu, M. Chen, and J. Wang, "Optimal energy-efficient sensing and power allocation in cognitive radio networks," *Mathematical Problems in Engineering*, vol. 2014, 2014.

[124] S.-U. Yoon and E. Ekici, "Voluntary spectrum handoff: a novel approach to spectrum management in crns," in *Communications (ICC), 2010 IEEE International Conference on*. IEEE, 2010, pp. 1–5.

[125] D. Luenberger and Y. Ye, "Linear and nonlinear programming, new york: Springer science+ business media," 2008.

[126] W. Dinkelbach, "On nonlinear fractional programming," *Management Science*, vol. 13, no. 7, pp. 492–498, 1967.

[127] S. Boyd and L. Vandenberghe, *Convex optimization*. Cambridge university press, 2004.

[128] C. Sun, W. Zhang, and K. B. Letaief, "Cooperative spectrum sensing for cognitive radios under bandwidth constraints," in *Wireless Communications and Networking Conference, 2007. WCNC 2007. IEEE*. IEEE, 2007, pp. 1–5.

[129] Z. Jin, S. Anand, and K. Subbalakshmi, "Performance analysis of dynamic spectrum access networks under primary user emulation attacks," in *Global Telecommunications Conference (GLOBECOM 2010), 2010 IEEE*. IEEE, 2010, pp. 1–5.

[130] Z. Jin, S. Anand, and K. P. Subbalakshmi, "Impact of primary user emulation attacks on dynamic spectrum access networks," *Communications, IEEE Transactions on*, vol. 60, no. 9, pp. 2635–2643, 2012.

[131] R. Yu, Y. Zhang, Y. Liu, S. Gjessing, and M. Guizani, "Securing cognitive radio networks against primary user emulation attacks," *Network, IEEE*, vol. 29, no. 4, pp. 68–74, 2015.

[132] C. Chen, H. Cheng, and Y.-D. Yao, "Cooperative spectrum sensing in cognitive radio networks in the presence of the primary user emulation attack," *Wireless Communications, IEEE Transactions on*, vol. 10, no. 7, pp. 2135–2141, 2011.

[133] M. Haghighat and S. M. S. Sadough, "Cooperative spectrum sensing for cognitive radio networks in the presence of smart malicious users," *AEU-International Journal of Electronics and Communications*, vol. 68, no. 6, pp. 520–527, 2014.

[134] M. Saber and S. Sadough, "Optimal soft combination for multiple antenna energy detection under primary user emulation attacks," *AEU-International Journal of Electronics and Communications*, vol. 69, no. 9, pp. 1181–1188, 2015.

[135] Z. Jin, S. Anand, and K. Subbalakshmi, "Detecting primary user emulation attacks in dynamic spectrum access networks," in *Communications, 2009. ICC'09. IEEE International Conference on*. IEEE, 2009, pp. 1–5.

[136] O. León, J. Hernández-Serrano, and M. Soriano, "Cooperative detection of primary user emulation attacks in crns," *Computer Networks*, vol. 56, no. 14, pp. 3374–3384, 2012.

[137] M. Dang, Z. Zhao, and H. Zhang, "Optimal cooperative detection of primary user emulation attacks in distributed cognitive radio network," in *Communications and Networking in China (CHINACOM), 2013 8th International ICST Conference on*. IEEE, 2013, pp. 368–373.

[138] M. J. Saber and S. M. S. Sadough, "Robust cooperative spectrum sensing in cognitive radio networks under multiple smart primary user emulation attacks," in *Electrical Engineering (ICEE), 2014 22nd Iranian Conference on*. IEEE, 2014, pp. 1745–1748.

[139] A. A. Sharifi, M. Sharifi, and M. J. M. Niya, "Secure cooperative spectrum sensing under primary user emulation attack in cognitive radio networks: Attack-aware threshold selection approach," *AEU-International Journal of Electronics and Communications*, vol. 70, no. 1, pp. 95–104, 2016.

[140] M. Haghighat, H. Fathi, and S. Sadough, "Robust resource allocation for ofdm-based cognitive radio in the presence of primary user emulation attack," *Radioengineering*, vol. 21, no. 4, pp. 1085–1091, 2012.

[141] J. Du, D. Guo, B. Zhang, and Y. Su, "A robust cooperative spectrum sensing-assisted multiuser resource allocation scheme," *Mathematical Problems in Engineering*, vol. 2015, 2015.

[142] M. J. Saber and S. M. S. Sadough, "Multiband cooperative spectrum sensing for cognitive radio in the presence of malicious users," *IEEE Communications Letters*, vol. 20, no. 2, pp. 404–407, 2016.

[143] A. Alahmadi, Z. Fang, T. Song, and T. Li, "Subband puea detection and mitigation in ofdm-based cognitive radio networks," *Information Forensics and Security, IEEE Transactions on*, vol. 10, no. 10, pp. 2131–2142, 2015.

[144] R. Umar, F. Mohammed, and A. U. Sheikh, "Hybrid cooperative energy detection techniques in cognitive radio networks," *Handbook of Research on Software-Defined and Cognitive Radio Technologies for Dynamic Spectrum Management*, p. 1, 2014.

[145] T. P. Dinh and H. A. Le Thi, "Recent advances in dc programming and dca," in *Transactions on Computational Intelligence XIII*. Springer, 2014, pp. 1–37.

[146] H. H. Kha, H. D. Tuan, and H. H. Nguyen, "Fast global optimal power allocation in wireless networks by local dc programming," *Wireless Communications, IEEE Transactions on*, vol. 11, no. 2, pp. 510–515, 2012.

[147] A. Khabbazibasmenj, F. Roemer, S. A. Vorobyov, and M. Haardt, "Sum-rate maximization in two-way af mimo relaying: Polynomial time solutions to a class of dc programming problems," *Signal Processing, IEEE Transactions on*, vol. 60, no. 10, pp. 5478–5493, 2012.

[148] P. A. Lopes and J. B. Gerald, "New normalized lms algorithms based on the kalman filter," in *Circuits and Systems, 2007. ISCAS 2007. IEEE International Symposium on*. IEEE, 2007, pp. 117–120.

[149] S. Al-Sultan, M. M. Al-Doori, A. H. Al-Bayatti, and H. Zedan, "A comprehensive survey on vehicular ad hoc network," *Journal of network and computer applications*, vol. 37, pp. 380–392, 2014.

[150] C. Yang, Y. Fu, Y. Zhang, S. Xie, and R. Yu, "Energy-efficient hybrid spectrum access scheme in cognitive vehicular ad hoc networks," *Communications Letters, IEEE*, vol. 17, no. 2, pp. 329–332, 2013.

[151] H. Zhang, Y. Ma, D. Yuan, and H.-H. Chen, "Quality-of-service driven power and sub-carrier allocation policy for vehicular communication networks," *Selected Areas in Communications, IEEE Journal on*, vol. 29, no. 1, pp. 197–206, 2011.

[152] D. B. Rawat and S. Shetty, "Enhancing connectivity for spectrum-agile vehicular ad hoc networks in fading channels," in *Intelligent Vehicles Symposium Proceedings, 2014 IEEE*. IEEE, 2014, pp. 957–962.

[153] M. Fathian and A. R. Jafarian-Moghaddam, "New clustering algorithms for vehicular ad-hoc network in a highway communication environment," *Wireless Networks*, vol. 21, no. 8, pp. 2765–2780, 2015.

[154] C. Jiang, Y. Chen, and K. R. Liu, "Data-driven optimal throughput analysis for route selection in cognitive vehicular networks," *Selected Areas in Communications, IEEE Journal on*, vol. 32, no. 11, pp. 2149–2162, 2014.

[155] D. B. Rawat, T. Amin, and M. Song, "The impact of secondary user mobility and primary user activity on spectrum sensing in cognitive vehicular networks," in *Computer Communications Workshops (INFOCOM WKSHPS), 2015 IEEE Conference on*. IEEE, 2015, pp. 588–593.

[156] X. Xu, J. Bao, Y. Luo, and H. Wang, "Cooperative wideband spectrum detection based on maximum likelihood ratio for cr enhanced vanet," *Journal of Communications*, vol. 8, no. 12, pp. 814–821, 2013.

[157] Y. Liu, S. Xie, R. Yu, Y. Zhang, X. Zhang, and C. Yuen, "Exploiting temporal and spatial diversities for spectrum sensing and access in cognitive vehicular networks," *Wireless Communications and Mobile Computing*, vol. 15, no. 17, pp. 2079–2094, 2015.

[158] K. Baraka, L. Safatly, H. Artail, A. Ghandour, and A. El-Hajj, "An infrastructure-aided cooperative spectrum sensing scheme for vehicular ad hoc networks," *Ad Hoc Networks*, vol. 25, pp. 197–212, 2015.

[159] N. Cheng, N. Zhang, N. Lu, X. Shen, J. W. Mark, and F. Liu, "Opportunistic spectrum access for cr-vanets: a game-theoretic approach," *Vehicular Technology, IEEE Transactions on*, vol. 63, no. 1, pp. 237–251, 2014.

[160] X. Qian and L. Hao, "On the performance of spectrum sensing in cognitive vehicular networks," in *Personal, Indoor, and Mobile Radio Communications (PIMRC), 2015 IEEE 26th Annual International Symposium on*. IEEE, 2015, pp. 1002–1006.

[161] T.-D. Nguyen, O. Berder, and O. Sentieys, "Energy-efficient cooperative techniques for infrastructure-to-vehicle communications," *Intelligent Transportation Systems, IEEE Transactions on*, vol. 12, no. 3, pp. 659–668, 2011.

[162] R. B. López, S. M. Sanchez, E. M. Fernandez, R. D. Souza, and H. Alves, "Genetic algorithm aided transmit power control in cognitive radio networks," in *Cognitive Radio Oriented Wireless Networks and Communications (CROWNCOM), 2014 9th International Conference on*. IEEE, 2014, pp. 61–66.

[163] Y. Wang, Q. Zhang, Y. Zhang, and P. Chen, "Adaptive resource allocation for cognitive radio networks with multiple primary networks," *EURASIP Journal on Wireless Communications and Networking*, vol. 2012, no. 1, pp. 1–18, 2012.

[164] D. Das and S. Das, "Optimal resource allocation for soft decision fusion-based cooperative spectrum sensing in cognitive radio networks," *Computers & Electrical Engineering*, 2016.

[165] Y. Zhang, J. Zheng, and H.-H. Chen, *Cognitive radio networks: architectures, protocols, and standards*. CRC press, 2010.

[166] D. Das and S. Das, "A survey on spectrum occupancy measurement for cognitive radio," *Wireless Personal Communications*, vol. 85, no. 4, pp. 2581–2598, 2015.

[167] M. Biggs, A. Henley, and T. Clarkson, "Occupancy analysis of the 2.4 ghz ism band," in *Communications, IEE Proceedings*, vol. 151, no. 5. IET, 2004, pp. 481–488.

[168] J. Kokkoniemi and J. Lehtomäki, "Spectrum occupancy measurements and analysis methods on the 2.45 ghz ism band," in *Cognitive Radio Oriented Wireless Networks and Communications (CROWNCOM), 2012 7th International ICST Conference on*. IEEE, 2012, pp. 285–290.

[169] M. Matinmikko, M. Mustonen, M. Höyhtyä, T. Rauma, H. Sarvanko, and A. Mämmelä, "Distributed and directional spectrum occupancy measurements in the 2.4 ghz ism band," in *Wireless Communication Systems (ISWCS), 2010 7th International Symposium on*. IEEE, 2010, pp. 676–980.

[170] M. Pakparvar, H. Gharibdoust, S. Pollin, and L. Tytgat, "Dynamic channel selection algorithms for coexistence of wireless sensor networks and wireless lans," in *Wireless and Mobile Computing, Networking and Communications (WiMob), 2013 IEEE 9th International Conference on*.   IEEE, 2013, pp. 33–38.

[171] S. A. Hanna and J. Sydor, "Spectrum metrics for 2.4 ghz ism band cognitive radio applications," in *Personal Indoor and Mobile Radio Communications (PIMRC), 2011 IEEE 22nd International Symposium on*.   IEEE, 2011, pp. 2344–2348.

[172] J. Xue, Z. Feng, and P. Zhang, "Spectrum occupancy measurements and analysis in beijing," *IERI Procedia*, vol. 4, pp. 295–302, 2013.

[173] M. López-Benítez, A. Umbert, and F. Casadevall, "Evaluation of spectrum occupancy in spain for cognitive radio applications," in *Vehicular technology conference, 2009. VTC Spring 2009. IEEE 69th*.   IEEE, 2009, pp. 1–5.

[174] Z. Jianli, W. Mingwei, and Y. Jinsha, "Based on neural network spectrum prediction of cognitive radio," in *Electronics, Communications and Control (ICECC), 2011 International Conference on*.   IEEE, 2011, pp. 762–765.

[175] I. A. Akbar and W. H. Tranter, "Dynamic spectrum allocation in cognitive radio using hidden markov models: Poisson distributed case," in *SoutheastCon, 2007. Proceedings. IEEE*.   IEEE, 2007, pp. 196–201.

[176] B. Najashi and W. Feng, "Cooperative spectrum occupancy based spectrum prediction modeling," *Journal of Computational Information Systems*, vol. 10, no. 10, pp. 4093–4100, 2014.

[177] V. K. Tumuluru, P. Wang, and D. Niyato, "A neural network based spectrum prediction scheme for cognitive radio," in *Communications (ICC), 2010 IEEE International Conference on*.   IEEE, 2010, pp. 1–5.

[178] N. Shamsi, A. Mousavinia, and H. Amirpour, "A channel state prediction for multi-secondary users in a cognitive radio based on neural network," in *Electronics, Computer and Computation (ICECCO), 2013 International Conference on*.   IEEE, 2013, pp. 200–203.

[179] Y.-H. Pao, S. M. Phillips, and D. J. Sobajic, "Neural-net computing and the intelligent control of systems," *International Journal of Control*, vol. 56, no. 2, pp. 263–289, 1992.

[180] J. C. Patra, R. N. Pal, B. Chatterji, and G. Panda, "Identification of nonlinear dynamic systems using functional link artificial neural networks," *Systems, Man, and Cybernetics, Part B: Cybernetics, IEEE Transactions on*, vol. 29, no. 2, pp. 254–262, 1999.

[181] R. Majhi, G. Panda, and G. Sahoo, "Development and performance evaluation of flann based model for forecasting of stock markets," *Expert Systems with Applications*, vol. 36, no. 3, pp. 6800–6808, 2009.

[182] J. C. Patra and A. C. Kot, "Nonlinear dynamic system identification using chebyshev functional link artificial neural networks," *Systems, Man, and Cybernetics, Part B: Cybernetics, IEEE Transactions on*, vol. 32, no. 4, pp. 505–511, 2002.

[183] R. De Francisco and A. Pandharipande, "Spectrum occupancy in the 2.36–2.4 ghz band: Measurements and analysis," in *Wireless Conference (EW), 2010 European*.   IEEE, 2010, pp. 231–237.

[184] S. Aslam, A. Shahid, and K.-G. Lee, "Ga-css: Genetic algorithm based control channel selection scheme for cognitive radio networks," in *Next Generation Mobile Apps, Services and Technologies (NGMAST), 2013 Seventh International Conference on*. IEEE, 2013, pp. 232–236.

[185] A. Batra, J. Balakrishnan, G. R. Aiello, J. R. Foerster, and A. Dabak, "Design of a multiband ofdm system for realistic uwb channel environments," *Microwave Theory and Techniques, IEEE Transactions on*, vol. 52, no. 9, pp. 2123–2138, 2004.

[186] P. Series, "Propagation data and prediction methods for the planning of indoor radiocommunication systems and radio local area networks in the frequency range 900 mhz to 100 ghz," 2012.

Deepa Das

CONTACT
INFORMATION

Signal Processing and Communication Lab
Department of Electrical Engineering
National Institute of Technology Rourkela
Dist : Sundargarh, Odisha PIN : 769008
deepadas.ctc@gmail.com
+91-9439012400

RESEARCH
INTERESTS

Cognitive Radio, Wireless Communication, Signal Processing, Soft Computing

EDUCATION

National Institute of Technology, Rourkela, INDIA

Ph.D., Electrical Engineering,

- *Submitted:* December 2016
  - Thesis Title: *Intelligent Approaches for Energy-Efficient Resource Allocation in the Cognitive Radio Network*
  - Thesis Advisor: Prof. Susmita Das, Ph.D

Kalinga Institute of Industrial Technology University, Bhubaneswar, INDIA

M.Tech., Electronics and Telecommunication Engineering, June 2008
- Thesis Title: *Multiuser detection in CDMA and MAI Cancellation*
- Thesis Advisor: Prof. Nirmal Kumar Rout, Ph.D
- CGPA: 8.75

Biju Patnaik University of Technology, Rourkela, INDIA

B.Tech., Electronics and Telecommunication Engineering, August 2005
- Percentage: 71.47

Dhenkanal Autonomous College, Dhenkanal , INDIA

+2 Sc., Physics, Chemistry, Biology, Mathematics 2000
- Percentage: 72.11

Panchayat HighSchool, Padiabhanga, Angul, INDIA

Tenth, March 1998
- Percentage: 86.4

RESEARCH
EXPERIENCE

Research Scholar   January 2013 to present
Department of Electrical Engineering,
National Institute of Technology Rourkela

DECLARATION

The information furnished above is true to the best of my knowledge & belief.

Date: July 3, 2017   Deepa Das
Place: Rourkela

Index